The Mineralogy of NYF Pegmatites from the Coldwell Alkaline Complex, Northwestern Ontario

Malcolm Alexander
Lakehead University
Thunder Bay, Ontario

ACKNOWLEDGEMENTS

ABSTRACT

The Coldwell Complex, northwestern Ontario, is a multiphase alkaline intrusion that is host to rare earth element, actinide and other high field strength element mineralization. Preliminary studies have shown that these minerals are concentrated in pegmatites associated with Center One ferrorichterite-ferroaugite syenites and Center Three syenites. The Center One syenites differentiate to pegmatitic residua and are characterized by cumulus perthitic-to-cryptoperthitic alkali feldspar, hedenbergite-aegirine pyroxenes, and intercumulous quartz, calcite, and calcic-to-sodic-calcic-to-sodic amphiboles. Center Three residua are similar, except that amphiboles are limited to calcic varieties (hastingsite) and precipitate before feldspar (as opposed to after). All pegmatitic residua are of the niobium-yttrium-fluorine (NYF) type. Back-scattered electron petrography has been used to characterize the mineral paragenesis. Pegmatitic syenitic residua emplaced in, but not derived from the border gabbro (Border Gabbro pegmatite), and residua within ferroaugite syenite units (Railway pegmatites) contain a wide range of rare element minerals which include britholite, chevkinite, fergusonite, monazite, allanite, kainosite, xenotime, REE fluorocarbonates bastnaesite, synchysite and parisite. Other rare element enriched minerals include apatite, thorite, zircon, zirconolite, niobium rutile and U-Th-Si-pyrochlore. Early-formed rare element minerals such as allanite, britholite, chevkinite, kainosite, and pyrochlore are commonly replaced by complex aggregates of later-forming phases such as REE-fluorocarbonates. Other riebeckite-quartz (Upper Marathon Shore pegmatites), richterite-quartz (Black pegmatites) and hastingsite-quartz (Center Three pegmatites) bearing pegmatitic residua contain a more restricted range of rare element minerals, which include zircon, xenotime, monazite and fluorocarbonates together with REE-bearing apatite, thorite and pyrochlore. The differences in rock forming and accessory mineralization suggest that most, if not all, residua are derived from different batches of ferroaugite syenite and syenite magma.

Intensive parameters have been estimated using the habit of perthites, the coexistence of zircon and baddeleyite, Fe-Ti-oxide compositions, amphibole mineralogy, and fluorocarbonate stability. These parameters indicate all pegmatitic units are similar, with initial silica activities of $10^{-0.75}$, alkali-feldspar precipitation at approximately 750 °C, magnetite-ilmenite subsolidus equilibration temperatures of 531 to 633 °C and oxygen fugacities of $10^{-16.5}$ to $10^{-22.9}$ bars, subsolidus quenching of magnetite occurs at approximately 450 °C, and subsequent 200 °C hydro- and carbothermal induced recrystallization of rare earth mineral and REE-bearing minerals.

CONTENTS

LIST OF FIGURES

LIST OF TABLES

CHAPTER ONE
INTRODUCTION AND GENERAL GEOLOGY

1.1 Introduction

The Coldwell alkaline complex of northwestern Ontario contains rocks that belong to three distinct differentiation trends. Compositions range from saturated-to-undersaturated, with alkalinity varying from miascitic-to-peralkaline. As such, the complex has been the subject of many petrogenetic studies (Currie 1980; McLaughlin and Mitchell 1989; Mitchell and Platt 1977). The complex is host to minerals containing abundant rare earth elements (REE), actinide and high field strength elements (HFSE). Initial studies by McLaughlin (1990) have shown that these minerals are dispersed throughout the complex, and concentrated in patch, vein and localized pegmatites. A comprehensive petrogenetic study of the pegmatite occurrences has yet to be undertaken, despite their exotic character and economic/mineralogical interest. The investigation of REE, thorium, and uranium minerals are, in particular, important as each mineral imparts a distinctive REE pattern to the rocks "documenting" the formational processes (Haskin 1990).

The objective of this study is to present the compositional variation of all minerals within the selected pegmatitic units, propose a paragenetic sequence of these mineral, and model the petrogenetic history of these pegmatites with a special focus on the REE mineralization. Preliminary work (McLaughlin 1990) has shown that the more exotic (and economic) minerals reside in Center One and Three pegmatitic rocks, which are the areas of focus for this study.

1.2 The Midcontinental Rift System

The initial igneous/magmatic activity of the Coldwell complex began with the onset of the North American Midcontinental Rift System (NAMRS). The rift system, according to Hutchinson et al. (1990) and Cannon and Hinze (1992), formed in response to the upwelling of a mantle plume. The NAMRS (Fig 1.1) is one of the largest known continental rifts in the world and can be traced for over 2000 km from Kansas to south-central Michigan (Van Schmus and Hinze 1985). A third arm, although not as apparent, may be the Nipigon embayment which is represented by extensive basaltic sheets and flows and dioritic intrusions.

In the Lake Superior basin, the central rift transects Archean and Early Proterozoic basement rock, with a maximum width of approximately 100 km. Seismic reflection data

(Behrendt et al. 1988) from the Lake Superior area indicate that the crust is approximately 40 km thick within the main rift segment, about 32 km of which consists of rift-related volcanic and sedimentary rocks. This thickness is greater or equal to the surrounding regions, which is different from all known Phanerozoic rifts (Behrendt et al. 1988).

Within the NAMRS is a reverse-to-normal magnetic pole reversal (Halls and Pesonen 1982). Magnetically-reversed rock is represented by exposed plutonic (i.e. Logan Sills) and volcanic (i.e. Lower Keweenawan basalt) rocks, whereas the magnetically normal rock is recorded in the volcanic Upper Keweenawan rocks of the Olser Group. The reversal has been constrained by Davis and Paces (1997) to a period of 1096.2±1.8 Ma to 1097.6±3.7 Ma.
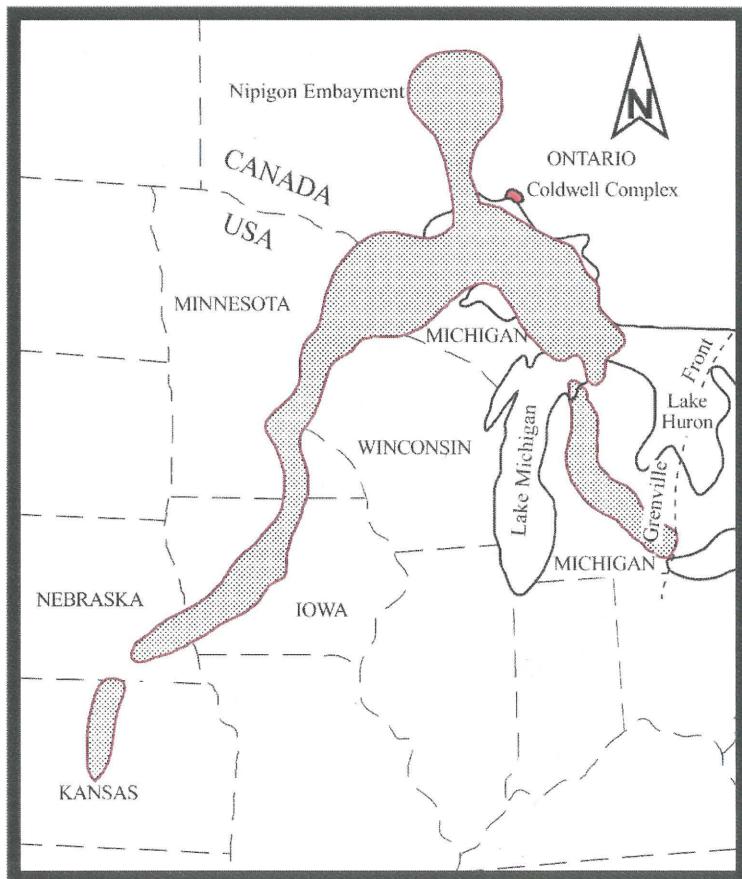
FIGURE 1.1: The midcontinental rift system positive Bouguer gravity anomaly, and location of the Coldwell complex. Adapted from Green (1983) and Cannon et al. (1989).

U-Pb zircon chronostratigraphic studies of the Lake Superior volcanics indicate that the initial activity began at 1113.6±6.5 Ma (Heaman et al. 2007; age of the Mount McKay dioritic

sill) and ended 1091.1±4.5 Ma (Heaman et al. 2007; age of the Blake Township gabbro), thus lasting a total of 23.6 Ma. U-Pb ages obtained for the normal polarity Portage Lake Volcanics (1094.0 to 1096.2 Ma) indicate that most of the exposed Keweenawan basalt erupted in an extremely short (2 Ma) period of time (Davis and Paces 1990). The eruption rates of the NAMRS have been estimated by Davis and Paces (1990) to be as low as 0.02-0.05 km^3/yr and as high as 0.2-0.6 km^3/yr.

Early volume estimates of the erupted lava in the rift indicated volumes exceeding 300,000 km^3 (Green 1983). Later estimates, which took into account the amount of rift-fill volcanics, were revealed from the Great Lakes International Multi-disciplinary Program on Crustal Evolution (GLIMPCE) study (Cannon et al. 1989) and indicate volumes in excess of 1.3 million km^3 (Hutchinson et al. 1990). This estimate could be extended to 2 million km^3 if some of the unaccounted volcanic rocks, thought initially to be sedimentary rocks, and eroded material are considered (Cannon 1992). This volume of lava is large when compared to other major mafic magmatic events in North America, e.g. the Mackenzie Igneous Events which produced approximately 250,000 km^3 of material (Le Cheminant and Heaman 1989).

One member included in the NAMRS plutonic suite is the Coldwell alkaline complex. With a diameter of 28 km, this complex is the largest alkaline intrusion in North America, and contains rocks that range from oversaturated, through saturated to undersaturated. The complex is located on the northern shore of Lake Superior between the Pic and Little Pic rivers (Fig. 1.2). The Coldwell complex is the southernmost member of a north-south-trending belt of alkaline intrusions which, according to Sage (1982), includes: the Prairie Lake carbonatite-ijolite complex, the Killala Lake nepheline syenite complex, the Chipman Lake carbonatite dykes, and the Dead Horse Creek, Gold Range, McKellar Creek, Neys, and Slate Islands volcaniclastic vents (Fig 1.3). All intrusions and vents have ages and mineralized/unmineralized structures that indicate a relationship to the magmatism of the Keweenawan mid-continental rifting. A contemporaneous belt of alkaline and carbonatitic intrusions is found along the Kapuskasing High, but no petrological or tectonic relation to the Coldwell complex is known to exist (Platt 1996).

The Coldwell complex is situated between two older Archean age tholeiitic volcanic belts: the Osler volcanic rocks to the west, and the Mamainse-Michipicoten volcanic rocks to the east. At least two episodes of folding, along with the intrusion of Archean felsic plutons, have affected the area, resulting in metamorphism ranging from greenschist to amphibolite facies. A

maximum grade of pyroxene hornfels facies, created by the emplacement of the complex, forms a 2 km wide contact aureole surrounding the west side of the complex (Walker 1967).
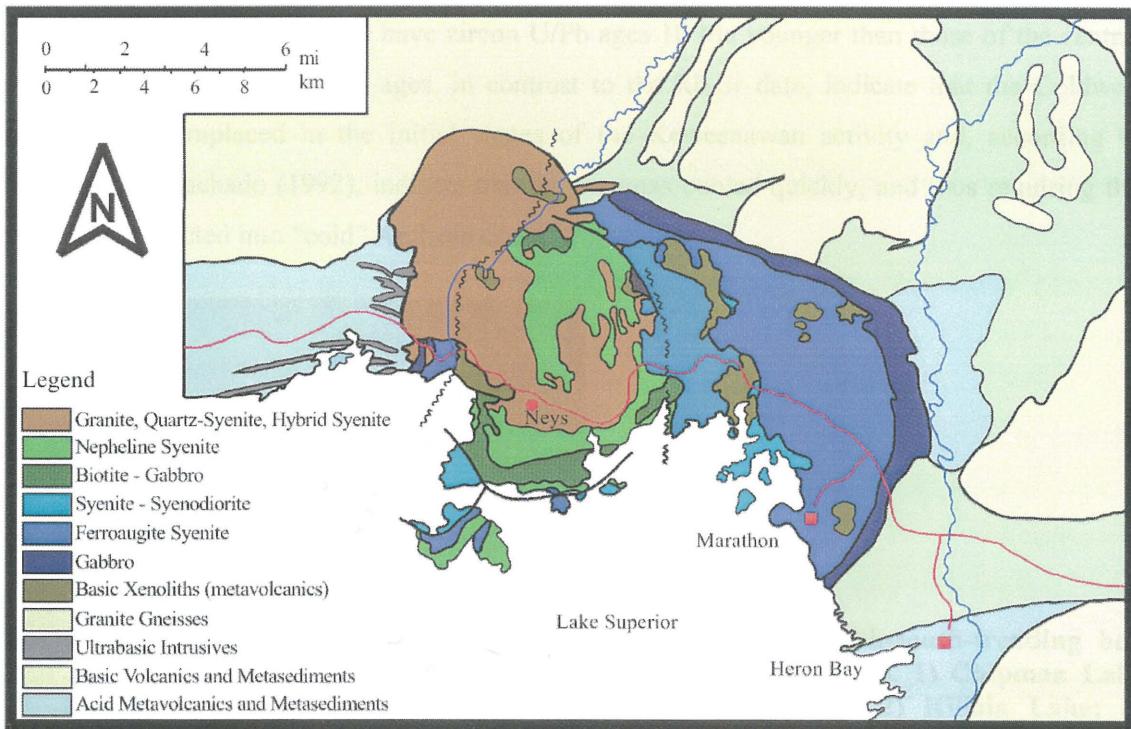
FIGURE 1.2: Geological map of the Coldwell alkaline complex. Center One shown in blues, Center Two in greens and Center Three in brown. Modified from Mitchell and Platt (1978).

1.3 Age of the Coldwell Complex

The age of the Coldwell complex has been determined using K-Ar, U-Pb and Rb-Sr methods. Initially, whole rock and mineral Rb/Sr ages by Chaudhuri et al. (1971) gave an age of 1052±15 Ma. The K-Ar ages of biotite from the Center One gabbro and ferroaugite syenite were determined by Currie (1976) to be 1005 Ma and 1015 Ma, respectively. A seventeen-point whole rock Rb-Sr isochron determined by Mitchell and Platt (1978) gave an age of 1044.5±6.2 Ma with an initial ratio of 0.70354±0.00016. These ages are late Neohelikian and indicate that the Coldwell complex was emplaced much later, by approximately 50 Ma, than the major period of Keweenawan igneous activity.

Following Chaudhuri et al. (1971), Rb/Sr geochronology was also reported by Bell et al. (1979) and Bell and Blenkinsop (1980). The age determined by Bell et al. (1979) from a five-point whole rock isochron gave an age of 1085±15 Ma with an initial ratio of 0.7019±0.0006,

whereas the Bell and Blenkinsop (1980) study determined an age of 1070±15 Ma and an initial $^{87}Sr/^{86}Sr$ ratio of 0.7035±0.0006. Using U-Pb, Heaman and Machado (1992) published an age of 1108±1 Ma. Heaman and Machado (1992) also determined that the quartz syenites from the western portion of the complex have zircon U/Pb ages 10 Ma younger than those of the central and eastern zones. These later ages, in contrast to the Rb-Sr data, indicate that the Coldwell complex was emplaced in the initial stages of the Keweenawan activity and, according to Heaman and Machado (1992), indicate that the magmas cooled quickly, and thus requiring the magmas be injected into "cold" Archean crust.
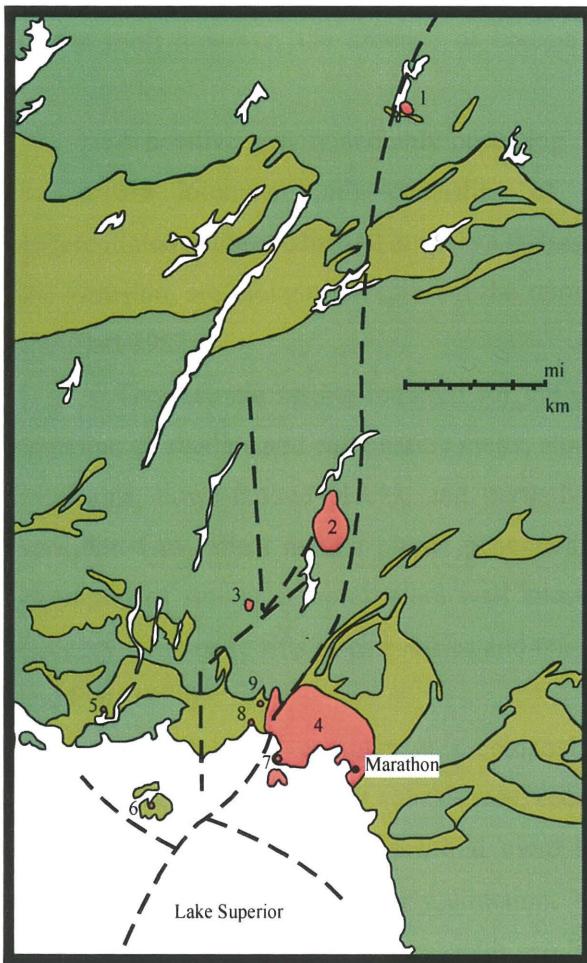
FIGURE 1.3: North-south-trending belt of alkaline intrusions. 1) Chipman Lake carbonatite dykes; 2) Killala Lake; 3) Prairie Lake; 4) Coldwell; 5) Gold Range; 6) Slate Islands; 7) Neys; 8) McKellar Creek; 9) Dead Horse Creek. North is up. After Sage (1982).

During alteration, the Rb-Sr and K-Ar systems are more susceptible to resetting than the U-Pb system and this could explain the significant discrepancy between the ages. It is apparent that sub-solidus reactions involving hydrothermal fluids have affected the Rb/Sr and K/Ar systems, rendering later events for determining the original age of emplacement, but providing

insight concerning alteration. The presence of fluorocarbonates and other late-stage minerals and textures also indicate that a later alteration episode occurred.

1.4 Structure

Exposure of the Coldwell complex is restricted mainly to the shorelines of Lake Superior and recent road and railway cuts. In part, the structure is characteristic of a cauldron subsidence (Mitchell and Platt 1978, 1982), with down-faulted blocks of the central portion of the complex representing a higher stratigraphic level (Mitchell and Platt 1977). Breccia and metasomatic zones in the western portion of the intrusion are believed to represent an area close to the roof; however, the absence of breccias in the eastern portion may indicate a deeper structural level.

A positive gravity anomaly occurring over the complex (Fig 1.4) suggests the complex has a 3-5 kilometer unit—consisting of pyroxenite and/or peridiotite—underlying the differentiated gabbro (Mitchell et al. 1983). Basaltic xenoliths, common in the central portions of the intrusion, are thought to represent the remnants of former basaltic cap rock lavas (Mitchell and Platt 1982).

The tectonic setting required for the extrusion of large volumes of basic magma and intrusion of alkaline and carbonatitic melts, along with tensile structures, i.e. concentric marginal intrusions, down-faulted blocks, and partially assimilated remnants of the capping lavas, is considered to reflect mantle plume generated intracratonic rifting (Mitchell and Platt 1982). Examples of similar complexes are well known from other rifted continental regions, e.g. the Gregory-Kavirondo rifts of east Africa and the Kangedlugssuaq area of east Greenland (Mitchell and Platt 1978).

The Coldwell complex is a composite intrusion with three magmatic episodes that represent individual cauldron subsidences, each characterized by a distinct differentiation trend (Mitchell and Platt 1978). The initial trend began in the east and, as the other two trends emerged, progressed in a westerly direction. The oldest phase of the Coldwell complex is the Center One saturated alkaline rocks with peralkaline oversaturated residua (gabbro with layered and unlayered ferroaugite syenites). Center One was followed by Center Two miascitic undersaturated alkali rocks (alkali biotite gabbro and undersaturated nepheline syenites). The final phase was Center Three alkaline rocks with oversaturated residua (syenites and quartz syenites).
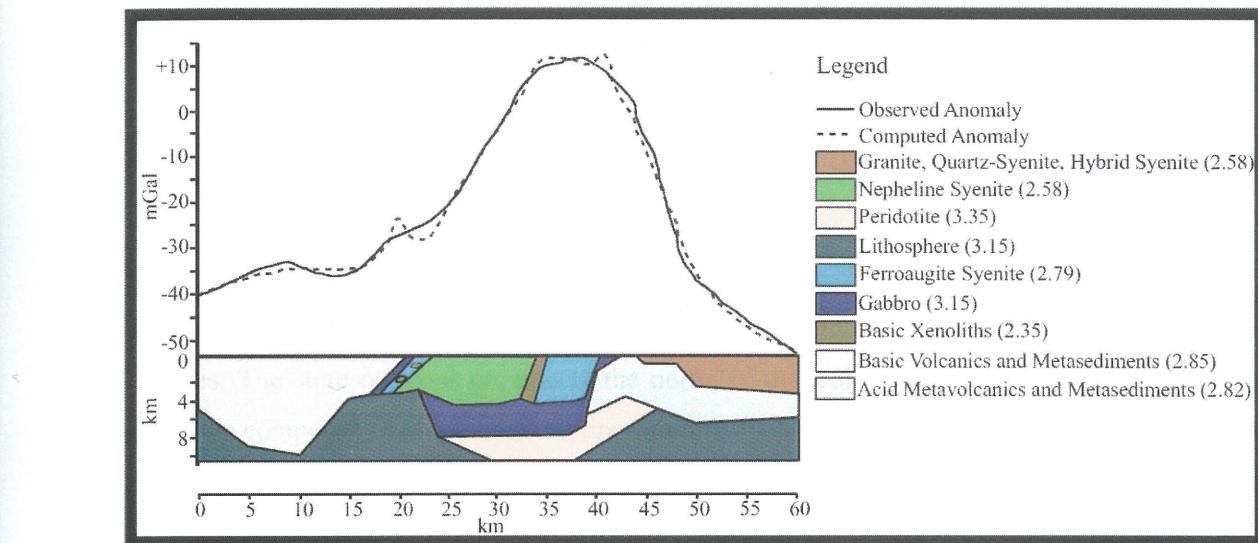
FIGURE 1.4: The observed and computed gravity anomaly profiles, and the interpreted infrastructure of the Coldwell complex. Density is in g/cm^3. After Mitchell et al. (1983).

1.5 Center One

The oldest intrusive rocks in Center One form a ring-like system consisting primarily of diverse oversaturated gabbros. These gabbros are massive-to-weakly layered with the bulk consisting of laminated cumulates of olivine, plagioclase, clinopyroxene and minor orthopyroxene. A prominent magnetic low, extensive metasomatism, brecciation, and the inclusion of basalt xenoliths characterize the eastern gabbro (Mitchell et al. 1983). The unit has sporadic development of graded layering with near vertical dip and mineral alignment and zones containing disseminated-to-coherent blebs of copper nickel sulphides and platinum group minerals. A similar gabbroic body in the western portion of the complex may, or may not (Currie 1980), be related to the eastern gabbro.

A large (130 m wide) north-south trending, coarse-grained gabbroic-to-monzonitic dyke intrudes the gabbro unit in Center One, and is associated with Cu-PGE mineralization (Dahl et al. 1987). The Two Duck Lake intrusion contains pyrrotite, chalcopyrite, pentlandite, cubanite, and platinum group minerals (Ohnenstetter et al. 1991). The Geordie Lake intrusion is approximately 500 x 2000 m in size and is bounded by Center One rocks. The intrusion consists of alternating zones of unlayered troctolite and olivine gabbro, which are divided by gradational contacts (Mulja and Mitchell 1990).

Intruding the gabbros is a series of massive-to-layered, red ferroaugite syenites. The lower series are layered and composed of alkali feldspar, fayalite olivine, ferroaugite,

titanomagnetite, and ferrohastingsite, ferroedenite and edenite amphiboles (Mitchell and Platt 1978). The upper series are poorly layered and consist of alkali feldspars, fayalite olivine, aegirine-to-hedenbergite pyroxene, aenigmatite, and katophorite and ferrorichterite amphiboles (Mitchell and Platt 1978).

1.6 Center Two

Center Two consists of an alkali biotite gabbro and undersaturated miascitic nepheline syenites. The suite outcrops on, and to the north, of the Coldwell Peninsula. The alkali biotite gabbro is composed of amphibole, biotite, olivine, plagioclase, pyroxene, and minor amounts of nepheline. Subsolidus reaction rims of amphiboles about olivines are common. The biotite gabbro is intruded by nepheline and natrolite syenites.

The nepheline syenites outcrop in three main areas; Pic and Allouez Islands, the Mink Creek-Redsucker Cove area and to the east of Killala Lake road. The nepheline syenites have moderate iron enrichment, and contain aluminous amphiboles and aegirine. The rocks are coarse-grained, leucocratic-to-melanocratic, hastingsite nepheline syenites, which contain minor and accessory apatite, biotite, fluorite, natrolite, sodalite, titanite, titanomagnetite, and zeolites (Mitchell and Platt 1982). The rocks exhibit a wide variety of textural types that are related to high temperature shearing and recrystallization of coarse grained nepheline syenite along faults along the margins of Center Two (Mitchell and Platt 1982). Subsolidus hydrothermal alteration in some areas has precipitated chlorite (chamosite), iron- (hematite), aluminum-oxides (boehmite) and zeolites (natrolite). According to Mitchell and Platt (1982) extensive fractional crystallization of an alkali basalt parent produced the nepheline syenites.

1.7 Center Three

Center Three consists of syenite, quartz syenite and granitic rocks. The suite is confined to the western half of the intrusion, with cross-cutting relationships and radiometric ages (Heaman and Machado 1992) indicating the suite was the last episode of activity. The syenites are characterized by an abundance of zircon, the near absence of pyroxene and the presence of Na-Fe amphiboles, fluorite and quartz. The suite commonly carries xenoliths of Archean country rock, metamorphosed/metasomatized contemporaneous basaltic rocks, consanguineous and earlier-formed syenites, and gabbros. Unlike Center One syenites, Center Three rocks do not differentiate to peralkaline residua, nor is their emplacement preceded by an intrusion of gabbro

(Mitchell et al. 1993). The reaction between Center Three magma and basaltic "cap" xenoliths has produced a diverse suite of contaminated syenites (Nicol 1990).

Mitchell et al. (1993) recognized four varieties of syenite, which in order of intrusion are magnesiohornblende syenite, ferroedenite syenite, contaminated ferroedenite syenite, and quartz syenite. The magnesiohornblende syenites are primarily alkali feldspar and amphibole, with minor biotite and quartz. Accessory minerals include magnetite, ilmenite, apatite, pyroxene, zircon, titanite, fluorite, pyrite, and olivine (Mitchell et al. 1993). The rocks are pink or red with clusters of mafic minerals. Textures include synneusis amphibole set in a hypidiomorphic-granular to porphyritic-hypidiomorphic-granular matrix. The synneusis clusters (Mitchell et al. 1993) have irregular margins with interstices between the amphiboles occupied by matrix alkali feldspar. The alkali feldspars are usually mantled, patch perthites, which are typically strongly sericitized and saussuritized (Mitchell et al. 1993). Hypidiomorphic-type syenites are characteristically subhedral-to-anhedral perthites. The porphyritic types of magnesiohornblende syenites have phenocrysts of patch perthite alkali feldspar, grading into microphenocrystal subhedral and randomly orientated laths (Mitchell et al. 1993). Late interstitial quartz and fluorite occur throughout the magnesiohornblende syenites.

The ferroedenite syenites are typically fine-to-medium-grained, with tabular alkali feldspar phenocrysts. The primary minerals include alkali feldspar and quartz with minor amphibole, biotite, and magnetite-ilmenite. Accessory minerals include apatite, titanite, pyroxene, fluorite, zircon, chevkinite, monazite, rare-earth fluorocarbonates, pyrochlore, columbite and allanite (McLaughlin and Mitchell 1989). The rocks contain phenocrysts of alkali feldspar set in a matrix of perthitic alkali feldspar prisms. Late stage quartz, sodic amphiboles, and fluorite occur in the interstices. Wide variations in the modal amount of amphibole and quartz may be found, as the ferroedenite syenites differentiate from relatively mafic-rich types to quartz-rich pegmatitic varieties (Mitchell et al. 1993).

The contaminated ferroedenite is recognized by its purple color, high content of xenolithic material, and the presence of oval clusters of metasomatic biotite. The rock consists primarily of alkali feldspar, amphibole and biotite. The contaminated ferroedenite is relatively poor in quartz relative to the contamination-free ferroedenite syenites and may contain significant quantities of plagioclase (Mitchell et al. 1993). Accessory minerals include apatite, magnetite, ilmenite, zircon, fluorite, pyroxene, fluorocarbonates, chevkinite, pyrochlore, columbite, zirconolite, allanite, and titanite (McLaughlin and Mitchell 1989). The rocks have mantled phenocrysts of vein and braid perthitic feldspar set in a xenomorphic-granular

groundmass of alkali feldspar, minor plagioclase and quartz. The groundmass is principally plagioclase, which occurs as discrete laths or as anhedral grains forming a sutured texture with alkali feldspar (Mitchell et al. 1993). The alkali feldspars are strongly hematized in contrast with those in the contamination-free ferroedenite syenites. Oval clusters of biotite characterize the contaminated ferroedenite syenites and are distributed uniformly throughout the groundmass and consist principally of randomly orientated interlocking plates of brown-green biotite.

The quartz syenites consist principally of alkali feldspar and amphibole, with minor quartz. Pyroxene, apatite, zircon, chevkinite, columbite, pyrochlore, rare-earth fluorocarbonates, fluorite, magnetite, Nb-rutile, allanite, monazite, fersmite, and fergusonite occur as accessory minerals (McLaughlin and Mitchell 1989). Quartz and fluorite occurs as late stage interstitial phase. The syenites have hypidiomorphic granular texture and are rarely porphyritic. Alkali feldspars are vein and braid antiperthites. The quartz syenites differ from ferroedenite syenites with respect to texture and type of feldspars, quartz content, relatively greater amounts of pyroxene, and the absence of titanite.

1.8 Minor intrusions

There are a series of minor plutonic intrusions throughout the Coldwell complex. The Neys, Dead Horse Creek and McKeller Creek vents are possibly associated with the complex. Superficially, only the Neys vent cuts the intrusive rocks of the complex. The Neys vent is located on the west side of the Coldwell Peninsula between Middleton and Coldwell. The vent cuts the coarse-grained amphibole syenites of Center Two, and is composed of coarse-grained nepheline syenites and hornfels. Xenoliths of country and intrusive rock, some of which are layered, are scattered throughout the Neys vent.

The other vents, the Dead Horse Creek and McKeller Creek, are related to the Coldwell complex but, unlike the Neys vent, do not cross-cut the plutonic rocks. Xenoliths found in the vents represent rock that was previously deposited in the vicinity. No plutonic xenoliths from the Coldwell complex have yet been found in the Dead Horse Creek and McKeller Creek diatremes.

Dike rocks are common in the Coldwell complex. The dikes are contemporaneous with Center Two activity and cut the complex and surrounding country rock (Mitchell et al. 1991). There are five varieties of lamprophyres, which in order of abundance are: ocellar camptonites, camptonites with quartz macrocrysts, amphibole camptonites, monchiquites, and sannaites (Mitchell et al. 1991). All lamprophyres associated with the Coldwell complex have similar incompatible element abundances and exhibit the same negative anomalies with respect to K, Sr,

Hf, and Ti (Mitchell et al. 1991). This suggests that all lamprophyres have been derived from a similar source.

Other dyke rocks associated with the Coldwell complex include feldspar glomeroporphyry and alkali basalt dykes, analcime tinguaites, and gabbroic to monzonitic dykes. The feldspar glomeroporphyry have rounded to tabular plates of orange feldspar that are commonly clumped together (Currie 1980). The analcime tinguaites consist of phenocrysts of analcime, alkali feldspar and nepheline set in a very fine-grained matrix of altered feldspars and acmitic pyroxene. Both mafic dykes commonly exhibit a sinuous and planar ground plan, bifurcations and off-sets (Currie and Ferguson 1970). The dykes range in width from 10 to 100 cm (Currie 1980).

1.9 Pegmatites

Pegmatites within Coldwell rocks occur as patches, veins and localized masses. The patch pegmatites range in size from 10 cm up to 2 m. Fed by pegmatitic veins, the patch pegmatites are especially abundant in the upper series of Center One ferroaugite syenites. Localized masses of pegmatite are essentially patch pegmatites, which exceed 2 m and can be in excess of 25 m in diameter. Margins of the three pegmatite types are rarely graded and commonly undisrupted, indicating emplacement occurred while the host was still relatively hot.

The accepted classification on pegmatites is believed to reflect the depth of formation (Cerny 1991). According to Cerny (1991), pegmatites formed in an extensional (anorogenic "A-type") environment evolve from both mantle and crust sources and produce niobium – yttrium – fluorine (NYF) type pegmatite. With extensional decompression, degassing occurs, causing trace ions to complex hydro- and carbo-thermally (Martin et al. 2008). These fluids migrate upwards, metasomatizing the crust into a relatively more alkaline anatectic magma and then crystallizing as syenite or granite (Martin et al. 2008).

Mineralogically and genetically, the pegmatites of the Coldwell complex are NYF-type. Mineral paragenesis in Center One and Three Coldwell rocks indicates three distinct magmatic stages of crystallization and at least one episode of alteration (Fig. 1.5). The first phase of the paragenetic scheme is the initial crystallization stage. The most diverse set of minerals are introduced in the initial stage of crystallization; the most notable being apatite, ilmenite, magnetite, pyrochlore, pyroxene, and zircon. These minerals are commonly euhedral-to-subhedral, surrounded with the main "cumulus" or "framework" crystallization stage (Fig. 1.5A), and account for approximately 5 to 7 vol. % of the rock.

The initial crystallization phase is followed by the main cumulus stage. This stage makes up approximately 85 to 90 vol. % of the rock, all of which is very coarse-grained alkali feldspar. The main crystallization phase forms a framework texture that entrains most of the initially-forming minerals and leaves voids, where late-forming minerals and gases accumulate (Fig. 1.5B).

The later interstitial stage (intercumulous) forms in the voids left behind by the initial- and main-crystallization stages (Fig. 1.5C). The common late-forming minerals include amphibole, biotite, calcite, fluorite, and quartz, and are generally anhedral. The minerals react and mantle previously formed minerals

The Coldwell pegmatites all contain alteration minerals that were introduced at a post magmatic, i.e. subsolidus, stage. There is at least one overprinting hydrothermal/metamorphic event(s) that has affected the Coldwell pegmatites. As shown in Figure 1.5D, this overprint has introduced water-bearing species, fluorine, and carbonate (e.g. chlorite, fluorocarbonates) and modifies textures (e.g. deuteric coarsening).

Five pegmatite occurrences were analyzed in this study. All are saturated syenites, which vary, some more than others, with respect to texture, mineralogy, and petrogenesis. The pegmatites are named on the basis of their occurrence or appearance: the Border Gabbro, Railway, Upper Marathon Shore, Black, and Center Three pegmatites.

1.10 Border Gabbro Pegmatites

The Border Gabbro pegmatites are located at N48 44.034 W086 19.865 on Highway 17 approximately 7 km southeast of the Marathon road turn off. The Border Gabbro pegmatites are peralkaline, representing residua derived from the ferroaugite syenite Center One unit, and emplaced into the main gabbroic unit of Center One. The pegmatites are syenitic in composition, with pale green feldspar, which range in size from 1 to 7 cm, accounting for 90 vol. % of the rock. Black (0.1-0.7 cm), euhedral-to-anhedral, aegirine-to-hedenbergite pyroxenes are intermittently dispersed throughout the unit and account for 5 vol. % of the modal abundance. Black, interstitially-forming, ferro-richterite, katophorite, ferrowinchite, edenite, and ferroedenite amphibole is relatively common and makes up 2 vol. % of the modal abundance. The amphibole crystals are anhedral, have striations parallel to elongation and range in size from < 1 mm to 2 cm. Small (0.1-0.5 cm), black intergrowths of magnetite/ilmenite are commonly concentrated in small 4 cm patches, and represent 1 vol. % of the modal abundance. Interstitial quartz and calcite occur late in the formation of these pegmatites. Modal abundance is

approximately 1 vol. % quartz, 0.25 vol. % calcite. There are also rare small (<0.1 cm) brown tetragonal zircon grains and very rare (only observed once in hand sample) brown euhedral chevkinite grains.
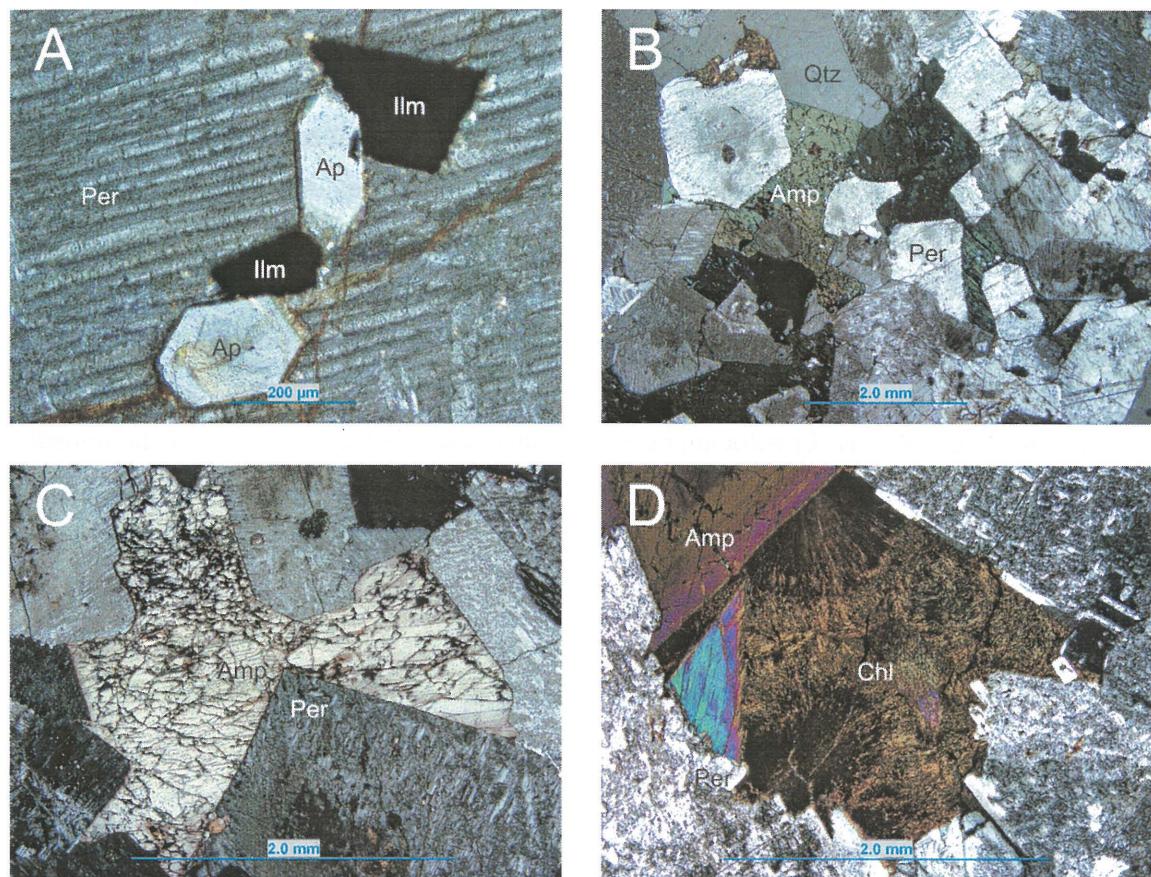
FIGURE 1.5: Cross polarized photomicrographs of the four stages of crystallization. A is initially-forming ilmenite (Ilm) and apatite (Ap) in perthite (Per). B is framework perthite with interstitial amphibole (Amp) and quartz (Qtz). C is interstitial amphibole surrounding perthite. D is secondary chlorite (Chl) surrounded by amphibole and perthite.

Using backscattered electron imagery (BSE) coupled with X-ray spectrometry (EDS), 33 minerals/mineral groups were identified in the Border Gabbro pegmatites. The paragenetic sequence of these minerals/mineral groups is illustrated in Figure 1.6. The initially-crystallizing minerals include thorite, galena, monazite, zirconolite, fergusonite, pyrochlore, allanite, magnetite, rutile, ilmenite, baddeleyite, zircon, chevkinite, titanite, apatite, olivine (fayalite), biotite, and pyroxene. The framework stage is composed entirely of alkali feldspars. The late stage includes amphibole, astrophyllite, barite, galena, chalcopyrite, molybdenite, sphalerite,

pyrite, quartz, fluorite, and calcite. Secondary or hydro-carbothermal minerals include muscovite, chlorite, ilmenite, rutile, quartz, fluorocarbonates and rhapdophane.

1.11 Railway Pegmatites

The Railway pegmatites are located in a railway cut of the Canadian Pacific Railway approximately 1 km east of the end of Pebble Beach Road (N48 46.231 W086 22.782). The pegmatites are thought to intrude Center One ferroaugite syenites, although no contact can be found. The pegmatites are very coarse grained, with most grain sizes ranging from 1 to 12 cm, and black in colour, reflecting the presence of dark feldspars, olivine, pyroxenes and amphiboles. The feldspar texture and composition from the Railway pegmatites are similar to the Border Gabbro feldspars, except for the lack of barium. Feldspars account for 90 vol. % of the modal abundance. Other Railway pegmatite minerals include initial-forming fayalite (3 vol. %), anhedral interstitial ferrorichterite and katophorite amphiboles (3 vol. %), and euhedral-to-subhedral initial-forming hedenbergite pyroxene (2 vol. %). Magnetite/ilmenite grains are relatively small (< 0.5 mm), making up approximately 1 vol. %, and are dispersed throughout the unit. Interstitial sulphides (mainly pyrite and chalcopyrite) are localized into small 1 x 1 cm aggregates. Very minor (0.05 vol. %) quartz is present throughout the unit.

Minerals not included in the macroscopic description, but identified using BSE-imagery and X-ray EDS, are shown in Figure 1.7 and include: thorite, fergusonite, baddeleyite, monazite, zirconolite, zircon, xenotime, pyrochlore, magnetite, ilmenite, titanite, allanite, chevkinite, apatite, and olivine in the initial stage; alkali feldspar in the cumulus stage; biotite, amphibole, astrophyllite, barite, lollingite, galena, chalcopyrite, molybdenite, sphalerite, pyrite, quartz, fluorite, and calcite in the interstitial stage; and rhapdophane, chlorite, ilmenite, quartz and fluorocarbonates in the secondary stage. This accessory mineral assemblage is very similar to the Border Gabbro pegmatites.

1.12 Upper Marathon Shore Pegmatites

The Upper Marathon Shore pegmatites are located on the northern shore of Lake Superior, south of the town of Marathon. The pegmatites intrude the upper series of the Center One ferroaugite syenite. The grain sizes of red alkali feldspars are smaller (0.5-5 cm) than the other units, and account for 85 vol. %. The pegmatites contain diverse (ferrorichterite, taramite, hastingsite, and riebeckite), and considerably more (7 vol. %), amphiboles than in the other pegmatite units. In common with the Border Gabbro and Railway pegmatites, the Upper

Marathon Shore pegmatites contain initial-forming hedenbergite pyroxene and magnetite/ilmenite, each making up 2 and 1 vol. %, respectively. Vugs are common, and lined with late-forming quartz and calcite. Fluorite is also present in minor amounts (0.1 vol. %). Chalcopyrite and pyrite are concentrated into small, usually 3 x 3 cm, aggregates, and make up 0.05 vol. % of the modal abundance.

With the use of BSE-imagery and X-ray EDS, the paragenetic sequence of the Upper Marathon Shore pegmatites (Fig. 1.8) includes: thorite, monazite, galena, pyrochlore, baddeleyite, zircon, xenotime, magnetite, rutile, ilmenite, allanite, apatite, and pyroxene in the initial stages of crystallization; feldspar in the framework stage; amphibole, barite, galena, arsenopyrite, chalcopyrite, molybdenite, sphalerite, pyrite, quartz, fluorite, and calcite in the interstitial stage; and muscovite, chlorite, rutile, ilmenite, quartz, and fluorocarbonates in the alteration stage.

1.13 Black Pegmatites

The Black pegmatites intrude the ferroaugite syenite unit of Center One, at N48 46.709, W086 25.006. The Black pegmatites are syenitic in composition, and contain a significant hedenbergite pyroxene component (10 vol. % of the modal abundance). The hedenbergite is brown/green in colour and generally forms elongate or tabular euhedral crystals. Feldspars are black-to-dark pink in colour and account for 85 vol. % of the modal abundance. Small, black, interstitial amphiboles (ferrorichterite and katophorite) are present, but in low concentrations (0.25 %). Magnetite/ilmenite crystals can get up to 1.5 cm across but are generally between < 1 mm to 0.5 cm. The magnetite/ ilmenite grains make up approximately 0.25 vol. % of the modal abundance.

Using BSE-imagery and X-ray EDS, 23 minerals were identified in the Black pegmatites. Figure 1.9 illustrates the paragenetic sequence and includes thorite, baddeleyite, pyrochlore, zircon, magnetite, ilmenite, biotite, apatite, and pyroxene in the initial stage of crystallization; alkali feldspar (mostly perthitic/cryptoperthitic) in the cumulous stage; biotite, amphibole, astrophyllite, barite, galena, molybdenite, sphalerite, pyrite, quartz, fluorite, and calcite in the interstitial stage; and chlorite, ilmenite, quartz and fluorocarbonate in the secondary stage of crystallization. Monazite forms in either the late-interstitial or secondary phase of crystallization.

1.14 Center Three Pegmatites

Center Three pegmatites were sampled from the syenitic (95 vol. % feldspar) residuum that intrudes the Center Three syenites located 5 km northwest of the Neys turnoff on highway 17. Compared to the other pegmatite units, which may all be from the same source, Center Three pegmatites are from a different source. This is reflected in the pegmatite's composition. Center Three albites consistently contain barium. The pegmatites also contain minor (0.5 vol. %) hastingsite amphibole. In common with all other pegmatite units, Center Three pegmatites contain hedenbergite pyroxene, but in minor amounts (0.1 vol. %). Pyrite is common either highly disseminated or as small (0.2 cm) euhedral crystals. Small magnetite/ilmenite crystals are also present, accounting for approximately 1 vol. % of the modal abundance.

In addition to the macroscopic minerals, BSE-imagery coupled with X-ray EDS identified thorite, baddeleyite, monazite, pyrochlore, zircon, magnetite, ilmenite, allanite, biotite, apatite, and pyroxene in the initial stage; feldspar in the framework stage; pyrochlore, biotite, amphibole, barite, galena, arsenopyrite, molybdenite, sphalerite, pyrite, quartz, fluorite, calcite, and magnetite in the interstitial stage; and muscovite, chlorite, ilmenite, quartz, and fluorocarbonates in the secondary stage (Fig. 1.10).

1.15 Chapter One Summary

The Coldwell alkaline complex is associated with the development of the North America Rift System and was emplaced approximately 1108±1 Ma ago. Emplacement of the Coldwell complex can be generalized into three distinct differentiation trends: Center One saturated alkaline rocks with peralkaline oversaturated residua; Center Two miascitic undersaturated alkali rocks; and Center Three alkaline rocks with oversaturated residua. Coldwell pegmatites are of the NYF-type and occur as patch, vein and localized masses. There have been no detailed studies on the Coldwell pegmatites, as studies to date have been of a reconnaissance character.
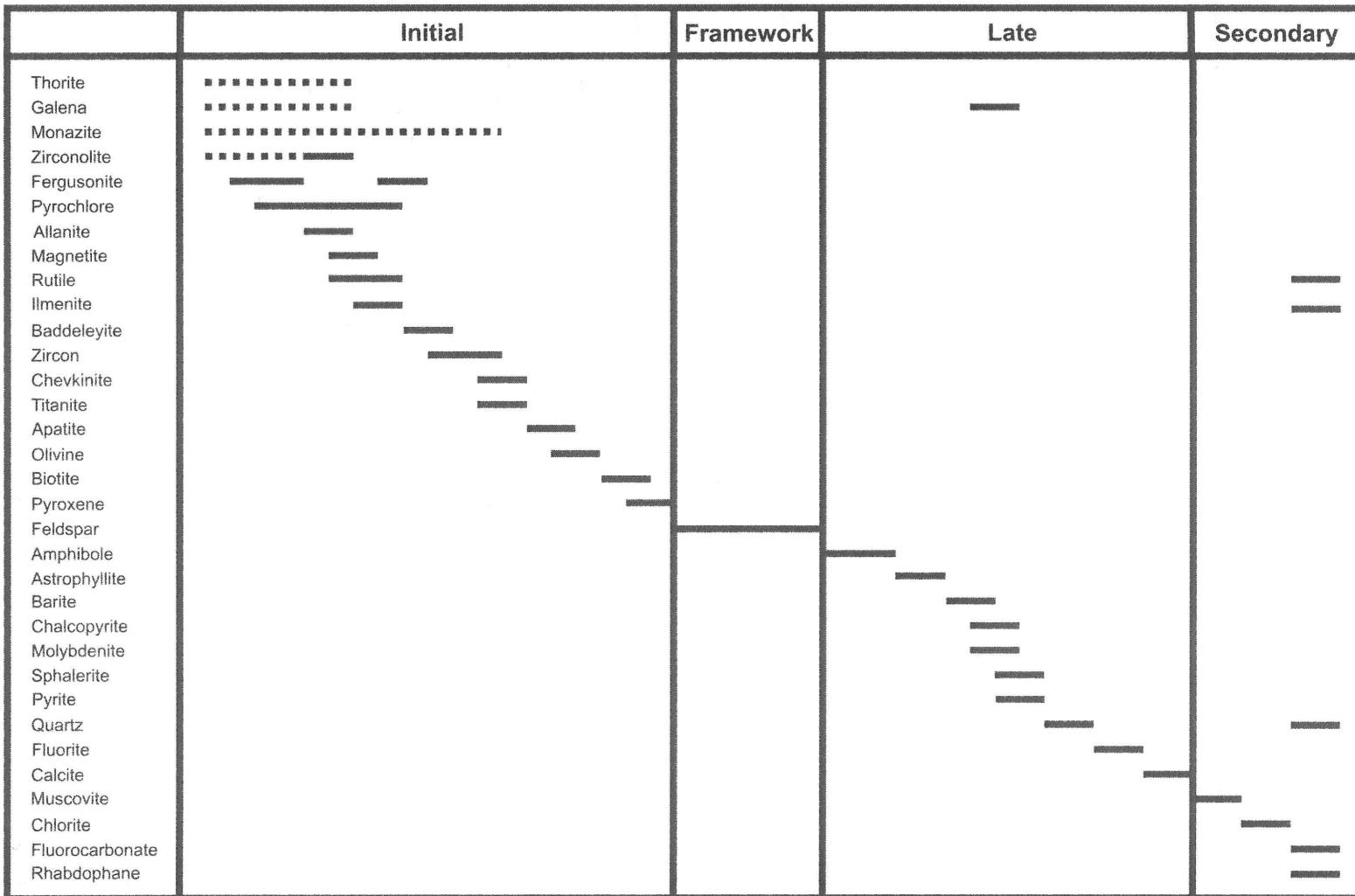
FIGURE 1.6: Paragenetic scheme for the Border Gabbro pegmatites.
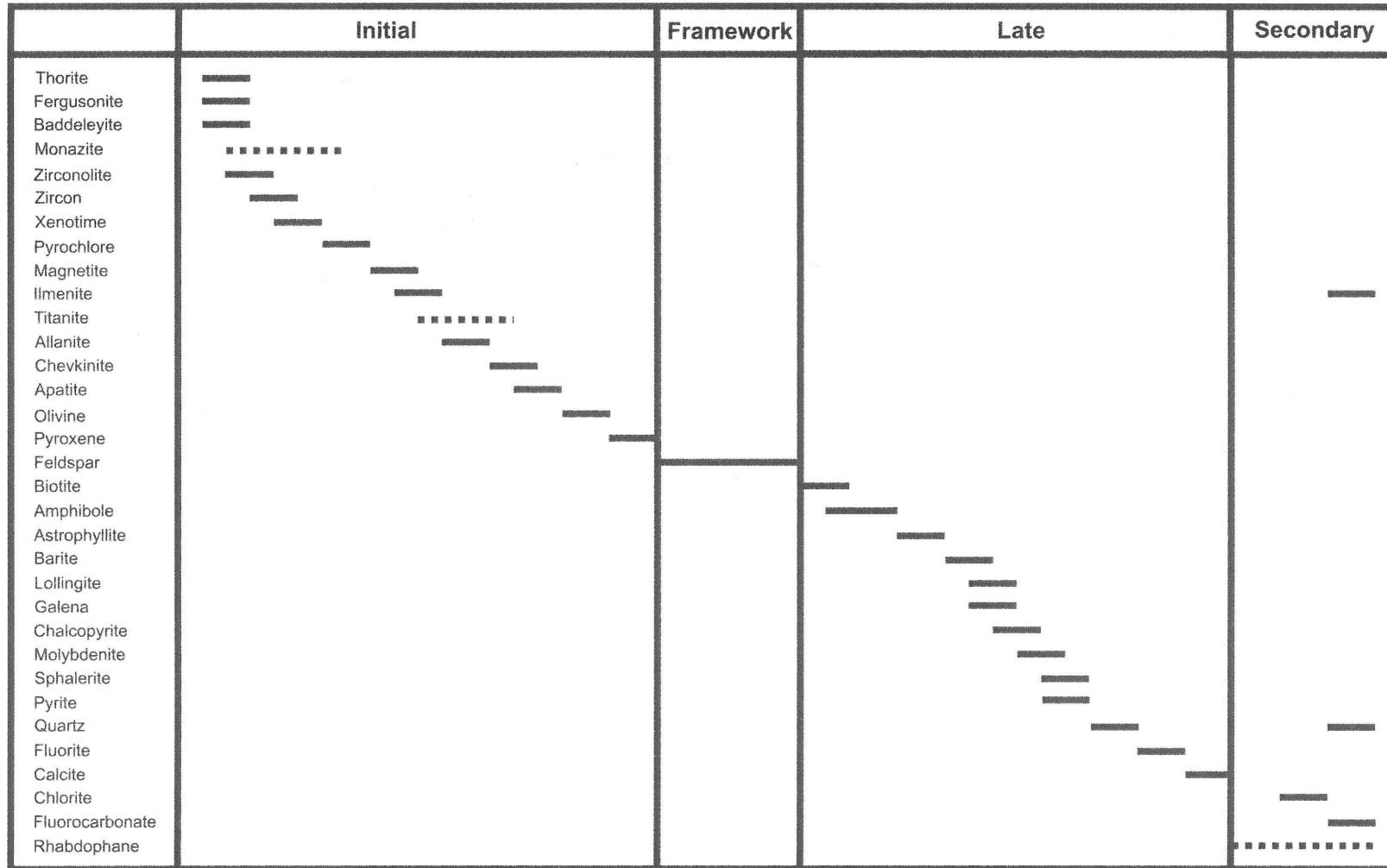
FIGURE 1.7: Paragenetic scheme for the Railway pegmatites.

	Initial	Framework	Late	Secondary
Thorite	▬			
Monazite	▬			
Galena	▬		▬	
Pyrochlore	▬			
Baddeleyite	▬			
Zircon	▬			
Xenotime	▬			
Magnetite	▬			
Rutile	▬			▬
Ilmenite	▬			▬
Allanite	▬			
Apatite	▬			
Pyroxene	▬			
Feldspar		▬		
Amphibole			▬	
Barite			▬	
Arsenopyrite			▬	
Chalcopyrite			▬	
Molybdenite			▬	
Sphalerite			▬	
Pyrite			▬	
Quartz			▬	▬
Fluorite			▬	
Calcite			▬	
Muscovite				▬
Chlorite				▬
Fluorocarbonate				▬
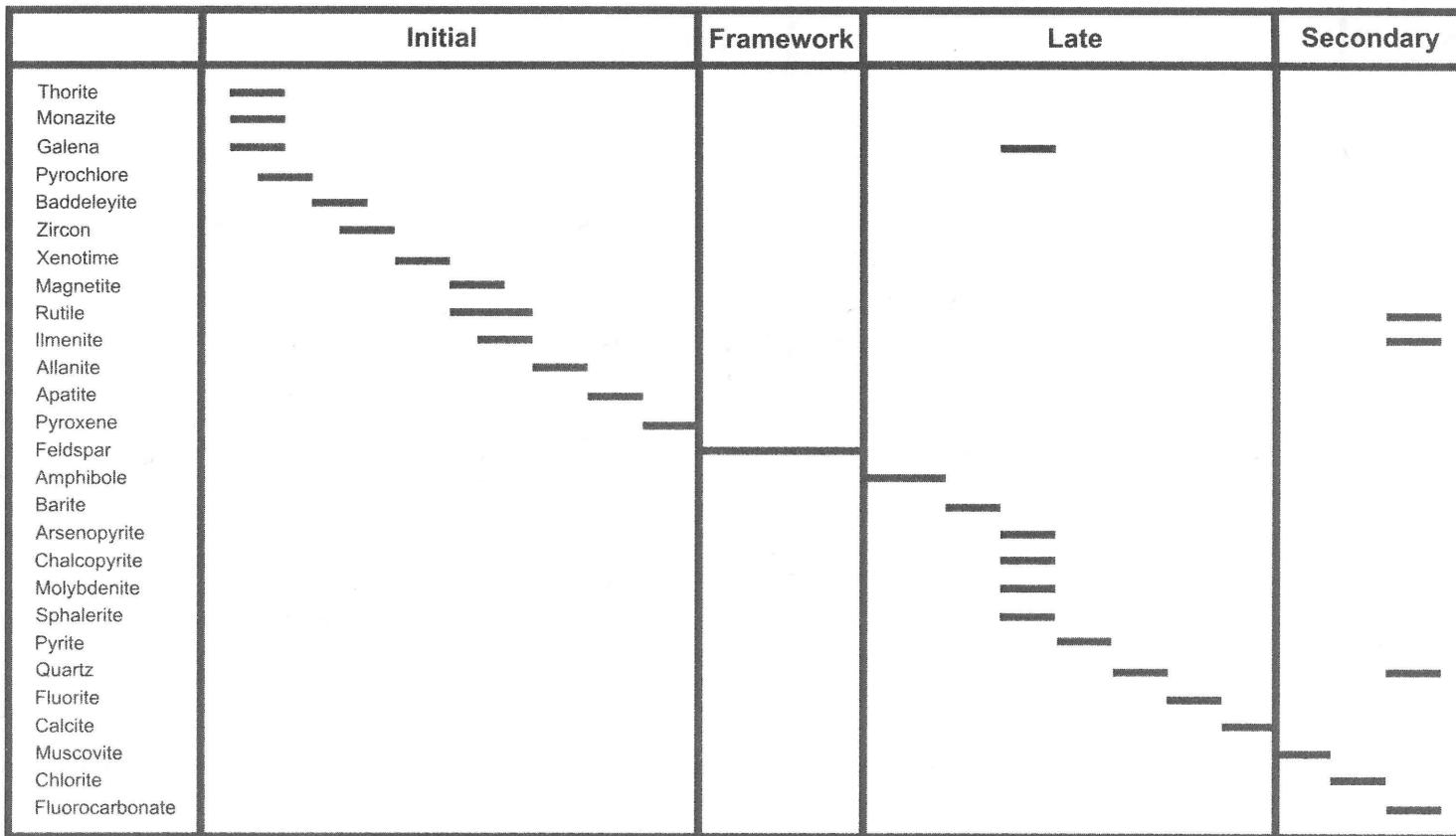
FIGURE 1.8: Paragenetic scheme for the Upper Marathon Shore pegmatites.

	Initial	Framework	Late	Secondary
Thorite	▬			
Baddeleyite	▬			
Pyrochlore	▬			
Zircon	▬			
Magnetite	▬			
Ilmenite	▬			
Biotite	▬		▬	▬
Apatite	▬			
Pyroxene	▬			
Feldspar				
Amphibole			▬	
Astrophyllite			▬	
Barite			▬	
Galena			▬	
Molybdenite			▬	
Sphalerite			▬	
Pyrite			▬	
Quartz			▬	
Fluorite			▬	▬
Calcite			▬	
Monazite			▪ ▪ ▪	
Chlorite			▬	
Fluorocarbonate				▬
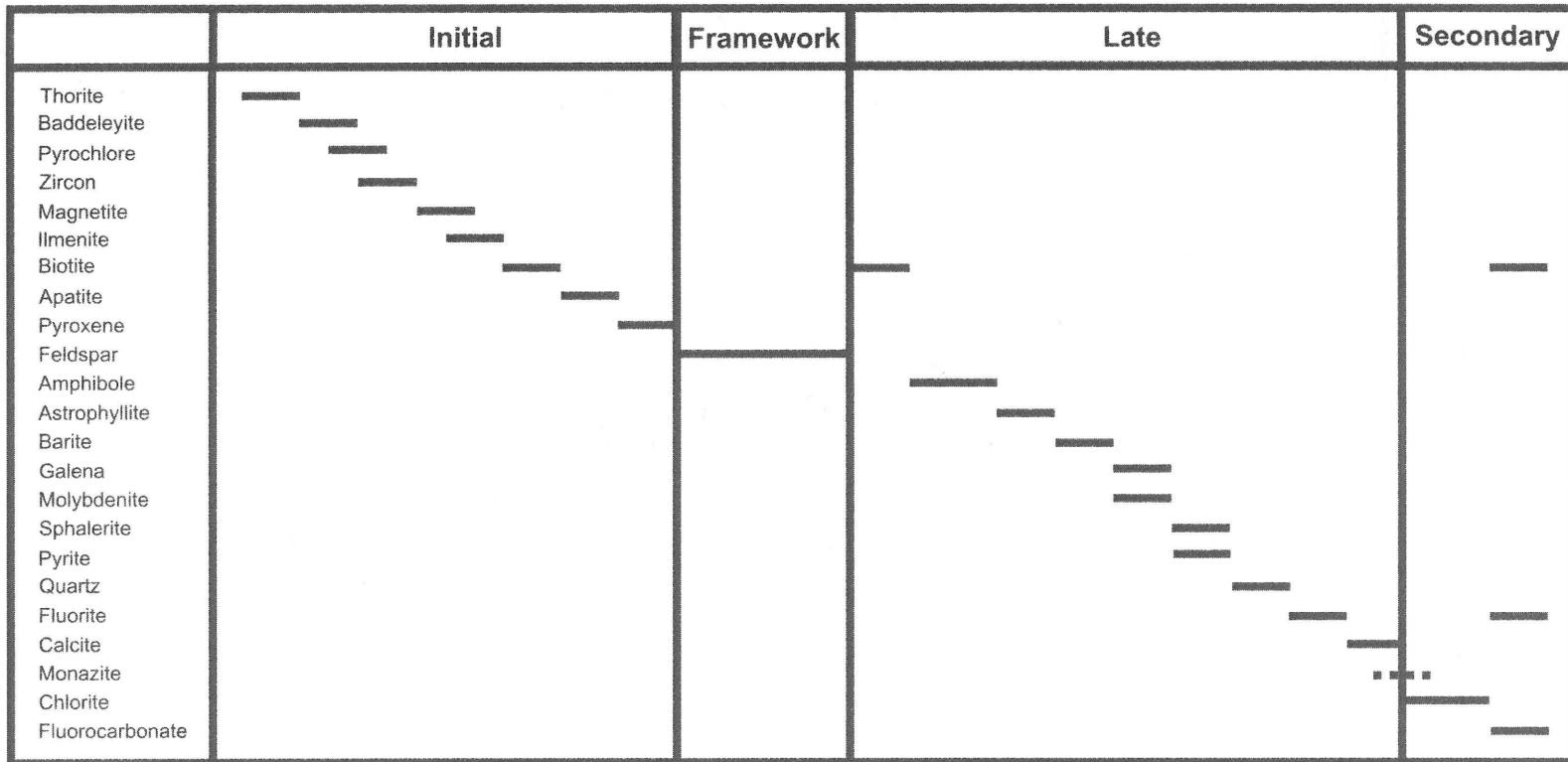
FIGURE 1.9: Paragenetic scheme for the Black pegmatites.
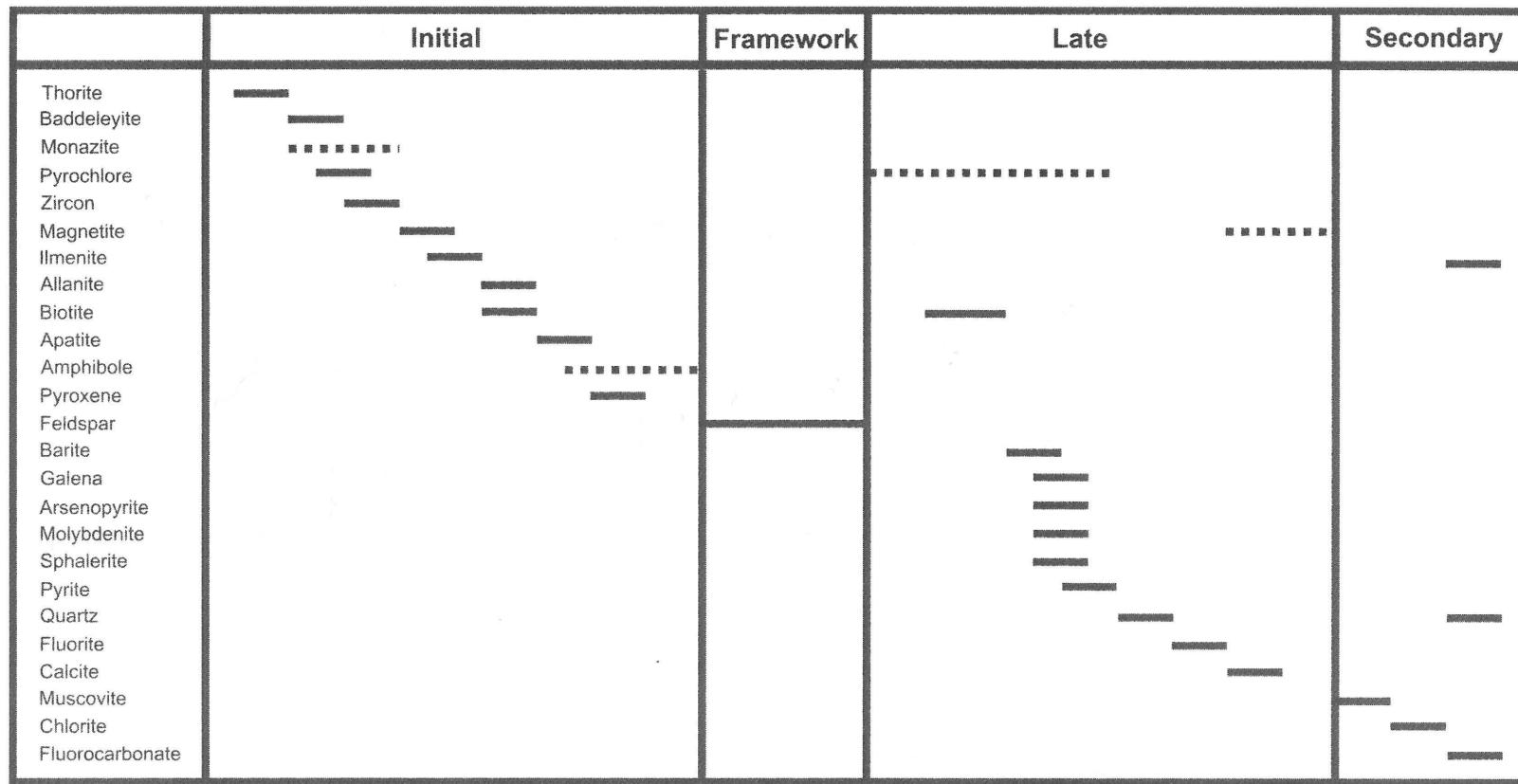
FIGURE 1.10: Paragenetic scheme for the Center Three pegmatites.

CHAPTER TWO
ANALYTICAL TECHNIQUES

2.1 Introduction

Two analytical techniques were used to characterize the mineralogy and petrogenesis of the Coldwell complex: standard optical microscopy using thin-sections; and backscattered electron petrography coupled with energy dispersive spectroscopy.

2.2 Back Scattered Electron Petrography and Energy Dispersive X-Ray Analysis

In addition to standard optical microscopy, the primary analytical tool used to identify and analyze samples was backscattered electron imagery and analytical X-ray spectrometry at Lakehead University. Data were obtained using a JEOL 5900, low-vacuum scanning electron microscope (LV-SEM) with an attached LINK ISIS 300 analytical system with incorporated Super ATW Light Element Detector (133 eV FwHm MnK) and energy dispersive X-ray spectrometer (EDS). Samples were thin-sectioned, polished and carbon coated in preparation for SEM-EDS analysis.

The EDS system identifies elemental compositions by bombarding the sample with electrons. Above a critical voltage, in this case 20 kV with a beam current set to 0.475 nA, the electrons in the sample become excited and the energy difference emitted upon returning to the unexcited state is converted into characteristic X-rays. The spectrometer, or detector, takes incoming characteristic X-rays and creates a voltage signal of proportional size. The spectrometer must always be under a vacuum so the detecting medium, in this case a lithium-drifted silicon crystal (Si[Li]) detector, retains its charge-free region. A beryllium window is used as a barrier to maintain the vacuum. The beryllium window, although maintaining the vacuum barrier, also absorbs low energy X-rays. The characteristic X-rays of the light elements (Be, Li, C) are either not detected or detected, but produce inaccurate data. Once the X-rays are converted into a voltage signal, the pulse processor measures the energy of the incoming X-ray and gives a digital readout of that value. The pulse processor in this study was energy calibrated against a nickel standard. The calibration input rates for a 50 second acquisition gave 4,800 to 5,100 cps.

X-ray spectra were acquired for 50-300 seconds, depending on the quality of acquisition and nature of the target, i.e. elements, structure, stability, etc. LINK ISIS SEMQUANT

quantitative software was used to process the spectra, and reduced using a full ZAF algorithm (three iterations). The standards used are listed in Table 2.1.

TABLE 2.1: Standards used in the SEM-EDS analyses.

Standard Name	ID	Element(s) Used
Apatite	1926 665	P
Barite	-	Ba, S
Cerium Fluoride	C-1215	Ce
Cerium Phosphate	-	Ce, P
Corundum	-	Al
Cuprite	-	Cu
Galena	-	Pb
Hafnium metal	00139	Hf
Ilmenite	-	Fe, Ti
Iron Metal	-	Fe
Lanthanum Fluoride	L-1114	La
Lanthanum Phosphate		La
Neodymium Fluoride	N-1010	Nd
Neodymium Phosphate	-	Nd
Niobium Metal	00240	Nb
Orthoclase	-	K
Praseodymium Fluoride	P-1074	Pr
Praseodymium Phosphate	-	Pr
Pyroxene Glass	DJ35	Si, Na, Mg, Al
Samarium Phosphate	-	Sm
Sphalerite	-	Zn
Strontium Titanate	-	Sr
Tantalum Metal	00448	Ta
Thorium Metal	-	Th
Thorium Silicate	-	Th, Si
Tungsten Metal	-	W
Uranium Metal	K5451	U
Wollastonite	68773	Ca
Yttrium Fluoride	-	Y, F
Yttrium Phosphate	-	Y
Zirconium Metal	-	Zr

Iron was standardized in the ferrous state. As such, in most cases recalculation to ferric iron was undertaken on a stoichiometric basis, as outlined by Droop (1987). For structures with site vacancies, the Fe^{2+}/Fe^{3+} recalculation was preformed independently. Specific procedures are outlined below. Unless otherwise stated, FeO* indicates that all iron was left in the ferrous state.

CHAPTER THREE
ROCK-FORMING AND MINOR MINERALIZATION

3.1 Introduction

Rock-forming and minor minerals of the Coldwell pegmatites are limited to 10 minerals/mineral groups. The major rock-forming minerals are feldspar, pyroxene, amphibole, and olivine. Minor minerals include: calcite, quartz, fluorite, biotite, chlorite, muscovite, calcite, and quartz.

The description of minerals in this chapter follows their relative abundance. Structural and compositional parameters are stressed, as they are used in modeling the petrogenesis.

3.2 Feldspar Group

In Coldwell pegmatites, subsolvus alkali feldspars form the main cumulus phase. The crystals precipitate euhedral-to-anhedral framework-type textures, with perthite and cryptoperthite intercrystalline textures. Typical perthite subtextures include braid, patch and film perthites. Braid perthites, as the name implies, are characterized by elongate interwoven microtextures, which commonly form in the body of the feldspar crystals (Fig. 3.1A). Deuterically coarsened perthite, termed "catastrophically coarsened" perthite by Parsons (1978), occur throughout the Coldwell units, and are distinguished by randomly oriented coarse "patches" of subgrains (Fig. 3.1B) or long parallel "film" subgrains that commonly form about crystal boundaries and fractures (Fig. 3.1C and D).

According to Worden et al. (1990) and Parsons and Lee (2005), deuterically coarsened perthites form when magmatic-derived waters (deuteric alteration), or waters introduced subsequently (hydrothermal alteration), move the feldspar solvus to a relatively "strain-free" position by internally rearranging ions. In both cases, water, which migrates through micropores that commonly develop between subgrain boundaries, fractures and inclusions, is the mechanism behind deuterically coarsened perthites.

In addition to perthitic textures, cryptoperthitic textures are also present. Under cross-polarized settings in optical microscopy, the cryptoperthitic crystals undulate when rotated. With SEM/EDS techniques, cryptoperthites are identified by their composition—with potassium and sodium compositions within the miscibility gap—and faint hummocky appearance.
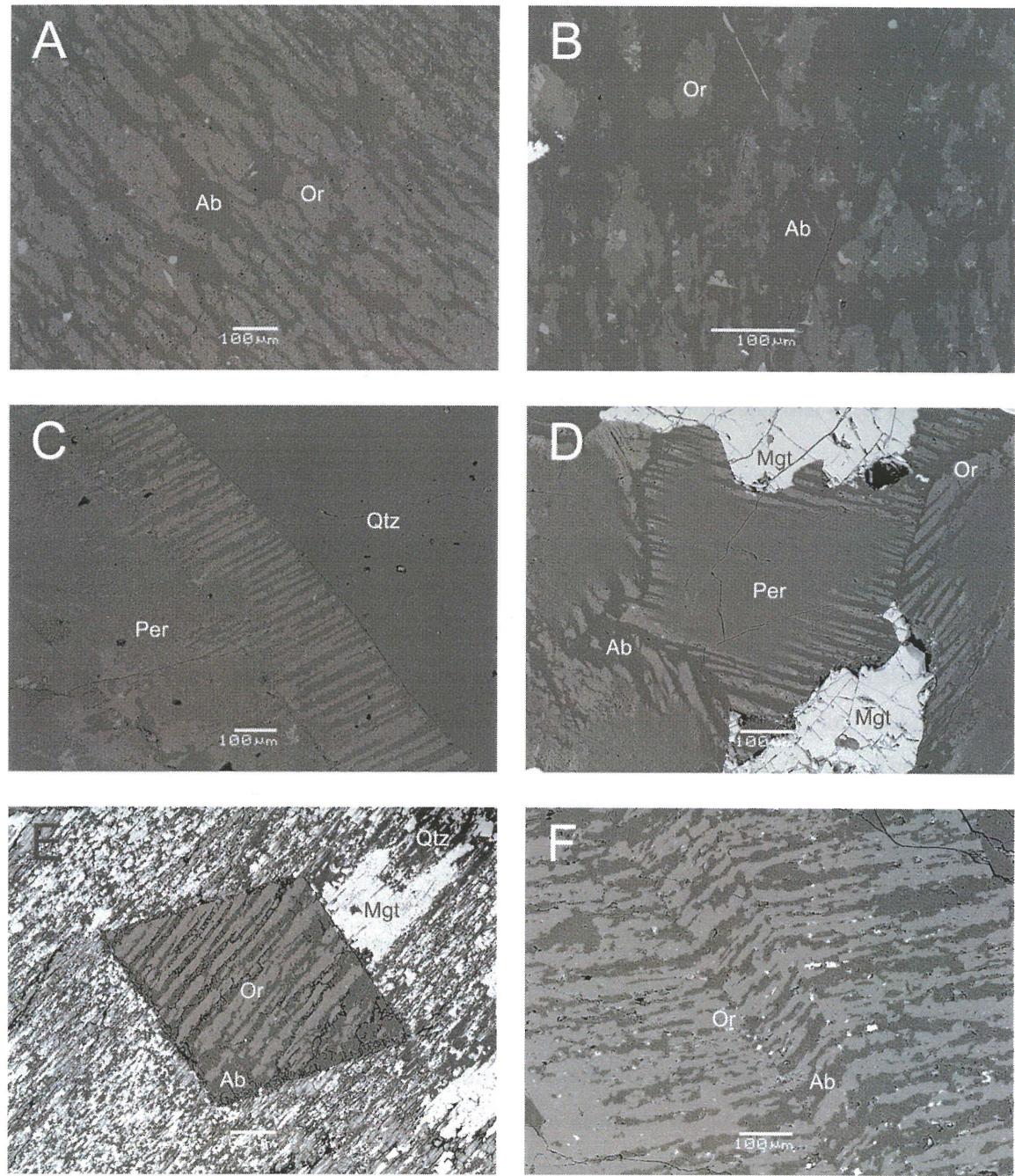
FIGURE 3.1: BSE-images of albite (Ab), orthoclase (Or) and cryptoperthites (Per). A is braid perthite. B is patch perthite. C is film perthite adjacent to quartz (Qtz) that grades into cryptoperthite. D is deuterically coarsened cryptoperthite and magnetite (Mgt). D is euhedral albite and orthoclase grain surrounded by magnetite and quartz. E is a euhedral perthite grain hosted by magnetite and quartz. F is film perthite that has undergone brittle deformation.

Feldspar compositions are generally similar throughout the units (Table 3.1 and Appendix II.I). No compositional change is observed between differing textures. The extent of solid solution between alkali and calcic feldspar is shown in the orthoclase-albite-anorthite ternary plots in Figures 3.2 and 3.3. Minor iron, which is found in both albite and orthoclase, and, to a lesser extent, calcium, which is found in albite, are present in Coldwell feldspars.

The Border Gabbro pegmatite feldspars account for 90 vol. % of the rock and are macroscopically pale green in colour. Green feldspar, specifically green orthoclase, is termed amazonitic. Amazonitic feldspar is restricted to NYF-granitic pegmatites and metamorphosed massive sulphide-hosted granitic pegmatites (Martin et al 2008). According to Hofmeister and Rossman (1985), the green colour is a direct result of trace lead and water that enter the structure by substituting for potassium:

$$Pb^{2+} + H_2O \rightarrow 2K^+$$ Hofmeister and Rossman (1985)

Lead is below the detection levels of the EDS system used, but trace amounts is inferred. Low amounts (0-1.07 wt. % Fe_2O_3) of iron, barium in one albite and three orthoclase analyses, and calcium in three of the albite samples are present in Border Gabbro feldspars. Feldspar textures range from coherent, to perthitic, to cryptoperthitic, with a maximum grain size of 7 cm.

Feldspars from the Railway pegmatites make up 90 vol. % of the rock, and are macroscopically black in colour. Feldspar grain sizes vary from 1 to 12 cm. These albites contain minor calcium (0-0.9 wt. % CaO). Iron in albite and orthoclase range from zero to 0.8 wt. % Fe_2O_3.

Red alkali feldspar forms the main cumulus phase (85 vol. %) in the Upper Marathon Shore pegmatites. Grain sizes range from 0.5 to 5 cm. The compositions of Upper Marathon Shore feldspars differ from others, with calcium detected in only one of the albites. They have the least amount of iron (0-0.4 wt. % Fe_2O_3).

In common with the Upper Marathon Shore pegmatites, feldspar from the Center Three syenites are macroscopically red in colour. Feldspar accounts for 95 vol. % of the rock. Grain sizes range from 0.5 to 4 cm. Iron is present in all analyses, and ranges from 0.07 to 0.25 wt. % Fe_2O_3. When detected, calcium in albites range upwards to 1.10 wt. % CaO.

Feldspar in the Coldwell pegmatites can be described by the three endmembers: potassium feldspar ($KAlSi_3O_8$), albite ($NaAlSi_3O_8$) and anorthite ($CaAl_2Si_2O_8$) (Figs. 3.2 and 3.3). Most ions in solid solution are accommodated by means of the simple substitutions:
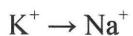
$$K^+ \rightarrow Na^+$$
$$Fe^{3+} \rightarrow Al^{3+}$$ Gaite and Michoulier (1970)

TABLE 3.1: Representative compositions of albite-orthoclase pairs.

	Border Gabbro[1]	Border Gabbro[2]	Railway[3]	Railway[4]	Upper Marathon Shore[5]	Upper Marathon Shore[6]	Center Three[7]	Center Three[8]	Thor Lake[9]	Thor Lake[10]
Na_2O	11.58	0.63	11.02	0.32	11.83	0.68	10.85	0.95	11.67	0.53
Al_2O_3	20.01	18.75	20.02	19.22	19.74	18.57	20.20	18.62	18.69	17.39
SiO_2	67.44	64.38	66.55	63.81	68.47	65.13	67.85	64.62	69.26	65.23
K_2O	0.40	15.43	0.21	16.03	0.11	15.91	0.22	15.34	0.10	16.47
CaO	0.48	-	0.79	-	-	-	0.55	0.20	-	0.71
Fe_2O_3	-	-	-	0.12	0.17	0.20	-	0.22	0.34	-
BaO	-	0.77	-	-	-		-	-	-	-
Total	**99.91**	**99.97**	**99.33**	**99.65**	**100.48**	**100.49**	**99.68**	**99.74**	**100.06**	**100.33**

[1] Border Gabbro pegmatite (4 analyses of sample MAS002) from the Coldwell complex.
[2] Border Gabbro pegmatite (6 analyses of sample MAS002) from the Coldwell complex.
[3] Railway pegmatite (4 analyses of sample MAS016) from the Coldwell complex.
[4] Railway pegmatite (5 analyses of sample MAS016) from the Coldwell complex.
[5] Upper Marathon Shore pegmatite (4 analyses of sample MAS019) from the Coldwell complex.
[6] Upper Marathon Shore pegmatite (6 analyses of sample MAS019) from the Coldwell complex.
[7] Center Three pegmatite (6 analyses of sample MAS035) from the Coldwell complex.
[8] Center Three pegmatite (6 analyses of sample MAS035) from the Coldwell complex.
[9] Altered/brecciated syenite (sample PT47) from the Lake Zone, Thor Lake, N.W.T., Canada Pinckston and Smith 1995).
[10] Altered/brecciated syenite (sample PT49) from the Lake Zone, Thor Lake, N.W.T., Canada Pinckston and Smith 1995).
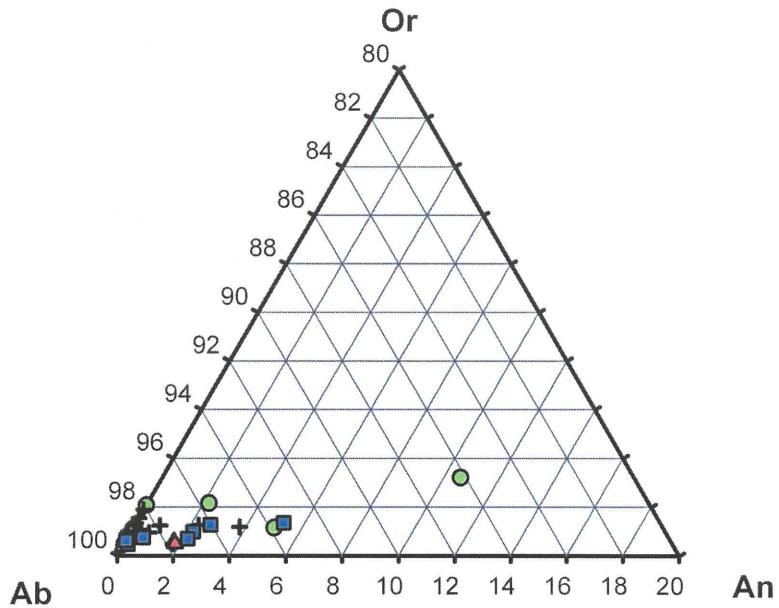
FIGURE 3.2: Albite compositions plotted in the orthoclase (Or) – Albite (Ab) – anorthite (An) ternary system (mol. %). Green circles, black crosses, red triangles, black diamonds, and blue squares are the Border Gabbro, Railway, Upper Marathon Shore, Black, and Center Three pegmatites, respectively.
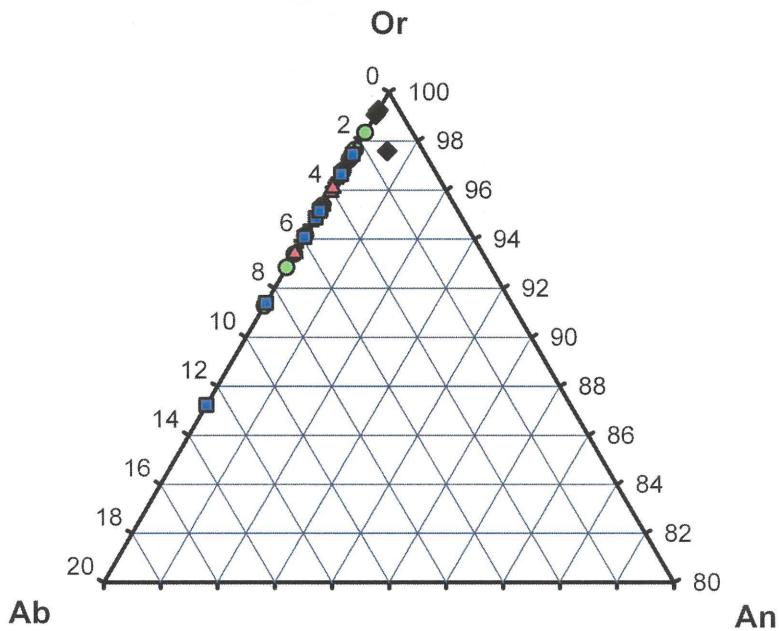
FIGURE 3.3: Potassium feldspar compositions plotted in the orthoclase (Or) – Albite (Ab) – anorthite (An) ternary system (mol. %). Green circles, black crosses, red triangles, black diamonds, and blue squares are the Border Gabbro, Railway, Upper Marathon Shore, Black, and Center Three pegmatites, respectively.

Substitution of other ions, mainly barium and calcium, enter the feldspar structure by A- and B-site coupled substitution:

$$(Ba,Ca)^{2+} + Al^{3+} \rightarrow (Na,K)^{+} + Si^{4+}$$
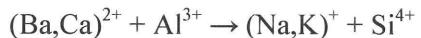
Smith and Brown (1988); Deer et al. (2001)

It has been shown by Yund (1984) and many others (Brown et al. 1983; Brown and Parsons 1984a,b; Waldron and Parsons 1992) that alkali feldspar exsolution textures are a function of cooling rate, deformational history and bulk composition. According to Brown et al. (1983) and Brown and Parsons (1984a,b), feldspar with compositions $Ab_{60}Or_{40}$ form braid-type perthites and feldspar with $Ab_{30}Or_{70} - Ab_{10}Or_{90}$ form film-type textures.

In general, the compositional range of $Ab_{85}Or_{15} - Ab_{15}Or_{85}$ form cryptoperthitic feldspar when exsolved (Deer et al. 2001). Cryptoperthitic feldspars develop in conjunction with crystallographic orientation and morphology, and are controlled by coherency strain (Willaime and Brown 1974). It has been shown by Brown et al. (1983) that cryptoperthitic feldspar results from an early cooling regime.

The bulk of perthites developing in the subsolidus, i.e. deuterically coarsened perthites, are film-type, indicating that initial cryptoperthitic textured compositions were closer to the $Ab_{30}Or_{70} - Ab_{10}Or_{90}$ compositional range.

3.3 Pyroxene Group

In Coldwell pegmatites, the pyroxene group minerals ($M2M1T_2O_6$) form in the initial stage of crystallization (Figs. 3.4 and 3.5). Pyroxene is euhedral-to-anhedral, enclosed by feldspar and associated with amphibole, apatite, ilmenite, magnetite, and olivine. Replacement of pyroxene by amphibole is common, and occurs as mantles along pyroxene grain boundaries. The pyroxenes have a green-to-green/brown pleochroism (Fig. 3.4).

Pyroxenes in Coldwell pegmatites are classified using the CNMMN nomenclature scheme (Morimoto et al. 1989). Figure 3.6 shows compositional variation in terms of three endmember components: hedenbergite ($CaFe^{2+}Si_2O_6$); diopside ($CaMgSi_2O_6$); and aegirine ($NaFe^{3+}Si_2O_6$); with aegirine and hedenbergite being the dominant species. Minor Al_2O_3, MnO, and TiO_2, represent the endmembers $CaAl_2SiO_6$, $CaTiAl_2O_6$, and $CaMnSi_2O_6$, respectively (Tables 3.2 and 3.3 and Appendix II.II). Unlike other A-type saturated pegmatites, e.g. Thor Lake, Coldwell pyroxenes do not contain any detectable zirconium.
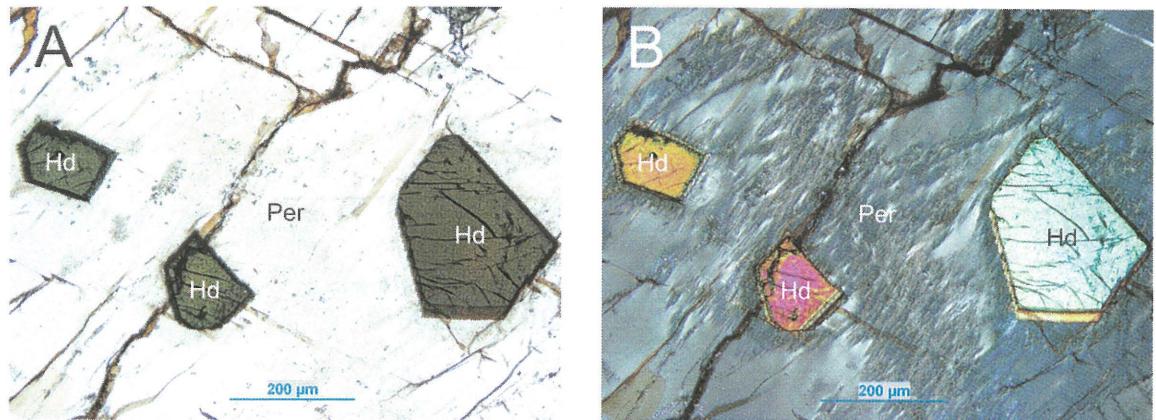
FIGURE 3.4: Photomicrographs of hedenbergite (Hd) and apatite (Ap) surrounded by perthite (Per), plane- (A) and cross-polarized (B) light.
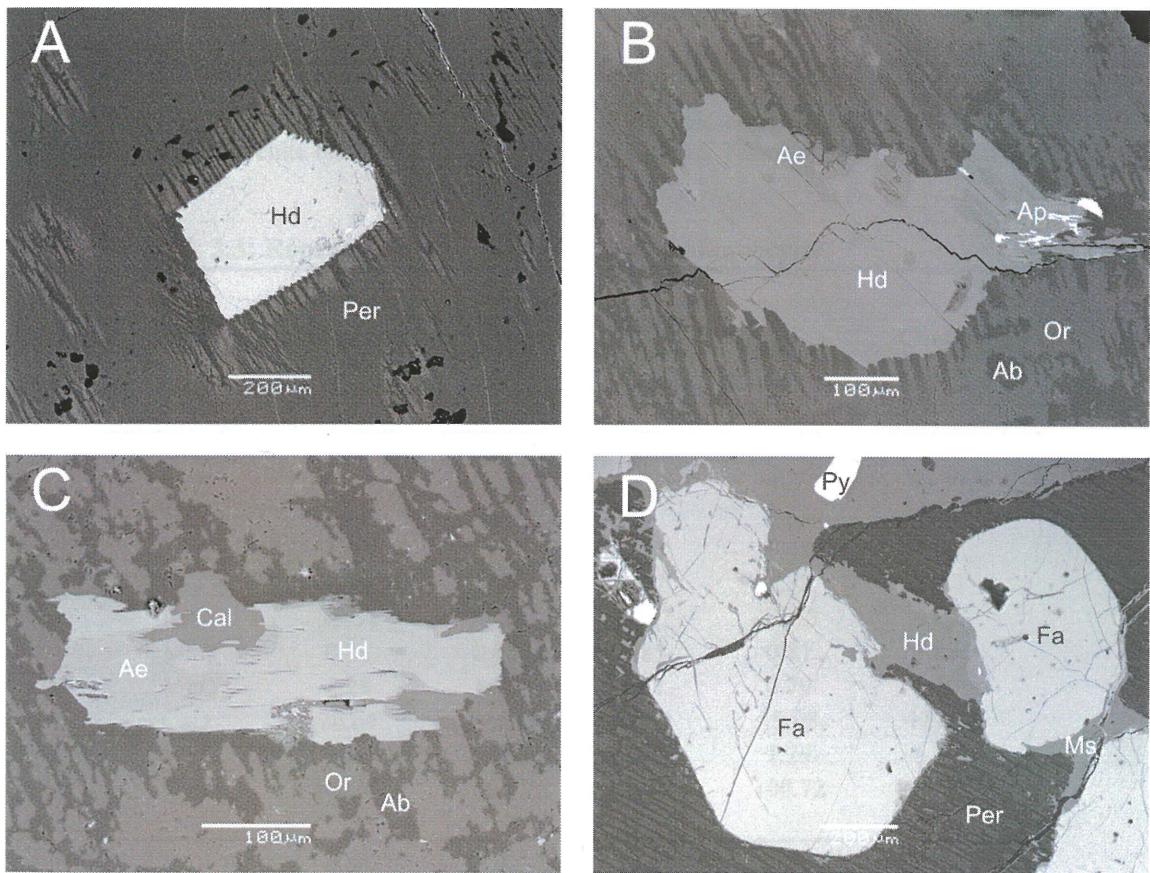
FIGURE 3.5: BSE-images of hedenbergite (Hd) and aegirine (Ae). A is a pyroxene in perthite (per). B is aegirine, hedenbergite and apatite (Ap) hosted by perthitic feldspar (Ab and Or). C is hedenbergite, Ca-Fe-amphibole and calcite (Cal) hosted by perthitic feldspar. D is hedenbergite intergrown with fayalite (Fa) and hosted by perthite (Per) and muscovite (Ms).

TABLE 3.2: Representative compositions of aegirine.

	Border Gabbro[1]	Thor Lake[2]
Na_2O	6.52	13.09
MgO	0.57	-
Al_2O_3	0.53	1.21
SiO_2	52.71	53.27
K_2O	0.15	-
CaO	0.15	1.36
TiO_2	0.34	-
MnO	0.15	0.11
FeO	22.61	-
Fe_2O_3	16.8	30.79
ZrO_2	-	0.73
Total	**100.54**	**100.59**

[1] Border gabbro pegmatite (5 analyses of MAS006) from the Coldwell complex.
[2] Altered/brecciated syenite (sample PT50) from the Lake Zone, Thor Lake, N.W.T., Canada (Pinckston and Smith 1995).

TABLE 3.3: Representative compositions of hedenbergite.

	Border Gabbro[1]	Railway[2]	Upper Marathon Shore[3]	Black[4]	Center Three[5]
SiO_2	48.21	48.23	50.25	48.76	50.39
TiO_2	0.70	0.60	-	0.55	0.18
Al_2O_3	1.03	0.55	1.25	0.48	1.04
Fe_2O_3	1.19	2.06	4.97	3.32	16.41
FeO	25.31	26.33	16.22	25.73	9.62
MnO	0.96	0.96	0.85	0.81	1.83
MgO	2.28	1.00	6.31	0.70	2.10
CaO	20.64	19.63	19.72	19.08	12.01
Na_2O	0.46	0.80	1.93	1.29	6.37
Total	**100.81**	**100.17**	**100.50**	**100.72**	**99.95**

[1] Border gabbro pegmatite (4 analyses of sample MAS001) from the Coldwell complex.
[2] Railway pegmatite (6 analyses of sample MAS016) from the Coldwell complex.
[3] Upper Marathon Shore pegmatite (2 analyses of sample MAS022) from the Coldwell complex.
[4] Black pegmatite (4 analyses of sample MAS021) from the Coldwell complex.
[5] Center Three pegmatite (4 analyses of sample MAS033) from the Coldwell complex.
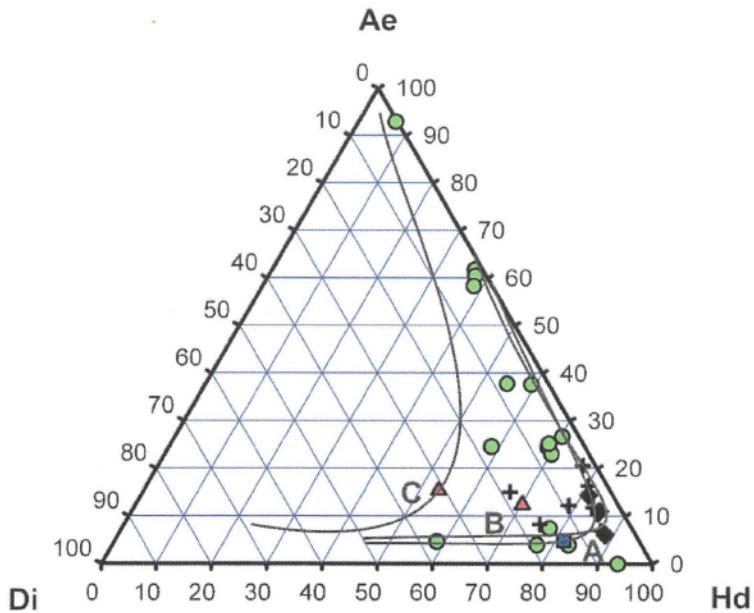
FIGURE 3.6: Aegirine (Ae) – diopside (Di) – hedenbergite (Hd) ternary plot. Green circles, Black crosses, red triangles, black diamonds, and blue squares are the Border Gabbro, Railway, Upper Marathon Shore, Black, and Center Three pegmatites, respectively. A is the Coldwell ferroaugite syenite trend (Mitchell and Platt 1978). B is the Ilimaussaq, Greenland trend (Larsen 1976). C is the South Oôroq, Greenland trend (Stephenson 1972).

The Border Gabbro pegmatite is the only unit containing aegirine and the pyroxenes form a complete compositional trend with hedenbergite (Fig. 3.6). From core to rim, magnesium content decreases (up to 8.29 wt % MgO) in some of the larger crystals. Pyroxenes from Border Gabbro pegmatites are commonly mantled by amphibole and/or chlorite.

Railway pyroxene analyses fall into the hedenbergite compositional field. The pyroxenes form in the initial stage of crystallization, and are commonly associated with apatite, magnetite, muscovite, and especially olivine (Fig. 3.5D).

Pyroxene in the Upper Marathon Shore pegmatite is present in only one of the four samples investigated. In these samples, pyroxene falls into the hedenbergite compositional field with magnesium ranging from 2.85 to 5.31 wt. % MgO.

The Black pegmatites contain hedenbergite that is commonly associated with amphibole and chlorite. Compositions have moderate manganese and magnesium (0.79-0.93 wt. % MnO and 0.73-0.94 wt. % MgO), and are poor (0.70-1.75 wt. % Na_2O) in sodium.

Hedenbergite pyroxene is present in two of the Center Three samples, and is mantled by amphibole. Pyroxenes from this unit contain higher than average manganese (1.80 and 1.83 wt.

% MnO), and magnesium (2.10 and 2.46 wt. % MgO) and moderate amounts of sodium (4.46 and 6.37 wt. % Na_2O).

Pyroxenes from other A- and S-type intrusives are similar in composition to Coldwell pyroxenes. Apart from minor amounts of zirconium, aegirine from the altered/brecciated syenite of Thor Lake, Canada is similar to that of the Border Gabbro pegmatite (Table 3.2). Zirconium in the Thor Lake aegirines may indicate that its rocks are slightly more evolved than Coldwell rock aegirines. The Mg-rich hedenbergite-to-hedenbergite-to-aegirine compositional trend of Coldwell pyroxenes (Fig. 3.6) is similar to the fractionation trends in Center One ferroaugite syenites (Mitchell and Platt 1978), Ilimaussaq (Larsen 1976) and South Oôroq (Stephenson 1972), and represents selective fractionation of magnesium and calcium.

Pyroxene group minerals are inosilicates, where two of the four oxygens are shared (Si : O = 1 : 3), thereby forming chain linked SiO_4 tetrahedra. In the Coldwell pegmatites, pyroxene compositions can be expressed by the general formula $M2M1T_2O_6$, where M2 can be any of Na^+, Ca^{2+}, K^+, Mn^{2+}, Fe^{2+}, Mg^{2+}; M1 denotes Mn^{2+}, Fe^{2+}, Mg^{2+}, Fe^{3+}, Al^{3+}, and Ti^{4+}; and T represents Si^{4+}, Fe^{3+} and Al^{3+} in the tetrahedral chain site (Klein 2002). The range of compositions present in Coldwell pyroxenes results from multiple substitution mechanisms, and include simple substitution, coupled substitution into one structural site, and coupled substitution between two or more structural sites:

$$Si^{4+} \rightarrow T^{4+}$$
$$(Mg,Fe,Ca,Mn)^{2+} \rightarrow (M1,M2)^{2+}$$
$$Ti^{4+} + \square \rightarrow 2(M1,M2)^{2+}$$
$$(Na,K)^+ + (Fe,Al)^{3+} \rightarrow (M1,M2)^+ + (M1,M2,T)^{3+}$$
$$(Na,K)^+ + Ti^{4+} + (Fe,Al)^{3+} \rightarrow (M1,M2)^{1+} + (M1,M2)^{4+} + (M1,M2,T)^{3+}$$
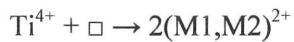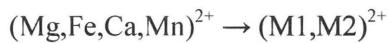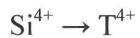
All Fe^{3+} is calculated from stoichiometry. There is a positive correlation ($r^2 = 0.985$) between mono- plus tri-valent ions and divalent ions (Fig. 3.7), indicating the Fe^{2+}/Fe^{3+} recalculation used is suitable for Coldwell pegmatites.

3.4 Amphibole Group

Amphiboles are present in all Coldwell pegmatites. In plane polarized light, the pleochroism ranges, depending on composition, from brown-to-dark brown, brown-to-green, green-to-dark green, or green-to-blue green (Fig. 3.8). All species of amphibole alter to chlorite, with some examples shown in Figure 3.9A and B. The amphiboles form in the initial and interstitial stages of crystallization. The initial-forming amphiboles are rare, subhedral-to-

anhedral, and adopt monoclinic 2/m prisms, as shown in Figure 3.9B. These amphiboles fall into the hastingsite compositional field, and only occur in the Center Three pegmatites. The initially formed amphiboles are associated with magnetite, ilmenite and rutile (Fig. 3.9E). Interstitial amphiboles are generally anhedral, and are associated with biotite, pyroxene, quartz and calcite.
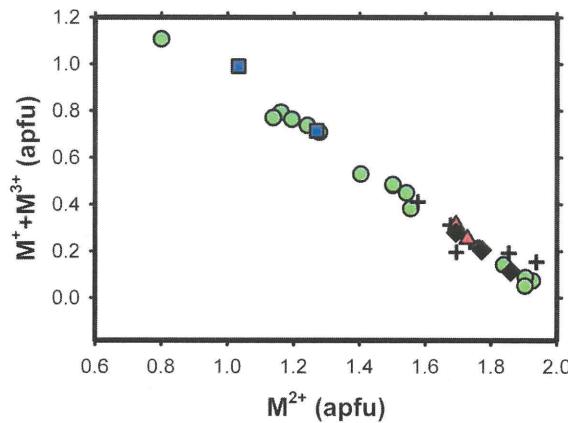
FIGURE 3.7: Pyroxene M^{2+} / $(M^+ + M^{3+})$ (apfu) binary diagram. $R^2 = 0.985$. Green circles, black crosses, red triangles, black diamonds, and blue squares are the Border Gabbro, Railway, Upper Marathon Shore, Black, and Center Three pegmatites.

As compositions of amphibole in Coldwell pegmatites vary significantly, the nomenclature scheme proposed by Leake et al. (1977; 2003) is used to identify the different species. Coldwell amphiboles fall in the monoclinic calcic, sodic-calcic and sodic amphibole compositional fields, as shown in Figures 3.10, 3.11, and are listed in Tables 3.4 and 3.5 and Appendix II.III.

Amphiboles from the Border Gabbro pegmatites make up approximately 2 vol. % of the modal abundance, and include sodic-calcic and calcic varieties. All Border Gabbro amphiboles, apart from edenite, have low *mg* numbers [$Mg/(Fe^{2+}+Mg)$] (Figs. 3.10 and 3.11). The calcic members include edenite and ferro-edenite; and the sodic-calcic members include ferroricherite, katophorite and ferrowinchite. The ferrorichterite and winchite amphiboles have a brown pleochroism, and form interstitially between the initial- and framework-forming minerals. The edenite and ferroedenite amphiboles commonly mantle pyroxene (Fig. 3.9B), and signify that pyroxene is being replaced by amphibole in the primary liquidus phase.

Railway amphiboles have compositions with low *mg* numbers and plot at the ferrorichterite/katophorite composition border. One crystal is zoned (Fig. 3.9C), with zoning

proportional to progressive depletion of iron. The katophorite amphiboles have a green pleochroism, whereas the ferrorichterite amphiboles have a brown pleochroism. Compared to the Border Gabbro pegmatites, amphibole modal abundance in the Railway pegmatites is low, at approximately 0.5 vol. %.
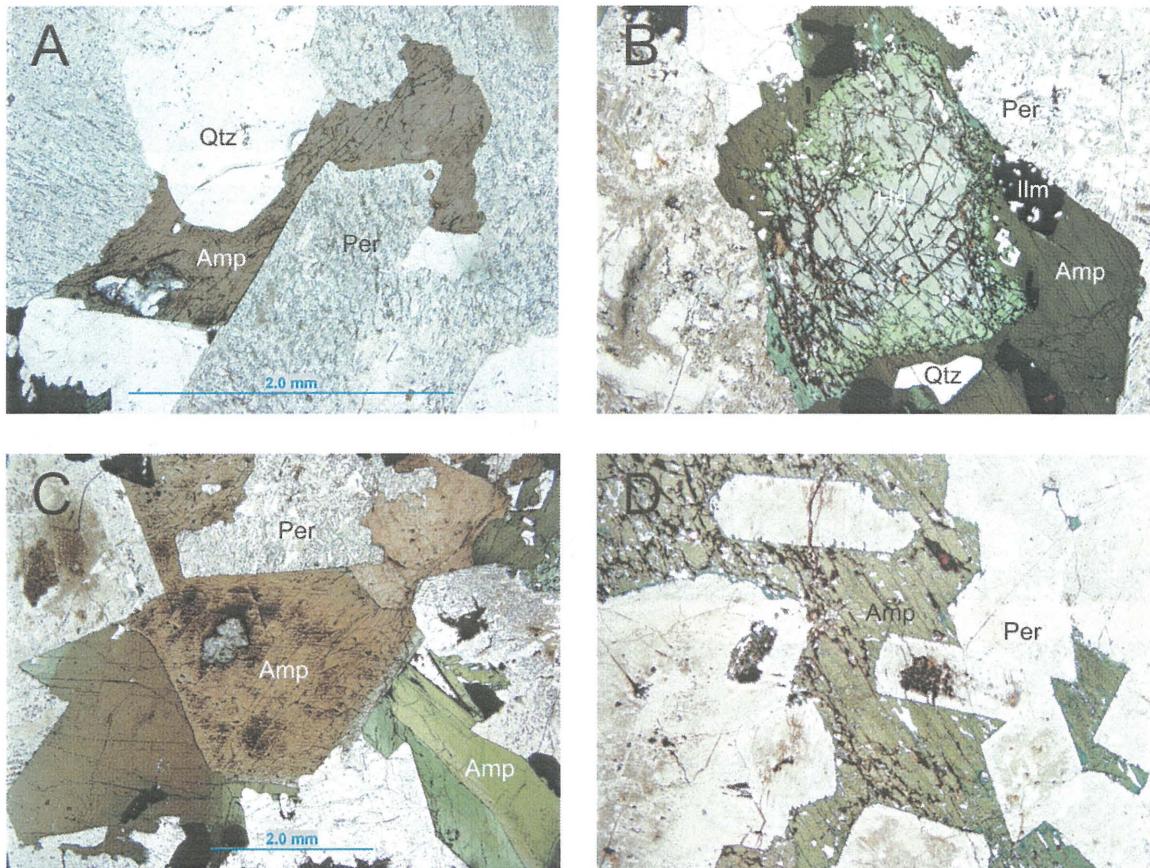
FIGURE 3.8: Photomicrographs of amphibole (Amp). A is ferrorichterite amphibole and quartz (Qtz) around perthite (Per) in plane-polarized (A) and cross-polarized (B) light. B is edenite amphibole mantling hedenbergite (Hd) and surrounded by ilmenite (Ilm), quartz and perthite. C is ferrorichterite (brown) and katophorite (green) amphiboles in perthite. D is riebeckite amphibole grown around perthite.

Amphiboles in the Upper Marathon Shore pegmatites include the sodic (riebeckite), sodic-calcic (ferrorichterite and taramite) and calcic varieties (hastingsite). All grains are either small (~ 50 μm) or extremely altered. Modal abundance is approximately 0.05 vol. %.

The Black pegmatites form a trend from the pleochroic green katophorite to pleochroic brown ferrorichterite (Fig. 3.8C). In common with Border Gabbro and Railway amphiboles, the
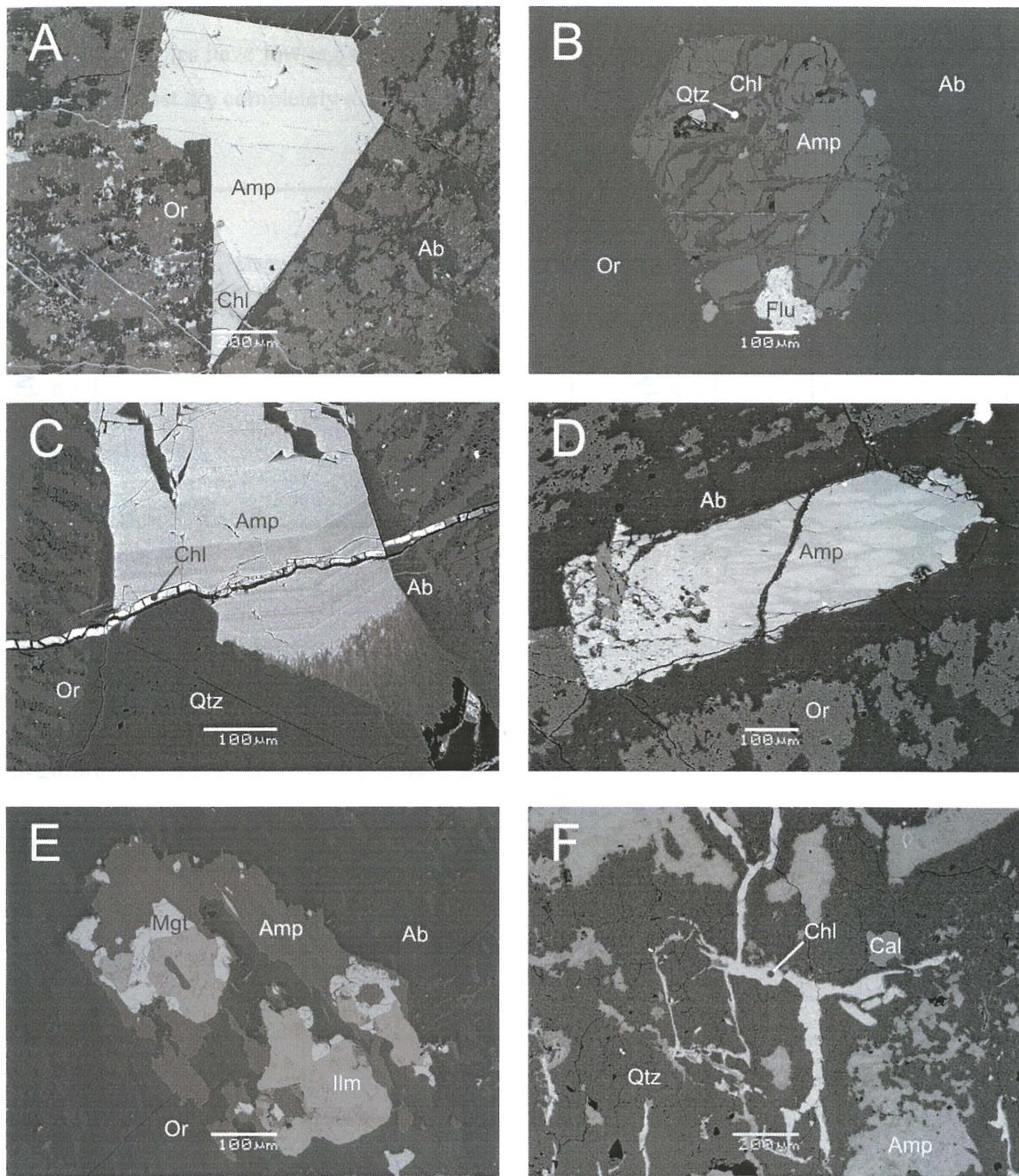
FIGURE 3.9: BSE-images of amphibole (Amp). A is amphibole (ferro-richerite) being altered to chlorite (Chl) and grown interstitially along albite (Ab) and orthoclase (Or) boundaries. B is amphibole (hastingsite) being altered along its grain boundary and fractures to chlorite and surrounded by albite and orthoclase (Flu is a fluorocarbonate inclusion). C is a magmatically zoned hastingsite amphibole (lighter areas are enriched in calcium and potassium) traversed by a chlorite vein and surrounded by quartz (Qtz), albite and orthoclase. D is riebeckite amphibole with hummocky texture (dark areas have aluminum, light areas do not) in albite. E is riebeckite amphibole surrounded by magnetite (Mgt), ilmenite (Ilm), albite and orthoclase. F is corroded taramite amphibole surrounded by calcite (Cal), quartz and chlorite.

Black amphiboles have low *mg* values. Amphibole grains in the Black pegmatites are rare (0.25 vol. %), as most are completely altered to chlorite.
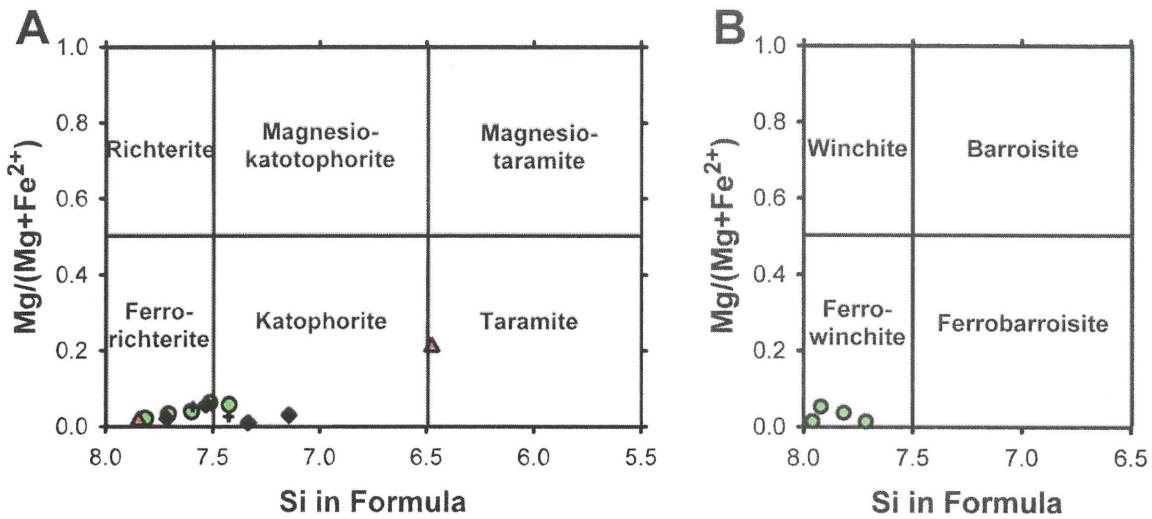
FIGURE 3.10: Sodic-calcic amphibole plots. A is for amphiboles with (Na + K) ≥ 0.50, (Ca + Na$_B$) ≥ 1.00, and 0.50 < Na$_B$ < 1.50. B is for amphiboles with (Na + K) < 0.50, (Ca + Na$_B$) ≥ 1.00, and 0.50 < Na$_B$ < 1.50. Green circles, black crosses, red triangles, and black diamonds are the Border Gabbro, Railway, Upper Marathon Shore, and Black pegmatites, respectively. From Leake et al. (1997).
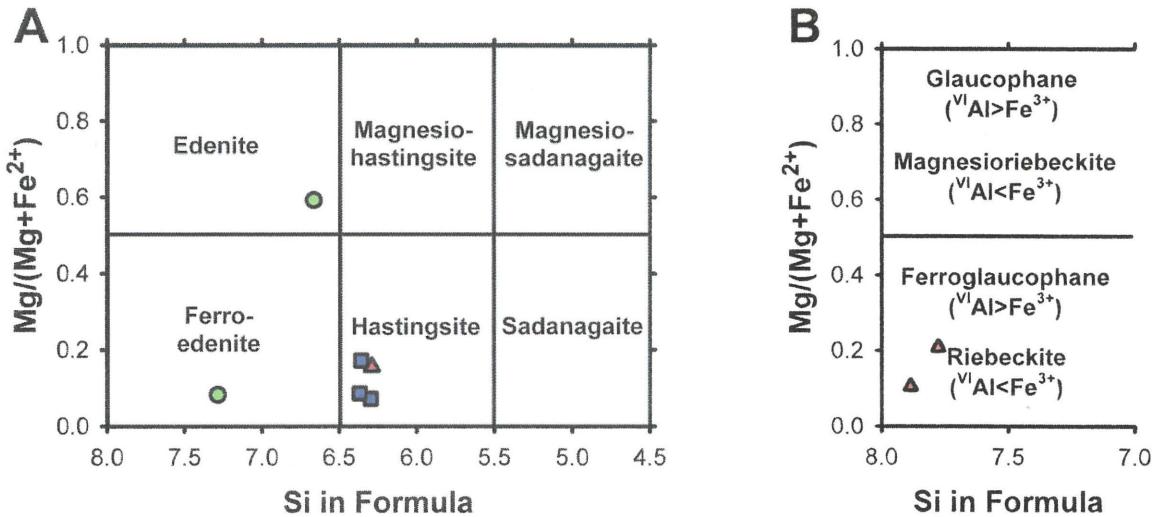
FIGURE 3.11: Calcic (A) and sodic (B) amphibole plots. A is for amphiboles with Ca$_B$ ≥ 1.50, (Na + K)$_A$ ≥ 0.50 and Ti < 0.50. B is for amphiboles with Na$_B$ ≥ 1.50, (Mg + Fe^{2+} + Mn^{2+}) > 2.5, (^{VI}Al or Fe^{3+}) > Mn^{3+}, Li < 0.5, (Mg or Fe^{2+}) > Mn^{2+}, and (Na + K)$_A$ < 0.50 (both averages are the riebeckite variety). Green circles, red triangles, and blue squares are the Border Gabbro, Upper Marathon Shore, and Center Three pegmatites, respectively. From Leake et al. (1997).

TABLE 3.4: Representative compositions of ferrorichterite, ferrowinchite, taramite, and riebeckite.

	Ferrorichterite				Ferrowinchite	Taramite	Riebeckite
	Border Gabbro[1]	Railway[2]	Upper Marathon Shore[3]	Black[4]	Border Gabbro[5]	Upper Marathon Shore[6]	Upper Marathon Shore[7]
SiO_2	47.99	47.45	50.15	48.08	50.05	40.77	50.15
TiO_2	1.16	1.79	-	1.52	0.16	0.89	-
Al_2O_3	1.69	2.22	0.97	1.71	0.90	8.56	0.97
Fe_2O_3	2.54	2.57	11.80	2.69	3.72	8.59	11.80
FeO	31.63	30.84	20.65	31.75	31.77	21.53	20.65
MnO	0.94	0.79	2.19	0.72	0.89	1.20	2.19
MgO	0.61	0.95	3.05	0.39	0.27	3.22	3.05
CaO	5.93	5.84	2.97	4.92	7.16	7.24	2.97
Na_2O	4.52	4.58	5.63	5.00	2.94	4.60	5.63
K_2O	1.10	1.12	1.09	1.49	0.42	1.57	1.09
Total*	**98.11**	**98.15**	**98.50**	**98.27**	**98.28**	**98.17**	**98.50**
H_2O_C	1.87	1.87	1.93	1.87	1.89	1.89	1.93
Total	**99.98**	**100.02**	**100.43**	**100.14**	**100.17**	**100.06**	**100.43**

[1] Border gabbro pegmatite (5 analyses of sample MAS006) from the Coldwell complex.
[2] Railway pegmatite (7 analyses of sample MAS017) from the Coldwell complex.
[3] Upper Marathon Shore pegmatite (4 analyses of sample MAS019) from the Coldwell complex.
[4] Black pegmatite (5 analyses of sample MAS029) from the Coldwell complex.
[5] Border Gabbro pegmatite (4 analyses of MAS009) from the Coldwell complex.
[6] Upper Marathon Shore pegmatite (4 analyses of MAS020) from the Coldwell complex.
[7] Upper Marathon Shore pegmatite (4 analyses of sample MAS019) from the Coldwell complex.
* Analytical total.

Center Three amphiboles consist of hastingsite (calcic) amphibole. Center Three hastingsite has a dark green pleochroism, anhedral-to-euhedral habits, and form in the initial stage of crystallization with magnetite and ilmenite (Fig. 3.9E). Most hastingsite grains alter to chlorite (Fig. 3.9B). The Center Three amphiboles are the only amphiboles to form in the initial stage of crystallization.

Apart from manganese and potassium, all other constituents vary considerably. In the Center One ferroaugite syenites, amphibole compositions range from hastingsite to ferroedenite in the lower series and ferrorichterite to katophorite and riebeckite to arfvedsonite in the upper series (Mitchell and Platt 1978). Trends that range from sodic-to-sodic-calcic-to-calcic are typical of highly differentiated complexes. Examples of similar trends include: Khibina, Russia –

pargasite (calcic) to arfvedsonite (sodic) (Yakovenchuk et al. 2005); Red Hill, United States – hastingsite (sodic) to katophorite (sodic-calcic) (Mitchell 1990); and many others (Mitchell 1990; Martin 2007).

TABLE 3.5: Representative compositions of katophorite, ferroedenite, edenite, and hastingsite.

	Katophorite			Ferroedenite	Edenite	Hastingsite	
	Border Gabbro[1]	Railway Syenite[2]	Black[3]	Border Gabbro[4]	Border Gabbro[5]	Upper Marathon Shore[6]	Center Three[7]
SiO_2	46.24	45.98	43.79	44.40	45.81	39.21	38.95
TiO_2	1.80	2.45	2.63	0.71	0.41	1.20	1.31
Al_2O_3	2.19	2.51	4.13	8.09	3.24	9.72	9.96
Fe_2O_3	4.59	2.04	0.20	0.71	6.18	5.89	4.50
Foe	30.07	31.99	32.96	15.27	29.14	24.55	27.07
MnO	0.77	0.81	0.54	0.28	0.64	0.98	1.09
MgO	1.03	0.48	0.57	12.45	1.47	2.54	1.18
CaO	6.06	5.98	7.65	12.03	9.92	9.29	9.86
Na_2O	4.62	4.65	4.01	3.61	1.44	3.46	2.85
K_2O	1.09	1.44	1.45	0.37	0.74	1.62	1.58
Total*	**98.46**	**98.33**	**97.93**	**97.92**	**98.99**	**98.46**	**98.35**
H_2O_C	1.87	1.86	1.84	2.00	1.88	1.87	1.85
Total	**100.33**	**100.19**	**99.77**	**99.92**	**100.87**	**100.33**	**100.20**

[1] Border gabbro pegmatite (4 analyses of sample MAS012) from the Coldwell complex.
[2] Railway pegmatite (5 analyses of sample MAS027) from the Coldwell complex.
[3] Black pegmatite (4 analyses of sample MAS031) from the Coldwell complex.
[4] Border Gabbro pegmatite (7 analyses of sample MAS004) from the Coldwell complex.
[5] Border Gabbro pegmatite (3 analyses of sample MAS002) from the Coldwell complex.
[6] Upper Marathon Shore pegmatite (4 analyses of sample MAS020) from the Coldwell complex.
[7] Center Three pegmatite (3 analyses of sample MAS035) from the Coldwell complex.
* Analytical Total.

Amphibole is an inosilicate with the general formula $AB_2^{VI}C_5^{IV}T_8O_{22}(OH)_2$ (Leake et al. 1997). The compositions of Coldwell amphiboles fall into the monoclinic varieties, and is based on double Si_4O_{11} chains that run parallel to the c axis (Leake et al. 1997). Coldwell amphiboles have the monovalent alkali metals Na, K entering the A-site; the mono- and di-valent alkali, alkali earth and transition metals Na^+, Ca^{2+}, Fe^{2+}, Mg^{2+} entering the B-site; C represents the transition metals and metalloids Al^{3+}, Mn^{2+}, Fe^{2+}, Fe^{3+}, Ti^{4+}; the tetrahedral T-site refers to Si^{4+}

and Al^{3+}; and O^{2-} and F^- can occupy the OH^--site. Fluorine is not determined, but may be present, as fluorine saturation (fluorite) occurs slightly after amphibole precipitation.

3.5 Chlorite

Chlorite is the most common alteration mineral in Coldwell pegmatites. There are several replacement textures, the most notable being radiating, massive and laminated (Fig. 3.12 and 3.13). In plane polarized light, chlorite has a moderate relief, honey brown or green-to-clear pleochroism and anomalous royal blue birefringence (Fig. 3.13). Coldwell chlorite replaces the silicate minerals amphibole, biotite and muscovite in the deuteric phase of crystallization.
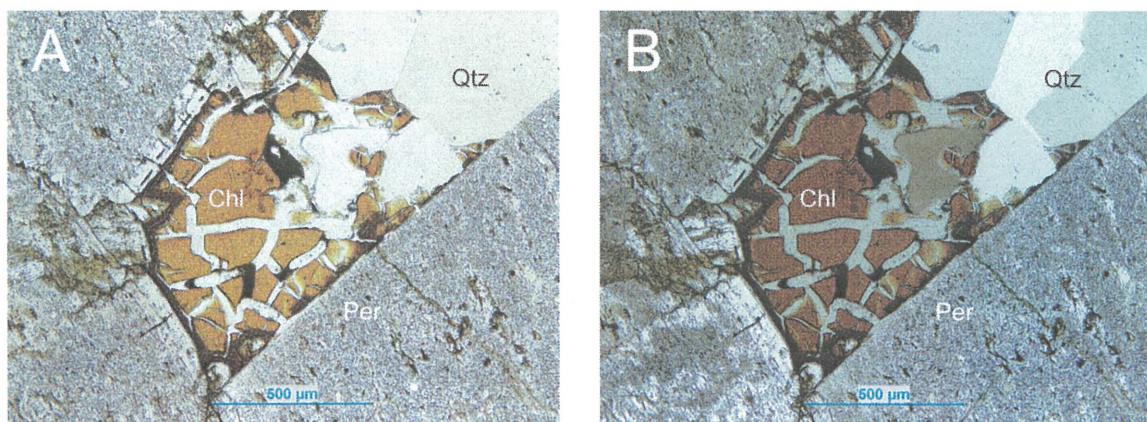
FIGURE 3.12: Optical micrographs of chlorite (Chl) and quartz (Qtz) surrounded by perthite (Per). A is normal-polarized, B is cross-polarized.

Aluminum, silica, iron, and magnesium vary between and within all units. Although representative compositions are given in Table 3.5, the extent of variability is better represented by the magnesium – total iron – aluminum ternary plot in Figure 3.14. In general, the Border Gabbro, Railway and Black pegmatites contain more iron than Upper Marathon Shore and Center Three chlorites. Both magnesium and octahedral aluminum change significantly between samples, ranging from 0 to 5.119 apfu and 0.698 to 2.820 apfu, respectively.

According to Holland et al. (1998), chlorite chemistry forming under low temperature conditions can be regarded as $[(R^{2+}_{6-x}Al_x)(Si_{4-x}Al_x)O_{10}(OH)_8]$. R-site ions include Ca^{2+}, Fe^{2+}, Fe^{3+}, K^+, Mg^{2+}, Mn^{2+}, Na^+, and Ti^{4+}. Coldwell chlorites belong to the clinochlore-chamosite series, with all analyses falling into the chamosite compositional field. Chamosite and clinochlore both belong to the trioctahedral-type of chlorites, consisting of 2:1 layers of $(R^{2+},R^{3+})_3(Si_{4-x}Al_x)O_{10}(OH)_2$ with interlayer octahedral $(R^{2+},R^{3+})_3(OH)_6$ sheets (Bailey 1988).
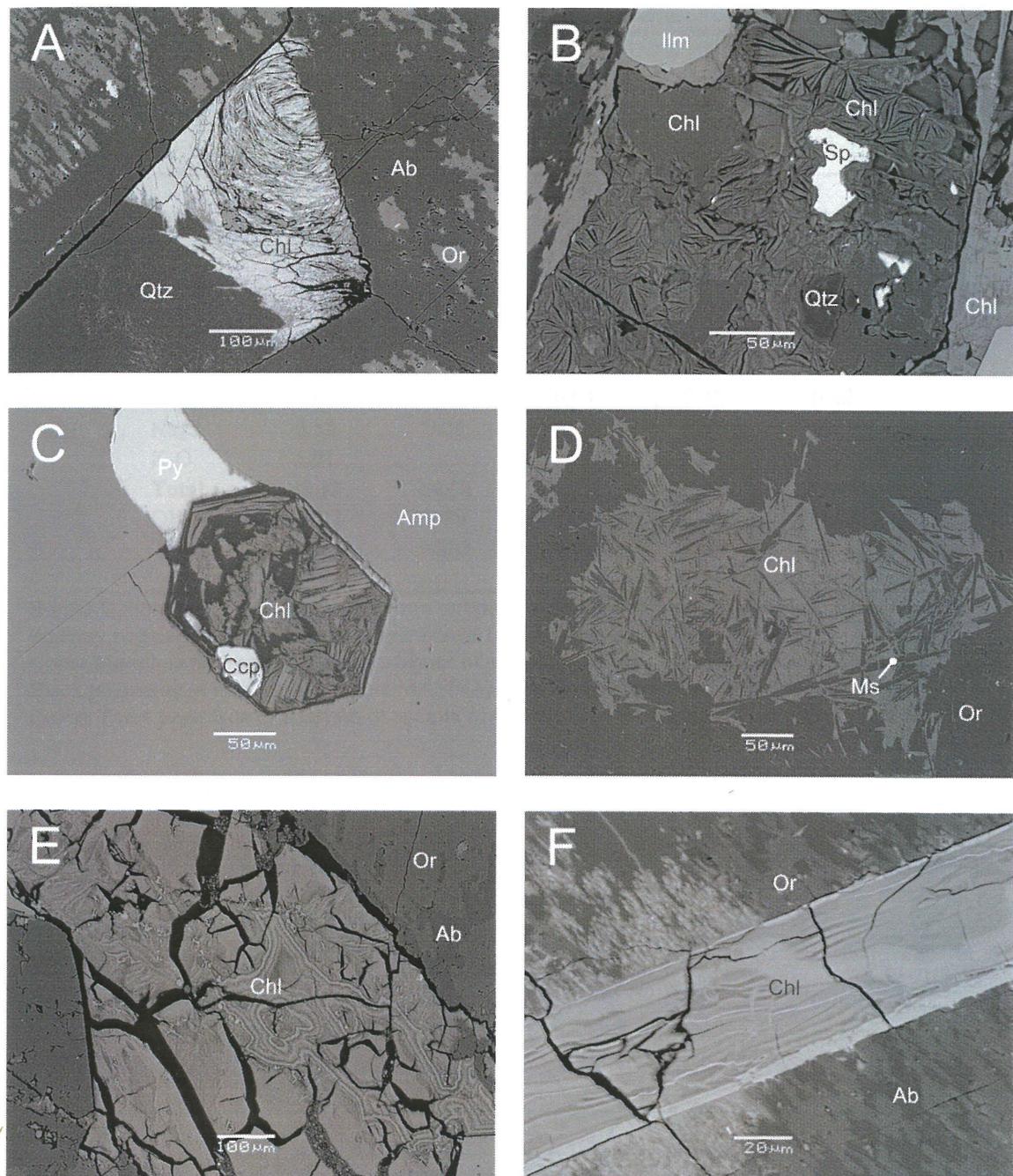
FIGURE 3.13: BSE images of chlorite (Chl). A is radiating chlorite with quartz (Qtz), albite (Ab) and orthoclase (Or). B is three phases of chlorite the lighter laminated type contains the highest iron, the radiating is moderate and the massive contains the least iron. The chlorite in B surrounds a sphalerite grain (Sp). C is a void set in pyrite (Py) and amphibole (Amp) filled with chlorite and chalcopyrite (Ccp). D is chlorite that formed interstitially between orthoclase and muscovite (Ms). E is massive chlorite with compositional zoning (light = iron-enriched). F is chlorite pseudomorphing biotite that precipitated adjacent to albite and orthoclase.

TABLE 3.6: Representative compositions of chlorite.

	Border[1]	Railway[2]	Upper Marathon Shore[3]	Black[4]	Center Three[5]
SiO_2	42.96	36.74	25.47	30.71	33.03
Al_2O_3	5.18	4.00	17.19	8.64	12.26
Fe_2O_3	10.79	7.60	-	0.68	2.81
FeO	24.26	33.75	40.59	40.29	28.15
MnO	1.84	0.98	1.33	0.75	0.38
MgO	1.02	0.54	4.75	4.82	11.80
CaO	0.83	0.35	0.04	0.45	0.82
Na_2O	0.53	0.08	0.21	0.59	0.22
K_2O	1.01	-	-	0.61	-
Total	**88.42**	**84.04**	**89.58**	**87.54**	**89.47**
OH_C	11.02	9.99	10.61	10.29	11.35
Total	**99.44**	**94.03**	**100.19**	**97.83**	**100.82**

[1] Border Gabbro pegmatite (4 analyses from sample MAS002) from the Coldwell complex.
[2] Railway pegmatite (6 analyses of sample MAS015) from the Coldwell complex.
[3] Upper Marathon Shore pegmatite (4 analyses of sample MAS018) from the Coldwell complex.
[4] Black pegmatite (4 analyses of sample MAS042) from the Coldwell complex.
[5] Center Three pegmatite (7 analyses of sample MAS038) from the Coldwell complex.
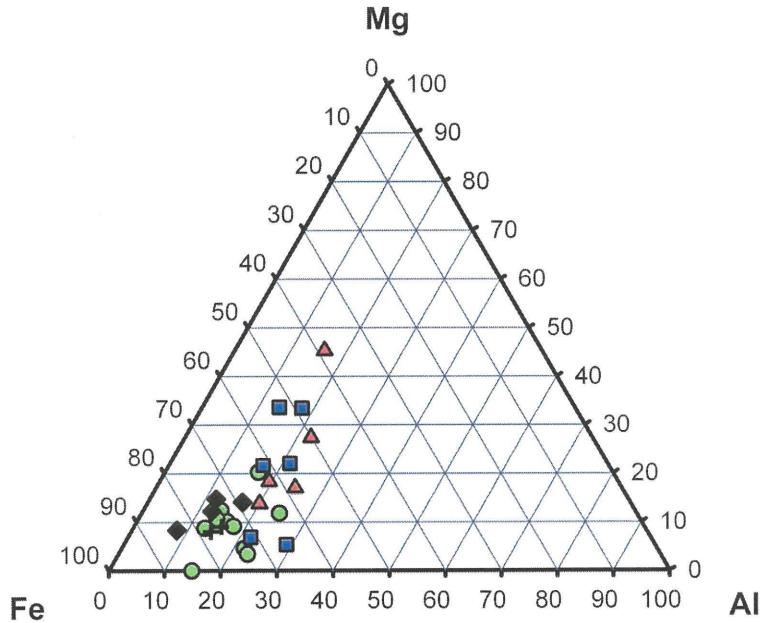
FIGURE 3.14: Chlorite magnesium (Mg) – total iron (Fe) – aluminum (Al) ternary plot (oxide wt. %). Green circles, black crosses, red and yellow triangles, black diamonds, and blue squares are the Border Gabbro, Railway, Upper Marathon Shore, Lower Marathon Shore, Black, and Center Three pegmatites, respectively.

Both chamosite and ferroan clinochlore adopt a monoclinic structure (Bayliss 1975; Rule and Bailey 1987).

Apart from tetrahedrally coordinated aluminum substituting for silicon, substitution into the chlorite structure is restricted to the R^{2+} site. Monovalent and trivalent ions in the R^{2+}-site indicates that coupled substitution was used to ensure charge neutrality:

$$(Al,Fe)^{3+} + (K,Na)^+ \rightarrow 2R^{2+}$$

The result from all divalent ions plotted against mono- tri and tetra-valent ions ($M^{2+}/M^++M^{3+}+M^{4+}$), as in Figure 3.15, gives an r^2 value of 0.797. Error may be related to the tetrahedral site, as the site may be not completely occupied or may contain ferric iron.
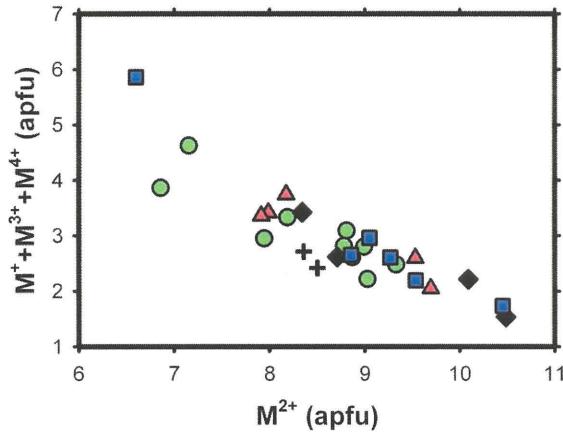
FIGURE 3.15: Chlorite M^{2+} (Fe^{2+}, Mn, Mg, Ca) vs $M^++M^{3+}+M^{4+}$ (Ti, Al(vi), Fe^{3+}, Na, K) binary diagram with a generated r^2 factor to 0.797. Green circles, black crosses, red triangles, black diamonds, and blue squares are the Border Gabbro, Railway, Upper Marathon Shore, Black, and Center Three pegmatites, respectively.

3.5 Olivine

Olivine is present in one of the Border Gabbro samples and nearly half of the Railway samples. Olivine forms in the initial phase of crystallization and is associated with amphibole, muscovite and pyroxene (Fig. 3.16). In all cases, compositions are iron rich, and fall into the fayalite compositional field (Table 3.7 and Appendix II.V).

Olivine occurs in one sample of the Border Gabbro pegmatite (Fig. 3.17). In this occurrence, fayalite has grown interstitially with an unknown mineral that was subsequently altered to chlorite. The crystals contain minor amounts of manganese and magnesium and trace amounts of aluminum and calcium.
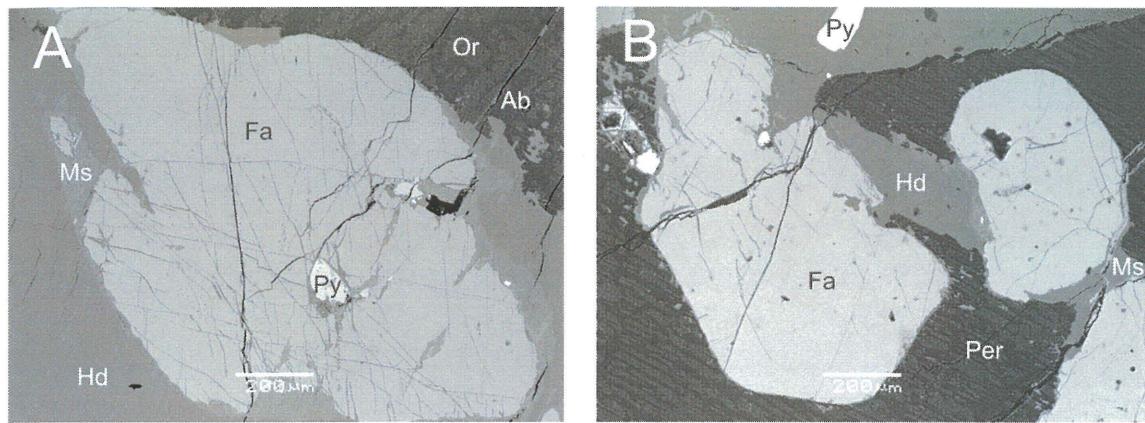
FIGURE 3.16: BSE-images of fayalite (Fa). Both images show fayalite with hedenbergite (Hd) and muscovite (Ms) overgrowths in perthite (Per, Ab-Or). A contains late pyrite (Py).

TABLE 3.7: Representative compositions of fayalite.

	Border Gabbro[1]	Railway[2]
SiO_2	30.15	29.76
Al_2O_3	0.20	0.22
FeO	66.19	67.13
MnO	2.40	2.61
MgO	1.19	0.36
CaO	0.39	0.39
Total	**100.51**	**100.47**

[1] Border Gabbro pegmatite (4 analyses of sample MAS001) from the Coldwell complex.
[2] Railway pegmatite (4 analyses of sample MAS025) from the Coldwell complex.

In contrast to Border Gabbro pegmatites, olivine is common in Railway pegmatites, occurring in four of the ten samples. The crystals are, as shown in Figure 3.17, rounded and commonly mantled by muscovite and hedenbergite. In common with the Border Gabbro, these olivines fall into the fayalite compositional field, with near identical compositions, except slightly lower (~ 1 wt. % MgO) magnesium.
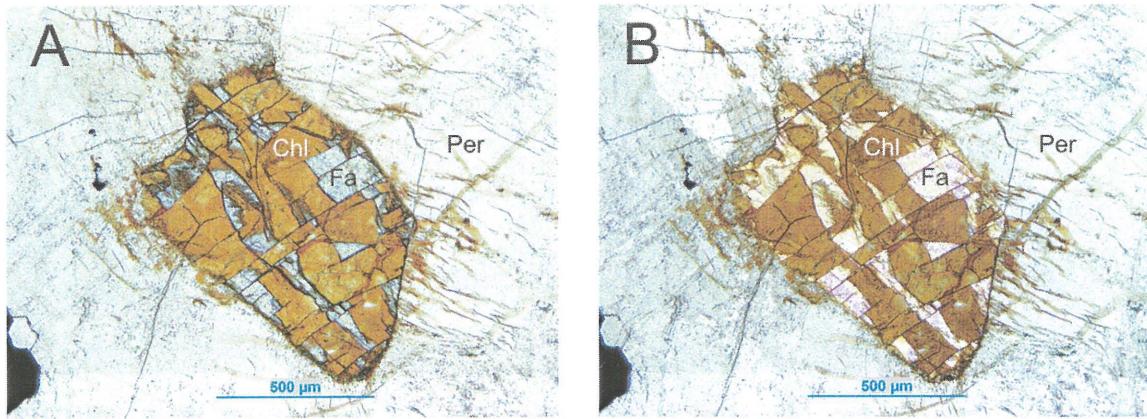
FIGURE 3.17: Photomicrographs of fayalite (Fa) and chlorite (Chl) in perthite (Per). A is normal-polarized, B is cross-polarized.

3.7 Calcite

Calcite is present in all pegmatitic units, and usually accounts for approximately 0.25 vol. % of the modal abundance. Calcite is one of the last minerals to form interstitially (Figs. 3.18, 3.19A and B). Calcite from Coldwell pegmatites is pure $CaCO_3$ with no magnesium, iron or strontium.
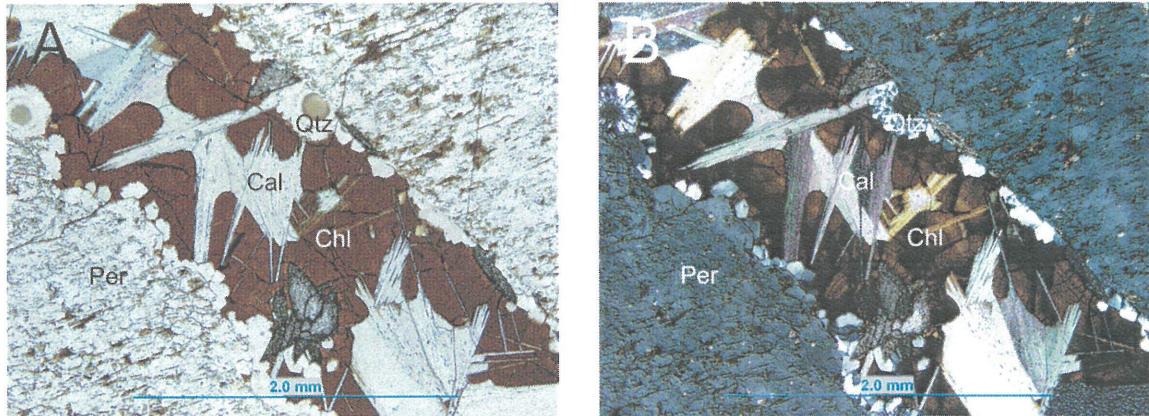
FIGURE 3.18: Photomicrographs of calcite (Cal) and quartz (Qtz) with late chlorite (Chl) in perthite (Per). A is normal-, B is cross-polarized.
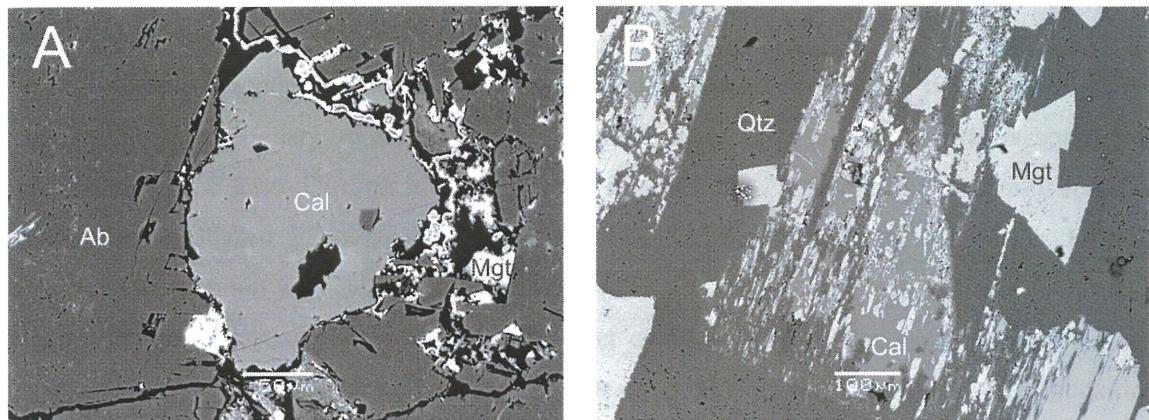
FIGURE 3.19: BSE-images of calcite (Cal). A is calcite hosted by albite (Ab) and magnetite (Mgt). B is calcite with magnetite inclusions hosted by quartz (Qtz).
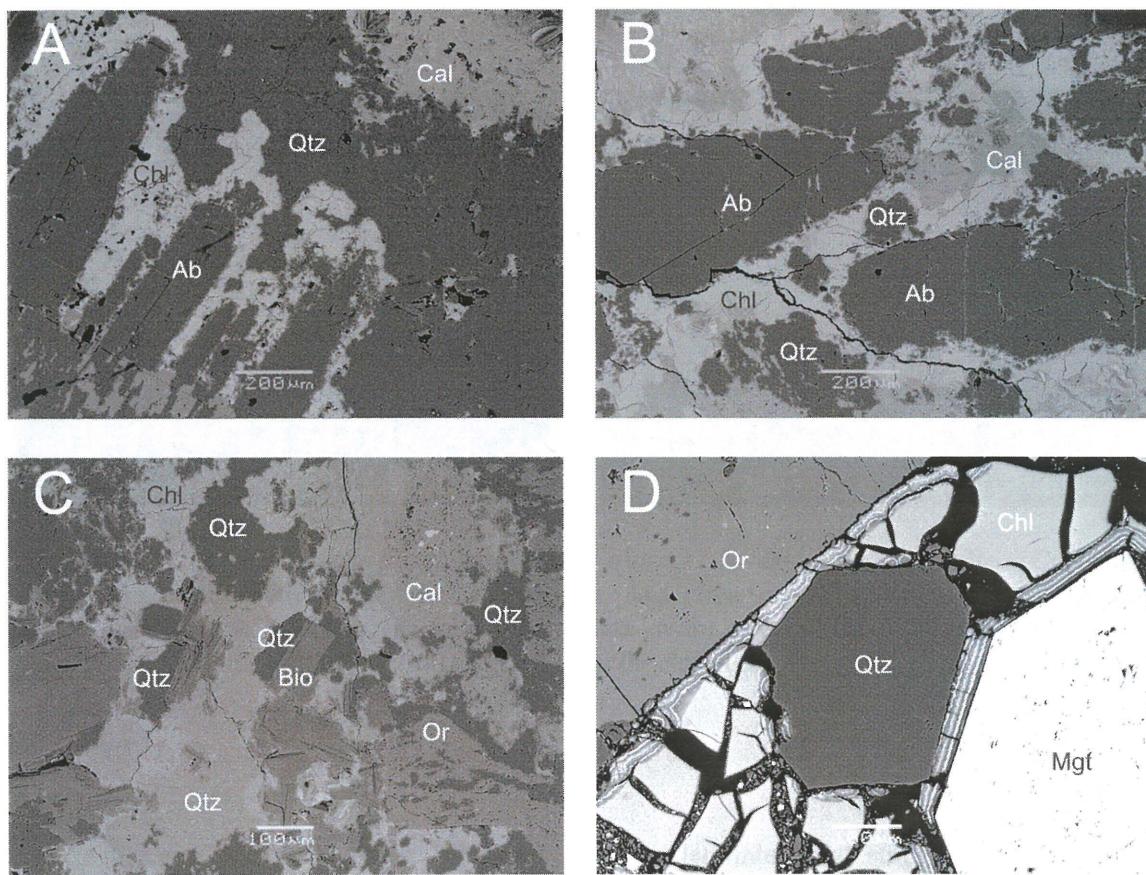
FIGURE 3.20: BSE-images of quartz (Qtz). A, B and C show quartz that has grown along chlorite (Chl), albite (Ab) and calcite (Cal) boundaries. C contains orthoclase (Or) instead of albite and also biotite (Bio). D is subhedral quartz hosted by chlorite, magnetite (Mgt) and orthoclase.

3.8 Quartz

Quartz is a common minor mineral found in Coldwell pegmatites. It forms in the late-interstitial and secondary stages of crystallization. Late interstitial stage quartz is commonly associated with calcite. The crystals, as shown in Figure 3.20A, B, and C, are generally anhedral (exception in Figure 3.20D), with crystal habit and size restricted by the earlier forming minerals. In common with calcite, quartz is one of the last primary minerals to form.

Secondary quartz is an alteration product commonly associated with fluorocarbonates (Fig. 3.21A). As most primary REMs are silicates, e.g. allanite and chevkinite, decomposition commonly creates fluorocarbonates plus quartz and other product(s). In common with the REE-silicates, the breakdown of amphibole (Fig. 3.21B) produces quartz:

$$NaCa_2Fe_5Si_7AlO_{22}(OH)_2 + 2CO_3 + 7OH^- \rightarrow Fe_5AlSi_4O_{10}(OH)_8 + 2CaCO_3 + NaOH + 3SiO_2 + 6O^{2-}$$
Ferro-edenite   Chamosite   Calcite   Quartz
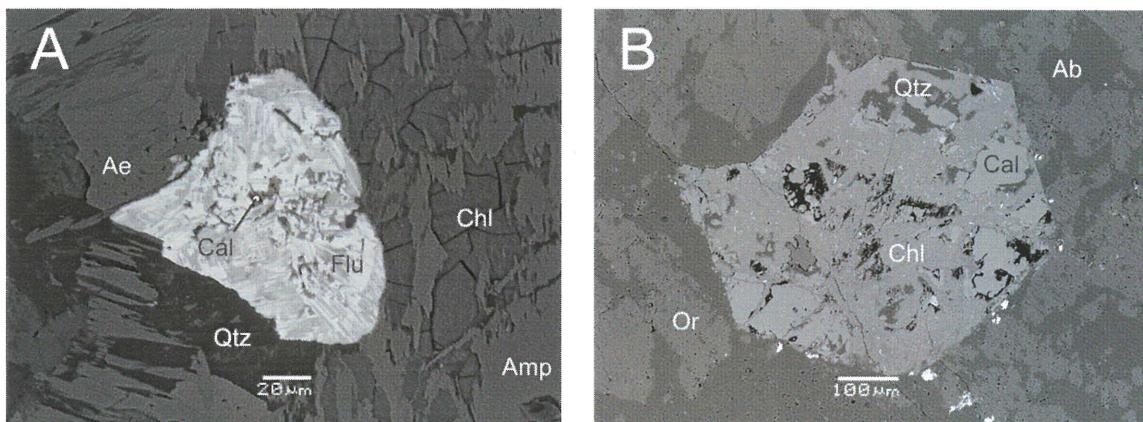
FIGURE 3.21: BSE-images of secondary quartz. A is quartz, calcite (Cal) and fluorocarbonates (Flu) surrounded by aegirine (Ae), chlorite (Chl), and amphibole (Amp). Some of the dark areas in the fluorocarbonate grain are quartz crystals. B is quartz, chlorite and calcite hosted by albite (Ab) and orthoclase (Or).

3.9 Fluorite

Fluorite occurs in nearly all samples in the late-interstitial stage of crystallization. Fluorite grains are anhedral, and generally isolated from other late-forming minerals (Fig. 3.22 and 3.23). No ions, other than calcium and fluorine, are detected in any of the analyses.

The occurrence of fluorite precipitating late in the paragenesis indicates that fluorine was present in the fluid and/or melt phases. Fluorine is important, as it complexes with REE,

HFSE, and other "incompatible" elements. As such, fluorine mobilizes these elements, whereby prohibiting these ions to reach early saturation.
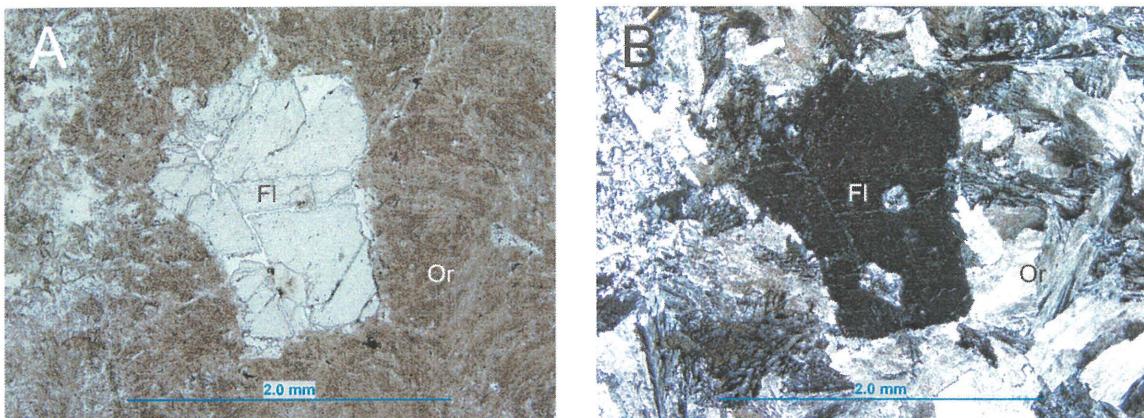
FIGURE 3.22: Photomicrographs of fluorite (Fl) in orthoclase (Or). A is normal-polarized, B is cross-polarized.
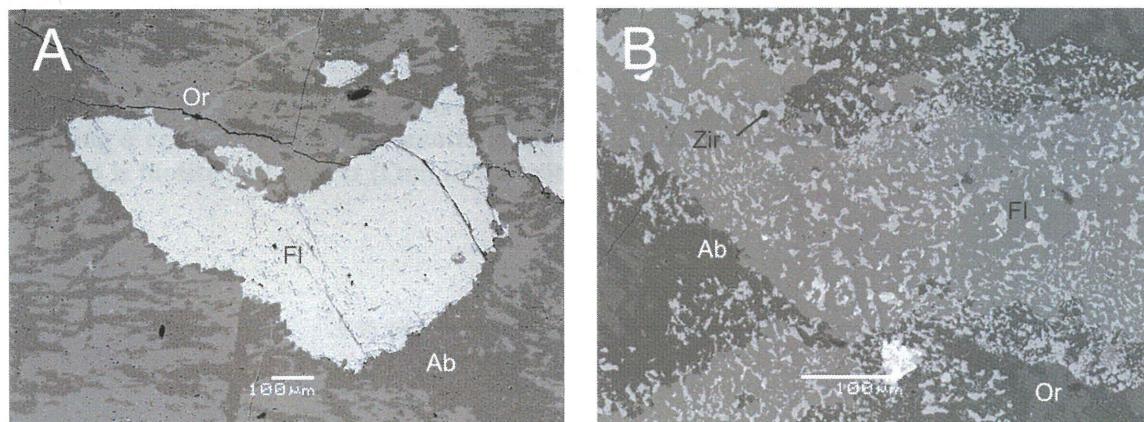
FIGURE 3.23: BSE-images of fluorite (Fl). A is interstitial fluorite in albite (Ab) and orthoclase (Or). B is fluorite with zircon (Zr) inclusions and hosted by albite and orthoclase.

3.10 Biotite

Biotite is present in the Border Gabbro, Railway and Black pegmatite units. Biotite forms in the interstitial and secondary stages of crystallization, and commonly alters to chlorite. In the interstitial stage, biotite forms early, before amphibole, and is characterized by discrete books that are confined by initial- and framework-phase minerals. Secondary biotite forms reaction rims around magnetite and ilmenite (Fig. 3.24).

In Coldwell biotites, the $IM_{2-3}\square_{0-1}T_4O_{10}A_2$ mica formula (Rieder et al. 1998) contains Ca^{2+}, K^+ and Na^+ in the I-site; Al^{3+}, Fe^{2+}, Fe^{3+}, Li^+, Mg^{2+}, and Mn^{2+}, in the M-site; and Cl^-, (F^-), O^{2-}, and (OH^-) in the A-site. I-site solid solution in respect to the dominant cation (potassium) is shown Figure 3.25. The amount of lithium, fluorine and hydrogen is undetermined, as these ions are not analyzed for. Coldwell biotites are enriched in potassium and iron, and thus, fall into the annite compositional field (Table 3.8 and Appendix II.IX).
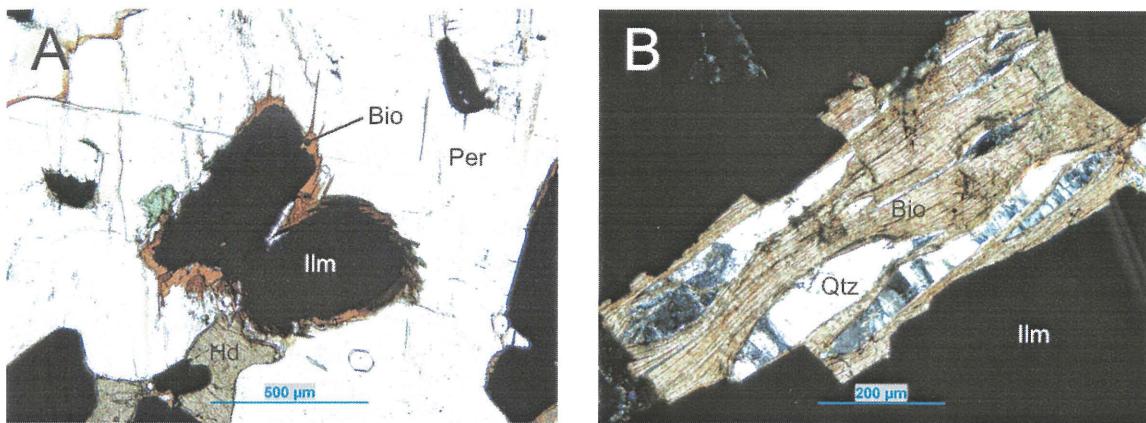
FIGURE 3.24: Photomicrographs of biotite (Bio). A (plane polarized light) is biotite forming a reaction rim with ilmenite (Ilm) and hosted by perthite (Per) and hedenbergite (Hd). B is biotite and quartz (Qtz) in ilmenite (Ilm) under cross polarized light.
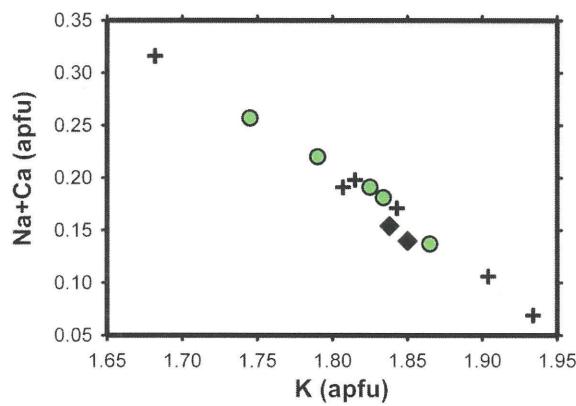
FIGURE 3.25: Biotite I-site substitution plot. The r^2 value is 0.960.

3.11 Muscovite

Muscovite is present in the Railway and Center Three pegmatite units. Muscovite crystallizes early in the secondary stage, before chlorite. The mineral forms small (50 to 150 μm) books of subhedral sheets that radiate from a nucleation point (Figs. 3.26, 3.27A). Coldwell muscovite is always associated with chlorite, and commonly mantles olivine and pyroxene. Both muscovite and chlorite are alteration products of a potassium-bearing mineral, presumably biotite:

$$3KFe_3AlSi_3O_{10}(OH)_2 + 6OH^- \rightarrow Fe_5AlSi_4O_{10}(OH)_8 + KAl_2Si_3O_{10}(OH)_2 + 2Fe_2O_3 + 2KOH + 2SiO_2$$

Biotite   Chamosite   Muscovite   Hematite   Quartz
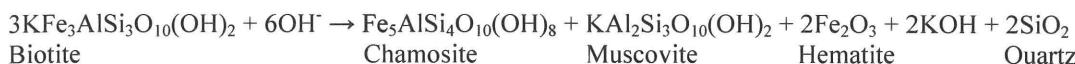
TABLE 3.8: Representative compositions of biotite.

	Border Gabbro[1]	Railway[2]	Black[3]
SiO_2	35.46	37.35	33.95
TiO_2	0.72	0.05	3.68
Al_2O_3	10.25	7.54	9.67
FeO	39.23	41.24	39.90
MnO	0.57	0.96	0.26
MgO	0.99	0.27	0.25
Na_2O	0.67	0.88	0.47
K_2O	8.35	7.78	8.54
Cl	-	0.10	-
O = Cl	-	0.02	-
Total	**96.24**	**96.15**	**96.72**
H_2O_C	3.57	3.51	3.55
Total	**99.81**	**99.66**	**100.27**

[1] Border gabbro pegmatite (4 analyses from sample MAS001) from the Coldwell complex.
[2] Railway pegmatite (4 analyses from sample MAS015) from the Coldwell complex.
[3] Black pegmatite (7 analyses from sample MAS030) from the Coldwell complex.

In common with biotite, muscovite readily alters to chlorite. Table 3.9 lists the compositions of typical unaltered muscovite, intermediately altered muscovite and a chlorite grain whose precursor was muscovite. With the onset of alteration, muscovite exhibits increases in magnesium, iron and water (hydroxyl). These increases are accompanied by decreases in silicon, aluminum and potassium. As muscovite itself is an alteration product, subsequent alteration must have affected the Coldwell pegmatites.

In the Coldwell muscovites, the $IM_{2-3}\square_{1-0}T_4O_{10}A_2$, formula contains K^+ and Na^+ in the I-site; Li^+, Fe^{2+}, Fe^{3+}, Mg^{2+}, Mn^{2+}, Al^{3+}, and/or Ti in the M-site; Al^{3+}, Fe^{3+}, and Si in the T-site; and OH^- in the A-site. Lithium and fluorine are able to substitute into the M and A sites, respectively, but are not quantified in this study. In addition to omitted elements, Fe^{2+}/Fe^{3+} recalculations were not preformed, which may add additional the error to the totals (Table 3.9 and Appendix II.X).
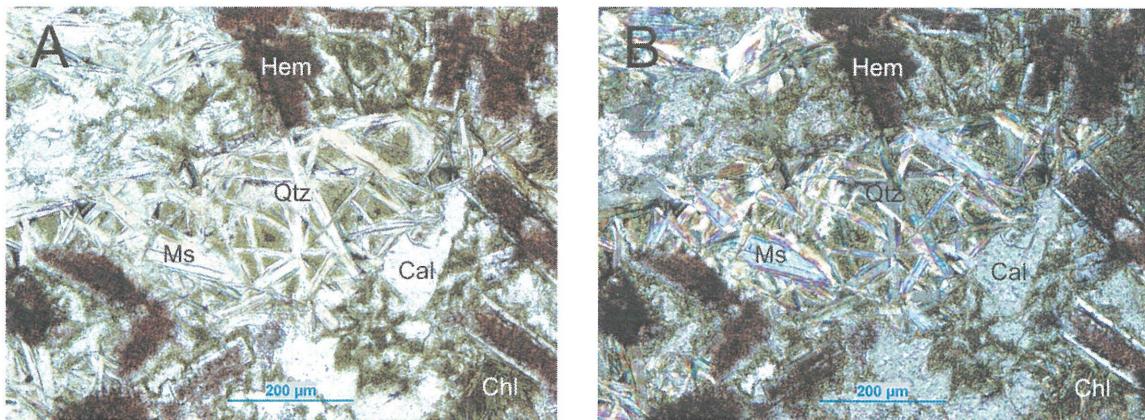
FIGURE 3.26: Optical photomicrographs of muscovite (Ms) intergrown with quartz (Qtz), chlorite (Chl), calcite (Cal), and hematite (Hem) in plane-polarized (A) and cross-polarized (B) light.
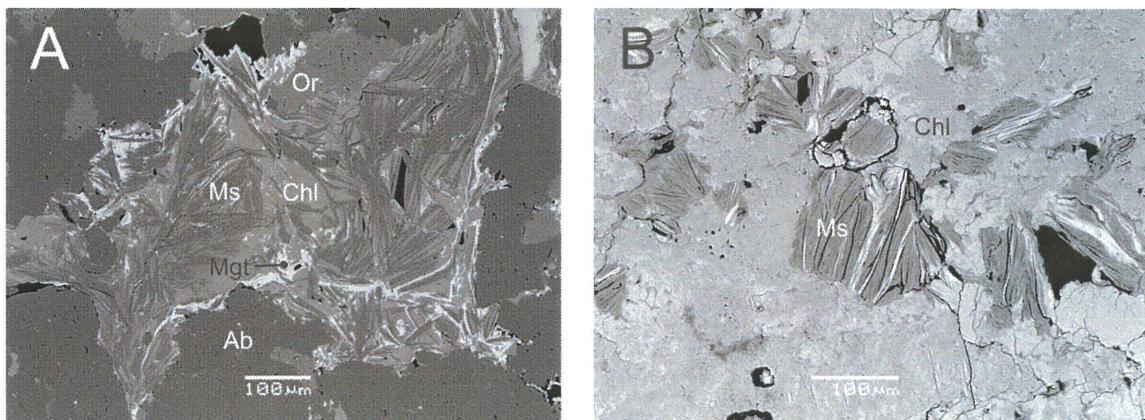
FIGURE 3.27: BSE-images of muscovite (Ms). A is muscovite, chlorite (Chl) and magnetite (Mgt) hosted by albite (Ab) and orthoclase (Or). B is muscovite surrounded by chlorite.

TABLE 3.9: Representative compositions of muscovite and altered varieties.

	Upper Marathon Shore[1]	Center Three [2]	Inter. Altered[3]	Chlorite[4]
SiO_2	47.41	44.11	47.91	32.81
TiO_2	0.39	0.14	-	-
Al_2O_3	33.68	38.47	27.45	14.37
Fe_2O_3	-	-	-	4.10
FeO	3.73	1.16	5.04	27.29
CaO	-	-	0.32	0.76
MnO	-	-	-	0.25
MgO	-	-	3.33	9.48
Na_2O	-	0.17	0.22	-
K_2O	11.11	10.85	7.29	0.42
Total	**96.32**	**94.77**	**91.56**	**89.40**
H_2O_C	4.50	4.48	N.D.	11.35
Total	**100.82**	**99.28**	**91.48**	**100.83**

[1] Upper Marathon Shore pegmatite (4 analyses of sample MAS019) from the Coldwell complex.

[2] Center Three pegmatite (3 analyses of sample MAS039) from the Coldwell complex.

[3] Intermediate altered muscovite from the Upper Marathon Shore pegmatite (4 analyses of sample MAS021) from the Coldwell complex.

[4] Chlorite from the Upper Marathon shore pegmatite (7 analyses of sample MAS022) from the Coldwell complex.

CHAPTER FOUR
ACCESSORY MINERALIZATION

4.1 Introduction

REEs (+ yttrium), the 3rd and 4th row transition elements zirconium, niobium, hafnium, tantalum, and tungsten along with the actinides thorium and uranium dominate the accessory mineralization of the Coldwell pegmatites. The majority of these elements are complexed with phosphates (apatite, monazite and xenotime), silicates (allanite, chevkinite, thorite, titanite, and zircon), oxides (baddeleyite, fergusonite, fersmite, ilmenite, pyrochlore, and rutile) and fluorocarbonates (bastnaesite, synchysite and parisite). Other minerals include the sulphates (barite), sulphides (arsenopyrite, chalcopyrite, galena, pyrite, and sphalerite), and oxides (magnetite).

The order of description of minerals in this chapter is alphabetical, as relative abundances are difficult to determine. Details on composition and structure are emphasized, due to the significance of crystallochemical controls on the formation of accessory mineralization.

4.2 Allanite

Allanite is the most compositionally diverse member of the epidote group and is one of the most important host of REEs in syenite, granite, granodiorite, monzonite, skarns, and felsic volcanics. Apart from the Black pegmatites, allanite occurs in all units of the Coldwell complex in the initial stage of crystallization. Allanite is closely associated with apatite, britholite, chevkinite, fergusonite, monazite and magnetite/ilmenite. In polarized light allanite is colourless, has high relief, and first order grey birefringence (Fig. 4.1).

In Coldwell pegmatites, allanite commonly alters to fluorocarbonates. Carbonate- and fluorine-saturated fluids migrate through fractures and crystal imperfections and replace silicon and oxygen in allanite producing fluorocarbonates and quartz (or other silicates):

$$REE_2M_3(SiO_4)(Si_2O_7)O(OH) + 2CO_2 + 2F^- \rightarrow 2(REE)(CO_3)F + 3SiO_2 + 3M^{n+} + OH^- + 4O^{2-}$$

Allanite   Bastnaesite   Quartz
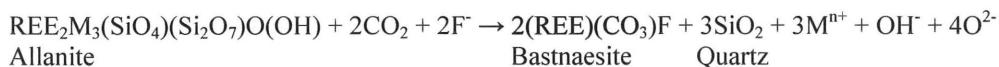
Allanite occurs in two of the Border Gabbro samples. In both cases, the crystals are strongly corroded and encased by amphibole. These compositions are similar to those in other units (Table 4.1) consisting of titanium (2.63 and 3.09 wt. % TiO_2), REEs (25.24 and 25.26 wt. % REE_2O_3), aluminum (9.59 and 9.99 wt. % Al_2O_3), ferrous iron (18.68 and 18.72 wt. % FeO), calcium (9.17 and 9.21 wt. % CaO), and other minor ions.
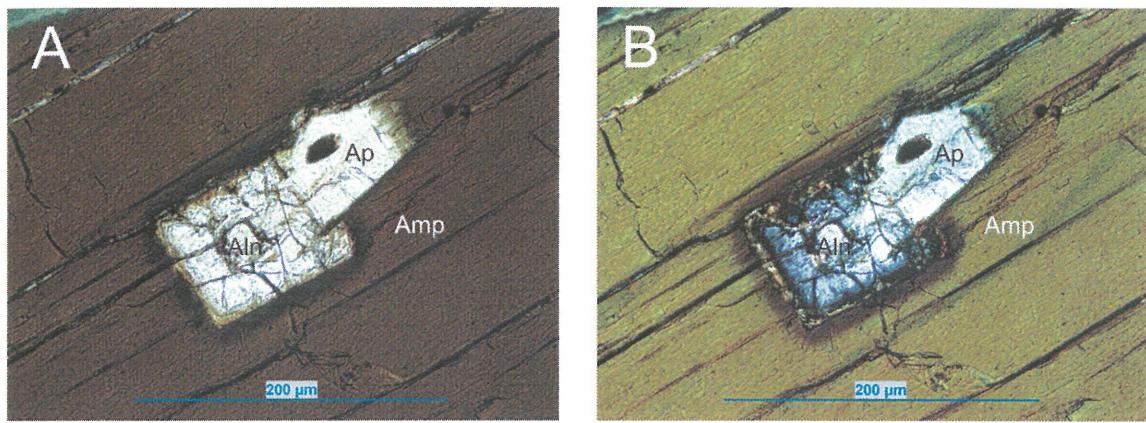
FIGURE 4.1: Photomicrographs of euhedral allanite (Aln) grown with apatite (Ap) and surrounded by amphibole (Amp) in plane-polarized (A) and cross-polarized light (B). Veinlets of monazite (brown with higher birefringence) crosscut the crystal.

Allanite is a common REM in the Railway pegmatites, is commonly mantled by chevkinite and/or monazite and contemporaneous with fergusonite (Fig. 4.2A and B). This mineral forms after ilmenite, but before apatite. Corroded allanite (Fig. 4.2D, E and F) is commonly associated with chalcopyrite, muscovite and chlorite.

Allanite from the Upper Marathon Shore pegmatites occurs in the initial-stage of crystallization and is later surrounded by interstitial quartz and sulphides, i.e. chalcopyrite and sphalerite. The allanite grain in Figure 4.2D consists of two phases both high in aluminum (16.02 and 19.15 wt. % Al_2O_3). In BSE, the lighter phase in Figure 4.2D contains higher amounts of REEs and lower titanium and calcium than the darker phase. Allanite in Figure 4.2D is associated with chlorite and muscovite, both of which are alteration minerals, indicating that this particular allanite grain has been either subjected to or a product of alteration.

In common with Coldwell allanite, compositional variations (Table 4.1) in calcium, REEs, aluminum, iron and titanium occur at other localities, i.e. the Corupá granites, Graciaso Province, southern Brazil (Vlach and Gualda 2007), Urdach massif, Western Pyrenees, France (Monchoux et al. 2006), and NYF pegmatites of the Vladislav-Pazderníkův mlýn, Czech Republic (Škoda et al. 2006). The main compositional difference between the Coldwell allanites and those from other localities is its aluminum-poor and iron-rich content.
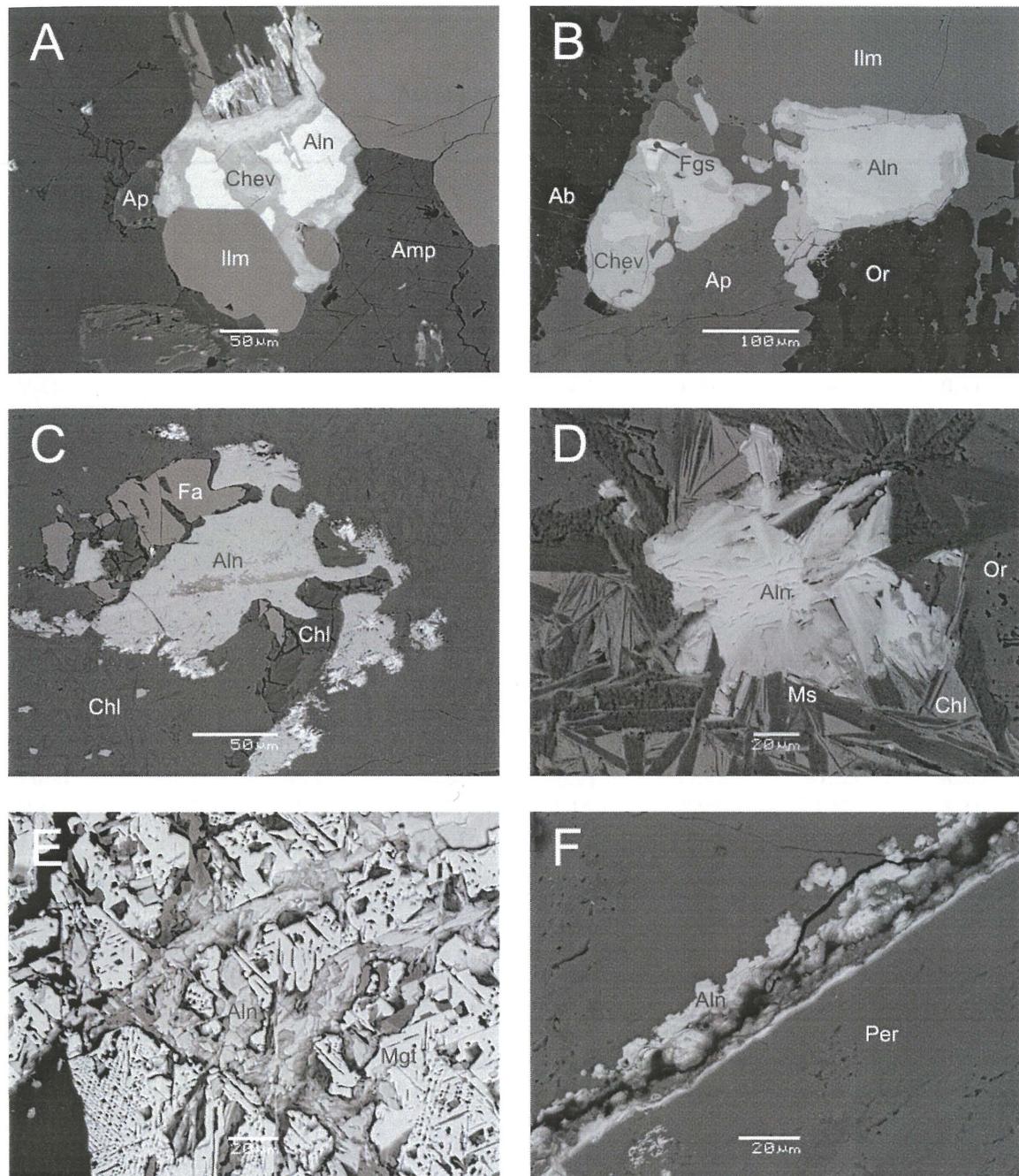
FIGURE 4.2: BSE-images of allanite (Aln). A is a mantled [by chevkinite (Chev)] allanite grain grown against two ilmenite (Ilm) grains and surrounded by amphibole. B is allanite mantled by chevkinite next to fergusonite (Fgs), apatite (Ap) and ilmenite and surrounded by albite (Ab) and orthoclase (Or). C is allanite and fayalite (Fa) in chlorite (Chl). D is allanite intergrown with muscovite and surrounded by chlorite and orthoclase. E is allanite which grew in fractured magnetite (Mgt). F is allanite along a perthite (Per) fracture.

TABLE 4.1: Representative compositions of allanite.

	Border Gabbro[1]	Railway[2]	Upper Marathon Shore[3]	Center Three[4]	Granite[5]	Albitite Dykes[6]	Granite[7]
P_2O_5	-	-	-	-	-	0.12	-
Ta_2O_5	-	-	-	-	-	0.42	-
SiO_2	30.89	31.08	32.12	32.69	29.85	30.04	31.37
TiO_2	1.46	0.89	1.14	-	1.91	0.45	1.64
ThO_2	-	-	-	-	0.10	0.25	0.44
Al_2O_3	11.61	11.86	16.02	12.45	8.51	16.33	15.45
Y_2O_3	-	-	-	-	0.16	-	0.31
La_2O_3	3.90	7.73	7.37	7.11	5.75	10.56	4.02
Ce_2O_3	9.10	12.73	12.17	11.93	12.80	14.07	12.45
Pr_2O_3	1.26	0.71	0.95	1.30	1.49	0.83	1.65
Nd_2O_3	5.57	1.55	2.40	1.65	5.30	1.77	4.96
Sm_2O_3	1.24	0.32	0.29	0.14	0.74	-	0.83
Gd_2O_3	-	-	-	-	-	-	1.11
Dy_2O_3	-	-	-	-	0.24	-	-
FeO	20.27	17.47	12.09	17.60	20.73	11.90	10.16
MgO	-	0.92	-	-	-	0.29	1.59
CaO	10.75	10.30	11.69	11.14	9.13	7.66	10.19
MnO	0.52	0.51	0.60	-	0.65	1.82	0.30
Na_2O	-	-	-	-	0.10	0.74	-
Total	**96.57**	**96.07**	**96.84**	**96.01**	**97.45**	**97.25**	**96.03**
H_2O_C	3.12	3.11	3.25	3.15	2.99	3.12	3.21
Total	**99.69**	**99.18**	**100.09**	**99.16**	**100.44**	**100.37**	**99.24**

[1] Border Gabbro pegmatite (5 analyses of sample MAS002) from the Coldwell complex.
[2] Railway pegmatite (3 analyses of sample MAS024) form the Coldwell complex.
[3] Upper Marathon Shore pegmatite (4 analyses of samples MAS018) from the Coldwell complex.
[4] Center Three pegmatite (2 analyses of sample MAS038) from the Coldwell complex.
[5] Granite (2 analyses of sample Co-2A) from the Corupá granites, Graciaso Province, southern Brazil (Vlach and Gualda 2007).
[6] Albitite dykes (sample P4-6) from the Urdach massif, Western Pyrenees, France (Monchoux et al. 2006).
[7] Granite (3rd allanite sample of Val gr) from the Vladislav-Pazderníkův mlýn pluton, Czech Republic (Škoda et al. 2006).

In Coldwell allanites, the A and M sites of the $A_2M_3(SiO_4)(Si_2O_7)O(OH)$ formula can be occupied by numerous ions; A: Ca, Mn, REE, Y, and M: Al, Fe^{3+}, Fe^{2+}, Mn, Ti, Mg. A-site vacancies have been known to occur in allanite. Because Fe^{2+}/Fe^{3+} recalculations can produce some error, the extent of A-site vacancies is difficult to determine. A list of commonly used methods for calculating Fe^{2+}/Fe^{3+} is given by Ercit (2002), with only one said to produce reliable results. This method normalizes the (M+T) site to 6 by adjusting the Fe^{2+}/Fe^{3+} until the total

number of positive charges equals 25. With Coldwell allanites, the Ercit (2002) method works well producing ionic totals from 8.502 to 8.901, which infers approximately 0.498 to 0.099 A-site vacancies (see Appendix III.I for structural formulae).

The A-site of Coldwell allanites is dominated by calcium, REEs (maximum of 0.945 apfu REEs) and vacancies. Plotting REEs against calcium, as shown in Figure 4.3A, gives an r^2 value of 0.869. Figure 4.3A also shows that the Border Gabbro and Railway allanites are enriched in REEs with reference to the Upper Marathon Shore allanites. In common with REEs and calcium, manganese may also enter the A-site (Hoshino et al. 2006). The r^2 value (0.820) in Figure 4.3B shows that Coldwell allanites are similar to other alkali complexes and do not allow manganese to preferentially enter the A-site (Hoshino et al. 2006).
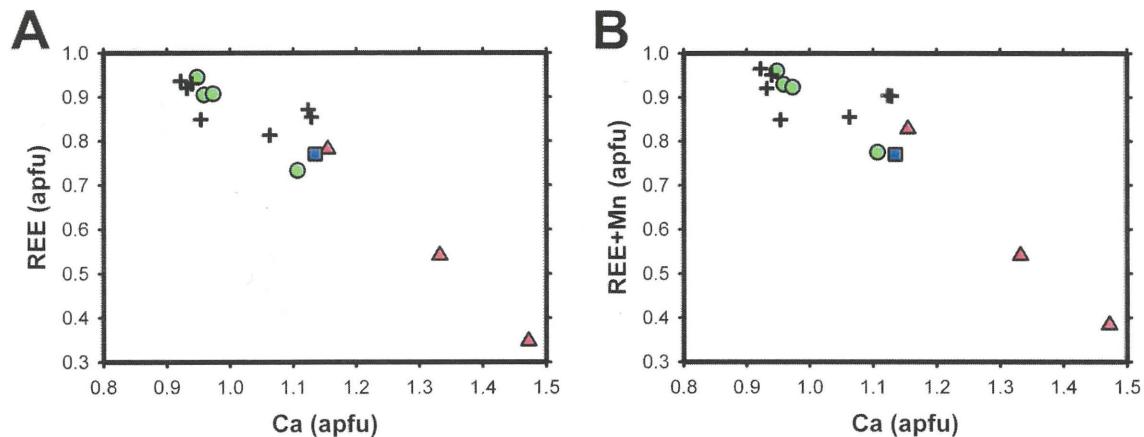
FIGURE 4.3: Allanite A-site substitution. A is calcium (Ca) vs. REEs (apfu), r^2 is 0.894. B is calcium vs. REEs and manganese (Mn) (apfu), r^2 is 0.855. Green circles, black crosses, red triangles and blue squares are the Border Gabbro, Railway, Upper Marathon Shore, and Center Three pegmatites, respectively.

The M-site of the Coldwell allanites is dominantly occupied by aluminum. Relatively small amounts of titanium (max 3.09 wt. % TiO_2), and, in one sample, minor magnesium (0.92 wt. % MgO) are also present. Coupled substitution of iron and titanium into the aluminum site or REEs and iron into the calcium and aluminum sites are mechanisms for allowing ferrous iron (Fig. 4.4) to enter the allanite structure:

$$Ti^{4+} + Fe^{2+} \rightarrow 2Al^{3+}$$

$$REE^{3+} + Fe^{2+} \rightarrow Ca^{2+} + Al^{3+}$$
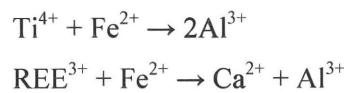
Alternatively, ferric iron can easily substitute for aluminum:

$$Fe^{3+} \rightarrow Al^{3+}$$
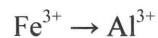
The binary diagrams in Figure 4.4 show the correlation of the M-site ions (Ti, Fe^{2+} and Fe^{3+}) with aluminum. The good correlation ($r^2 = 0.919$) in Figure 4.4A indicates that Fe^{2+}/Fe^{3+} recalculations using method 10 of Ercit (2002) are applicable to the Coldwell allanites. The addition of magnesium and manganese into Fig. 4.4B reduces the r^2 value to 0.901, indicating that these two ions are not related to aluminum.

The addition of manganese into Figure 4.3B and 4.4B increases the error. A discussion of manganese accommodation is given in Ercit (2002) who shows evidence that the ion can impartially enter both sites. No preference is shown in the Coldwell allanites, although low concentrations (0-0.60 wt. % MnO) and assumed divalent oxidation states may account for this lack of bias.
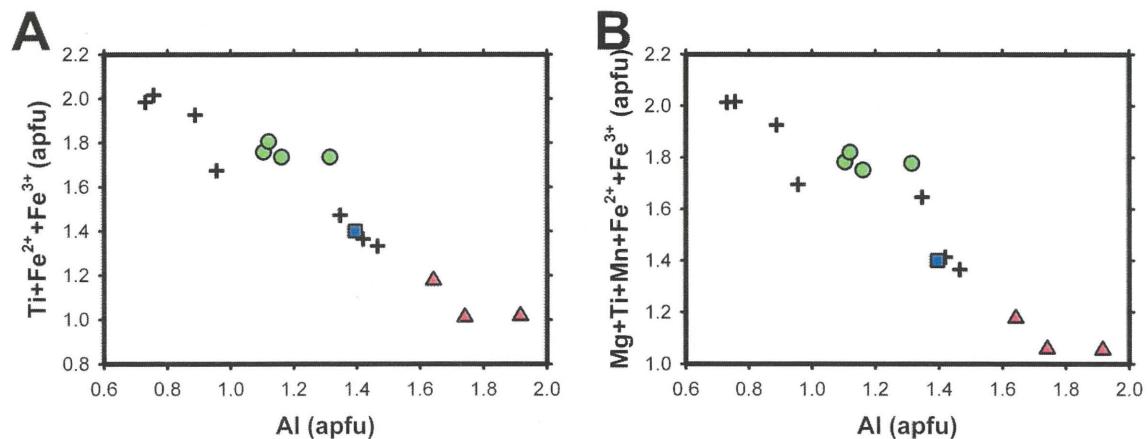
FIGURE 4.4: Allanite binary diagrams of M-site substitution. A is aluminum vs. titanium (Ti) and total iron ($Fe^{2+}+Fe^{3+}$), r^2 is 0.919. B includes magnesium and manganese into A, and results in lowering the r^2 factor to 0.901. Green circles, black crosses, red triangles and blue squares are the Border Gabbro, Railway, Upper Marathon Shore, and Center Three pegmatites, respectively.

4.3 Apatite and Britholite

Apatite is calcium phosphate [$Ca_5(PO_4)_3(F,Cl,OH)$] and occurs in all units of the Coldwell complex. Apatite precipitates in the initial stages of crystallization forming euhedral-to-anhedral discontinuously (Fig. 4.5A) and continuously (Fig. 4.5B) zoned crystals, generally on the μm to mm scale.
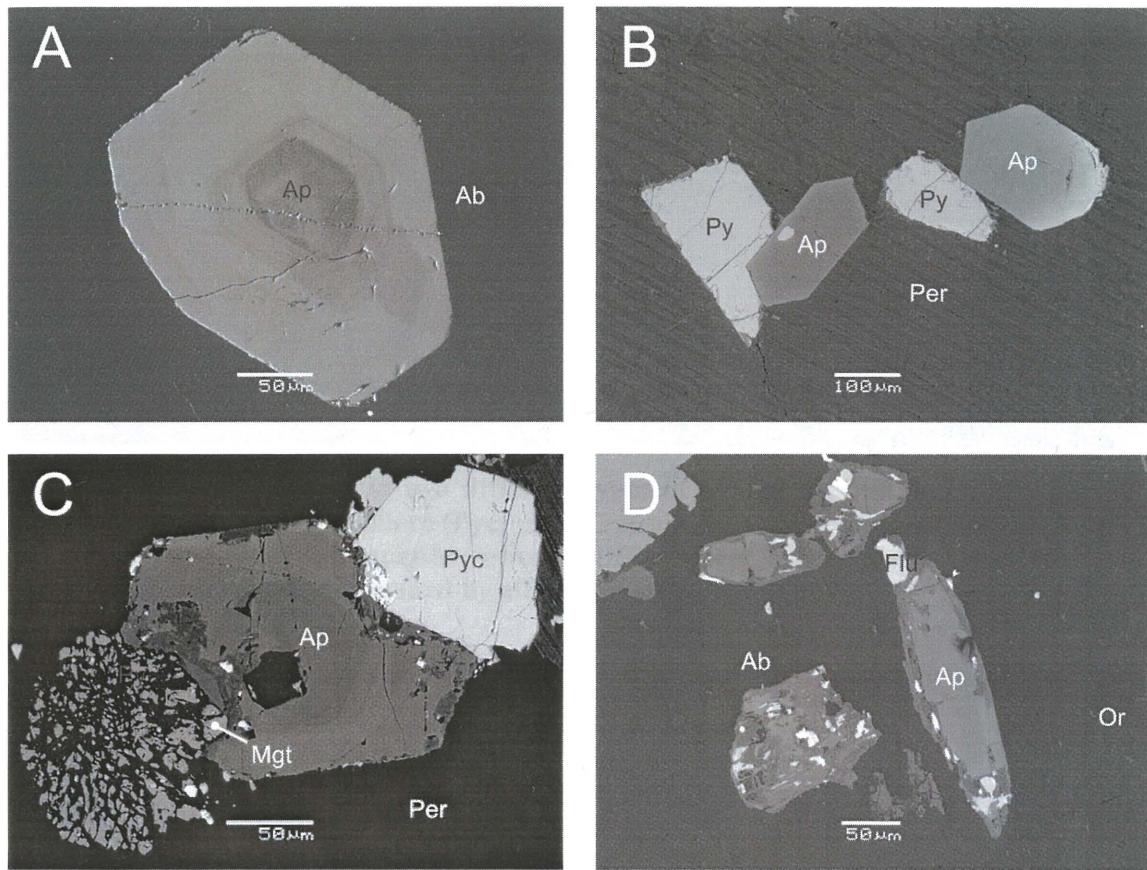
FIGURE 4.5: BSE-images of apatite (Ap). A is a zoned apatite in perthite (Per). B is apatite and pyrite (Py) surrounded by albite (Ab) and orthoclase (Or). C is apatite intergrown with pyrochlore (Pyc) and magnetite (Mgt) in perthite. D is apatite that is partially altered to fluorocarbonates (Flu) and surrounded by albite and orthoclase.

The crystal habits of Coldwell apatites can be either equant (Fig. 4.5B) or prismatic (Fig. 4.5D). Studies on apatite morphology (Wyllie et al. 1962; Höche et al. 2001a,b) suggest that equant grains are representative of equilibrium growth and elongate apatite grains predominate in supersaturated environments where diffusion is uncontrolled. Both morphologies are present in all units.

There is evidence of dissolution of apatite in some of the samples from across the Coldwell complex. This dissolution can occur early in the paragenesis, before the crystallization of cumulus minerals. Apatite that has undergone dissolution early in the paragenesis contains feldspar inclusions (Fig. 4.6A). Further dissolution is evident in either the late-interstitial or secondary phases. As apatite dissolves, the insoluble elements, i.e. REEs, are left immobile and form fluorocarbonates (Fig. 4.6B).
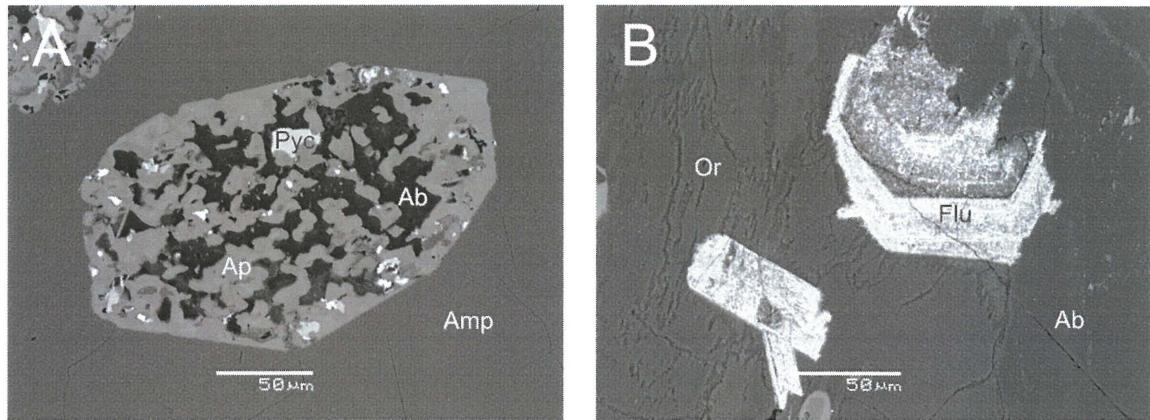
FIGURE 4.6: BSE-images of two different types of apatite dissolution. A is a partially dissolved apatite with pyrochlore (Pyc) inclusions and surrounded by amphibole (Amp). B is completely dissolved apatite whose REEs were subsequently used to form fluorocarbonates (Flu) surrounded by albite and orthoclase (Or).
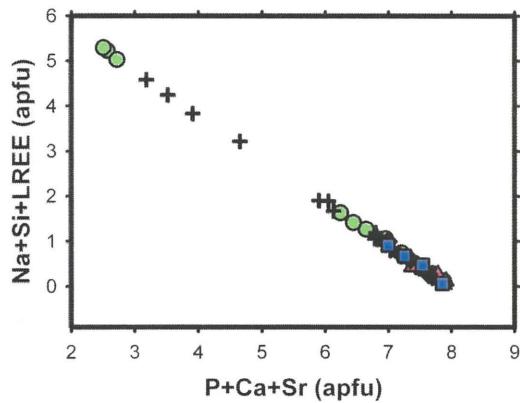
FIGURE 4.7: Apatite P+Ca+Sr / Si+Na+LREE (apfu) binary diagram, $r^2 = 0.999$. Green circles, black crosses, red triangles, black diamonds and blue squares represent the Border Gabbro, Railway, Upper Marathon Shore, Black, and Center Three pegmatites, respectively.

Apatite compositions (Table 4.2) are similar in all pegmatite units. Minor differences are mostly related to REE and silicon content. REEs increase from the Upper Marathon Shore to the Border Gabbro, that is, Upper Marathon Shore < Black < Center Three < Railway < Border Gabbro (Fig. 4.7). These differences also occur within samples and individual crystals. In crystals, concentric zoning (both continuous and discontinuous) reflect enrichment of REE, Si, and actinides. Minor amounts of iron and strontium (maximum 1.24 wt. % FeO and 0.40 wt. %

SrO) are detected in some of the samples. Significant amounts of yttrium (up to 11.19 wt. % Y_2O_3) are present in some crystals. Thorium and uranium are present in a few examples, especially if high REE and silicon are present (Table 4.3).

TABLE 4.2: Representative compositions of apatite/britholite.

	Border Gabbro[1]	Railway[2]	Upper Marathon Shore[3]	Black[4]	Center Three[5]	Nepheline Syenite[6]
P_2O_5	35.36	25.31	40.14	40.35	35.56	40.18
SiO_2	3.72	9.33	1.38	1.63	4.02	0.18
Y_2O_3	-	-	-	0.89	-	-
La_2O_3	2.06	6.64	1.16	1.89	2.28	2.69
Ce_2O_3	5.06	12.54	2.06	0.10	4.88	2.60
Pr_2O_3	0.45	1.64	0.38	0.69	0.59	-
Nd_2O_3	2.42	5.23	1.26	0.21	1.75	0.31
Sm_2O_3	0.33	1.03	0.18	-	0.34	-
CaO	47.57	35.64	50.12	52.11	48.07	47.64
FeO	-	0.61	-	0.17	0.12	-
SrO	-	-	-	-	-	3.11
Na_2O	-	-	0.54	-	-	1.00
Total	**96.97**	**97.97**	**97.22**	**98.04**	**97.61**	**97.71**
F_C	3.51	3.19	3.67	3.73	3.56	2.59
O = F	1.48	1.34	1.55	1.57	1.50	1.09
Total	**99.00**	**99.82**	**99.34**	**100.20**	**99.67**	**99.21**

[1] Border Gabbro pegmatite (5 analyses of sample MAS006) from the Coldwell complex.
[2] Railway pegmatite (2 analyses of sample MAS015) from the Coldwell complex.
[3] Upper Marathon Shore pegmatite (2 analyses of sample MAS022) from the Coldwell complex.
[4] Black pegmatite (4 analyses of sample MAS028) from the Coldwell complex.
[5] Center Three pegmatite (3 analyses from sample MAS034) from the Coldwell complex.
[6] Nepheline syenite (sample 3) from the Pilansberg alkaline complex, South Africa (Liferovich and Mitchell 2006).

One sample from the Black pegmatite contains exceptionally high (16.99 wt. % ThO_2) thorium. The crystal is metamict with an analytical total of 87.05 oxide wt. % (assuming the halogen site is completely occupied by fluorine). The high thorium crystal is mantled by thorite, and enclosed in chlorite.

Apatite adopts the hexagonal $P6_3m$ space group. Ca, Fe^{2+}, LREE, Na, Th, and U commonly occupy the A-site of Coldwell apatite; the B-site contains Si and P; and the halogen site is assumed to be completely filled by fluorine. Britholite ($LREE_{10}(Si,P)_6O_{24}(OH,F)_2$) is hexagonal, but adopts the $P6_3$ space group, which is similar to the $P6_3m$ space group of apatite

(Kalsbeek et al. 1990; Oberti et al. 2001). Because apatite and britholite are structurally similar, a solid solution between LREE and silicon occurs in the calcium and phosphorus sites:

$$LREE^{3+} + Si^{4+} \rightarrow Ca^{2+} + P^{5+}$$
                                                            Rønsbo (1989)

TABLE 4.3: Selected compositions of apatite/britholite.

	High Yttrium and Thorium[1]	High Yttrium and Thorium[2]	High Yttrium[3]	High Thorium[4]	High Iron[5]
P_2O_5	3.29	4.29	12.89	12.60	26.91
SiO_2	20.32	20.50	16.29	15.12	8.07
ThO_2	1.82	2.55	0.60	16.99	-
UO_2	0.30	0.62	-	-	-
Y_2O_3	2.99	2.93	11.19	-	1.75
La_2O_3	16.15	14.97	21.64	5.03	5.50
Ce_2O_3	26.39	24.89	2.19	10.93	10.84
Pr_2O_3	1.60	0.94	7.87	1.29	1.17
Nd_2O_3	7.96	7.21	0.98	3.46	4.06
Sm_2O_3	1.11	0.42	0.60	0.57	0.44
CaO	15.57	16.50	22.66	6.65	37.21
FeO	0.47	0.44	0.64	10.96	1.24
SrO	0.20	0.39	-	0.68	-
Na_2O	-	-	-	-	-
Total	**98.17**	**96.65**	**97.55**	**88.82**	**97.19**
F_C	2.47	2.50	2.85	2.41	3.23
$O = F$	1.04	1.05	1.20	1.01	1.36
Total	**99.60**	**98.10**	**99.20**	**87.05**	**99.06**

[1] High yttrium and thorium crystal from the Border Gabbro pegmatite (3 analyses of sample MAS002) from the Coldwell complex.

[2] High yttrium and thorium crystal from the Border Gabbro pegmatite (4 analyses of sample MAS002) from the Coldwell complex.

[3] High yttrium crystal from the Railway pegmatite (3 analyses of sample MAS028) from the Coldwell complex.

[4] High thorium crystal from the Black pegmatite (2 analyses of sample MAS029) from the Coldwell complex.

[5] High iron crystal from the Railway pegmatite (3 analyses of sample MAS027) from the Coldwell complex.

Rønsbo (1989) showed that sodium can enter the apatite structure if accompanied by LREEs:

$$LREE^{3+} + Na^+ \rightarrow 2Ca^{2+}$$
                                                            Rønsbo (1989)

Combining LREEs, silicon, and sodium and plotting against calcium and phosphorus, a negative correlation with nearly perfect r^2 value of 0.999 (Fig. 4.7) is achieved. Minor sodium (max 0.97 wt. % Na_2O) in Coldwell apatites reflect low Na/Si ratios, and, according to Rønsbo (1989), indicates that the silicon content in Coldwell pegmatites, despite being peralkaline, is high enough to prevent partitioning of sodium into the apatite structure.

The tetravalent ions (thorium and uranium) are also detected in some of the apatites. Hughson and Sen Gupta (1964) detected 5.62 wt. % ThO_2 in their britholite, thus suggesting that thorium and uranium may substitute for calcium:

$$(Th,U)^{4+} + \square \rightarrow 2Ca^{2+} \qquad \text{Hughson and Sen Gupta (1964)}$$

The precipitation of apatite from a melt has been related to silicon, phosphorus and aluminum concentrations and temperature, with equilibrium concentrations being 0.04 to 0.28 wt. % P_2O_5 at 1 kbar and temperatures from 750 to 900 °C in peralkaline systems (Watson and Capobianco 1981). With increasing aluminum in melt, the equilibrium crystallization temperature of apatite seems to decrease (Piccoli and Candela 2002).

When compared to other rock types, i.e. nepheline syenites (Liferovich and Mitchell 2006a), Coldwell apatites are sodium- and strontium-poor. Coldwell apatites are dominated by the $Ca_5(PO_4)_3X$ endmember. Although alkali-rich, the initial stage of crystallization was dominated by silicon saturation relative to sodium. The dominance of silicon is responsible for the lack of $Na_{2.5}REE_{2.5}(PO_4)_3F$ compositional trends observed.

4.4 Arsenopyrite

Arsenopyrite, FeAsS, is a trace mineral occurring in the Border Gabbro, Upper Marathon Shore, and Center Three pegmatites. This mineral forms in the late interstitial stage of crystallization with sphalerite, calcite, and galena (Fig. 4.8). Apart from iron, arsenic and sulphur, no other ions are present. Arsenopyrite is the main arsenic-bearing mineral in Coldwell pegmatites.

4.5 Astrophyllite

Trace astrophyllite group minerals form in the interstitial stage in the Border Gabbro, Railway, and Black pegmatite units (Fig. 4.9). All compositions plot in the astrophyllite subgroup (Fig. 4.10), that is, high iron relative to magnesium plus sodium and manganese. There are two astrophyllite group members (Fig. 4.11) within Coldwell pegmatites, astrophyllite and Fe-zircophyllite, the latter being an extremely rare mineral.
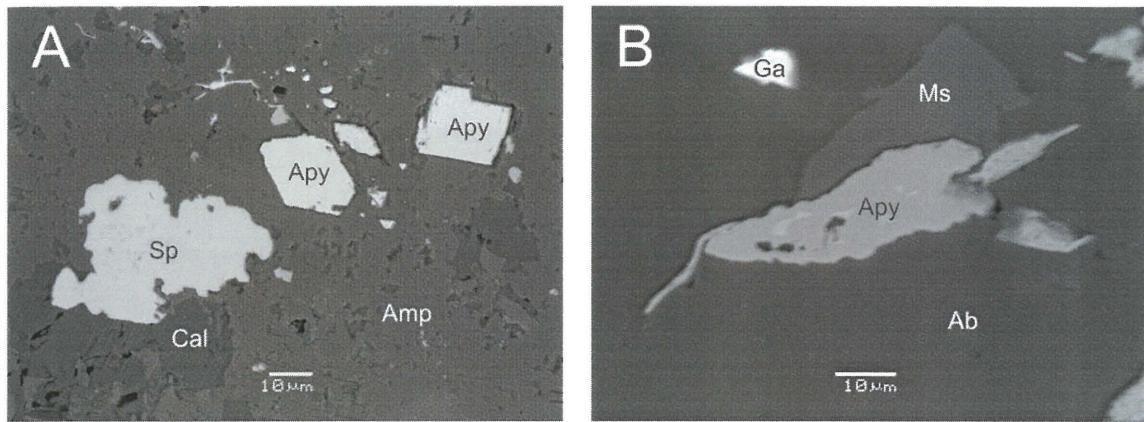
FIGURE 4.8: BSE-images of arsenopyrite (Apy). A is arsenopyrite associated with sphalerite (Sp) and calcite (Cal), and surrounded by amphibole (Amp). B is arsenopyrite associated with galena (Ga) and surrounded by muscovite (Ms) and albite (Ab).

In the Border Gabbro pegmatites, astrophyllite group minerals are present in one sample (MAS005). In this sample, the mineral is associated with amphibole, and surrounded by perthite (Fig. 4.9A). Compositionally, as seen in Figure 4.11, the crystal plots in the Fe-zircophyllite field, containing high zirconium (10.48 wt. % ZrO_2), niobium (3.76 wt. % Nb_2O_5), and titanium (2.35 wt. % TiO_2). In common with all Coldwell astrophyllite-bearing units, the Border Gabbro astrophyllite contains minor amounts of aluminum, manganese, calcium, and sodium (Tables 4.4 and 4.5).

In the Railway pegmatites, there are two samples containing astrophyllite-group minerals: one containing astrophyllite (MAS015) and the other containing Fe-zircophyllite (MAS026). In the MAS015 sample (Fig. 4.9B), astrophyllite is tabular, has cleavage parallel to elongation and is compositionally zoned. Darker areas in Figure 4.9B contain higher titanium and lower zirconium than the lighter areas, and are concentrated away from the fractures, and thus away from altering fluids,

The Fe-zircophyllite crystal in sample MAS026 is intergrown with amphibole (Fig. 4.9C). In common with the Railway astrophyllite from MAS015, MAS026 has zirconium-rich zones occurring along fractures, as seen in Figure 4.9A, but, in contrast to MAS015, niobium is also enriched.

The Black pegmatite has one sample containing Fe-zircophyllite. The crystal is tabular with cleavage parallel to elongation (Fig. 4.9D). It is associated with chlorite, calcite and Fe-

sphalerite. Given the close association with chlorite, it is likely that astrophyllite in this setting has undergone some alteration.
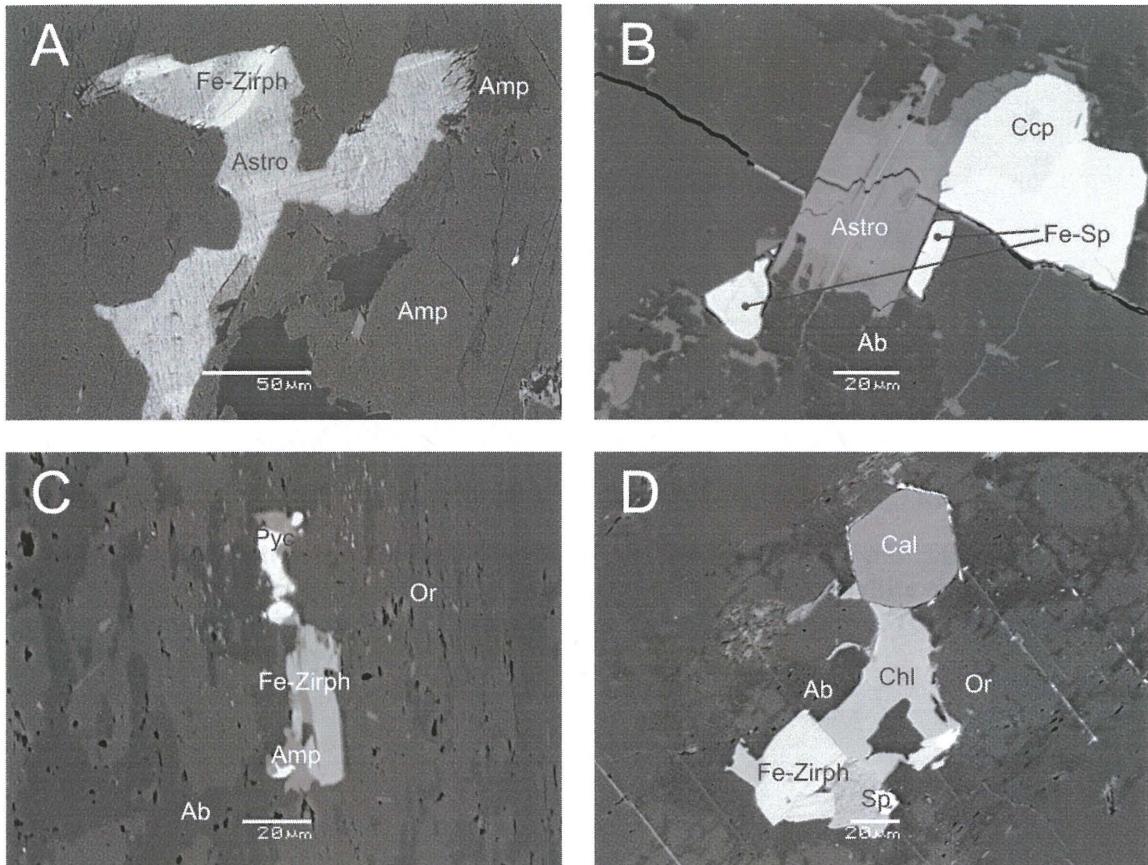
Figure 4.9: BSE-images of astrophyllite (Astro) and Fe-zircophyllite (Fe-Zirph). A contains interstitial astrophyllite with lighter Fe-zircophyllite zones set in Fe- and (Fe,Ca)-amphibole (Amp). B is astrophyllite in albite (Ab) and orthoclase (Or) with chalcopyrite (Ccp) and Fe-sphalerite (Fe-Sp). C is Fe-zircophyllite intergrown with amphibole and surrounded by albite, orthoclase and pyrochlore (Pyc). D is a euhedral Fe-zircophyllite grain surrounded by albite and chlorite.

Table 4.4 list Coldwell astrophyllite with astrophyllite from other localities, i.e. granitic pegmatites from Zomba-Malosa, Africa, pegmatite veins from Monte, Galiñeiro, Spain, and undersaturated pegmatites from Barkevik, Norway. Astrophyllite from the saturated pegmatites contain higher manganese, tantalum and tin. The undersaturated pegmatites from Barkevik, Norway also contain higher manganese and tin, but, in common with Coldwell astrophyllite, low tantalum. Coldwell potassium/sodium ratio is slightly higher than the other localities.
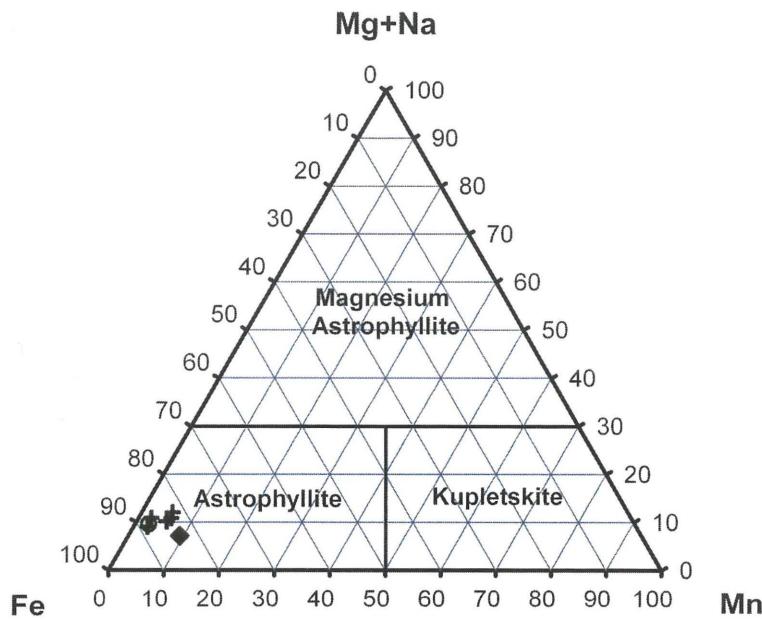
FIGURE 4.10: Astrophyllite Fe – Mg+Na – Mn (apfu) ternary plot. All astrophyllite group minerals from the Coldwell pegmatites plot in the astrophyllite subgroup. Green circles, black crosses and black diamonds are the Border Gabbro, Railway and Black pegmatites, respectively.
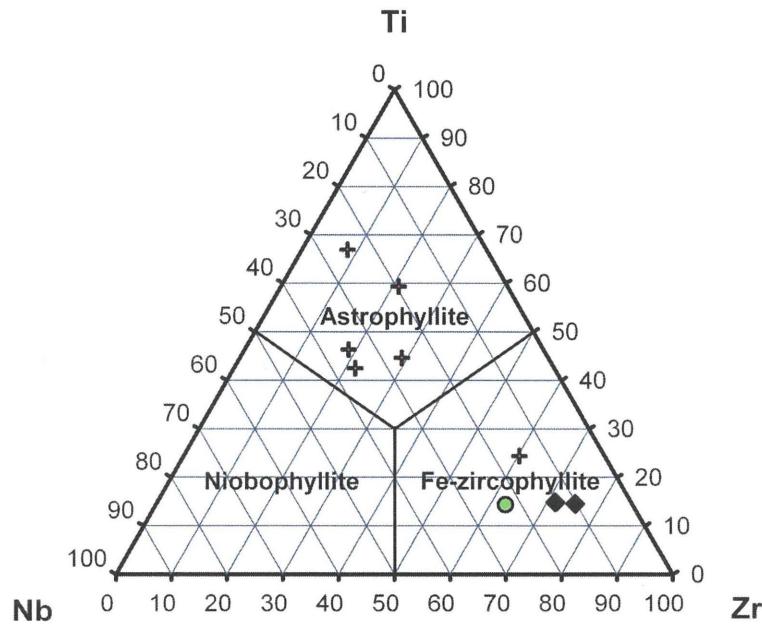
Figure 4.11: Ti – Nb – Zr (apfu) ternary plot for astrophyllite group members with iron dominating the C-site. Green circles, black crosses and black diamonds are the Border Gabbro, Railway and Black pegmatites, respectively.

TABLE 4.4: Representative compositions of astrophyllite group minerals.

	Railway[2]	Granitic Pegmatite[2]	Non-deformed pegmatite[3]	Under-saturate Pegmatite[4]
Nb_2O_5	5.07	2.03	3.45	1.07
Ta_2O_5	-	1.18	0.46	-
SiO_2	34.94	33.98	33.93	34.18
TiO_2	6.70	7.48	8.87	9.04
ZrO_2	2.69	2.59	1.60	3.70
SnO_2	-	1.80	0.38	0.14
HfO_2	-	0.18	-	-
Al_2O_3	1.18	0.44	1.46	1.54
FeO	35.89	30.03	34.01	27.62
MgO			0.19	0.97
MnO	0.95	5.17	2.10	7.41
CaO	0.11	0.52	0.82	1.43
ZnO	-	0.50	0.11	0.24
SrO	-	0.07	-	-
BaO	-	0.15	-	-
Na_2O	1.86	2.53	2.00	2.83
K_2O	5.26	5.49	4.99	5.48
Rb_2O	-	0.46	0.49	0.31
Cs_2O	-	0.10	0.19	0.15
Total	**94.65**	**94.70**	**95.05**	**96.11**
H_2O_C	2.70	2.61	2.67	2.71
F_C	1.42	1.37	1.41	1.43
O=F	0.60	0.58	0.59	0.60
Total	**98.17**	**98.10**	**98.53**	**99.65**

[1] Railway pegmatite (2 analyses of sample MAS015) from the Coldwell complex.
[2] Granitic pegmatite (6 analyses of sample AFR-1) from Zomba-Malosa, Malawi, Africa (Piilonon et al. 2003).
[3] Undeformed pegmatite (sample 8) from south of Monte Galiñeiro, Virgo, Spain (Macdonald and Saunders 1973).
[4] Undersaturated pegmatite (sample 4) from Barkevik, Langesundfjord, Norway (Macdonald and Saunders 1973).

The unusually high iron and zirconium content in the Coldwell Fe-zircophyllite is the first ever documented. The occurrence of this mineral in all three units may be related to subsequent alteration of astrophyllite. Enrichment of zirconium in MAS015 and zirconium/niobium in sample MAS026 from Railway pegmatites along fractures indicates that typical "incompatible" zirconium and niobium ions were mobile (relative to titanium) during the

interstitial or secondary crystallization stages. Astrophyllite is the only mineral to be subsequently enriched in the secondary stage of crystallization in zirconium and niobium, and makes astrophyllite the primary sink for these elements in the alteration stage of the paragenesis.

TABLE 4.5: Representative compositions of Fe-zirco-phyllite.

	Border Gabbro[1]	Railway [2]	Black[3]
Nb_2O_5	3.76	2.48	1.76
SiO_2	33.32	34.31	33.35
TiO_2	2.35	3.94	2.51
ZrO_2	10.48	9.73	12.97
Al_2O_3	1.39	1.29	1.06
FeO	34.48	34.69	33.33
MnO	0.95	2.23	3.69
CaO	1.24	1.41	2.05
Na_2O	1.62	1.71	1.23
K_2O	5.05	5.10	4.70
Total	**94.64**	**96.89**	**96.65**
H_2O_C	2.62	2.65	2.62
F_C	1.38	1.40	1.38
O=F	0.58	0.59	0.58
Total	**98.06**	**100.35**	**100.07**

[1] Border Gabbro pegmatite (5 analyses of sample MAS005) from the Coldwell complex.
[2] Railway pegmatite (4 analyses of sample MAS026) from the Coldwell complex.
[3] Black pegmatite (2 analyses of sample MAS032) from the Coldwell complex.

The monoclinic structure (Piilonen et al. 2003) of Coldwell astrophyllite can be described as $A_2BC_7D_2T_8O_{26}(OH)_4X_{0-1}$, and includes K, Na and □ in the A-site; Ca and Na in the B-site; Fe^{2+}, Mg, Mn, and Na in the C-site; Nb, Ti and Zr in the D-site; and Al and Si in the T-site. Iron is extremely high, such that $Fe/(Fe+Mn) \geq 0.89$. Simple substitutions include:

$(K,Na)^+ \rightarrow A^+$

$(Mg,Mn,Fe)^{2+} \rightarrow C^{2+}$
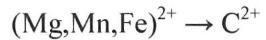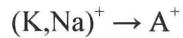
Coupled substitution of sodium and niobium is similar to the substitution described by Macdonald et al. (2007):
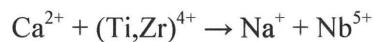
$Ca^{2+} + (Ti,Zr)^{4+} \rightarrow Na^+ + Nb^{5+}$ 　　　　　　　　　Macdonald et al. (2007)

As shown in Figure 4.12, substitution of sodium and niobium for calcium, titanium and zirconium gives a good correlation (r^2 value of 0.929). Variation in the sodium plus niobium substitution plot (Piilonen et al. 2000), is related to a coupled substitution between fluorine and oxygen, that is:
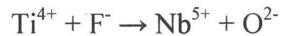
$$Ti^{4+} + F^- \rightarrow Nb^{5+} + O^{2-}$$
<div align="right">Piilonen et al. (2000)</div>
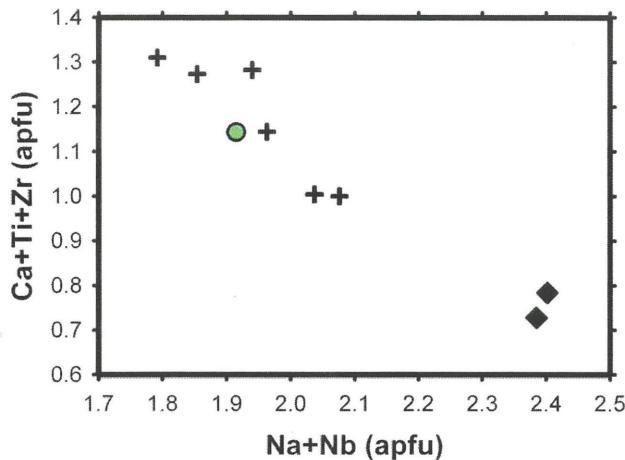
FIGURE 4.12: Astrophyllite Na+Nb / Ca+Ti+Zr (apfu) binary plot. R^2 = 0.929. Green circle, black crosses and black diamonds are Border Gabbro, Railway and Black pegmatite units, respectively.

As fluorine is not determined using the analytical setup, it is not possible to tell if fluorine varies to accommodate niobium.

In Coldwell astrophyllite, the $K_2(Na,Ca)-(Fe^{2+},Mn)_7(Zr,Nb)_2Si_8O_{26}(OH)F$ formula of Fe-zircophyllite suggested by Pilonen et al. (2003) is oversimplified. In Coldwell astrophyllite, potassium does not occupy two structural sites (see calculated ionic proportions in Appendix III.III) and titanium is present in appreciable concentrations (2.35 - 6.88 oxide wt. %). Thus, the expanded formula $(K,Na,Ca)_3(Fe^{2+},Mn)_7(Zr,Nb,Ti)_2Si_8O_{26}(OH)F$ is suggested for this study.

The work of Macdonald and Saunders (1973) suggests that substitution of Na for K is related to silica content such that high potassium/sodium ratios are generally found in undersaturated rocks. This relationship indicates that the Black pegmatites are saturated when compared with the Border Gabbro and Railway pegmatites. Alternatively, since niobium correlates to sodium, increases in sodium may be dependant on Nb-Ti-Zr activities. A high zirconium content in astrophyllite minerals indicates that residual melts which produced the pegmatites had very high alkalinities.

4.6 Baddeleyite

Baddeleyite, or ZrO_2, is present in all pegmatite units. In polarized light, baddeleyite has a high relief, brown pleochroism, and second order birefringence (Fig. 4.13). Common ions for which the baddeleyite structure accommodates are hafnium and iron, and less frequently, tantalum, silicon and titanium (Table 4.6). Crystals are euhedral-to-anhedral, and occur with a variety of minerals, namely ilmenite, magnetite, monazite, pyrochlore, zircon, and zirconolite (Fig. 4.14).
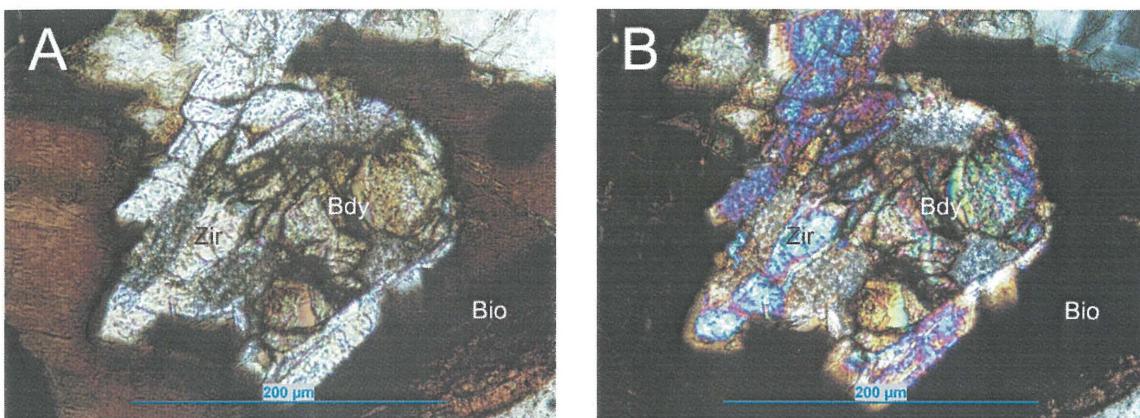
FIGURE 4.13: Photomicrographs of baddeleyite (Bdy) mantled by zircon (Zir) and surrounded by biotite (Bio). A is plane-polarized, B is cross-polarized.

Baddeleyite is commonly mantled and/or intergrown with zircon (Figs. 4.13 and 4.14A,D). Primary baddeleyite intergrown with zircon can be used to constrain either temperature or oxygen fugacity, as each mineral has a limited stability when associated with the other (see Petrogenesis Chapter).

The paragenesis of baddeleyite between units is not always the same. In the Border Gabbro baddeleyite forms after pyrochlore and magnetite, whereas in the Railway, Upper Marathon Shore, Black and Center Three pegmatites baddeleyite begins precipitation before the commencement of pyrochlore and magnetite precipitation. There is also significant corrosion of baddeleyite grains in Railway pegmatites that is not observed in the other units.

The breakdown of zircon can produce baddeleyite as a product:

$$(Ca,Mg)CO_3 + ZrSiO_4 \rightarrow ZrO_2 + CaMgSi_2O_6 + CO_2 \qquad \text{Rizvanova et al. (2000)}$$

The reaction quoted by Rizvanova et al. (2000) is not observed in Coldwell pegmatites, as no diopside is present and would require all calcium, magnesium, silicon and carbon to be
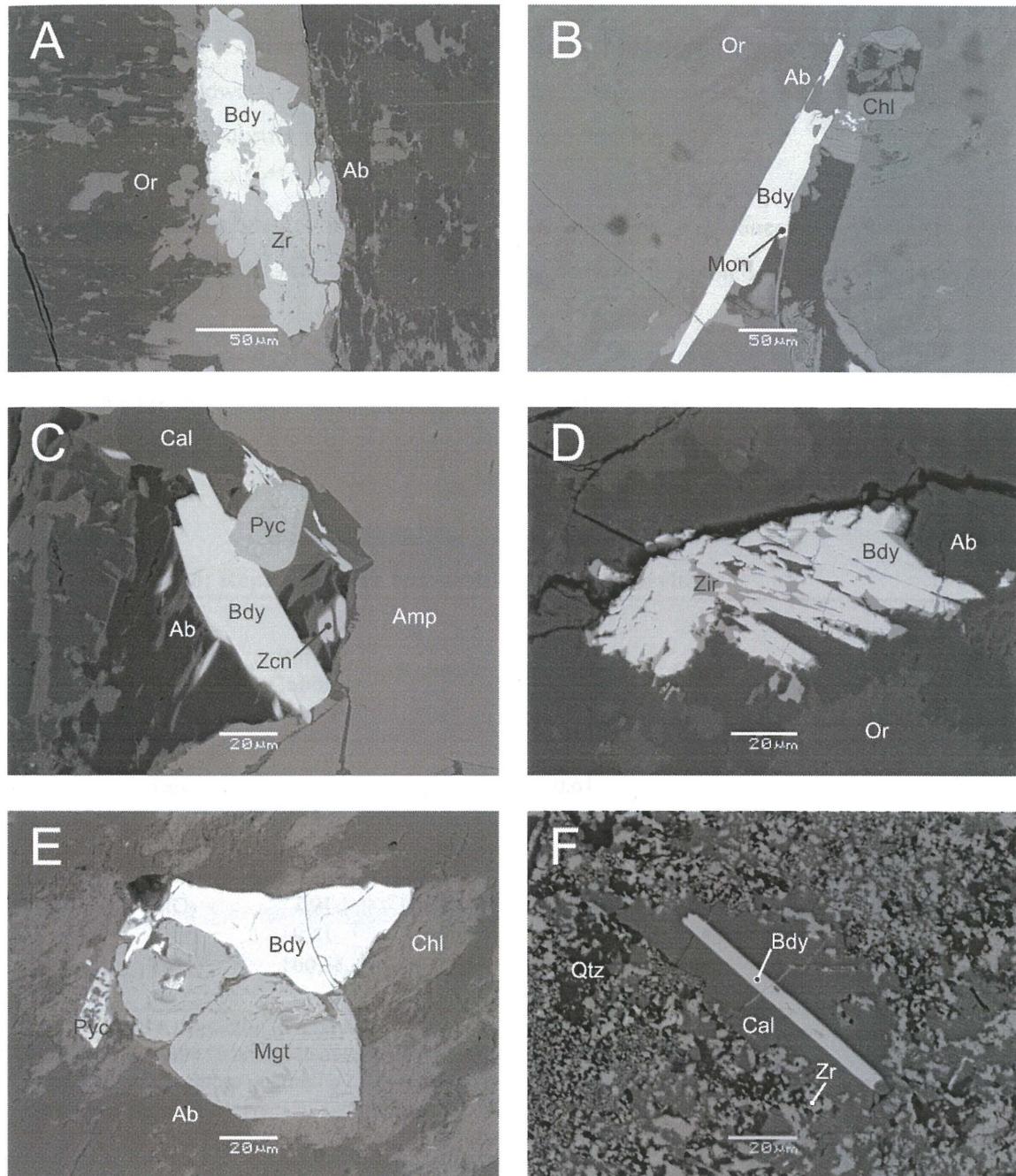
FIGURE 4.14: BSE-images of baddeleyite (Bdy). A is baddeleyite surrounded by zircon (Zir), albite (Ab) and orthoclase (Or). B is baddeleyite with monazite (Mon) growing onto it, and surrounded by albite, orthoclase, chlorite (Chl), and quartz (Qtz). C is baddeleyite grown onto pyrochlore (Pyc), and surrounded by albite, calcite (Cal), amphibole (Amp) and zirconolite (Zcn). D is radial baddeleyite intergrown with zircon and surrounded by albite and orthoclase. E is baddeleyite grown with magnetite (Mtg) and pyrochlore, and surrounded by albite and chlorite. F is euhedral baddeleyite grown in calcite.

taken up into solution. Euhedral crystals encased by cumulus-forming minerals and intergrown zircon-baddeleyite textures indicate that most, if not all, baddeleyite is primary.

In the Coldwell pegmatites, the baddeleyite Zr-site accommodates Ca, Fe^{3+}, Fe^{2+}, Hf, Si, Ta, and Ti. Simple substitutions account for the tetravalent ions:

$$(Hf, Si, Ti)^{4+} \rightarrow Zr^{4+}$$
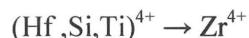
The accommodation of tantalum requires trivalent ions to balance the crystal lattice. The only possibility is, at least in the tantalum-bearing baddeleyites, some of the iron is in its ferric state:

$$Fe^{3+} + Ta^{5+} \rightarrow 2Zr^{4+}$$
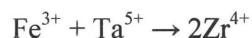
As for the divalent ions (calcium and iron), the structure requires a vacancy to remain electrically neutral:

$$2(Ca, Fe)^{2+} \rightarrow Zr^{4+} + \square$$
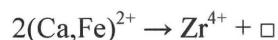
TABLE 4.6: Representative compositions of baddeleyite.

	Border Gabbro[1]	Railway[2]	Upper Marathon Shore[3]	Black[4]	Center Three[5]
Ta_2O_5	-	-	0.61	-	-
SiO_2	0.41	-	-	0.16	-
TiO_2	-	-	0.18	-	-
ZrO_2	97.63	98.84	95.89	98.26	98.55
HfO_2	1.91	0.81	1.87	1.06	1.26
FeO	0.41	1.02	0.55	0.53	0.39
Total	**100.36**	**100.67**	**99.10**	**100.01**	**100.20**

[1] Border Gabbro pegmatite (4 analyses of sample MAS006) from the Coldwell complex.
[2] Railway pegmatite (5 analyses of sample MAS016) from the Coldwell complex.
[3] Upper Marathon Shore pegmatite (3 analyses of sample MAS018) from the Coldwell complex.
[4] Black pegmatite (4 analyses of sample MAS031) from the Coldwell complex.
[5] Center Three syenite pegmatite (5 analyses of sample MAS036) from the Coldwell complex.

4.7 Barite

Barite, $BaSO_4$, occurs in the Border Gabbro, Railway, Upper Marathon Shore and Center Three pegmatite units. All barite precipitates in the late interstitial stage and forms elongate tabular crystals generally in the mm range (Fig. 4.15) or anhedral vein-like textures if constrained by grain boundaries. Although only present in 4 samples, when barite does occur, it is generally concentrated into relatively high volumes.
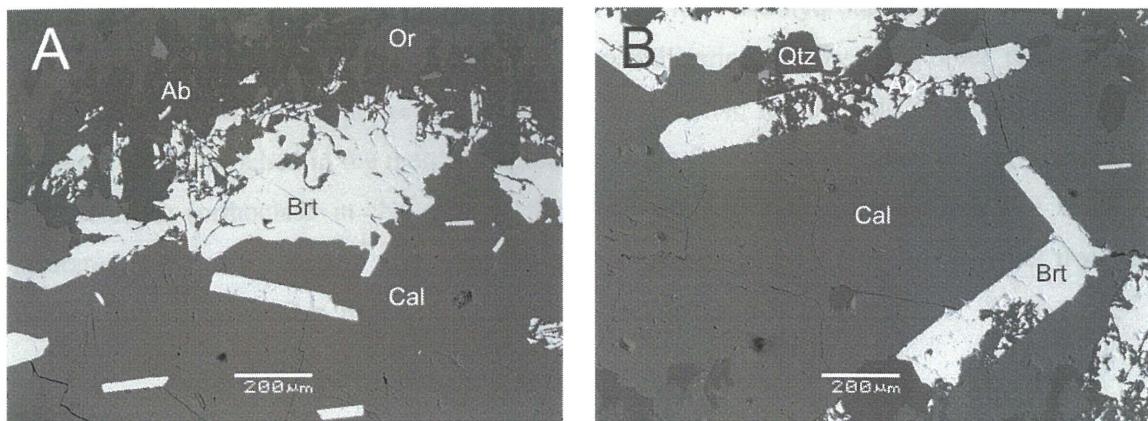
FIGURE 4.15: BSE-images of barite (Brt). A is barite that has precipitated along an albite (Ab)/orthoclase (Or) grain boundary and then surrounded by calcite (Cal). B is barite surrounded by quartz (Qtz) and calcite.

Strontium is a minor element found in Coldwell barite (Table 4.7). The *Pnma* structure of barite is isostructural with celestite ($SrSO_4$), thus allowing strontium to easily substitute for barium:

$$Sr^{2+} \rightarrow Ba^{2+}$$

TABLE 4.7: Representative compositions of barite.

	Border Gabbro[1]	Railway[2]	Upper Marathon Shore[3]	Center Three[4]
SO_3	23.11	34.29	34.94	34.72
CaO	-	-	-	0.65
SrO	0.62	1.71	1.18	0.29
BaO	63.89	63.59	64.15	64.41
Total	**99.62**	**100.27**	**99.59**	**100.07**

[1] Border Gabbro pegmatites (4 analyses of sample MAS012) from the Coldwell complex.
[2] Railway pegmatite (3 analyses of sample MAS023) from the Coldwell complex.
[3] Upper Marathon Shore pegmatites (4 analyses of sample MAS018) from the Coldwell complex.
[4] Center Three pegmatite (4 analyses from sample MAS037) from the Coldwell complex.

In one sample (MAS037) calcium is present, and, in common with strontium, enters the barite structure by simple substitution:

$$(Ca,Sr)^{2+} \rightarrow Ba^{2+}$$
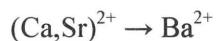
Barium and strontium are very soluble in both melt and hydrothermal mediums, and do not normally reach saturation early on in the crystallization history. The order that feldspar precipitates can affect whether or not barite will be available for the fluid phase (Hanor 2000). Barium will be enriched in the melt if plagioclase is the first of the feldspars to precipitate. But, if K-feldspar (orthoclase in the case of the Coldwell pegmatites) crystallizes and water is saturated, most of the barium will enter the K-feldspar structure (Hanor 2000). Apart from the Border Gabbro pegmatites, barium is below the detection limits in all feldspars.

4.8 Chalcopyrite

Chalcopyrite is a trace sulphide occurring in the Border Gabbro, Railway and Upper Marathon Shore pegmatites. The mineral is commonly concentrated into anhedral aggregates within the pegmatites. Sampling may have missed the mineral in the Black and Center Three units. The mineral forms in the late interstitial stage of crystallization with sphalerite (Fig. 4.15). Coldwell chalcopyrite does not contain any ions other than iron, copper and sulphur.
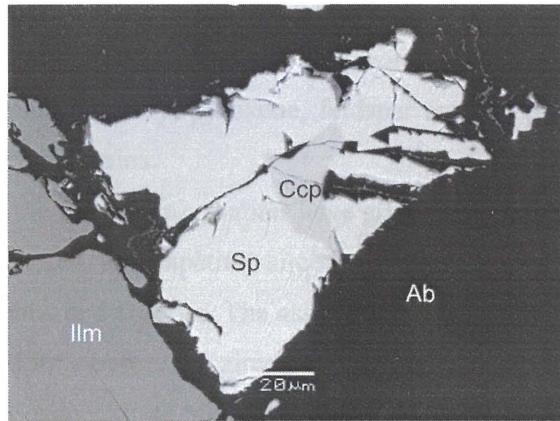
FIGURE 4.16: BSE-image of chalcopyrite (Ccp) associated with sphalerite (Sp) and surrounded by albite (Ab) and ilmenite (Ilm).

4.9 Chevkinite

Chevkinite in the Coldwell pegmatites form tabular euhedral-to-anhedral yellow, brown and red pleochroic crystals (Fig. 4.17). Chevkinite is observed in two of the pegmatite units: the Border Gabbro and Railway pegmatites. In both units, nearly all chevkinite grains are altered to some degree. This alteration is most pronounced along grain boundaries and fractures, indicating that the alteration is secondary.
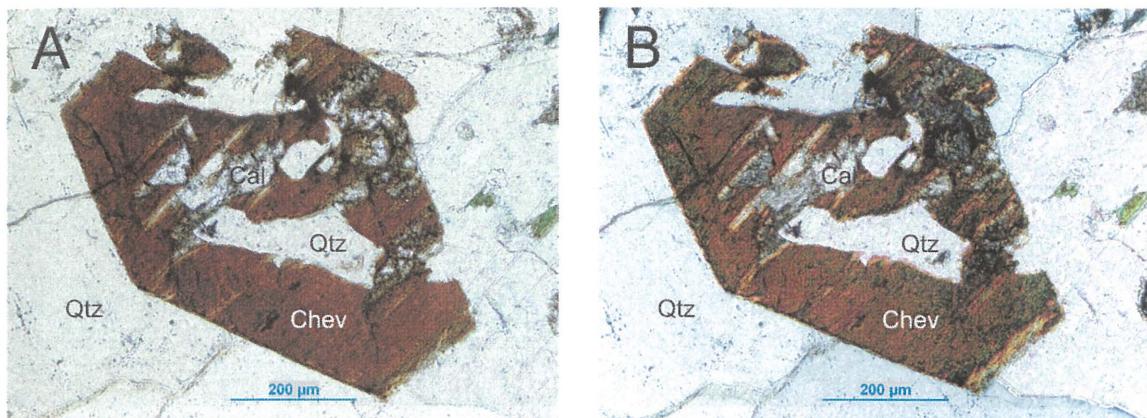
FIGURE 4.17: Photomicrographs of chevkinite (Chev) with quartz (Qtz) and calcite (Cal) inclusions and surrounded by quartz in plane-polarized (A) and cross-polarized (B) light.

In Border Gabbro pegmatites, chevkinite forms euhedral-to-anhedral grains ranging in size from 2.8 mm - 20 μm. In terms of composition, the Border Gabbro chevkinites contain more calcium than that of the Railway pegmatites, but otherwise the compositions are very similar (Table 4.8). Chevkinite is intimately associated with ilmenite and apatite, enclosed by feldspar, pyroxene and chlorite, and altered to rutile and fluorocarbonates. Both ilmenite and magnetite form before chevkinite. Subsequently, pyroxene, feldspar and the precursor to chlorite (likely biotite) enclose the chevkinite grains.

Chevkinite from the Railway pegmatites have grain sizes ranging from 25 μm – 460 μm. Here, chevkinite is associated with apatite, zircon and fluorocarbonates, and surrounded by amphibole, feldspar, olivine, and chlorite. The association with zircon, as seen in Figure 4.18A, indicates that chevkinite forms before the zircon and its inclusions (thorite, galena, etc.). Figure 4.18A also shows an apatite/chevkinite boundary that is indicative of chevkinite before apatite.

The compositions of chevkinite from Coldwell pegmatites are similar to those in other saturated A-type intrusions. As seen in Table 4.8, both the quartz syenite from Cape Ashizuri complex, Shikoku Island, Japan (Imaoka and Nakashima 1994) and the Corupá granites of the Graciaso Province, southern Brazil (Vlach and Gualda 2007) closely resembles the unaltered Coldwell chevkinites. In contrast, undersaturated bodies, such as the nepheline syenites of the Chilwa complex, Malawi (Platt et al. 1987), are REE-poor and titanium- and calcium-rich relative to Coldwell chevkinites.
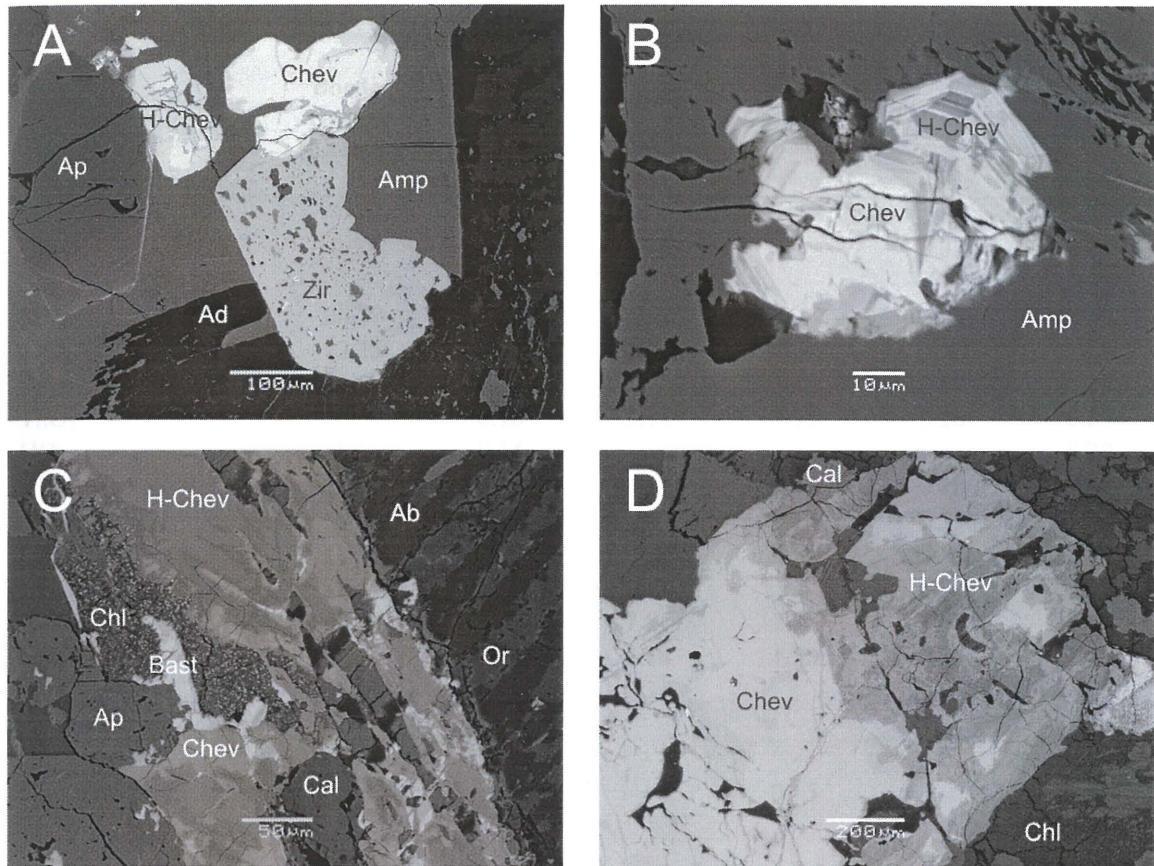
FIGURE 4.18: BSE-images of selected chevkinite (Chev) grains. A is chevkinite and hydrous variety (H-Chev) associated with zircon (Zir) and apatite (Ap), and enclosed by albite (Ab) and amphibole (Amp). B is chevkinite with the hydrous variety zoning the crystal. C is chevkinite associated with apatite and partially decomposing into bastnaesite (Bast). D is a large chevkinite grain in calcite (Cal) and chlorite that has undergone extensive alteration in the upper right half.

Alternatively, altered chevkinite from Coldwell pegmatites closely resemble chevkinite from undersaturated localities (Table 4.8). There is an alteration pattern which emerges from plotting a $CaO+SrO+MgO+Al_2O_3$ - Sum La_2O_3-Sm_2O_3 - FeO^* ternary plot (Fig. 4.19). All unaltered analyses plot in the evolved oversaturated field. As alteration increases, shown by the red arrow in Figure 4.18, a trend moving towards, and past, the evolved undersaturated field occurs. This illustrates that the amount of REEs leached is relatively small, compared to the leaching of iron.

TABLE 4.8: Representative compositions of chevkinite and its altered variety.

	Border Gabbro[1]	Border Gabbro (altered)[2]	Railway[3]	Railway (altered)[4]	Quartz Syenite[5]	Granite[6]	Nepheline Syenite[7]
Nb_2O_5	1.15	0.32	1.52	3.16	-	0.33	8.20
Ta_2O_5	-	-	-	-	-	-	0.33
SiO_2	19.49	20.77	19.37	15.72	19.49	19.76	27.80
TiO_2	16.93	23.25	18.22	18.42	16.98	19.52	29.20
ZrO_2	1.28	0.24	0.26	-	-	0.88	0.59
ThO_2	-	-	0.70	3.17	3.55	0.26	0.89
UO_2	-	0.71	0.14	-	-	-	0.28
Al_2O_3	0.55	0.71	0.25	0.27	0.10	0.18	0.68
Y_2O_3	-	-	-	-	-	0.37	3.33
La_2O_3	6.30	9.09	13.57	15.04	23.75	13.44	0.54
Ce_2O_3	21.15	18.69	23.05	21.16	19.63	22.65	2.97
Pr_2O_3	3.24	2.48	2.06	1.84	2.36	2.02	0.56
Nd_2O_3	12.12	6.15	5.88	4.48	1.52	6.24	4.49
Sm_2O_3	2.05	0.23	0.75	0.31	-	0.55	0.78
Eu_2O_3	-	-	-	-	-	-	0.35
Gd_2O_3	-	-	-	-	-	0.28	0.84
Dy_2O_3	-	-	-	-	0.15	-	0.75
Er_2O_3	-	-	-	-	-	-	0.40
Yb_2O_3	-	-	-	-	-	-	0.31
Fe_2O_3	4.16	-	1.63	-	-	-	-
FeO	7.99	6.50	10.09	3.88	9.13	10.41	8.47
MnO	-	0.23	-	0.26	-	0.20	0.28
CaO	2.79	3.12	2.04	0.51	2.09	2.97	8.43
SrO	-	-	-	-	0.28	-	-
Total	**99.20**	**92.49**	**99.53**	**88.22**	**99.03**	**100.06**	**100.47**

[1] Border Gabbro pegmatite (5 analyses of sample MAS005) from the Coldwell complex.
[2] Border Gabbro pegmatite (3 analyses of sample MAS007) from the Coldwell complex.
[3] Railway pegmatite (6 analyses of sample MAS016) from the Coldwell complex.
[4] Railway pegmatite (3 analyses of sample MAS015) from the Coldwell complex.
[5] Quartz Syenite (sample 1) from the Cape Ashizuri complex, Shikoku Island, Japan (Imaoka and Nakashima 1994).
[6] Granite (6 analyses of sample Co-3B) from the Corupá granites, Graciaso Province, southern Brazil (Vlach and Gualda 2007). Values under 0.1 wt. % omitted.
[7] Nepheline syenite (2 analyses of sample A,D) from the Chilwa complex, Malawi (Platt et al. 1987).

In altered leucosyenites of the Shuiquangou syenitic province, alteration produces an allanite-ilmenite-titanite-epidote-quartz corona (Jiang 2006). This is not observed in Coldwell chevkinites, instead associations indicate that breakdown of chevkinite is a two-stage process. The first being hydration of chevkinite and desilicification, followed by saturation with

carbonate and fluorine to produce fluorocarbonates, quartz, magnetite, and Nb-rutile and/or Nb-ilmenite:

$(REE,Ca)_4Fe(Fe,Nb)_2Ti_2Si_4O_{22} + 4CO_2 + 4F^- \rightarrow 4(REE,Ca)(CO_3)F + 4SiO_2 + Fe_2O_3 + 3(Ti,Nb)O_2 + OH^-$

Chevkinite   Bastnaesite   Quartz Magnetite Ilmenite
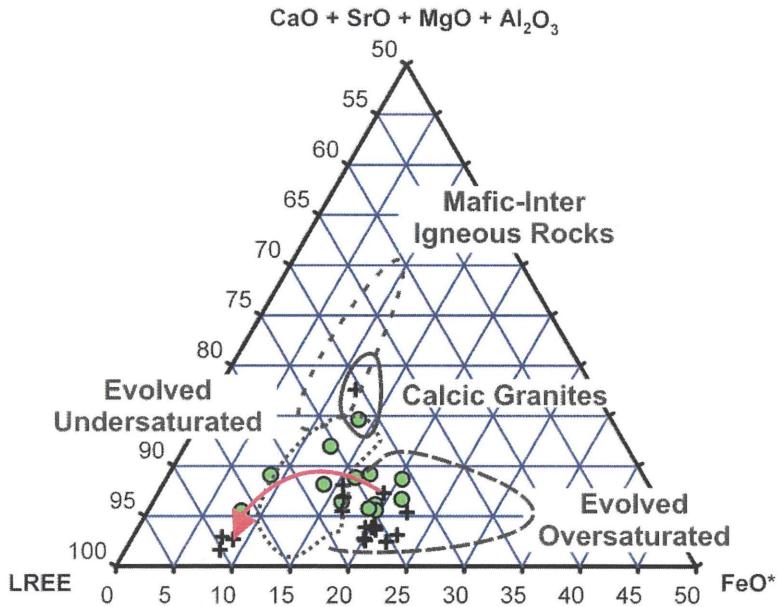
FIGURE 4.19: Chevkinite CaO+SrO+MgO+Al$_2$O$_3$ – Sum La$_2$O$_3$-Sm$_2$O$_3$ – FeO* ternary diagram (oxide wt. %) with CaO+SrO+MgO+Al$_2$O$_3$ and FeO* reduced to 50 %. All unaltered chevkinite analyses plot in the evolved oversaturated field, while altered analyses follow a trend (shown by the red arrow) past the evolved oversaturated field. Designated fields taken from Macdonald and Belkin (2002). Green circles are Border Gabbro, black crosses are Railway pegmatites.

The mineral perrierite is commonly mistaken for chevkinite, as it has similar composition and structure. It has been shown, initially by Lima-de-Faria (1962) and subsequently by Mitchell (1966) that with increasing temperature and fO_2, perrierite undergoes a phase change to chevkinite. A common method, used initially by Calvo and Faggiani (1974) to distinguish between these two minerals is the Si-O-Si angle, chevkinite being 157.5° and perrierite 165.5°. Other studies (de Hoog and van Bergen 2000) associate the phase change with composition. Chevkinite generally contains more iron and less calcium than perrierite. The minerals can be distinguished by plotting FeO* against CaO. Figure 4.20A, indicates that minerals in the Coldwell pegmatites with the A$_4$BC$_4$O$_8$(Si2O$_7$)$_2$ formula have both the chevkinite

and perrierite compositions. On closer inspection, all altered $A_4BC_4O_8(Si2O_7)_2$-type minerals fall into the perrierite subcategory, while all unaltered $A_4BC_4O_8(Si2O_7)_2$-type minerals fall into the chevkinite subcategory. Figure 4.20B contains all $A_4BC_4O_8(Si2O_7)_2$-type minerals with total oxides above 95%.
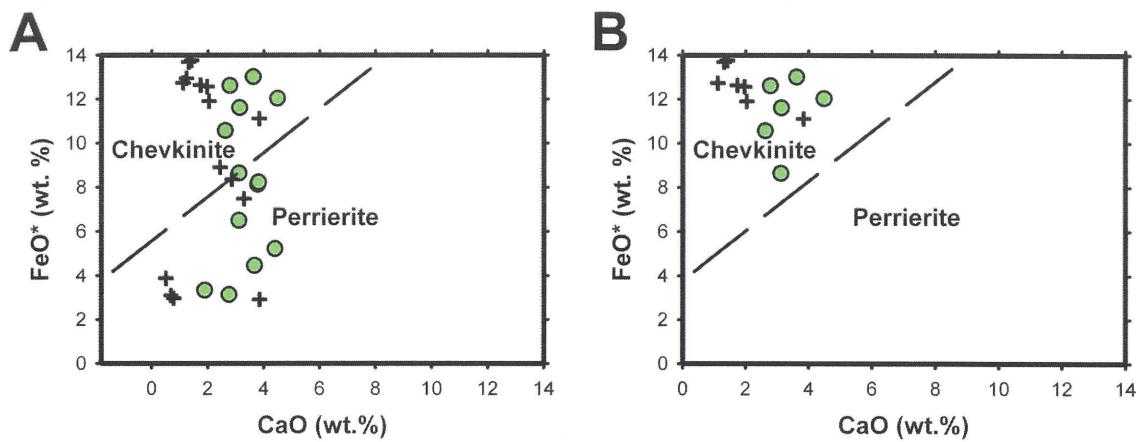
FIGURE 4.20: Chevkinite FeO* / CaO discriminant plots. A includes all chevkinite grains analyzed; B contains analyses that have total oxide wt. % above 95. Green circles represent the Border Gabbro pegmatites, black crosses depict Railway pegmatites.

All examples of Coldwell chevkinite are of the iron-rich variety. Thus, the B-site is completely filled with iron. Significant iron is also present in the C-site. Recalculations were preformed following Parodi et al. (1994). The method fills the tetrahedral site to a total of 4.0 with silicon, and aluminum if needed; the B-site is then filled with ferrous iron and the remainder with magnesium (this was not performed as no magnesium was detected in any of the samples); the Ti-site is then filled to 2.0 with titanium; any excess aluminum, iron and titanium along with niobium, zirconium and manganese are then assigned to the C-site, with Fe^{2+}/Fe^{3+} recalculated using the methodology of Droop (1987); and REE, calcium, thorium, and uranium are assigned to the A-site.

Chevkinite in the Coldwell complex can be expressed by the formula $A_4Fe^{2+}C_2Ti^{4+}_2Z_4O_{22}$, where the A-site can be any of Ca^{2+}, REE^{3+}, Th^{4+} and U^{4+}; the C-site can be Mn, Ti, Fe^{2+}, Fe^{3+}, Al^{3+}, Zr, and Nb^{5+}; and the Z-site can include either Si and/or Al. The structure of the Fe-rich variety of chevkinite adopts a *C2/m* space group, and consists of two sets of sheets: an octahedra sheet, and Si/Fe-site tetrahedra sheet with rare earth and large atoms situated in the nine coordinated A-sites (Song et al. 1999). Although Macdonald and Belkin (2002) concluded that there was no universal balancing scheme for chevkinite, some substitution

correlations do occur in Coldwell pegmatites. The main substitution scheme, according to McDowell (1979) and Macdonald and Belkin (2002), is calcium, titanium and zirconium substituting for REE, aluminum and iron:
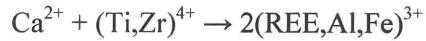
$$Ca^{2+} + (Ti,Zr)^{4+} \rightarrow 2(REE,Al,Fe)^{3+}$$ McDowell (1979)

This mechanism is illustrated in Figure 4.21A. Deviation from the 1:1 ratio is likely related to selective leaching. The relationships between some of the major ions and total wt. % are shown in Figure 4.21. A correlation between calcium and zirconium has been observed by Macdonald and Belkin (2002), but is not apparent, as seen in Figure 4.21B, in Coldwell chevkinite. There is a negative correlation between the total oxide wt. % and titanium (Fig. 4.22A), positive correlations between the total oxide wt. % and ferric/ferrous iron (Fig. 4.22B) and REEs (Fig. 4.22C), and no correlation between the total oxide wt. % and calcium (Fig. 4.22D). These correlations are similar to those from the Shuiquangou syenitic intrusion (Jiang 2006).
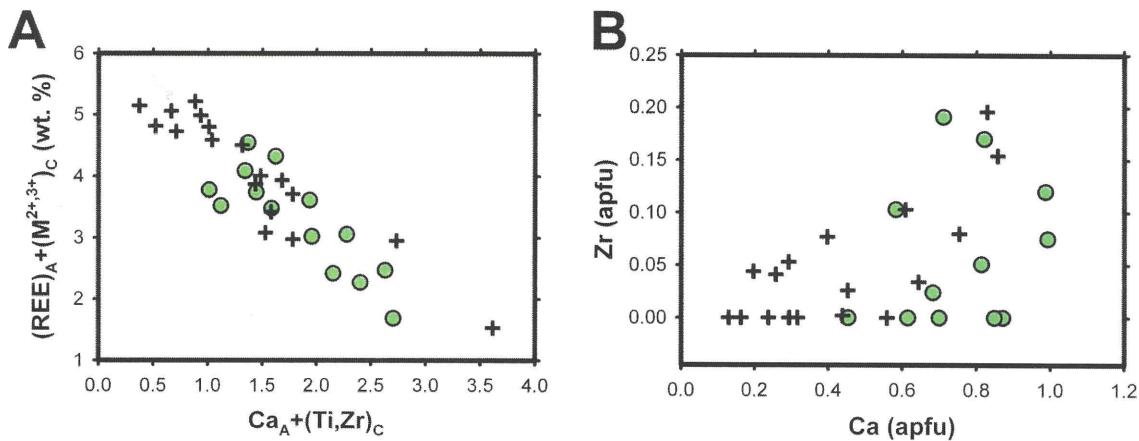
FIGURE 4.21: Chevkinite $Ca_A+(Ti,Zr)_C$ versus $(REE)_A+(M^{2+,3+})_C$ and Ca versus Zr binary plots (apfu).

Hydrous anionic groups were detected in a Mössbauer spectroscopy study by Yang et al. (2002). As altered and some unaltered chevkinite gives low analytical totals, the possibility of hydrous groups is inferred.

4.10 Fergusonite

Yttrium niobate, or fergusonite, is a trace mineral in Border Gabbro and Railway pegmatites. The mineral has a brown-red pleochroism, high relief and anomalous birefringence

(Fig. 4.22). In all cases, fergusonite forms in the initial stage of precipitation, with other initial-forming minerals, i.e. pyrochlore, allanite, chevkinite, zircon, etc. (Fig. 4.23). Fergusonite is one of two, the other being xenotime, to contain substantial HREEs (Table 4.9). Apart from thorium content, compositions between the two units are very similar (Table 4.9). Otherwise differences among units are related to occurrence.
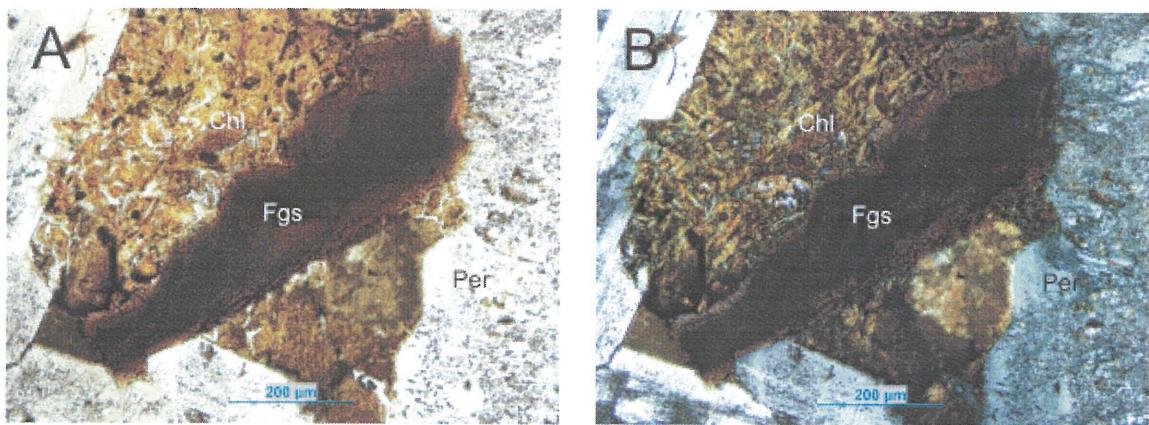
FIGURE 4.22: Standard optical micrographs of fergusonite (Fgs) associated with chlorite (Chl) and surrounded by perthite (Per). A is plane-polarized, B is cross-polarized.

In the Border Gabbro pegmatites, fergusonite is found intergrown with zircon and mantling pyrochlore. Some fluorocarbonate grains are adjacent to fergusonite crystals, indicating that, in common with xenotime, yttrium- and HREE-bearing minerals are relatively stable under alteration conditions. Even so, compositional variations related to alteration are observed, and are marked by increases in silica and LREEs.

Fergusonite from the Railway pegmatites is commonly associated with allanite, chevkinite, pyrochlore, and fluorocarbonates. Pyrochlore occurs before the precipitation of fergusonite; allanite and fergusonite occur contemporaneously; and chevkinite occurs after fergusonite. In common with the Border Gabbro fergusonite, silica and LREEs increase with increasing alteration.

Most of the observed fergusonite is altered. With increased alteration titanium increases, and iron and REEs decrease (Fig. 4.24). There is no alteration trend observed between calcium and alteration (Fig. 4.24D).
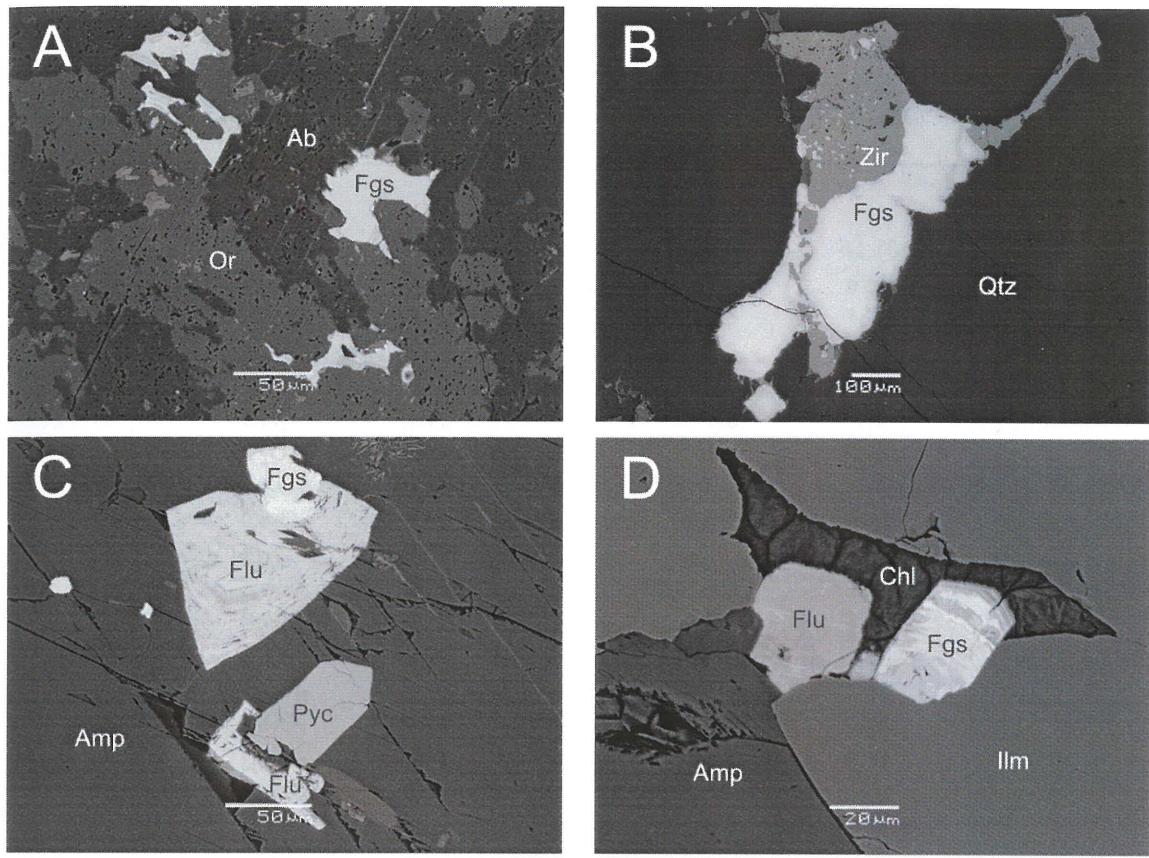
FIGURE 4.23: BSE-images of fergusonite (Fgs). A is fergusonite in albite (Ab) and orthoclase (Or). B is fergusonite and zircon (Zir) in quartz (Qtz). C is fergusonite, fluorocarbonates (Flu) and pyrochlore (Pyc) in amphibole (Amp). D in a subhbedral fergusonite grain (darker areas are enriched in niobium and silicon) and fluorocarbonate grain (Flu) in ilmenite (Ilm), chlorite (Chl) and amphibole (Amp).

Compared to other pegmatitic bodies, i.e. granitic pegmatite from the Amerlia District, United States (Lumpkin 1998) and granitic pegmatite from Bakkane-Steane, Norway (Tomašić et al. 2006), Coldwell fergusonite is enriched in MREEs, HREEs and tungsten while also being depleted in uranium (Table 4.9). The REE distribution is HREE selective, as yttrium is the dominant A-cation. Figure 4.25 is a ternary diagram illustrating the extent of REE composition in respect to LREE, MREE and HREE. The solid outline in Figure 4.25 is alkali rock and the dashed outline is calc-alkali rock (Weiliang 1991).

TABLE 4.9: Representative compositions of fergusonite.

	Border Gabbro[1]	Railway [2]	Granitic Pegmatite[3]	Granitic Pegmatite[4]
WO_3	2.95	3.82	0.9	-
Nb_2O_5	43.95	45.18	42.9	44.10
Ta_2O_5	2.50	0.72	5.0	6.50
TiO_2	0.59	0.45	0.5	1.20
SnO_2	-	-	0.3	-
ThO_2	2.75	4.49	2.9	-
UO_2	1.70	1.66	7.8	4.9
Y_2O_3	20.06	20.23	29.9	32.10
La_2O_3	0.33	0.26	-	-
Ce_2O_3	1.63	2.55	0.2	0.61
Pr_3O_3	0.67	0.78	-	-
Nd_2O_3	4.90	5.02	0.6	1.35
Sm_2O_3	2.62	2.56	0.8	1.64
Eu_2O_3	0.70	-	-	-
Gd_2O_3	4.20	3.56	1.2	1.42
Tb_2O_3	0.68	0.44	-	0.43
Dy_2O_3	3.95	4.00	1.7	2.31
Ho_2O_3	0.56	-	-	-
Er_2O_3	2.39	1.94	0.6	0.37
Tm_2O_3	0.82	-	-	0.30
Yb_2O_3	1.23	1.10	2.1	0.27
Lu_2O_3	0.25	-	-	-
CaO	0.69	1.21	1.4	1.91
MnO	-	0.19	-	-
FeO	0.77	0.02	-	0.11
PbO	-	-	0.5	-
Total	**100.89**	**100.18**	**98.4**	**99.52**

[1] Border Gabbro pegmatite (2 analyses of sample MAS006) from the Coldwell complex.
[2] Railway pegmatite (2 analyses of sample MAS026) from the Coldwell complex.
[3] Granitic pegmatite (wall zone core sample) from the Amelia district, United States (Lumpkin 1998).
[4] Granitic pegmatite (sample FER-BS) from the Bakkane-Steane, Norway (Tomašić et al. 2006).

Fergusonite can adopt monoclinic (Komkov 1959) and tetragonal (Weitzel and Schröcke 1980) structures. As fergusonite compositions are usually accompanied by high levels of actinides, metamictization can destroy the structure. On heating, fergusonite can regain its original structure, but higher temperature polymorphs can give misleading results (Xueming et al. 1993). Unfortunately, the small crystal size and low modal abundance made finding a suitable crystal for structural analysis impractical. The structure of Y-fergusonite is monoclinic, but other

varieties, e.g. formanite, Nd-fergusonite, Ti-fergusonite, adopt the tetragonal crystal system (Weiliang 1991). As yttrium is greater than 0.337 apfu in all samples, it is probable that all fergusonite grains are of the monoclinic $I4_1/a$ variety (Komkov 1959).
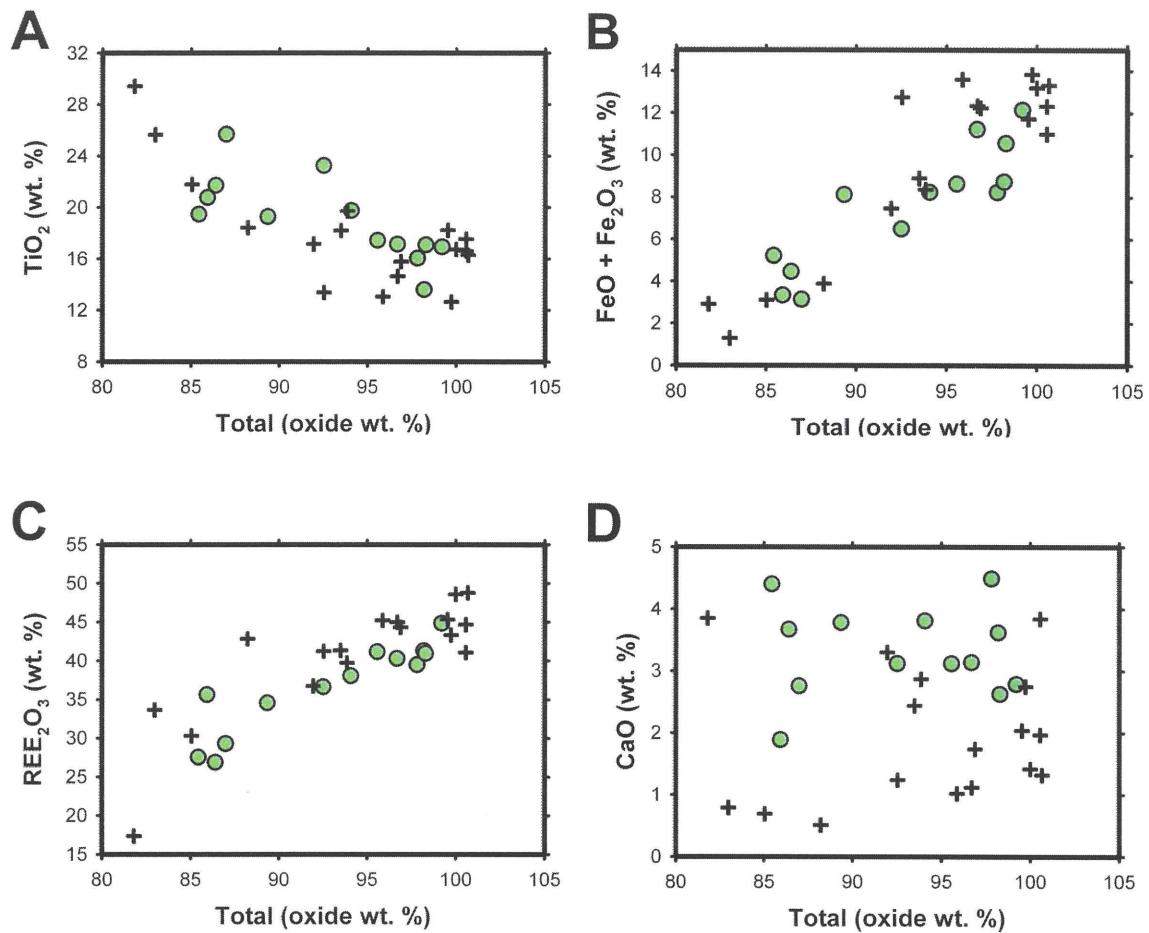
FIGURE 4.24: Various ions/ionic groups vs. total oxide weight %. Green circles and black crosses are the Border Gabbro and Railway pegmatites.

Fergusonite ($YNbO_4$) from the Coldwell pegmatites contains a wide range of ions. Substitution into the yttrium site is generally restricted to REEs but also includes Ca^{2+}, Fe^{2+}, Fe^{3+}, Mn^{2+}, Na^+, Th^{4+}, and U^{4+}, while Ta^{5+}, Ti^{4+} and W^{6+} are typically found in the niobium site. REEs, ferric iron and tantalum enter the fergusonite structure via simple substitution:

$$(Fe,REE)^{3+} \rightarrow Y^{3+}$$
$$(Ta)^{5+} \rightarrow Nb^{5+}$$
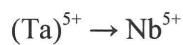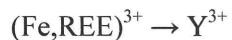
The presence of calcium, manganese and possibly ferrous iron indicate a coupled substitution into the yttrium structural site. These divalent ions can accompany tetravalent ions (titanium, thorium and uranium) into two yttrium sites:

$$(Ca,Fe,Mn)^{2+} + (Th,Ti,U)^{4+} \rightarrow 2Y^{3+}$$

A positive linear trend emerges when plotting divalent versus tetravalent species (Fig. 4.26A). With an r^2 value of 0.427, Figure 4.26A indicates that not all divalent species are in proportion to the tetravalent species. Coldwell fergusonite also contains significant amounts of tungsten (up to 5.78 % WO_3). The plot in Figure 4.26B of divalent ions versus tungsten shows an ill-defined positive relationship. As such, in common with tetravalent ions, tungsten can enter the fergusonite structure if accompanied by divalent ions:

$$(Ca,Fe,Mn)^{2+} + W^{6+} \rightarrow Y^{3+} + Nb^{5+}$$
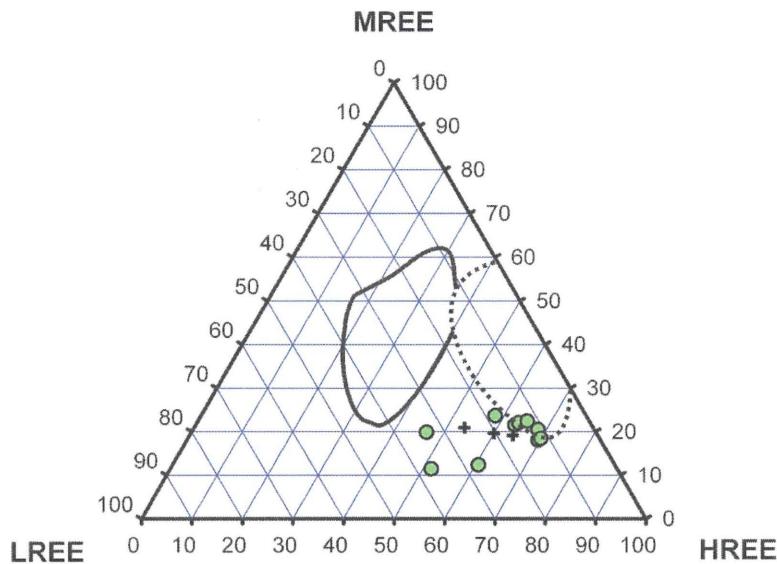
FIGURE 4.25: Fergusonite MREE (Sm-Ho) – LREE (La-Nd) – HREE (Er-Lu+Y) ternary plot. Solid line is alkali rock, dashed is calc-alkali rock (Weiliang 1991). Green circles and black crosses are the Border Gabbro and Railway pegmatites, respectively.

Plotting divalent, tetravalent, tantalum, tungsten and REEs against yttrium and niobium gives an r^2 value of 0.914 (Fig. 4.27). Although never in great amount (0.12-1.83 wt. % FeO), uncalculated ferric iron could likely be contributing to the less than perfect r^2 value.
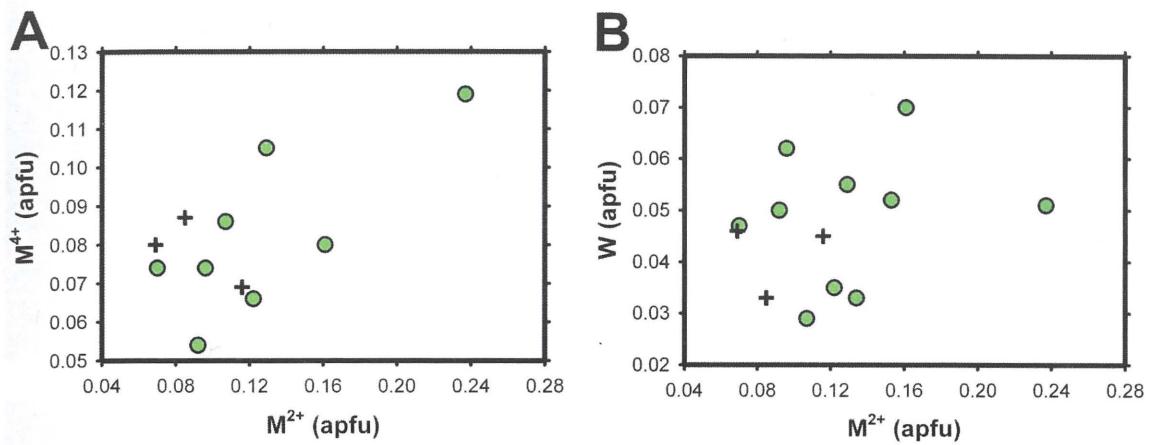
FIGURE 4.26: Fergusonite binary diagrams. A illustrates the positive correlation between divalent (M^{2+}) and tetravalent (M^{4+}) ions ($r^2 = 0.472$). B is tungsten vs. the divalent ions ($r^2 = 0.074$). Green circles and black crosses are the Border Gabbro and Railway pegmatites, respectively.
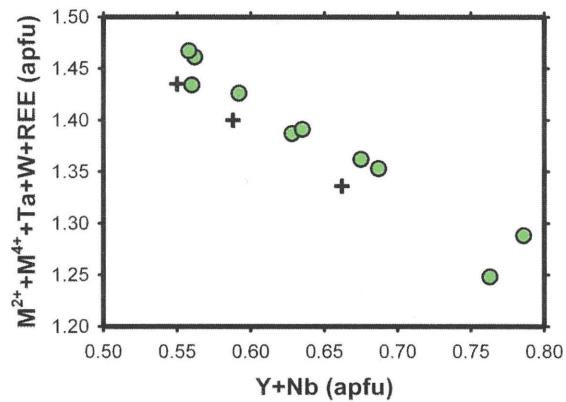
FIGURE 4.27: Fergusonite binary plot of all ions that substituted into yttrium and niobium ($r^2 = 0.914$). Green circles and black crosses are the Border Gabbro and Railway pegmatites, respectively.

4.12 Fluorocarbonate (Bastnaesite) Group

In polarized light fluorocarbonates are brown/red, have a high relief, and anomalous birefringence. Textures range considerably as shown in Figure 4.28. The bastnaesite groups general formula is $n(REE)(OH,F)CO_3 \bullet mCaCO_3$ and consists of four members: bastnaesite
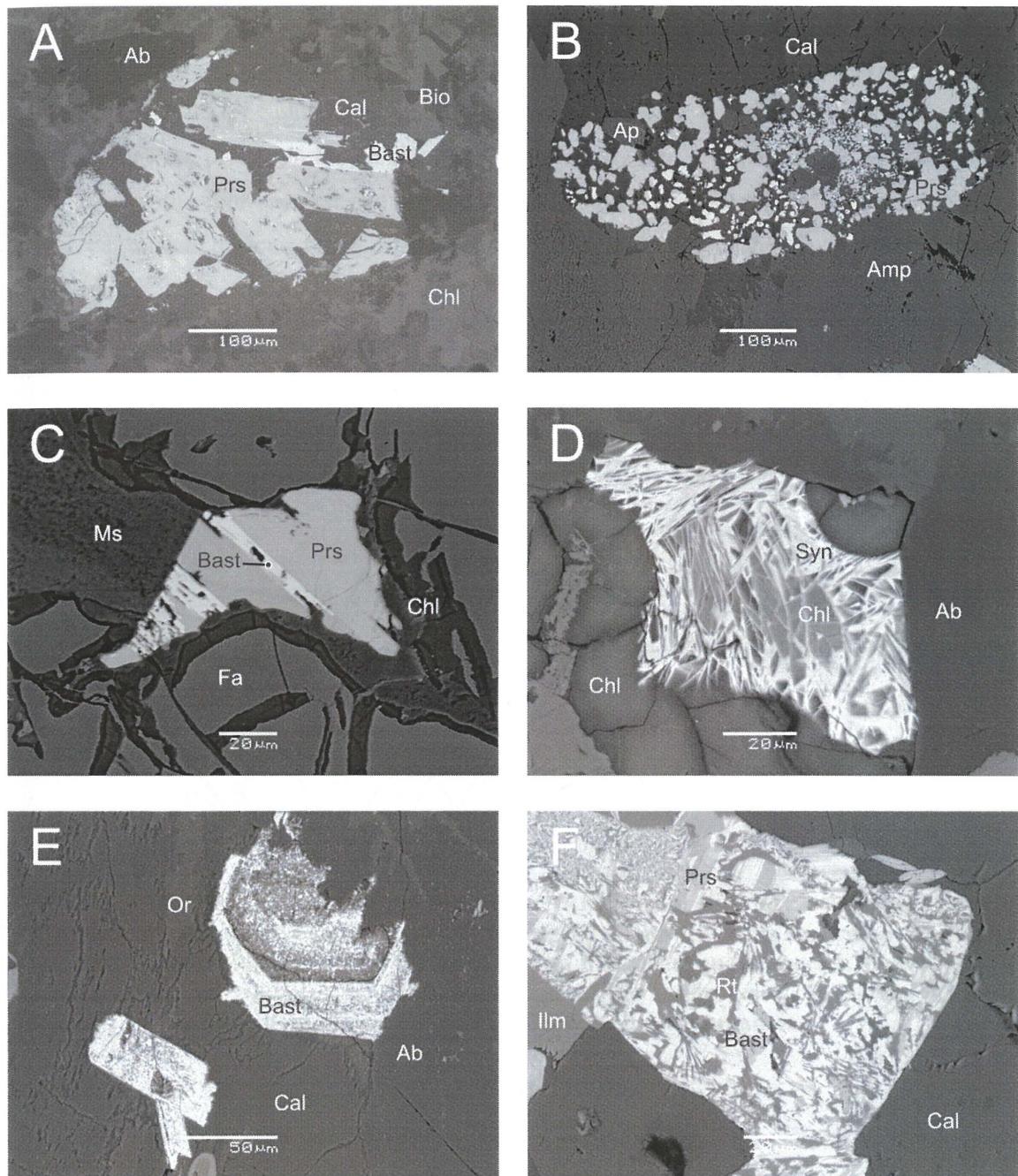
FIGURE 4.28: BSE-images of bastnaesite (Bast), synchysite (Syn) and parisite (Prs). A is parisite and bastnaesite in calcite (Cal), chlorite (Chl) biotite (Bio) and albite (Ab). B is parisite and apatite (Ap) in calcite and riebeckite amphibole (Amp). C is syntaxial bastnaesite and parisite growing in muscovite (Ms), chlorite and fayalite (Fa). D is radial synchysite (high yttrium) intergrown and surrounded by chlorite, grown on albite. E is a bastnaesite that replaced REE-rich apatite in calcite, albite and orthoclase (Or). F is bastnaesite intergrown with parisite and Nb-rutile (Rt) in calcite and ilmenite (Ilm).

(REE)(CO$_3$)F, synchysite (REE)Ca(CO$_3$)$_2$F, röentgenite (REE)$_3$-Ca$_2$(CO$_3$)$_3$F$_3$, and parisite (REE)$_2$Ca(CO$_3$)$_3$F$_2$. Layered intermediaries have been identified in other localities (van Landuyk and Amelinckx 1975; Smith et al. 2000), and may be present in Coldwell pegmatites. When compositions are plotted in the calcium-REE-iron ternary plot, as in Figure 4.29, mean values plot between the four species, and are indicative of layered intermediaries. Alternatively, this could be related to ions other than calcium, REEs and iron entering the fluorocarbonate structure.
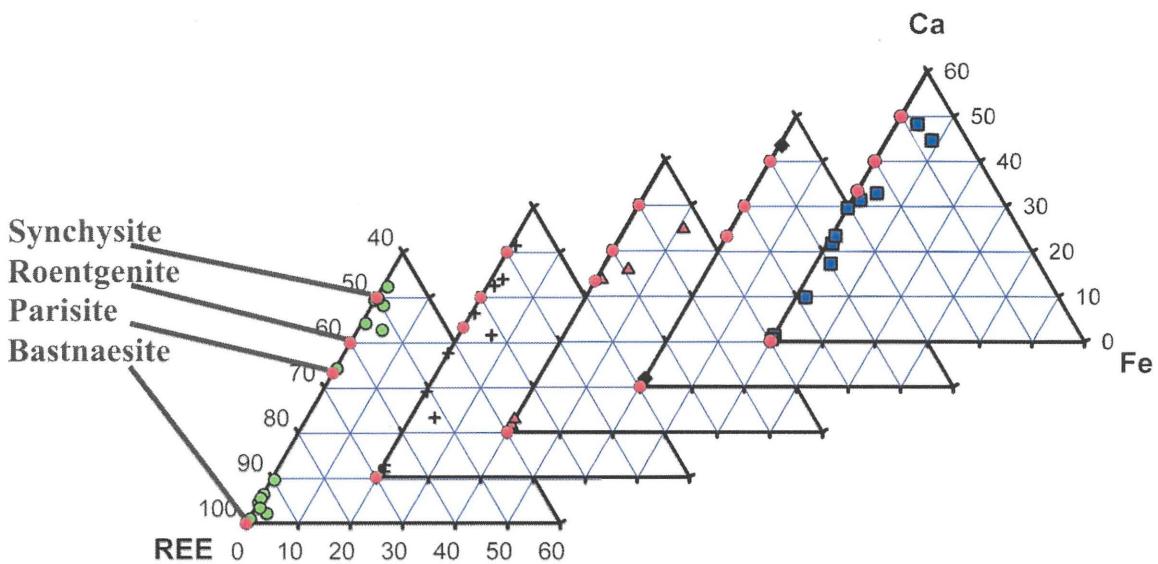
FIGURE 4.29: Fluorocarbonate calcium (Ca) – REE – iron (Fe) ternary plot (apfu) with calcium and iron reduced by 60 %. Field is magnified and the units separated for clarity. Red dots indicate ideal location for each of the fluorocarbonate species. Green circles, black crosses, red triangles, black diamonds, and blue squares are the Border Gabbro, Railway, Upper Marathon Shore, Black, and Center Three pegmatites.

Coldwell fluorocarbonate textures (Figs. 4.28 and 4.30), sizes (10 µm to 100 µm) and compositions (Tables 4.10, 4.11, 4.12, 4.13 and Appendix III.VII) are generally the same between Coldwell units. Exceptions to this are the absence of röentgenite and parisite in the Black pegmatites and rare outliner compositions (Table 4.14). The fluorocarbonates form anhedral crystals in the secondary stage of crystallization, and are commonly associated with primary REMs. In addition to discrete crystals (Fig. 4.30B), syntaxial, or "polycrystal" (Donnay and Donnay 1953), intergrowths are common (Fig. 4.30C). The syntaxial intergrowths are commonly between bastnaesite and synchysite and/or parisite. According to Gieré (1996) and

Williams-Jones and Wood (1992), as CO_3^{2-} and Ca^{2+} activities equilibrate, a response likely to occur with the precipitation of calcite, the activities fluctuate to form syntaxial intergrowths:

$$2REE(CO_3)F + 2CO_3^{2-} + Ca^{2+} + F^- \rightarrow REE_2Ca(CO_3)_3F_2$$

Bastnaesite   Parisite
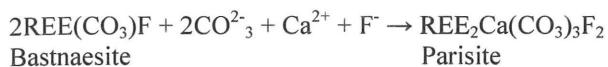
TABLE 4.10: Representative compositions of bastnaesite.

	Border Gabbro[1]	Railway[2]	Upper Marathon Shore[3]	Black[4]	Center Three[5]	Carbon-atite[6]	Carbon-atite[7]
SiO_2	0.41	0.35	0.62	0.81	0.37	0.16	-
ThO_2	-	0.41	-	-	-	0.23	-
Y_2O_3	0.31	-	0.65	0.33	-	0.12	-
La_2O_3	19.31	21.65	22.10	19.81	26.02	25.22	26.35
Ce_2O_3	35.27	36.21	35.55	36.11	37.20	36.40	37.41
Pr_2O_3	3.40	2.58	4.02	3.29	2.94	3.80	2.50
Nd_2O_3	10.92	11.77	9.81	11.12	7.88	9.22	6.60
Sm_2O_3	1.00	0.85	1.40	1.29	0.29	0.51	0.36
Gd_2O_3	-	-	-	-	-	1.17	-
Fe_2O_3	0.18	0.18	-	0.36	-	-	-
CaO	1.38	0.25	0.43	0.46	0.14	-	0.84
SrO	1.05	-	-	0.12	0.26	-	0.85
BaO	-	-	-	-	-	0.13	-
Total	**73.23**	**74.25**	**74.58**	**73.70**	**75.10**	**77.24**	**74.91**
F_C	8.84	8.72	8.97	8.98	8.81	8.9	8.75
$O=F$	3.72	3.67	3.78	3.78	3.71	3.75	3.68
CO_{2C}	20.47	20.19	20.78	20.80	20.41	20.70	20.25
Total	**98.82**	**99.49**	**100.55**	**99.78**	**100.61**	**102.81**	**100.23**

[1] Border Gabbro pegmatite (4 analyses of sample MAS012) from the Coldwell complex.
[2] Railway pegmatite (3 analyses of sample MAS028) from the Coldwell complex.
[3] Upper Marathon Shore pegmatite (2 analyses of sample MAS021) from the Coldwell complex.
[4] Black pegmatite (4 analyses of sample MAS032) from the Coldwell complex.
[5] Center Three pegmatite (4 analyses of sample MAS040) from the Coldwell complex.
[6] Carbonatite (25 analyses of the P4 aegirine vein/vug hosted sample) from the Bayan Obo deposit, Inner Mongolia, China (Smith et al. 2000).
[7] Carbonatite (6 analyses of sample 633A/414.1) from the Khibina complex, Kola Peninsula, Russia (Zaitsev 1998).

Apart from isolated occurrences, the compositions of most Coldwell fluorocarbonates are similar to other fluorocarbonates in anorogenic rocks, i.e. carbonatites from the Bayan Obo deposit, China and Khibina, Russia (Zaitsev et al. 1998). Bastnaesite (Table 4.10), synchysite (Table 4.11) and parisite (Table 4.13) from all three localities are LREE selective. While the

REE abundance of the Coldwell and Bayan Obo fluorocarbonates are very similar, REE abundances from Khibina are more LREE, specifically lanthanum and cerium, selective.

In some cases, the fluorocarbonates contain elevated concentrations of yttrium (up to 6.55 wt. % Y_2O_3). Initially discovered by Smith et al. (1960), Y-fluorocarbonates are typical of yttrium-enriched granitic complexes (Wang et al. 2003). Accompanying yttrium are elevated amounts of HREEs: gadolinium, dysprosium and erbium (Table 4.14). HREEs in the fluorocarbonate structure are rare, as the mineral group is LREE selective.

TABLE 4.11: Representative compositions of synchysite.

	Border Gabbro[1]	Railway[2]	Black[3]	Carbonaite[4]
SiO_2	1.80	0.51	1.70	-
ThO_2	3.00	-	-	-
Y_2O_3	2.03	0.51	2.68	-
La_2O_3	7.64	12.55	9.19	16.54
Ce_2O_3	19.03	24.03	19.74	26.19
Pr_2O_3	2.70	2.67	2.64	2.15
Nd_2O_3	9.89	8.02	8.97	6.14
Sm_2O_3	1.90	0.63	1.03	0.38
Dy_2O_3	0.25	-	-	-
Er_2O_3	0.11	-	-	-
Fe_2O_3	1.37	1.40	0.70	-
CaO	16.91	17.93	18.00	17.47
SrO	0.73	-	0.18	0.24
Total	**66.36**	**68.25**	**64.83**	**69.11**
F_C	6.21	6.18	6.24	5.94
O=F	2.61	2.60	2.63	2.50
CO_{2C}	28.75	28.63	28.94	27.55
Total	**99.71**	**100.46**	**97.38**	**100.10**

[1] Border Gabbro pegmatite (2 analyses of sample MAS004) from the Coldwell complex.
[2] Railway pegmatite (3 analyses of sample MAS026) from the Coldwell complex.
[3] Black pegmatite (4 analyses of sample MAS032) from the Coldwell complex.
[4] Carbonatite (8 analyses of sample 633A/414.1) from the Khibina complex, Kola Peninsula, Russia (Zaitsev 1998).

Some Coldwell fluorocarbonates are characterized by high iron contents, and, as listed in Table 4.14, some of the highest ever recorded. Average iron content (in wt. % Fe_2O_3) is 1.44 in bastnaesite, 1.72 in synchysite, 4.61 in röentgenite, and 2.10 in parisite, with a maximum of 11.98 wt. % Fe_2O_3 (0.433 apfu) in a röentgenite grain. Considering the environment in which the

fluorocarbonates formed, i.e. oxidizing, all iron is assumed to be in its ferric state. Ferric iron can replace REEs by simple substitution:

$$Fe^{3+} \rightarrow REE^{3+}$$
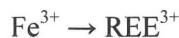
TABLE 4.12: Representative compositions of röentgenite.

	Border Gabbro[1]	Railway[2]	Upper Marathon Shore[3]	Center Three[4]
SiO_2	0.53	0.44	1.44	1.00
ThO_2	0.90	0.56	2.24	0.87
Y_2O_3	0.70	1.02	0.43	0.69
La_2O_3	8.98	13.56	11.20	10.70
Ce_2O_3	25.49	25.99	19.32	20.70
Pr_2O_3	3.20	3.01	1.61	2.81
Nd_2O_3	11.66	8.22	5.26	8.82
Sm_2O_3	1.72	0.78	0.25	1.17
Fe_2O_3	1.02	1.59	11.98	4.68
CaO	14.23	13.71	13.22	15.53
SrO	0.39	0.66	-	-
Total	**68.82**	**69.51**	**66.95**	**66.97**
F_C	6.84	6.94	7.69	7.20
O=F	2.88	2.92	3.24	3.03
CO_{2C}	26.40	26.81	29.68	27.79
Total	**99.18**	**100.37**	**101.08**	**98.93**

[1] Border Gabbro pegmatite (4 analyses of sample MAS012) from the Coldwell complex.
[2] Railway pegmatite (3 analyses of sample MAS017) from the Coldwell complex.
[3] Upper Marathon Shore pegmatite (3 analyses of sample MAS022) from the Coldwell complex.
[4] Center Three pegmatite (3 analyses of sample MAS036) from the Coldwell complex.

Other ions commonly found in the Coldwell pegmatites include Al^{3+}, Si^{4+}, Sr^{2+}, Th^{4+} in the REE-site, and SO^{2-}_4 in the (CO_3)-site. These other ions enter the fluorocarbonate structure by simple and coupled substitution. Simple substitutions occur in all three calcium-, REE-, and CO_3-sites:

$$Sr^{2+} \rightarrow Ca^{2+}$$
$$Al^{3+} \rightarrow REE^{3+}$$
$$SO^{2-}_4 \rightarrow CO^{2-}_3$$
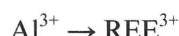
Coupled solid solution into one structural site also occurs in Coldwell fluorocarbonates:

$$(Th,Si)^{4+} + Sr^{2+} \rightarrow 2REE^{3+}$$
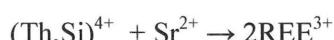
TABLE 4.13: Representative compositions of parisite.

|	Border Gabbro[1]	Railway[2]	Upper Marathon Shore[3]	Center Three[4]	Carbon-atite[5]	Carbon-atite[6]
SiO_2	0.32	0.39	0.52	0.27	0.16	-
ThO_2	-	0.18	0.69	-	0.28	-
Y_2O_3	0.56	0.13	0.12	-	0.12	-
La_2O_3	11.41	15.36	15.37	16.92	9.46	19.63
Ce_2O_3	27.98	28.49	26.59	31.57	29.73	31.72
Pr_2O_3	4.02	2.93	2.01	2.92	4.13	2.30
Nd_2O_3	12.97	8.69	6.28	9.57	16.49	6.83
Sm_2O_3	1.35	0.72	0.98	0.81	1.40	0.45
Eu_2O_3	-	-	-	-	0.20	-
Fe_2O_3	0.41	0.77	5.82	-	-	-
CaO	10.40	11.11	10.62	8.84	9.27	9.72
SrO	-	0.11	-	0.18	0.22	0.56
BaO	-	-	-	-	0.14	-
Total	**69.42**	**68.92**	**69.00**	**71.08**	**71.60**	**71.21**
F_C	7.06	7.13	7.51	6.95	6.90	6.98
O=F	2.97	3.00	3.16	2.93	2.91	2.94
CO_{2C}	24.54	24.78	26.10	24.15	24.10	24.27
Total	**98.05**	**97.79**	**99.45**	**99.25**	**99.69**	**99.52**

[1] Border gabbro pegmatite (3 analyses of sample MAS006) from the Coldwell complex.
[2] Railway pegmatite (4 analyses of sample MAS014) from the Coldwell complex.
[3] Upper Marathon Shore pegmatite (5 analyses of sample MAS022) from the Coldwell complex.
[4] Center Three pegmatite (5 analyses of sample MAS040) from the Coldwell complex.
[5] Carbonatite (7 analyses of the P3 fluorite stage sample) from the Bayan Obo deposit, Inner Mongolia, China (Smith et al. 2000).
[6] Carbonatite (2 analyses of sample 633A/414.1) from the Khibina complex, Kola Peninsula, Russia (Zaitsev 1998).

According to Wedepohl (1995), fluorocarbonates form where subsolidus hydrothermal fluids react with pre-existing REE-silicates and phosphates to replace oxygen and/or hydroxyl with fluorine. Fluorine was likely expelled from the melt and into fluid during crystallization leaving carbon dioxide in the residual melt fractions. As such, each REM underwent "bastnasitization" (Gieré 1996), a process which occurs when calcium, fluorine and carbonate saturated fluids preferentially use REEs to form the fluorocarbonates and various daughter mineral/soluble complexes. This "bastnasitization" is observed in monazite, allanite, xenotime, and chevkinite:

$$REEPO_4 + HF + H_2O + CO_2 \rightarrow REE(CO_3)F + H_3PO_4$$
Monazite   Bastnaesite

$$REE_2Fe_3(SiO_4)(Si_2O_7)O(OH) + CO_2 + F^- \rightarrow 2(REE)(CO_3)F + 3SiO_2 + Fe_3O_4 + OH^- + O^{2-}$$

Fe-Allanite   Bastnaesite   Quartz   Magnetite

$$YPO_4 + HF + H_2O + CO_2 \rightarrow Y(CO_3)F + H_3PO_4$$

Xenotime   Y-Bastnaesite

$$(REE,Ca)_4Fe(Fe,Nb)_2Ti_2Si_4O_{22} + 4CO_2 + 4F^- \rightarrow 4(REE,Ca)(CO_3)F + 3(Ti,Nb)O_2 + Fe_2O_3 + 4SiO_2 + OH^-$$

Chevkinite   Bastnaesite   Rutile   Hematite Quartz
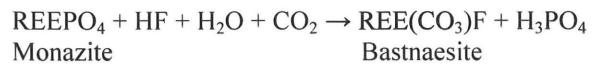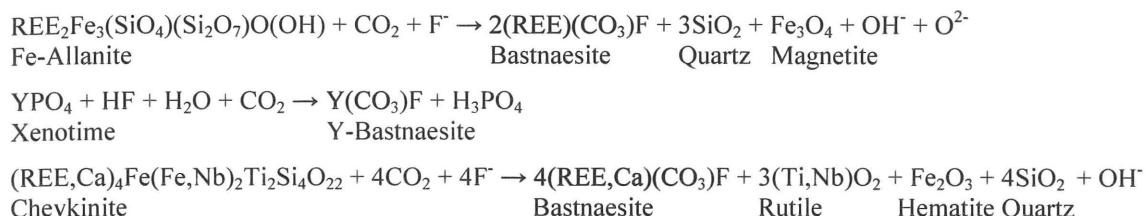
TABLE 4.14: Unique fluorocarbonate compositions from the Coldwell pegmatites.

	High Iron[1]	High Iron[2]	High Iron and Sulfur[3]	High Iron and Thorium[4]	High Iron and Thorium[5]	High Yttrium[6]
SO_3	-	-	3.87	-	-	-
SiO_2	1.44	0.73	0.75	2.10	1.99	0.63
ThO_2	2.24	1.97	0.54	4.70	4.29	1.66
Y_2O_3	0.43	0.85	0.66	2.19	0.46	6.55
La_2O_3	11.20	10.22	15.45	11.98	17.50	8.46
Ce_2O_3	19.32	17.71	28.35	24.36	27.69	18.59
Pr_2O_3	1.61	1.65	2.75	2.61	1.99	2.02
Nd_2O_3	5.26	6.02	9.23	9.73	6.59	8.64
Sm_2O_3	0.25	0.72	1.02	1.09	0.55	1.35
Gd_2O_3	-	-	-	-	-	1.08
Dy_2O_3	-	-	-	-	-	1.36
Er_2O_3	-	-	-	-	-	0.73
Fe_2O_3	11.98	8.35	4.59	7.91	5.61	0.36
CaO	13.22	17.21	4.32	2.96	4.06	16.28
SrO	-	0.26	0.16	0.35	0.30	0.43
Total	**66.95**	**65.69**	**71.69**	**69.98**	**70.97**	**68.14**
F_C	7.69	6.54	9.86	10.43	10.02	6.10
O=F	3.24	2.75	4.15	4.39	4.22	2.57
CO_{2C}	29.68	30.28	20.72	24.16	23.21	28.23
Total	**101.08**	**99.76**	**98.12**	**100.18**	**100.04**	**99.90**

[1] High iron content from röentgenite grain from Border Gabbro pegmatite (3 analyses of sample MAS012) from the Coldwell complex.

[2] High iron content in synchysite grain from Center Three pegmatite (3 analyses of sample MAS035) from the Coldwell complex.

[3] High sulfur content in bastnaesite grain from the Railway pegmatite (3 analyses of sample MAS014) from the Coldwell complex.

[4] High iron and thorite from bastnaesite grain from Railway pegmatite (3 analyses of sample MAS028) from the Coldwell complex.

[5] High thorite content in bastnaesite grain from Center Three pegmatite (2 analyses of sample MAS033) from the Coldwell complex.

[6] High yttrium content in synchysite grain from Border Gabbro pegmatite (4 analyses of sample MAS012) from the Coldwell complex.

4.13 Galena

Galena is a common suphide occurring in all pegmatite units. It forms in the initial stage of crystallization as < 1 µm inclusions in zircon and thorite, and in the late stage of crystallization with sulphides (sphalerite, pyrite, and molybendite). In all cases, crystals are anhedral, and compositions are devoid of any other detectable elements.

The late-forming variety of galena is syngenetic with molybdenite (Fig. 4.30A) and sphalerite (Fig. 4.30B) and usually entrained by the very late-interstitial minerals, i.e. fluorite, quartz and calcite. Late-forming galena crystals are generally much larger (up to 250 µm) than those of the initial-forming variety.
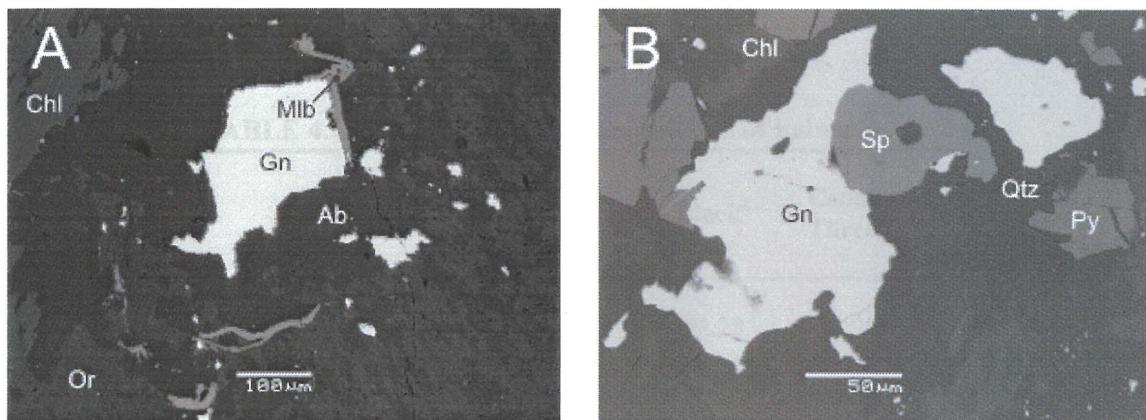
FIGURE 4.30: BSE-images of galena (Gn). A is galena intergrown with molybdenite (Mlb) and surrounded by albite (Ab), orthoclase (Or) and chlorite (Chl). B is galena intergrown with sphalerite (Sp) and surrounded by chlorite, quartz (Qtz) and pyrite (Py).

4.13 Kainosite

Kainosite (cenosite) is an extremely rare mineral occurring in the Border Gabbro, Railway, Black, and Center Three pegmatites. All grains are less that 60 µm in size, form in the initial stage of crystallization and are often associated with pyrochlore and fluorocarbonates (Fig. 4.31). Apart from one grain in Center Three pegmatites, all kainosite crystals are very altered, and, as they do not exhibit stoichiometric kainosite proportions, are identified by their high REEs and silicon, low aluminum, and moderate-to-high calcium (Table 4.15 and Appendix III.IX). Kainosite is often zoned and commonly alters to fluorocarbonates and quartz:

$$Ca_2REE_2Si_4O_{12}(CO_3)H_2O + 4CO_2 + 2F^- \rightarrow 2(REE)Ca(CO_3)_2F + 4SiO_2 + 2OH^- + 2O^{2-}$$
Kainosite   Synchysite   Quartz
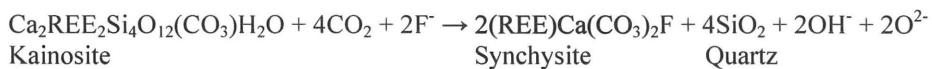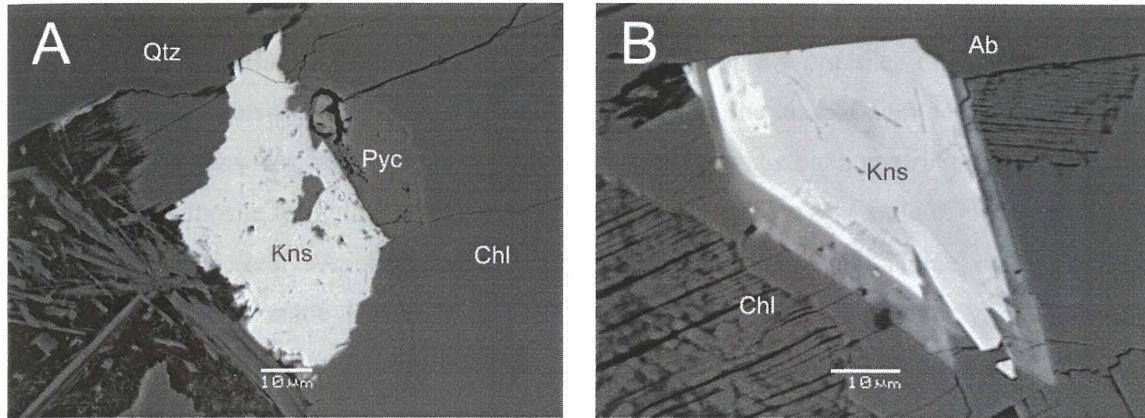
FIGURE 4.31: BSE-images of kainosite (Kns). A is kainosite associated with pyrochlore (Pyc) and surrounded by chlorite (Chl) and quartz (Qtz). B is zoned kainosite surrounded by albite (Ab) and chlorite (Chl).

TABLE 4.15: Representative compositions of kainosite.

	Border Gabbro[1]	Railway[2]	Black[3]	Center Three[4]
SiO_2	30.60	21.53	22.28	33.98
Al2O3	0.33	0.15	1.15	0.28
Y_2O_3	6.11	2.58	7.29	13.54
La_2O_3	1.25	10.09	12.98	0.95
Ce_2O_3	8.47	27.25	24.28	7.36
Pr_2O_3	1.55	3.51	2.02	1.43
Nd_2O_3	10.26	11.59	6.40	8.55
Sm_2O_3	2.78	1.54	0.99	1.24
Gd_2O_3	2.04	-	0.56	2.54
Tb_2O_3	0.51	-	0.22	0.15
Dy_2O_3	1.87	-	0.45	1.69
Ho_2O_3	0.21	-	-	0.24
Er_2O_3	0.89	-	0.31	1.01
Yb_2O_3	1.38	-	0.47	1.59
CaO	11.27	10.99	3.96	16.05
FeO*	6.22	0.60	0.86	0.27
Total	**85.74**	**89.83**	**84.22**	**90.87**
CO_{2C}	5.66	4.90	4.73	6.23
H_2O_C	2.32	2.01	1.93	2.55
Total	**93.72**	**96.74**	**90.88**	**99.65**

[1] Border Gabbro pegmatite (3 analyses of sample MAS003) from the Coldwell complex.
[2] Railway pegmatite (3 analyses of sample MAS014) from the Coldwell complex.
[3] Black pegmatite (4 analyses of sample MAS032) from the Coldwell complex.
[4] Center Three pegmatite (3 analyses of sample MAS038) from the Coldwell complex.

Kainosite is a rare mineral found in pegmatitic granites (Adams et al. 1964; Pouliot et al. 1964; Salvi and Williams-Jones 1996). Most studies mention the presence of kainosite, but do not include quantitative analyses. As in Coldwell kainosite, the lack of complete compositional data in other studies may be related to the difficulty with finding stoichiometric crystals.

The kainosite formula $[Ca_2REE_2Si_4O_{12}(CO_3)H_2O]$ includes Al^{3+} and Fe^{2+} in the REE-site and Ca-site, respectively. As most kainosite crystals are altered to some degree, no substitution correlations could be made. However, there are correlations with the total oxide % and calcium, silicon and iron. These correlations indicate that calcium and silicon are being leached and iron is slightly enriched with decreasing total oxide %. It should be noted that REEs are relatively immobile during the alteration of kainosite (Fig. 4.32B).
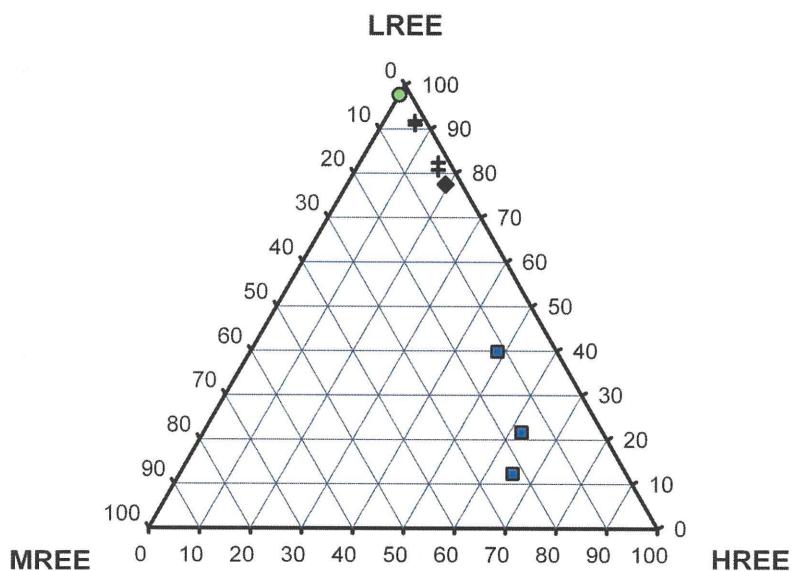
FIGURE 4.32: Kainosite MREE (Sm-Ho) – LREE (La-Nd) – HREE (Er-Lu+Y) ternary plot. Green circles, black crosses, black diamonds, and blue squares are the Border Gabbro, Railway, Black, and Center Three pegmatites, respectively.

4.14 Ilmenite

Ilmenite is a common initial-forming and, less frequently, secondary mineral present in all units. When not discrete, as in Figure 4.33A, ilmenite forms with magnetite. Ilmenite/magnetite intergrowths, as seen in Figure 4.33C, are common, but ilmenite is also observed mantling magnetite (Fig. 4.33C).

Secondary ilmenite is an alteration product, along with fluorocarbonates and quartz, of chevkinite. Ilmenite crystals produced in this fashion are generally enriched in niobium, anhedral and intergrown with the other alteration products (Fig. 4.33D).
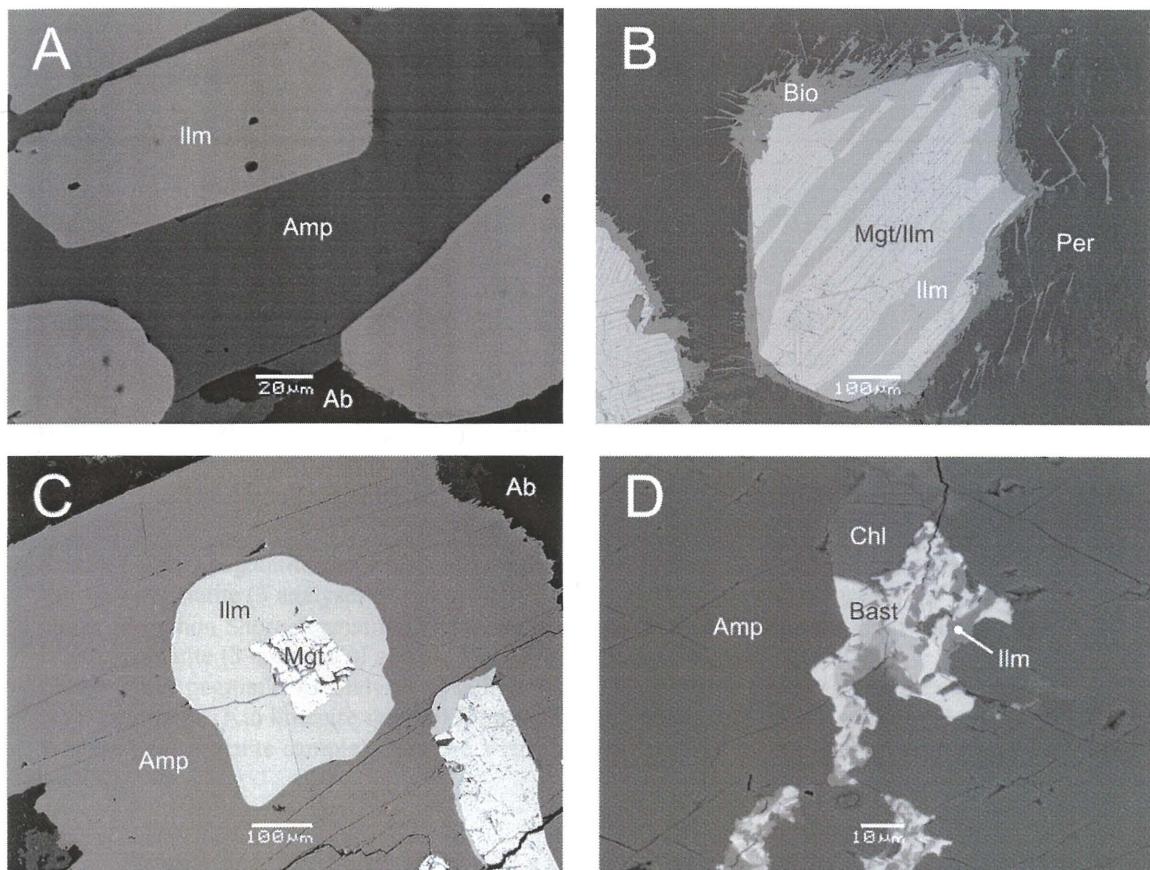
FIGURE 4.33: BSE-images of ilmenite (Ilm). A is subhedral crystals of ilmenite surrounded by amphibole and albite. B is ilmenite and magnetite (Mgt) intergrown together, mantled by biotite (Bio) and surrounded by perthite (Per). C is magnetite mantled by ilmenite and surrounded by amphibole. D is niobium-ilmenite associated with bastnaesite (Bast) and surrounded by chlorite (Chl) and amphibole.

As shown in Table 4.15, ilmenite commonly contains significant amounts of niobium (max 2.57 wt. % Nb_2O_5), and manganese (max 14.09 wt % MnO). Other ions present in minor amounts include: Al^{3+}, Ca^{2+}, and Fe^{3+}. The hexagonal (R-3) ilmenite structure accommodates niobium by pairing with divalent or trivalent ions:

$$(Fe,Mn)^{2+} + 2Nb^{5+} \rightarrow 3Ti^{4+}$$
$$(Fe,Al)^{3+} + Nb^{5+} \rightarrow 2Ti^{4+}$$
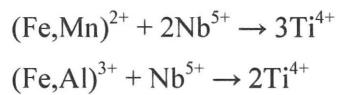
As silicon is tetravalent, it enters the ilmenite structure by simple substitution:

$$Si^{4+} \rightarrow Ti^{4+}$$

TABLE 4.16: Representative compositions of ilmenite.

	Border Gabbro[1]	Railway[2]	Upper Marathon Shore[3]	Black[4]	Center Three[5]	NYF-Pegma-tite[6]	Granite[7]
Ta_2O_5	-	-	-	-	-	0.10	0.11
Nb_2O_5	-	0.31	1.38	0.50	0.62	0.41	0.43
SiO_2	0.32	0.30	0.33	0.25	0.38	-	-
TiO_2	50.49	50.95	49.17	50.77	49.55	52.83	52.93
Al_2O_3	0.10	0.09	-	0.13	0.14	-	-
Fe_2O_3	3.42	2.50	5.07	2.34	4.29	-	-
FeO	43.82	40.34	42.20	43.81	34.19	41.19	40.82
MnO	1.96	4.88	2.40	2.13	10.70	5.40	5.53
CaO	-	0.71	-	-	-	-	-
Total	**100.11**	**100.08**	**100.55**	**99.93**	**99.87**	**99.93**	**99.82**

[1] Border Gabbro pegmatite (3 analysis of sample MAS001) from the Coldwell complex.
[2] Railway pegmatite (3 analyses of sample MAS017) from the Coldwell complex.
[3] Upper Marathon Shore pegmatite (3 analyses of sample MAS019) from the Coldwell complex.
[4] Black pegmatite (3 analyses of sample MAS030) from the Coldwell complex.
[5] Center Three pegmatite (3 analyses of sample MAS037) from the Coldwell complex.
[7] NYF-pegmatite (Klu ilmenite sample) from the Klučov intrusive, Czech Republic (Škoda et al. 2006).
[7] Granite (Val ilmenite sample) from the Vladislav-Pazderníkův mlýn pluton, Czech Republic (Škoda et al. 2006).

Ferrous and ferric iron allow for a partial solid solution to exist between ilmenite and hematite:

$$FeTiO_3 + Fe_2O_3 \rightarrow (Fe^{2+},Fe^{3+})TiO_3 + Fe^{2+}Fe^{3+}_2O_4$$
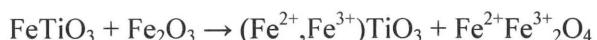
Ilmenite can accommodate higher amounts of ferric iron with increasing oxygen fugacity (fo_2) and temperature. As such, the amount of trivalent iron present in the ilmenite can be used to determine these parameters (Petrogenesis Chapter).

4.15 Löllingite

Löllingite is present in one of the Railway pegmatite (MAS017) samples. Here it forms a small (~ 8 μm) euhedral grain in the late interstitial stage of crystallization, next to chalcopyrite (Fig. 4.34).

The only detected ion that is not part of the ideal lollingite "$FeAs_2$" formula is sulfur (Table 4.16). In common with other arsenides, i.e. glaucodot, cobaltite, etc., lollingite can accommodate sulfur into the arsenic site, expanding the formula to $Fe(As,S)_2$. Löllingite is one of two minerals, the other being arsenopyrite, to contain detectable arsenic.
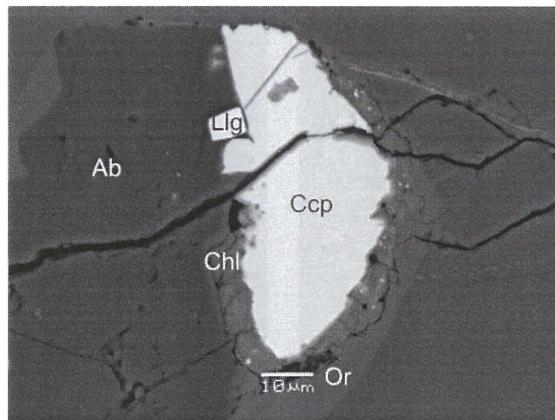
FIGURE 4.34: BSE-image of löllingite (Llg) associated with chalcopyrite (Ccp), and surrounded by chlorite (Chl), albite (Ab) and orthoclase (Or).

TABLE 4.17: Representative compositions of löllingite.

	Railway[1]
S	1.88
Fe	26.55
As	71.93
Total	**100.36**

[1] Railway pegmatite (2 analyses of sample MAS017) from the Coldwell complex.

4.16 Magnetite

Magnetite is present in all units, and forms in the initial, in one unit, interstitial, and secondary stages of crystallization. Initial-forming magnetite forms crystals with octahedral and dodecahedral habits, but rarely cubes (Fig. 4.35A and B). The initial-forming magnetite is commonly associated with ilmenite, crystallizing with a subsolidus texture (Fig. 4.35C) or, less frequently, mantling textures. The exsolution of ilmenite forms along magnetite cleavage planes.

Interstitial magnetite is rare, and only occurs in Center Three pegmatites. As seen in Figure 4.35D, interstitial magnetite grows in intercumulous voids. The crystals are characteristically anhedral, low in titanium and are the last to form. Secondary magnetite is observed in all units, as it is an alteration product of allanite, chevkinite and amphibole.
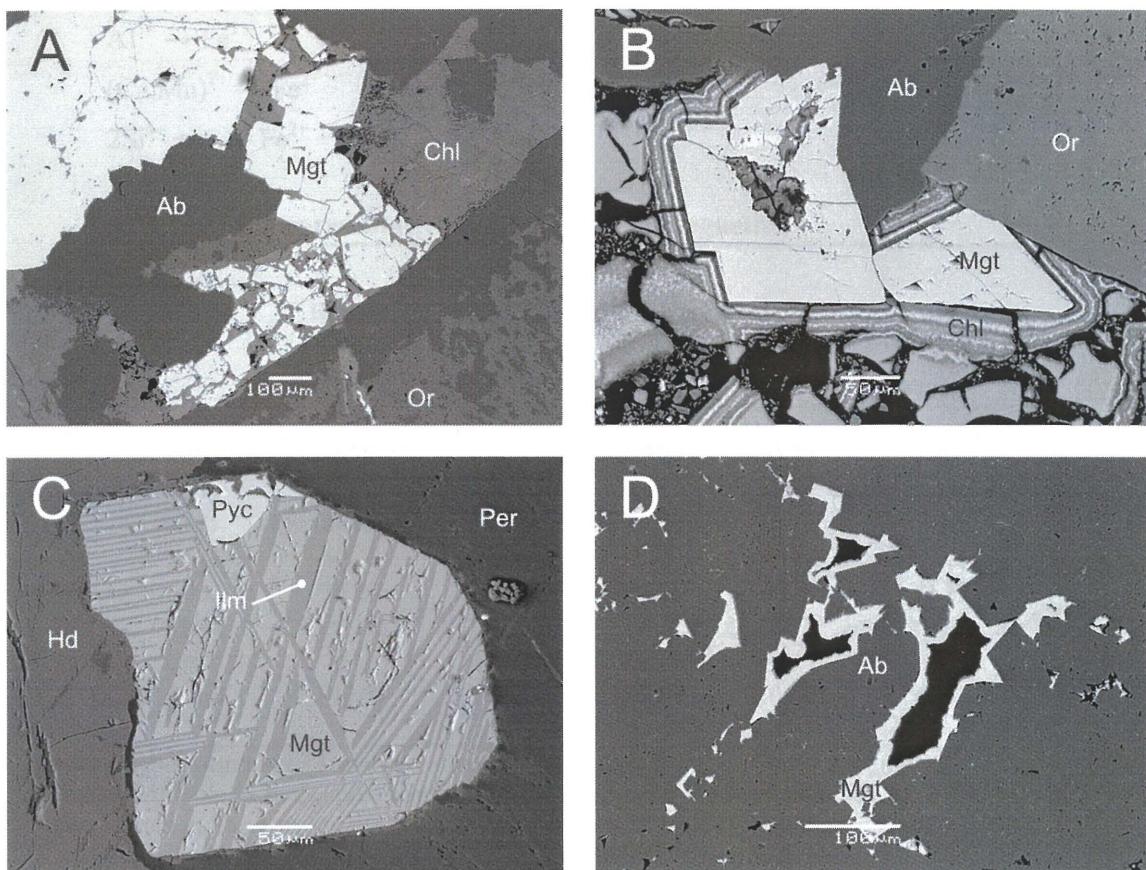
FIGURE 4.35: BSE-images of magnetite (Mgt). A is a concentration of subhedral and anhedral magnetite crystals surrounded by albite (Ab), orthoclase (Or) and chlorite (Chl). B is euhedral magnetite surrounded by albite, orthoclase and concentrically zoned chlorite. C is magnetite and ilmenite intergrown with one another and surrounded by pyrochlore (Pyc), hedenbergite (Hd) and perthite (Per). D is secondary magnetite which forms in voids left by, in this case, albite crystals.

Titanium is a common ion present in Coldwell magnetite. The range, 0.49 to 4.95 oxide wt. % TiO_2, is similar to granitic pegmatites, granites, and ultramafics (Buddington and Lindsley 1964). Titanium can enter the magnetite structure via a partial solid solution with ulvöspinel (Fe_2TiO_4):

$$Fe_2TiO_4 \rightarrow (Fe,Ti)_3O_4$$
Ulvöspinel Magnetite
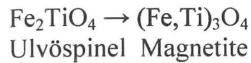
With increasing oxygen fugacity (fo_2) and temperature, the magnetite-ulvöspinel miscibility gap shrinks. The titanium component in magnetite is used in the Petrogenesis Chapter of this study to determine fo_2 and temperature.

Other impurities include aluminum, calcium, manganese, and silicon:

$$Al^{3+} \rightarrow Fe^{2+}$$

$$(Ca,Mn)^{2+} \rightarrow Fe^{2+}$$

$$2Si^{4+} + \square \rightarrow Fe^{2+} + 2Fe^{3+}$$
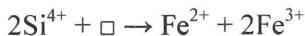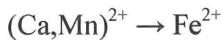
TABLE 4.18: Representative compositions of magnetite.

	Border Gabbro[1]	Railway[2]	Upper Marathon Shore[3]	Black[4]	Center Three[5]
SiO_2	0.38	-	0.37	0.30	0.41
TiO_2	3.82	0.49	2.65	1.44	0.84
Al_2O_3	0.46	0.11	0.17	0.20	0.38
Fe_2O_3	60.42	67.66	62.97	65.68	65.75
FeO	35.29	31.12	34.03	32.86	32.12
MnO	-	-	-	0.13	0.22
CaO	-	0.22	-	-	-
Total	**100.37**	**99.60**	**100.09**	**100.61**	**99.72**

[1] Border Gabbro pegmatite (4 analysis of sample MAS001) from the Coldwell complex.
[2] Railway pegmatite (5 analyses of sample MAS017) from the Coldwell complex.
[3] Upper Marathon Shore pegmatite (4 analyses of sample MAS019) from the Coldwell complex.
[4] Black pegmatite (3 analyses of sample MAS032) from the Coldwell complex.
[5] Center Three pegmatite (3 analyses of sample MAS037) from the Coldwell complex.

4.17 Molybdenite

Molybdenite is a relatively common sulphide present in all of the Coldwell pegmatites. The mineral forms in the late stages of crystallization with galena and sphalerite (Fig. 4.36). The crystals are wispy and elongate, with cleavages parallel to elongation. Apart from molybdenum and sulphur, no other elements are detected.

4.18 Monazite and rhabdophane

Trace amounts of monazite are present in all lithologies. The mineral precipitates in the initial and secondary stages of crystallization. Common associations are with apatite, chevkinite,

thorite, and fluorocarbonates, with the latter being an alteration product. Monazite crystals range from subhedral to anhedral (Fig. 4.37A and B). The compositions of Coldwell monazites, as listed in Table 4.18, is relatively constant, and commonly contain minor silicon, thorium, iron, strontium, and HREEs. Compositional changes are mostly related to calcium, REE, and thorium, i.e. the Border Gabbro and Railway pegmatites contain a range of calcium (and minor strontium) that is not present in the other units (Fig. 4.38). Monazites from the Railway pegmatites contain the largest range of calcium (Fig. 4.37).
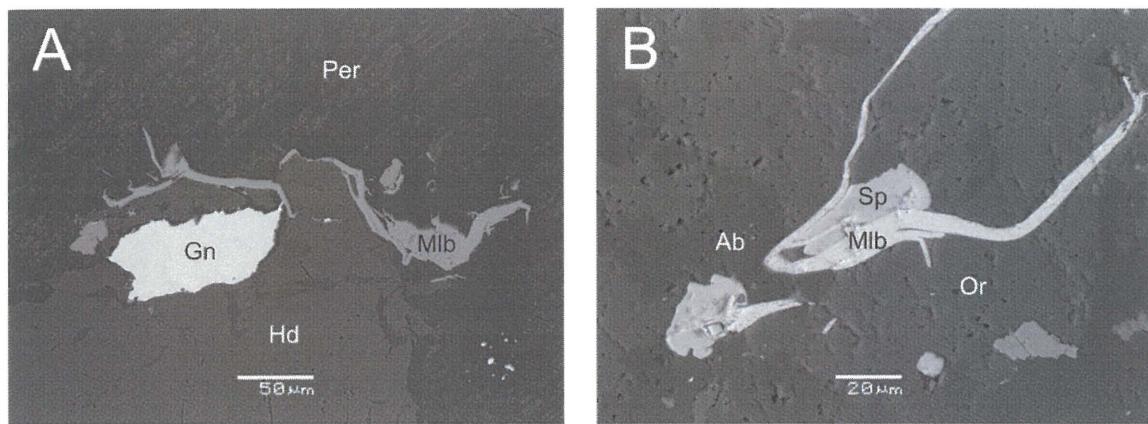
FIGURE 4.36: BSE-images of molybdenite (Mlb). A is molybdenite and galena (Gn) surrounded by perthite (Per) and hedenbergite (Hd). B is molybdenite and sphalerite (Sp) in albite (Ab) and orthoclase (Or).

Monazite forms with apatite and its hydrous variety "rhabdophane" in the initial phase of crystallization (Fig. 4.37D). Minor constituents include silicon, thorium, iron, and strontium. One crystal contains detectable gadolinium (1.17 wt. % Gd_2O_3), but no other MREEs.

Monazite from the Upper Marathon Shore pegmatites has higher thorium (0.8-1.2 oxide wt. %) and HREE (up to 1.7 oxide wt. %) than the other lithologies. Otherwise, the associations are the same as in the other units.

In the Black pegmatites, monazite only occurs in one sample. The grains are either late primary or secondary, forming from the breakdown of REE-rich apatite. As such, the crystals are disseminated, form after euhedral apatite, and are intergrown with chlorite.

Monazites from other A-type intrusions have similar compositions to Coldwell monazites. As listed in Table 4.17, monazite compositions from the Thor Lake intrusion and the

It is likely that apatite ($CaPO_4$) and britholite ($LREE_{10}(Si,P)_6O_{24}(OH,F)_2$), as both minerals are nearly isomorphous, form a limited solid solution with monazite. However, in order to balance the crystal lattice a tetravalent ion, such as thorium, is required:

$$Th^{4+} + (Ca,Sr)^{2+} \rightarrow 2REE^{3+}$$
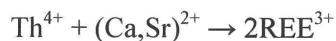
Gramaccioli and Segalstad (1978)
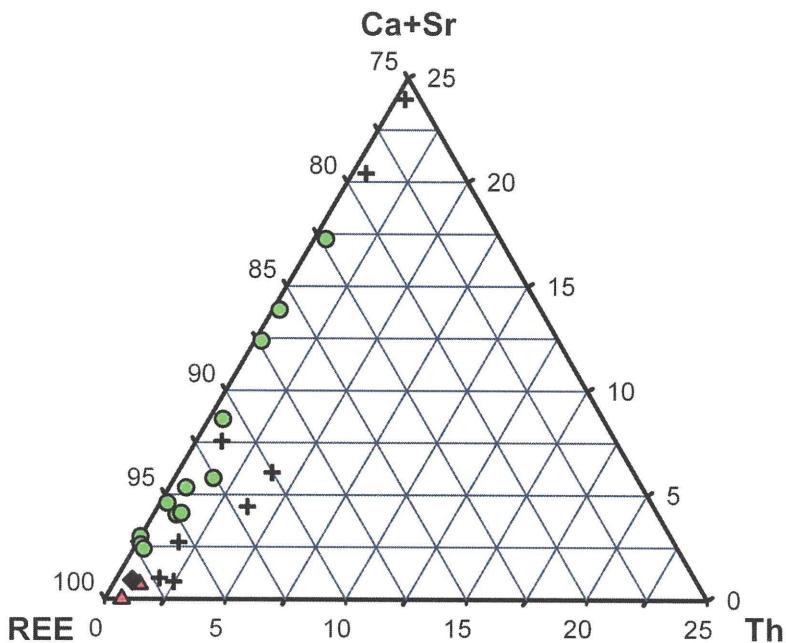
FIGURE 4.38: Monazite calcium + strontium (Ca+Sr) – REE – thorium (Th) ternary diagram (apfu) with Ca+Sr and Th reduced by 75 %. Green circles, black crosses, red triangles, black diamonds, and blue squares are the Border Gabbro, Railway, Upper Marathon Shore, Black, and Center Three pegmatites, respectively.

The coupled substitution of thorium and divalent ions for LREE is uncertain. The monazite structure cannot accommodate ions as large as thorium and calcium in the same crystal lattice. Instead, these large ions are likely paired with silicon:

$$(Ca,Sr)^{2+} + Si^{4+} \rightarrow 2REE^{3+}$$
$$Th^{4+} + Si^{4+} \rightarrow REE^{3+} + P^{5+}$$
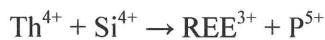
Gramaccioli and Segalstad (1978)

As shown in Figure 4.39A, there is a correlation between silicon and phosphorus. When the same diagram is expanded to include all tetra-, tri- and di-valent ion, the combination of substitution mechanisms has a strong negative correlation, and a resulting r^2 factor of 0.937 (Fig. 3.39B).

TABLE 4.19: Representative compositions of monazite.

	Border Gabbro[1]	Railway[2]	Upper Marathon Shore[3]	Black[4]	Center Three[5]	Thor Lake[6]	Granite[7]
P_2O_5	30.98	29.46	29.73	28.54	28.86	29.40	28.61
SiO_2	1.67	0.32	0.63	1.09	1.07	-	0.66
ThO_2	0.62	0.99	0.78	0.81	0.68	-	1.84
UO_2	-	-	-	-	-	-	0.16
Al_2O_3	-	0.64	0.38	-	0.30	-	-
Fe_2O_3	0.25	-	-	0.38	0.47	-	-
Y_2O_3	-	0.10	-	1.58	1.10	-	0.58
La_2O_3	10.60	17.55	12.48	16.86	13.20	13.88	15.38
Ce_2O_3	30.99	33.42	34.52	33.98	33.76	38.51	34.26
Pr_2O_3	3.58	3.27	4.18	3.21	3.91	3.05	3.57
Nd_2O_3	14.21	10.29	13.55	11.07	14.33	12.65	11.21
Sm_2O_3	1.89	1.17	2.57	1.37	1.41	1.16	1.73
Gd_2O_3	-	1.17	1.48	-	-	-	0.44
Tb_2O_3	-	-	-	-	-	-	-
Dy_2O_3	-	-	0.27	-	-	-	-
Er_2O_3	-	-	-	-	-	-	0.12
CaO	4.14	0.64	-	0.21	0.63	0.06	0.16
SrO	0.41	-	-	-	-	-	-
H_2O	-	-	-	-	-	0.38	-
Total	**99.34**	**100.31**	**100.57**	**99.10**	**99.72**	**98.71**	**98.72**

[1] Border gabbro pegmatite (5 analyses of sample MAS010) from the Coldwell complex.
[2] Railway pegmatite (4 analyses of sample MAS023) from the Coldwell complex.
[3] Upper Marathon Shore pegmatite (4 analyses of sample MAS018) from the Coldwell complex.
[4] Black pegmatite (5 analyses of sample MAS029) from the Coldwell complex.
[5] Center Three pegmatite (4 analyses of sample MAS034) from the Coldwell complex.
[6] Altered/brecciated syenite (sample PT77) from the Lake Zone, Thor Lake, N.W.T., Canada Pinckston and Smith 1995).
[7] Granite (4th monazite sample of Val gr) from the Vladislav-Pazderníkův mlýn pluton, Czech Republic (Škoda et al. 2006).

The hydrous variety of monazite, named rhabdophane [(REE,Ca)$PO_4 \bullet H_2O$], is present in the Border Gabbro and Railway pegmatites, and forms along the fractures and grain boundaries of monazite. Rhabdophane is an alteration mineral targeting weakened crystals, the monazites containing high actinides (suggesting a metamict nature) are more susceptible to this form of alteration. As listed in Table 4.18 and Appendix III.X, Coldwell rhabdophane is characterized by having low analytical totals, low sulfur (0.83-10.09 wt. % SO_3), low fluorine, and elevated amounts of calcium (2.86-4.87 wt. % CaO) and elevated iron (0.66-6.30 wt. % Fe_2O_3). Fluorine

and sulfur can enter the monazite/rhabdophane structure if accompanied by tetravalent and divalent ions, respectively:

$$F^- + Th^{4+} \rightarrow O^{2-} + LREE^{3+}$$

$$S^{3-} + (Ca,Fe,Sr)^{2+} \rightarrow O^{2-} + LREE^{3+}$$
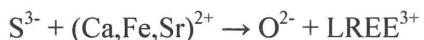
As sulfur may reach 0.398 apfu, most, if not all of the iron may be in its divalent oxidation state in order to satisfy charge neutrality. Alternatively, high sulfur in some samples may be accommodated with hydroxyl and/or fluorine for balance:

$$S^{3-} + (OH,F)^- \rightarrow 2O^{2-}$$
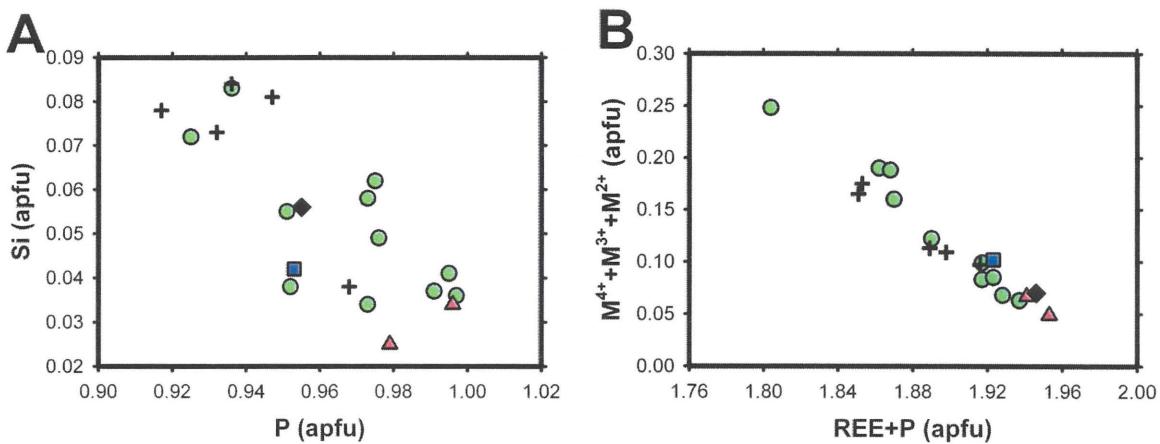
FIGURE 3.39: Monazite substitution diagrams (apfu). A is silicon (Si) vs. phosphorus (P). $R^2 = 0.629$. B is tetra-, tri-, and di-valent ions ($M^{4+}+M^{3+}+M^{2+}$) vs. REEs and phosphorus (P). $R^2 = 0.937$.

Monazite can be used to show the amount of fractionation between units by plotting La_2O_3/Nd_2O_3 versus $La_2O_3+Ce_2O_3+Pr_2O_3$. Figure 4.40 shows the extent of this relationship, and that there is a exponential trend from the most fractionated, and relatively HREE-enriched, Border Gabbro pegmatites to the least fractionated, and relatively LREE-enriched, Railway pegmatites. This suggests that the Border Gabbro is more evolved than the other pegmatites.

4.19 Pyrite

Pyrite forms euhedral-to-anhedral crystals (Fig. 4.41A), which are often associated with ilmenite and magnetite (Fig. 4.41B). In Coldwell pegmatites, pyrite forms syngenetically with sphalerite and calcopyrite, and before quartz and calcite (Fig. 4.41C). Mantling of pyrite by magnetite, as in Figure 4.41D, is rare and only occurs in Center Three pegmatites. Pyrite is intersticial and is consistently of stoichiometric FeS_2 composition, with no other detectable ions.

TABLE 4.20: Representative compositions of rhabdophane.

	Border Gabbro[1]	Railway[2]
SO_3	0.82	10.09
P_2O_5	20.70	22.23
SiO_2	5.92	0.65
ThO_2	0.08	0.38
Al_2O_3	0.37	1.26
Y_2O_3	0.33	1.87
La_2O_3	16.74	8.68
Ce_2O_3	32.75	21.31
Pr_2O_3	2.41	2.46
Nd_2O_3	7.14	9.02
Sm_2O_3	0.30	0.91
CaO	2.86	4.87
FeO	0.67	5.67
SrO	0.81	-
Total	**91.90**	**89.40**

[1] Border Gabbro pegmatite (3 analyses of sample MAS005) from the Coldwell complex.
[2] Railway pegmatite (4 analyses of sample MAS023) from the Coldwell complex.
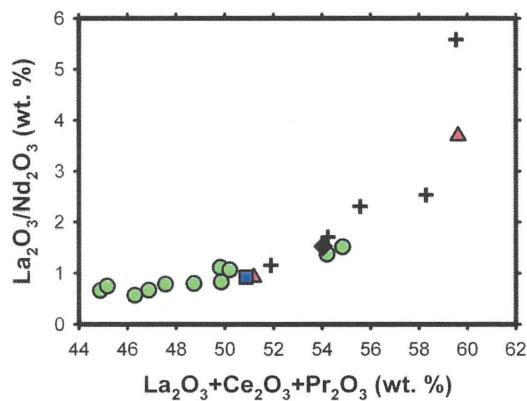
FIGURE 4.40: Fractionation of REEs in monazite. The Border Gabbro (green circles) is the most fractionated and the Railway (black crosses) is the least, with the Black (black diamonds), Upper and Lower Marathon Shore (red and yellow triangles, respectively), and Center Three (blue square) falling in transition. Diagram after Fleischer and Altschuler (1969).
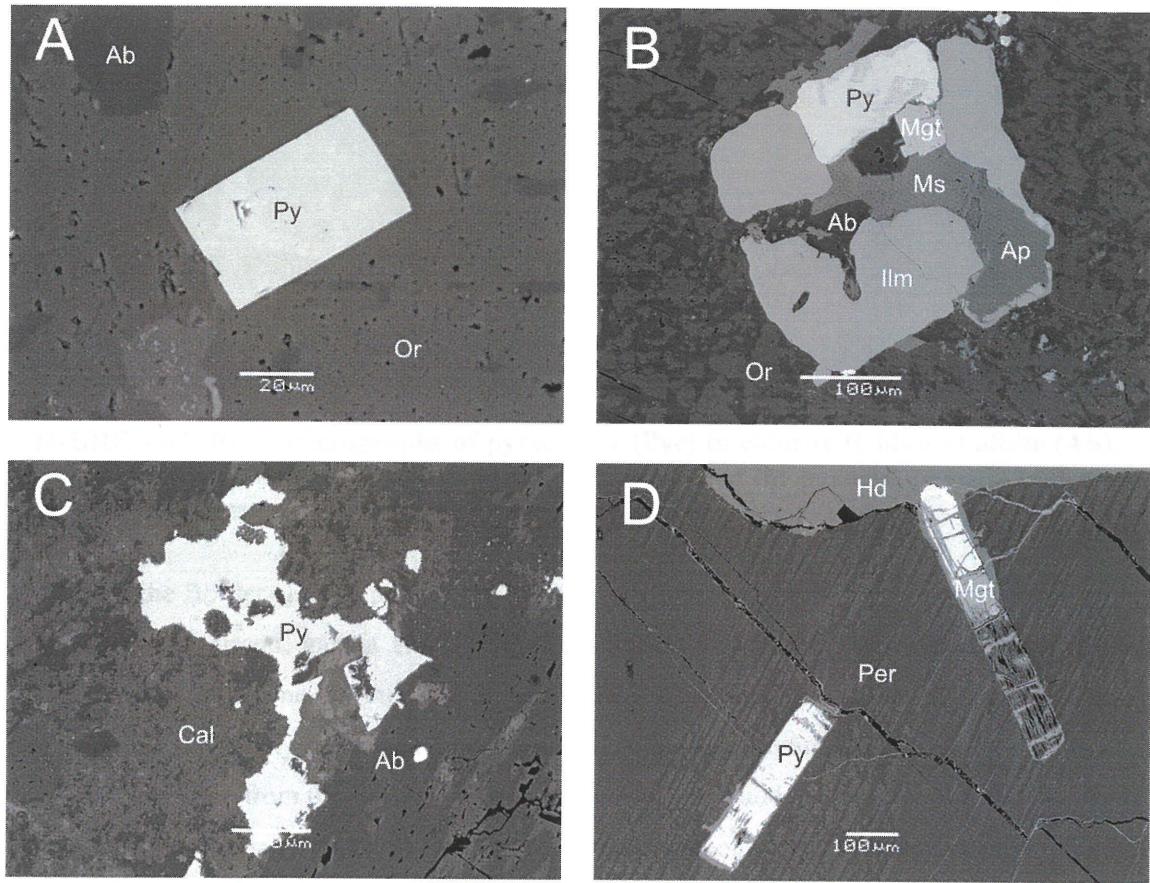
FIGURE 4.41: BSE-images of pyrite (Py). A is euhedral pyrite in orthoclase (Or) and albite (Ab). B is pyrite, ilmenite (Ilm), apatite (Ap), muscovite (Ms), and magnetite in albite and orthoclase. C is anhedral pyrite in albite and calcite (Cal). D is subhedral elongate pyrite and magnetite (Mgt) in perthitic feldspar (Per) and hedenbergite (Hd).

4.20 Pyrochlore Group

Pyrochlore is a trace mineral present in all Coldwell pegmatites. As shown in Figure 4.42, pyrochlore is colourless, has a high relief and first-order grey birefringence. Pyrochlore crystals are euhedral-to-anhedral, and form in the initial- (Fig. 4.43A to E) and, less commonly, interstitial-stages of crystallization (Fig. 4.43F). Oscillatory, continuous and patchy zoning of pyrochlore—reflecting variations in silica content—occur in all of the pegmatites. Pyrochlore is the primary niobium host in Coldwell pegmatites and, apart from apatite, the most important REE-bearing mineral. Pyrochlore is one of two minerals, the other being zirconolite, to accommodate significant amounts of tantalum and tungsten. Table 4.20 and Appendix III.XI list the compositionally diverse pyrochlores in the Coldwell complex.
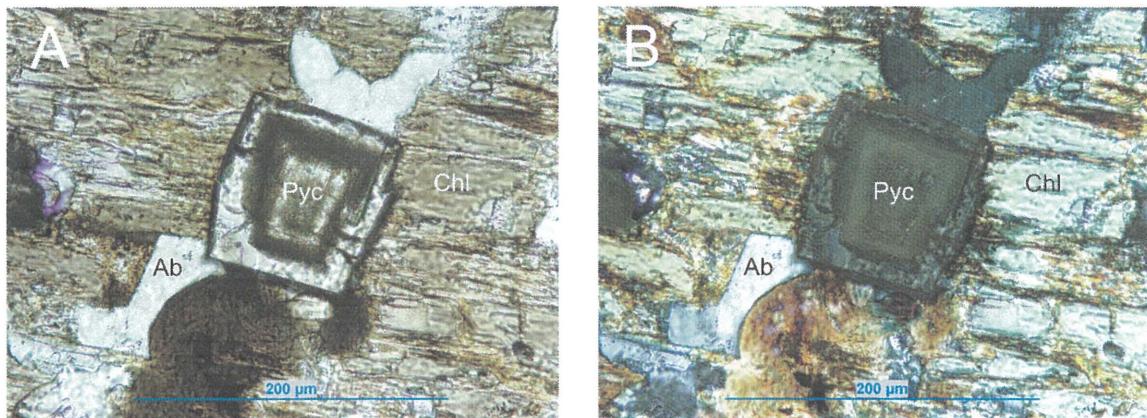
FIGURE 4.42: Photomicrographs of pyrochlore (Pyc) in chlorite (Chl) and albite (Ab). A is plane-polarized, B is cross-polarized. The center area of the pyrochlore grain is strongly silicified/metamict.

In the Border Gabbro pegmatites, pyrochlore forms euhedral-to-anhedral crystals, and is associated with zircon, galena and thorite. In common with thorite, pyrochlore forms before zircon, and is thus one of the first minerals in the paragenetic sequence. Border Gabbro pyrochlore is commonly silicified along grain boundaries and fractures.

Pyrochlore from the Railway pegmatites forms with baddeleyite, ilmenite and magnetite. The grains are normally euhedral, and form contemporaneously with baddeleyite (Fig. 4.43C). High iron is characteristic of most Railway pyrochlores with a maximum value of 0.777 apfu and an average of 0.394 apfu.

Pyrochlore from the Upper Marathon Shore pegmatites are euhedral-to-anhedral. The mineral in this setting forms in the initial stage of crystallization, before magnetite/ilmenite. Galena inclusions are present in most of the crystals. In one sample (MAS020), shown in Figure 4.43D, pyrochlore decomposes into Y-fluorocarbonate.

Pyrochlore from the Black pegmatites is commonly associated with chevkinite and zircon, with pyrochlore forming before both of these two minerals. The Black pyrochlores are characterized by high niobium.

Pyrochlore from Center Three pegmatites crystallizes at two times; one in the early-initial stage, the other in the interstitial stage. In common with the other units, the early-initial stage is associated with magnetite/ilmenite, zircon, etc. The interstitial stage pyrochlore rims initial and cumulous minerals, and crystallizes before quartz (Fig. 4.43F).
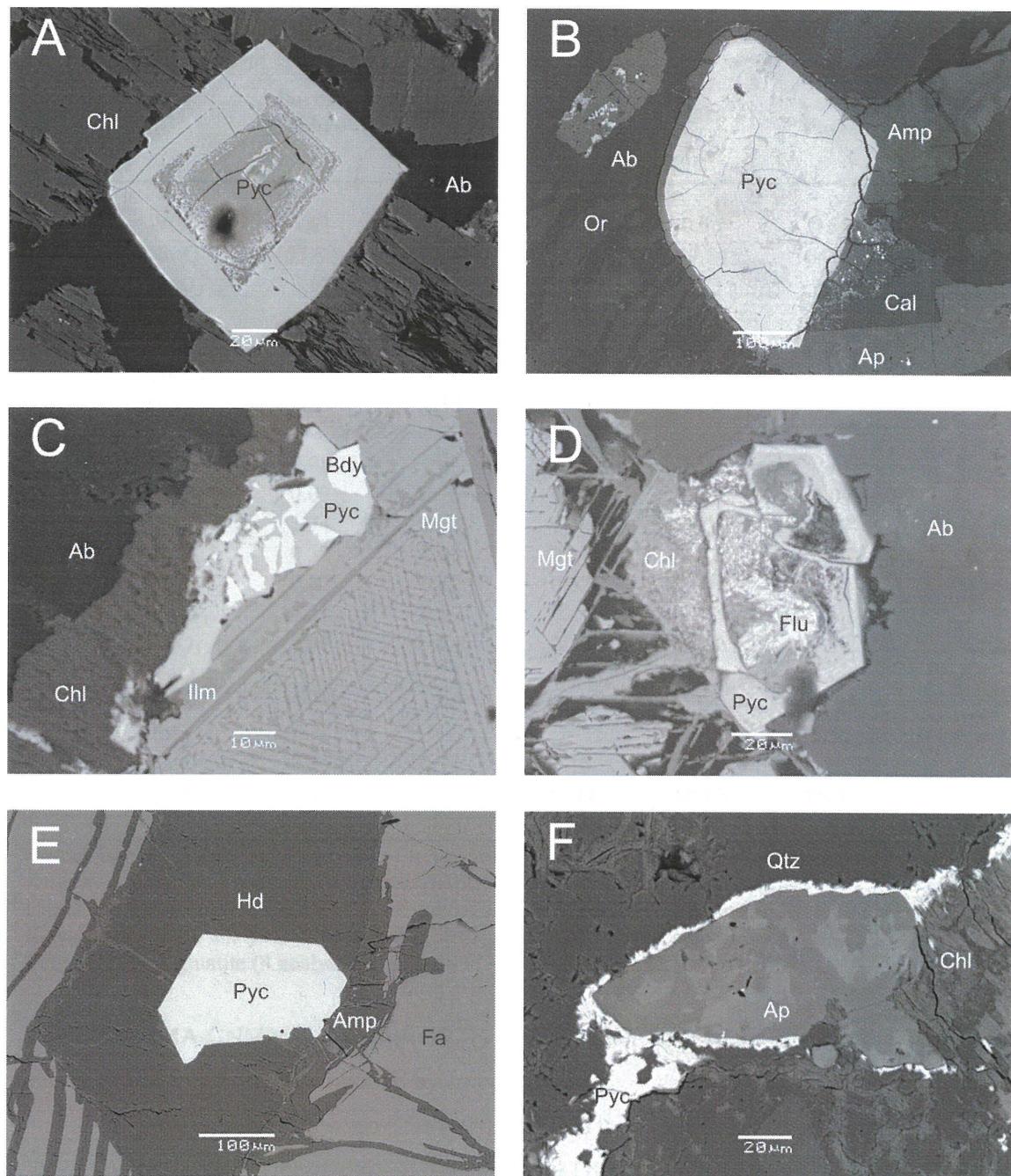
FIGURE 4.43: BSE-images of pyrochlore (Pyc). A is the BSE image of Figure 4.39. B is subhedral pyrochlore mantled by amphibole (Amp) and surrounded by calcite (Cal), apatite (Ap), albite, and orthoclase (Or). C is pyrochlore intergrown with baddeleyite and surrounded by chlorite, magnetite (Mgt) and ilmenite (Ilm). D is pyrochlore that is decomposed into Y-fluorocarbonate (Flu) and surrounded by chlorite, magnetite and albite. E is euhedral pyrochlore in hedenbergite (Hd), amphibole and fayalite (Fa). F is pyrochlore that has grown in a fracture and along an apatite grain.

TABLE 4.21: Representative compositions of Coldwell pyrochlore.

	Border Gabbro[1]	Railway[2]	Upper Marathon Shore[3]	Black[4]	Center Three[5]
WO_3	1.61	-	-	0.56	0.39
Nb_2O_5	53.83	51.30	63.02	49.54	64.15
Ta_2O_5	3.69	2.67	0.88	0.73	2.34
SiO_2	-	3.22	0.67	2.72	0.30
TiO_2	5.51	5.70	5.09	0.19	5.11
ThO_2	1.19	0.56	-	4.46	-
UO_2	5.44	3.35	-	1.08	-
Al_2O_3	-	-	-	-	0.11
Y_2O_3	0.08	-	-	1.97	-
La_2O_3	0.09	0.79	0.23	0.59	0.09
Ce_2O_3	1.74	2.08	1.42	4.86	0.83
Pr_2O_3	0.32	0.09	0.31	1.17	-
Nd_2O_3	0.82	0.42	0.62	6.46	0.39
Sm_2O_3	0.21	0.09	-	1.90	-
Fe_2O_3	4.97	24.07	0.27	7.24	0.74
MnO	-	1.75	-	-	-
CaO	17.75	1.46	16.91	4.61	17.28
PbO	-	-	-	-	6.72
Na_2O	0.20	0.19	7.16	-	-
Total	**97.45**	**97.74**	**96.11**	**88.08**	**98.45**

[1] Border Gabbro pegmatite (8 analyses of sample MAS003) from the Coldwell complex.
[2] Railway pegmatite (2 analyses of sample MAS016) from the Coldwell complex.
[3] Upper Marathon Shore pegmatite (3 analyses of sample MAS020) from the Coldwell complex.
[4] Black pegmatite (3 analyses of sample MAS029) from the Coldwell complex.
[5] Center Three pegmatite (4 analyses of sample MAS040) from the Coldwell complex.

The IMA-CNMMN (Hogarth 1977) classification scheme for pyrochlore uses three general groups to describe the mineral by composition:

1) betafite subgroup when $[2Ti \geq (Nb + Ta)]$ at the B position of the formula,

2) pyrochlore subgroup when $[(Nb + Ta) > 2Ti]$ and $[Nb > Ta]$, and

3) microlite subgroup when $[(Nb + Ta) > 2Ti]$ and $[Ta > Nb]$

Pyrochlore from the Coldwell pegmatites all belong to the pyrochlore subgroup, as shown in Figures 4.44 and 4.45, and adopt the cubic $Fd3m$ space group. In Coldwell pyrochlores, the formula, $A_{2-m}B_2O_6(OH,F,O)_{1-n} \cdot pH_2O$ (De Vito 2006), accommodates Ca^{2+}, Fe^{3+}, Mn^{2+}, Na^+, REE^{3+}, Sr^{2+}, Th^{4+}, U^{4+}, and Y^{3+} in the tetrahedrally-coordinated A site; and Al^{3+}, Fe^{3+}, Nb^{5+}, Si^{4+}, Ta^{5+}, Ti^{4+}, W^{6+} and Zr^{4+} in the octahedrally-coordinated B site. As iron can enter the

A-site of pyrochlore in its ferric state, all iron is recalculated into the ferric state, despite the likelihood of ferrous iron in the A-site. It should be noted that fluorine was omitted in the analyses, as fluorine/iron peak overlap preventing accurate results.
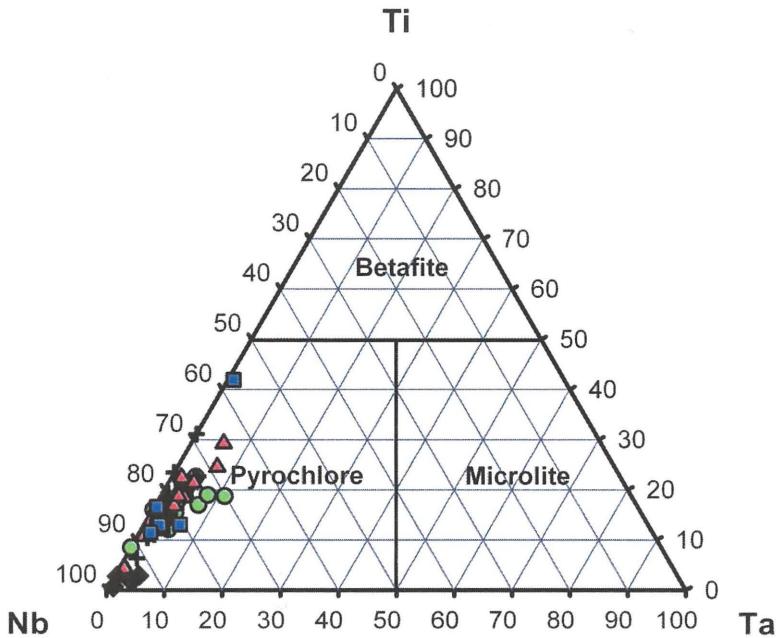
FIGURE 4.44: Titanium (Ti) – niobium (Nb) – tantalum (Ta) ternary plot (apfu). Green circles, black crosses, red, black diamonds, and blue squares are the Border Gabbro, Railway, Upper Marathon Shore, Black, and Center Three pegmatites, respectively.

The extent of B-site substitution is shown in Figure 4.46. The B-cation in pyrochlore is relatively inert, as the B_2O_6 framework is very stable, and is not usually affected by alteration. As such, the pyrochlore structure more readily subject to A-cation exchange or total A-cation loss:

$Na^+ + REE^{3+} \rightarrow 2Ca^{2+}$	Lumpkin and Ewing (1995)
$REE^{3+} + (Ti,Zr)^{4+} \rightarrow Ca^{2+} + Nb^{5+}$	Lumpkin and Ewing (1995)
$Ca^{2+} + (Ti,Zr)^{4+} \rightarrow Na^+ + Nb^{5+}$	Lumpkin and Ewing (1995)
$A \rightarrow \square$	
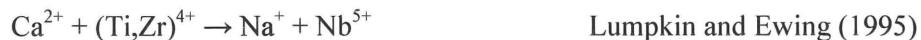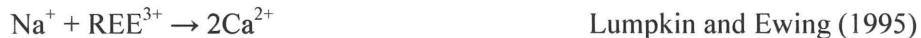
The extent of A-site vacancies is shown in Figure 4.47. The trend from full occupancy to complete vacancy is related to selective leaching. If metamictization is a factor, there will be a correlation, shown by the red arrow in Figure 4.47, between the actinide contents and A-site vacancies.
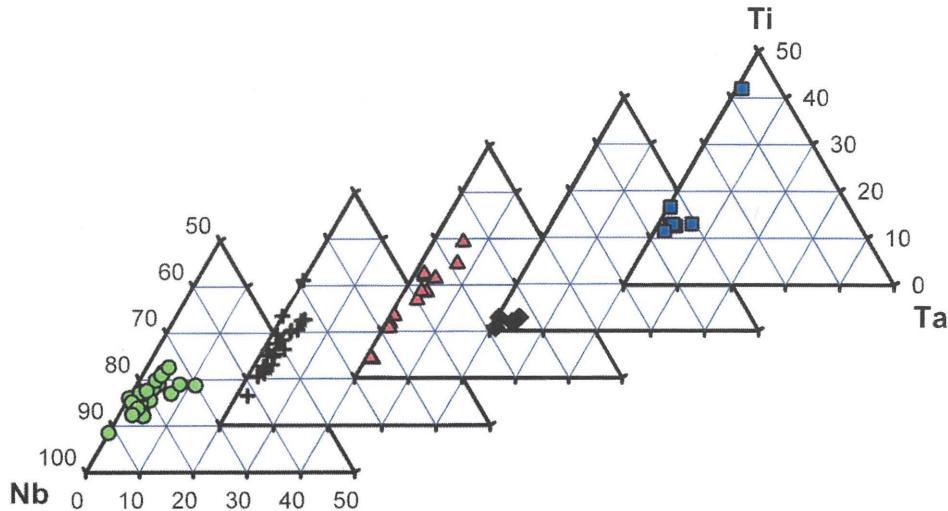
FIGURE 4.45: Expanded view of Figure 4.43 with all lithologies separated.

The maximum occurrence of 0.777 apfu ferric/ferrous, iron is significant in Coldwell pyrochlores. As shown in Figure 4.48, there is a correlation between both calcium- and niobium-sites and iron. Similar trends are observed in the Lueshe (Democratic Republic of Congo) and Araxá (Brazil) carbonatites (Nasraoui and Waerenborgh 2001). In general there is a better correlation between calcium and iron in the Coldwell complex although this is not the case in Railway pyrochlores. As such, iron in the niobium-site explains why there is such a large error in Railway B-site substitution diagram (Figure 4.46A).
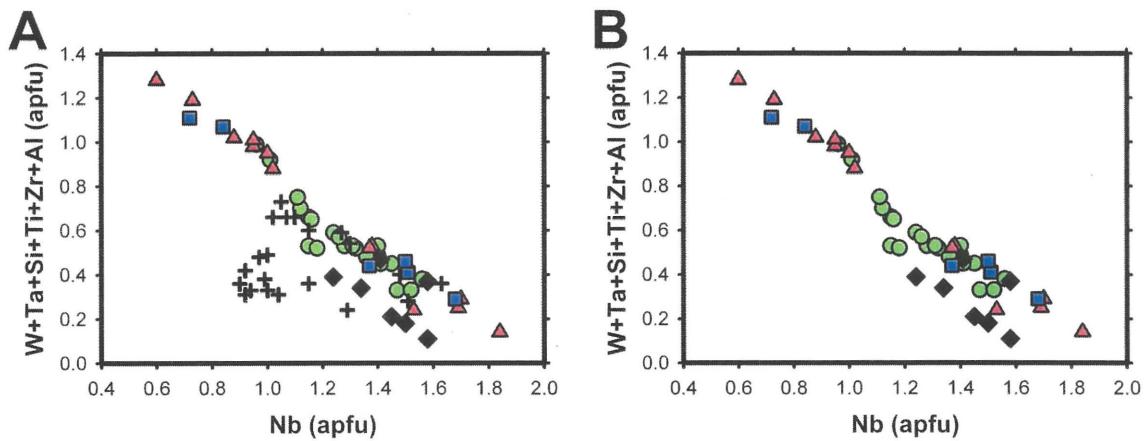
FIGURE 4.46: Pyrochlore niobium vs other B-site ions. A ($r^2 = 0.528$) includes all lithologies, B ($r^2 = 0.898$) has the Railway pegmatites omitted. Green circles, black crosses, red triangles, black diamonds, and blue squares are the Border Gabbro, Railway, Upper Marathon Shore, Black, and Center Three pegmatites, respectively.

Silicon is another important ion in Coldwell pyrochlores. Silicification of pyrochlore occurs in primary liquidus (Fig. 4.43A) and secondary stages (Fig. 4.43B). Silica content in Coldwell pyrochlores reaches a maximum of 0.909 apfu and an average of 0.248 apfu.

Lumpkin and Ewing (1995) recognized primary, transitional and secondary alteration trends, each of which having their own distinctive textures and exchange characteristics. These authors distinguish primary alteration as having exchange characteristic—i.e. calcium, sodium and fluorine for strontium, oxygen, minor manganese, iron and barium without any textural heterogeneity. Transitional alteration, having oscillatory zoning that reflects loss of sodium, calcium and fluorine and gains in REEs and iron, and secondary alteration having fracture-controlled patchy zoning reflecting loss of calcium, sodium and fluorine and increases in manganese, iron, REEs, and water. Coldwell pyrochlores display all three mechanisms. Primary alteration is predominant, with seemingly "unaltered" grains devoid, or extremely low, sodium and low calcium, and increasing iron and A-site vacancies. Transitional alteration is characterized by oscillatory zoning that reflect high silicon and water content. As all grains are altered in the primary stage, changes in composition, other than silica and water, are difficult to quantify. The same happens to pyrochlore grains altered in the secondary stage of crystallization, which are characterized by their feathered textures, and extremely high water and silicon content. The A-site vacancy (A-vac) – divalent ions (A^{2+}) – monovalent ions (A^{+}) ternary plot in Figure 4.49 shows a trend that, according to Lumpkin and Ewing (1995), is typical of transitional alteration, but, as all pyrochlores are significantly altered in the primary stage, high A-site deficiencies prohibit any other useful information from being extracted from this particular diagram.

Alternatively, Ercit (2005) described six mechanisms that can be used to generalize what kind, if any, of alteration the pyrochlore grains may have been subjected to. These mechanisms include: hydration; high-field-strength-element (HFSE) gain (e.g. Si and Al); large-ion-lithophile-element (LILE) gain (e.g. K, Ba and Sr); calcium addition; exchange of HREE and Y for LREE; and A-cation loss. In general, hydration, metamictization and the addition of F, Si, Al, Ba, K, and Sr all result in the reduction of the analytical total by either creating vacant sites, or addition of ions that are undetectable using SEM/EDS analysis. High Nb/Ti ratios and low REEs, uranium and silica, characterize the primary pyrochlores. The totals for secondary pyrochlore are characteristically low, as deuteric environments tend to be enriched in F and H_2O (undeterminable elements), and HFSE-enriched. Replacement of ions and leaching of A-site ions of metamictized crystals alter the margins of pyrochlore.
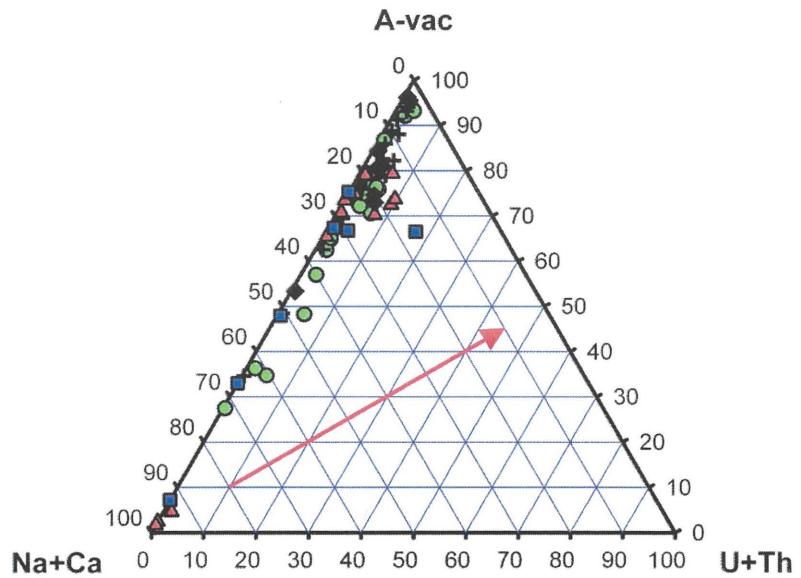
FIGURE 4.47: Pyrochlore A-site vacancy (A-vac) – sodium + calcium (Na+Ca) – uranium + thorium (U+Th) ternary plot (apfu). The red arrow is the ideal trend if actinide were responsible for vacating the A-site. Green circles, black crosses, red triangles, black diamonds, and blue squares are the Border Gabbro, Railway, Upper Marathon Shore, Black, and Center Three pegmatites, respectively.
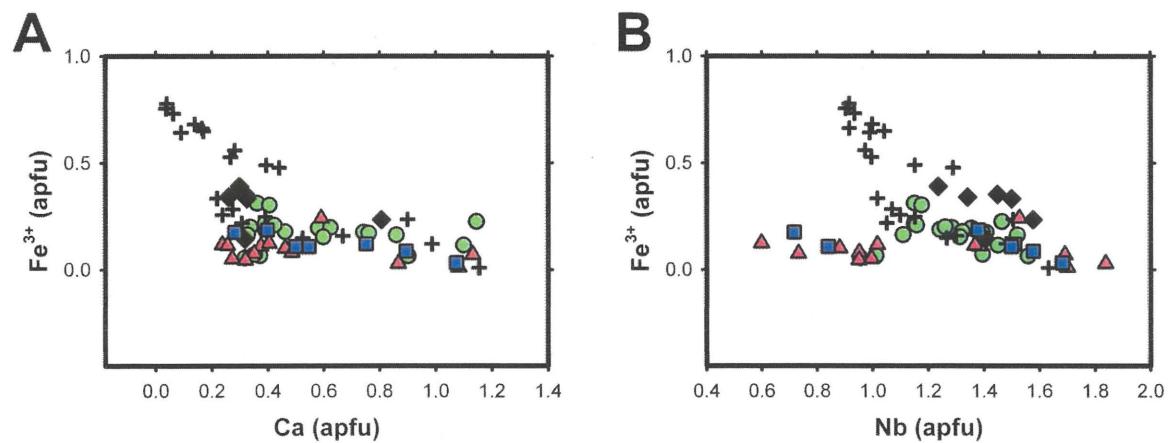
FIGURE 4.48: Pyrochlore iron substitution binary diagrams. A is calcium (Ca) vs. iron (Fe), B is niobium (Nb) vs. iron.

TABLE 4.22: Pyrochlore from other localities.

	Altered Breccia Syenite[1]	NYF-Pegmatite[2]	Per-alkaline Granite[3]	Sövite Carbonatite[4]	Sövite Carbonatite[5]
WO_3	-	1.31	-	-	-
Nb_2O_5	52.54	21.02	50.77	64.74	66.94
Ta_2O_5	1.62	5.58	1.71	-	0.27
SiO_2	4.70	1.37	-	0.66	-
TiO_2	5.60	24.36	10.25	5.50	3.34
ZrO_2	-	-	-	1.66	-
ThO_2	1.39	6.68	1.18	0.62	0.09
UO_2	6.35	11.22	12.22	-	0.16
Al_2O_3	0.08	-	-	-	-
Y_2O_3	-	3.10	-	-	-
La_2O_3	0.47	1.09	2.21	0.11	0.32
Ce_2O_3	3.09	5.78	7.03	1.29	0.68
Pr_2O_3	0.24	0.92	-	-	-
Nd_2O_3	0.70	3.97	-	-	-
Sm_2O_3	-	1.16	-	-	-
Gd_2O_3	-	0.86	-	-	-
Dy_2O_3	-	0.49	-	-	-
Er_2O_3	-	0.29	-	-	-
Yb_2O_3	-	0.35	-	-	-
Fe_2O_3	-	-	-	0.24	-
FeO	4.88	1.37	-	-	-
MnO	0.45	0.53	-	-	-
CaO	3.76	5.04	1.68	17.26	14.69
SrO	-	-	-	-	1.33
PbO	-	-	3.05	0.41	-
BaO	-	-	-	-	0.11
Na_2O	0.31	-	4.28	6.96	7.90
K_2O	-	-	-	-	-
Total	**86.18**	**96.49**	**94.38**	**99.45**	**95.83**

[1] Altered/brecciated syenite (sample PT61) from the Lake Zone, Thor Lake, N.W.T., Canada (Pinckston and Smith 1995).

[2] NYF-pegmatite (Koz B yttropyrochlore sample) from, the Kožichovice intrusive, Czech Republic (Škoda et al. 2006).

[3] Peralkaline granite (sample Pyc-I from grain 1) from the Kuiqi peralkaline A-type granites, China (Xie et al. 2006).

[4] Sövite carbonatite (sample 31-350.2d) from the Oka carbonatite complex (Hay 2003).

[5] Sövite carbonatite (31 analyses of sövite sample) from the Lueshe carbonatite complex (Nasraoui and Bilal 2000).

Coldwell pyrochlores (Table 4.20) are similar in composition (ACTS, iron, REEs, and silicon) to occurrences in other anorogenic intrusive, i.e. A-type syenites, granites, pegmatites and carbonatites (Table 4.21). Ta/Nb ratios can be used to identify the source of pyrochlores (Nasraoui and Bilal 2000). The Coldwell pegmatites Ta/Nb ratio (1/15.5) is similar to syenites from Lueshe (1/43 < Ta/Nb < 1/19) and from the analyses given by Pinckston and Smith (1995) from Thor Lake, Canada, NYF-pegmatites from the Kožichovice intrusive, Czech Republic (Škoda et al. 2006) and granites from the Kuiqi peralkaline A-type intrusion, China (Xie et al. 2006). Alternatively, carbonatites have a much lower Ta/Nb ratios, e.g. Lueshe has a ratio of 1/71 (Nasraoui and Bilal 2000).
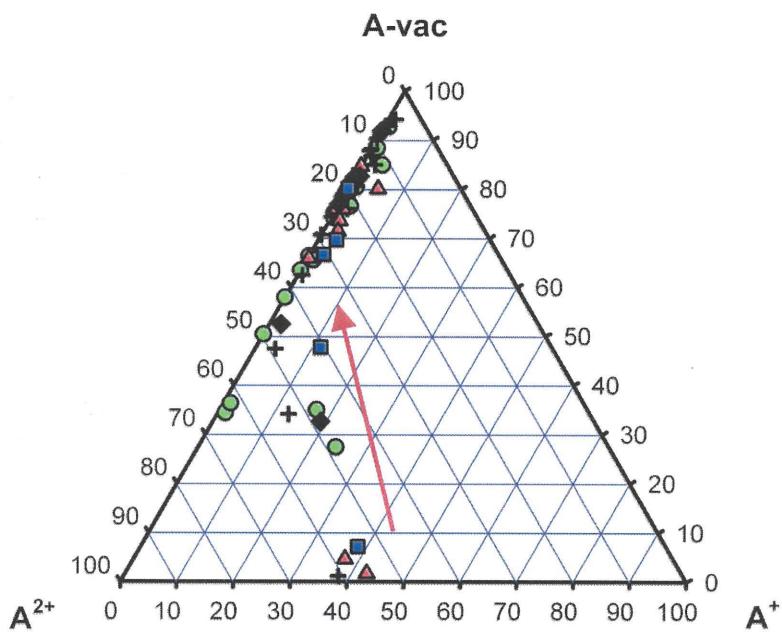
FIGURE 4.49: Pyrochlore A-site vacancy (A-vac) – divalent ions (A^{2+}) – monovalent ions (A^+) ternary plot (apfu). The red arrow is the trend typical of transitional alteration (Lumpkin and Ewing 1995).

4.21 Rutile

Rutile (TiO_2) is a common accessory mineral occurring in a variety of rock types. In the Coldwell pegmatites, rutile occurs in the Border Gabbro and Upper Marathon Shore units. Rutile forms in the interstitial and secondary stages of crystallization. As an interstitial mineral, rutile forms with calcite and quartz. Figure 4.50A shows interstitial rutile forming stubby ditetragonal dipyramids. Secondary rutile is intimately associated with fluorocarbonates and chevkinite. The association with fluorocarbonates, shown in Figure 4.50C, relates to the breakdown of

chevkinite, with REEs and calcium partitioning into the fluorocarbonate structure, and titanium and niobium into the rutile structure (discussed in the chevkinite section).
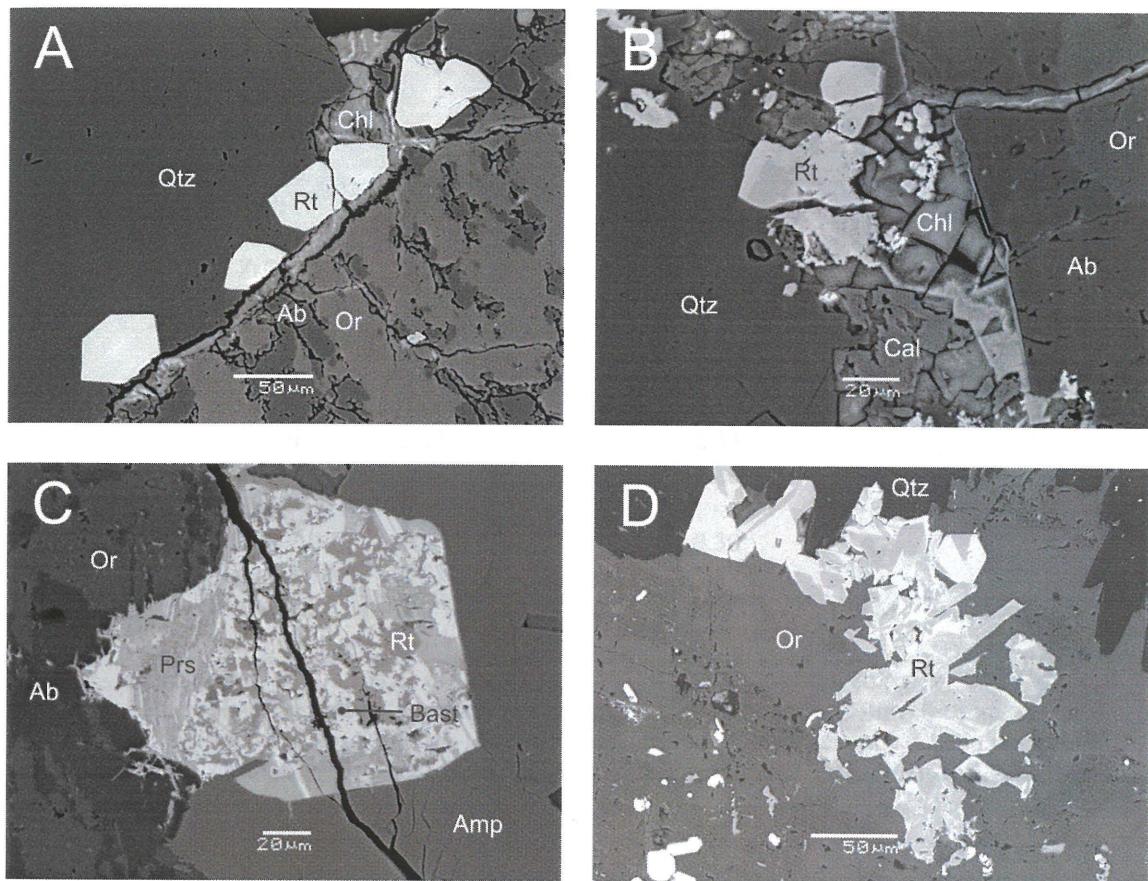
FIGURE 4.50: BSE-images of rutile. A has euhedral rutile (Rt) in quartz (Qtz) and chlorite (Chl) grown adjacent to perthite (Or and Ab). B has subhedral rutile associated with chlorite, quartz and calcite (Cal). C contains rutile associated with the fluorocarbonates bastnaesite (Bast) and parisite (Prs) enclosed in perthite and amphibole (Amp). D is rutile in orthoclase and quartz. The lighter areas in D are enriched in Nb.

In addition to niobium, which ranges from 0.67 to 23.19 wt. % Nb_2O_5, other ions such as silicon (0.14 to 2.33 wt. % SiO_2), ferrous iron (0.00- 6.21 wt. % FeO), and ferric iron (0.00-4.84 wt. % Fe_2O_3) range considerably (Table 4.22 and Appendix III.XII). Zirconium is present in the Border Gabbro rutile and, to a much lesser extent, the Upper Marathon Shore pegmatites, with values from zero to 2.07 oxide wt. % ZrO_2 (Table 4.22 and Appendix III.XII). Minor uranium and tin are detected in some of the Border Gabbro and Upper Marathon Shore rutile, respectively.

TABLE 4.23: Representative compositions of rutile.

	Border Gabbro[1]	Upper Marathon Shore[2]	NYF-Pegma-tite[3]	NYF-Pegma-tite[4]
WO_3	-	-	0.67	-
Ta_2O_5	-	-	0.59	2.05
Nb_2O_5	8.48	16.10	7.71	5.95
SiO_2	1.26	2.33	-	-
TiO_2	82.79	77.17	84.32	89.19
ZrO_2	2.07	0.27	-	-
SnO_2	-	-	3.58	0.51
UO_2	0.51	-	-	-
Al_2O_3	-	0.09	0.52	-
Sc_2O_3	-	-	0.13	-
Fe_2O_3	3.53	1.23	0.83	1.87
FeO	-	3.53	1.20	1.06
CaO	0.26	0.16	-	-
MnO	-	-	0.38	-
CuO	0.51	-	-	-
Total	**99.41**	**100.88**	**99.93**	**100.63**

[1] Border Gabbro pegmatite (1 analysis of sample MAS007) from the Coldwell complex.
[2] Upper Marathon Shore pegmatite (2 analyses of sample MAS012) from the Coldwell complex.
[3] NYF-pegmatite (Kra rutile sample) from the Kracovice intrusion, Czech Republic (Škoda et al. 2006).
[4] NYF-pegmatite (Val rutile sample) from the Vladislav-Pazderníkův mlýn pluton, Czech Republic (Škoda et al. 2006).

Compared to NYF pegmatites from the Kracovice intrusion, Czech Republic and the Vladislav-Pazderníkův mlýn pluton, Czech Republic (Škoda et al. 2006), Coldwell rutiles are low in tantalum, titanium and tin, and enriched in niobium (Table 4.22). The compositions of primary rutile are more similar to Kracovice and Vladislav-Pazderníkův, as the niobium-rich variety is secondary.

Rutile adopts the tetragonal P_2mnm structure (Soffer 1961). There are two distinct compositions of rutile that occur in the Coldwell pegmatites: stoichiometric rutile (TiO_2) and Nb-rutile [$(Nb,Ti)O_2$]. Other minor elements include: Ca^{2+}, Cu^{2+}, Fe^{2+}, Fe^{3+}, Mn^{2+}, REE^{3+}, Si^{4+}, U^{4+}, and Zr^{4+} in the Ti site; and OH^- in the O site. Common simple substitutions include tetravalent ions into the titanium site:

$$(U,Zr,Si)^{4+} \rightarrow Ti^{4+}$$
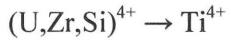
Figure 4.51A plots tetravalent ions (M^{4+}) against titanium (Ti). No real correlation is present, but this may be a result of low abundances of the tetravalent species, and overlap of other mechanism.
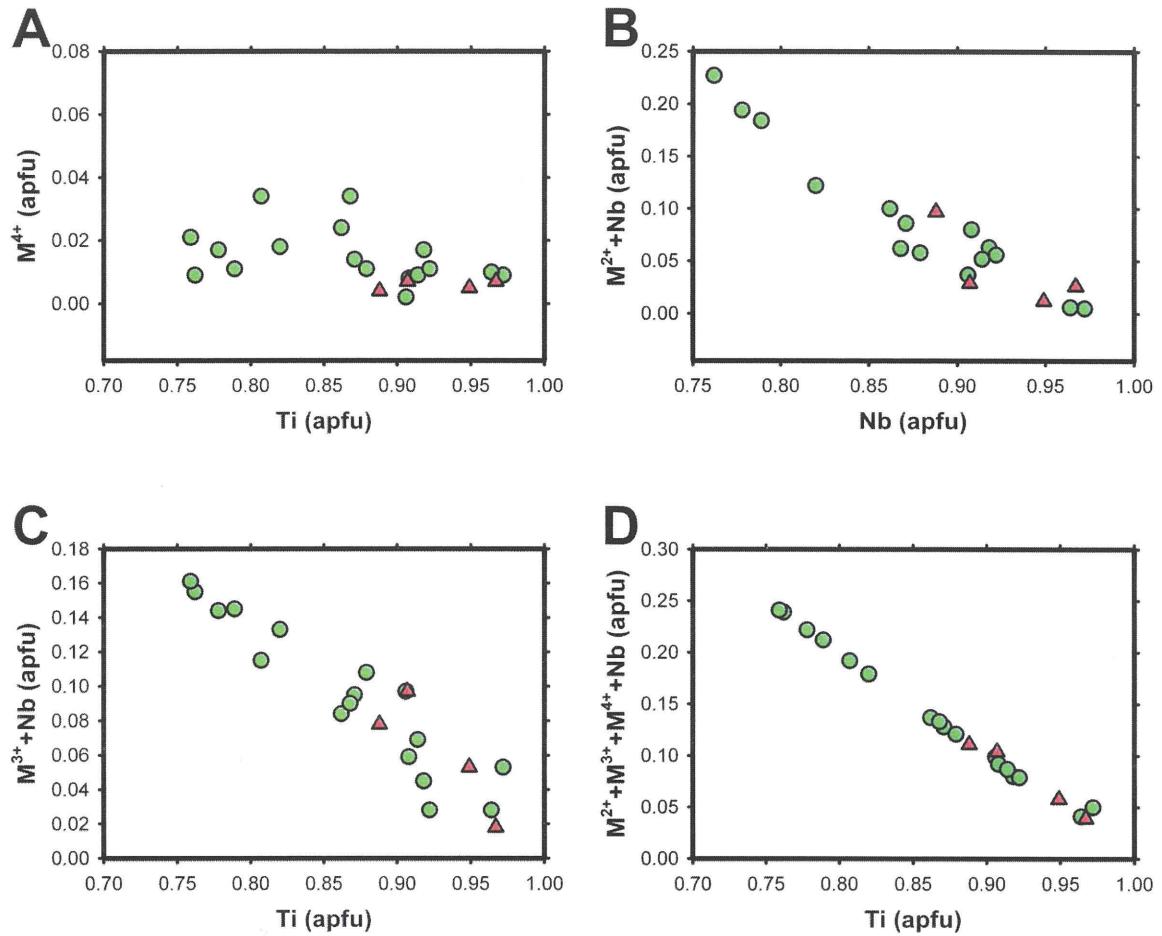
FIGURE 4.51: Various binary diagrams of titanium substitution. A is M^{4+} ions (Si, Zr, and U) plotted against Ti, R^2 is 0.199. B is M^{2+} (Fe, Ca, and Cu) and Nb ions plotted against Ti, r^2 is 0.920. C is M^{3+} (Fe^{3+} and Al) and Nb ions plotted against Ti, r^2 is 0.886. D is the combined mechanisms [M^{2+} (Fe^{2+}, Ca, and Cu), M^{3+} (Fe^{3+} and Al), M^{4+} (Si, Zr, and U)], and Nb against Ti, r^2 is 0.995. Green circles are the Border Gabbro pegmatites. Red triangles are the Upper Marathon Shore pegmatites.

Solid solutions between rutile and columbite [$(Fe,Mn)Nb_2O_6$], produce coupled substitutions into the titanium structural site:

$$(Fe,Mn)^{2+} + 2Nb^{5+} \rightarrow 3Ti^{4+}$$
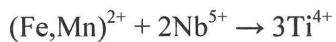
Vlassopoulos et al. (1993)

In the case of the Coldwell pegmatites, this mechanism is expanded to include the other divalent metals:

$$(Ca,Cu,Fe,Mn)^{2+} + 2Nb^{5+} \rightarrow 3Ti^{4+}$$
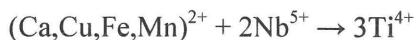
All divalent metals are plotted with niobium against titanium in Figure 4.51B. With an r^2 value of 0.920, the divalent metals plus niobium vs. titanium indicate that another substitution mechanism is present.

The presence of ferric iron was quoted by Vlassopoulos et al. (1993), and in the case of the Coldwell pegmatites, aluminum is also included. Fe^{3+}/Fe^{2+} recalculations are obtained using the Droop (1987) method, and all ferric iron is combined with aluminum and niobium to occupy two titanium sites:

$$(Fe,Al)^{3+} + Nb^{5+} \rightarrow 2Ti^{4+} \qquad \text{Vlassopoulos et al. (1993)}$$

The above mechanism is plotted in Figure 4.51C, and gives an r^2 value of 0.886. In addition to niobium, the combination of di-, tri, and tetra-valent ions into the titanium site form a convincing correlation, as depicted in Figure 4.51D.

Many studies have detected hydroxyl in rutile (Soffer 1961; Hill 1968; Hammer and Beran 1991; Vlassopoulos 1993). The incorporation of hydroxyl into the rutile structure allows for trivalent and pentavalent ions to substitute into the rutile structure:

$$(Fe,REE)^{3+} + OH^- \rightarrow Ti^{4+} + O^{2-} \qquad \text{Vlassopoulos et al. (1993)}$$
$$Nb^{5+} + OH^- \rightarrow Ti^{4+} \qquad \text{Vlassopoulos et al. (1993)}$$

The hydrogen content in rutile can be used to define intensive parameters such as fugacity, and water activity (Vlassopoulos et al. 1993). Certain pitfalls, as described by Vlassopoulos et al. (1993), are equilibration temperatures of the hydrous phase and the reduction or oxidation of iron or niobium. In the case of the rutile in Coldwell pegmatites, there is no significant hydroxyl component detected—as totals are within the margin of error—and utilizing the hydrogen content for petrogenetic information may be misleading.

It has been shown by Keppler (1993) that melts with high fluorine content will affect the solubilities of columbite, rutile and zircon. As such, HFSE and REEs tend to be incompatible during fractional crystallization and, with the exception of zircon (see zircon section), only occur in the later stages of crystallization. Secondary rutile is not related to incompatibility. On the other hand, interstitial rutile indicates that the incompatible elements titanium and niobium were stable in melt.

4.22 Sphalerite

Sphalerite is the most common sulphide to occur within pegmatitic Coldwell rocks. In common with other sulphides, sphalerite forms in the late interstitial stage of crystallization (Fig. 4.52). All sphalerite crystals are anhedral, and closely associated with chalcopyrite (Fig. 4.52B). Other associations are with arsenopyrite, galena and pyrite. An inclusion of a cobaltian arsenic sulphide (alloclastite?) occurs in one sphalerite grain from the Border Gabbro pegmatites, but as the grain is small, no accurate analyses could be preformed (Fig. 4.52B).
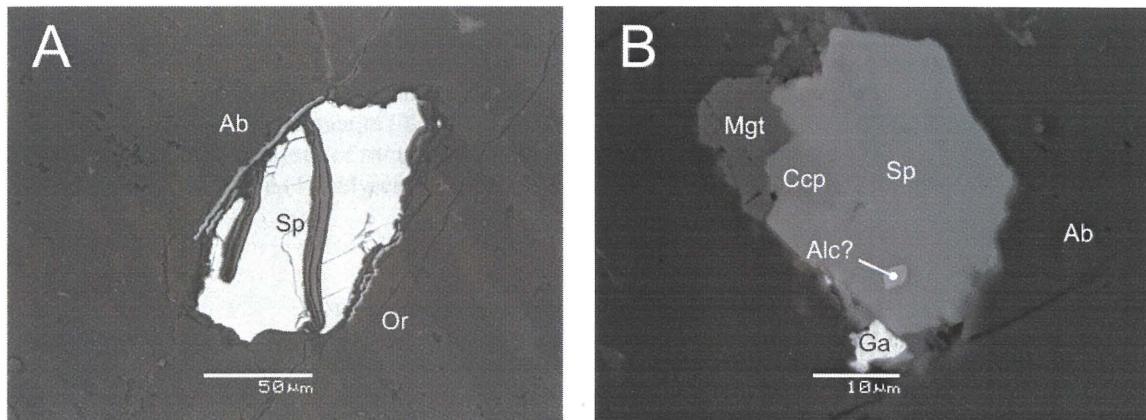
FIGURE 4.52: BSE-images of sphalerite (Sp). A is sphalerite in albite (Ab) and orthoclase (Or). B is sphalerite associated with chalcopyrite (Ccp), galena (Ga) and alloclastite? (Alc?). The sphalerite grain in B is surrounded by albite and magnetite (Mgt).

Within the Coldwell units analyzed, sphalerite is able to accommodate Fe and Cu (Table 4.24) by simple substitution:

$$(Cu,Fe)^{2+} \rightarrow Zn^{2+}$$
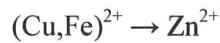
4.23 Thorite

Thorite, $ThSiO_4$, is a trace mineral present in all Coldwell pegmatites. Thorite has a light yellow-to-brown pleochroism, high relief and first order grey birefringence (Fig. 4.53). High thorium and uranium content is responsible for metamictization of the individual thorite crystals and surrounding materials, whereby producing opaque pleochroic halos (Fig. 4.52). Thorite crystallizes in the initial stage of the paragenesis, usually with zircon, and occasionally with fergusonite, xenotime, and galena (Fig. 4.54). The composition of Coldwell thorite is variable, but can be grouped to produce the REE ternary diagram in Figure 4.55, sub-grouped into two varieties: LREE-thorite and HREE-thorite.

TABLE 4.24: Representative compositions of sphalerite.

	Border Gabbro[1]	Railway[2]	Upper Marathon Shore[3]	Black[4]	Center Three[5]
Fe	12.87	11.29	10.51	2.35	1.13
Zn	52.71	55.56	56.89	63.85	64.25
Cu	0.51	-	-	0.34	0.63
S	33.76	33.84	33.05	33.28	33.49
Total	**99.85**	**100.69**	**100.45**	**99.82**	**99.50**

[1] Border gabbro pegmatite (3 analyses of sample MAS005) from the Coldwell complex.
[2] Railway pegmatite (5 analyses of sample MAS015) from the Coldwell complex.
[3] Upper Marathon Shore pegmatite (3 analyses of sample MAS019) from the Coldwell complex.
[4] Black pegmatite (6 analyses of sample MAS030) from the Coldwell complex.
[5] Center Three pegmatite (4 analyses from sample MAS034) from the Coldwell complex.
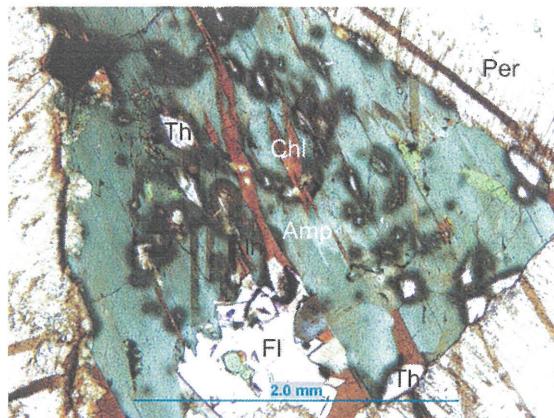
FIGURE 4.53: Photomicrograph of thorite (Th) in amphibole (Amp), perthite (Per), fluorite (Fl), and chlorite (Chl). Metamictization produces the pleochroic haloes along the thorite boundaries.

LREE-thorite is of the cerium variety, with cerium ranging up to 7.32 wt. % Ce_2O_3. Relative maximum abundances (in wt. %) are 5.58 La_2O_3, 1.17 Pr_2O_3, 3.52 Nd_2O_3, and 0.77 Sm_2O_3. HREE-thorite is dominated by yttrium (up to 8.65 wt. % Y_2O_3), but also includes significant amounts of gadolinium (max1.06 wt. % Gd_2O_3), dysprosium (max 1.49 wt. % Dy_2O_3), erbium (max 1.22 wt. % Er_2O_3), and ytterbium (max 1.20 wt. % Yb_2O_3). A limited solid solution between LREE and HREE thorite varieties is shown in Figure 4.55, with a possible miscibility gap between 30 and 50 total REE apfu %.
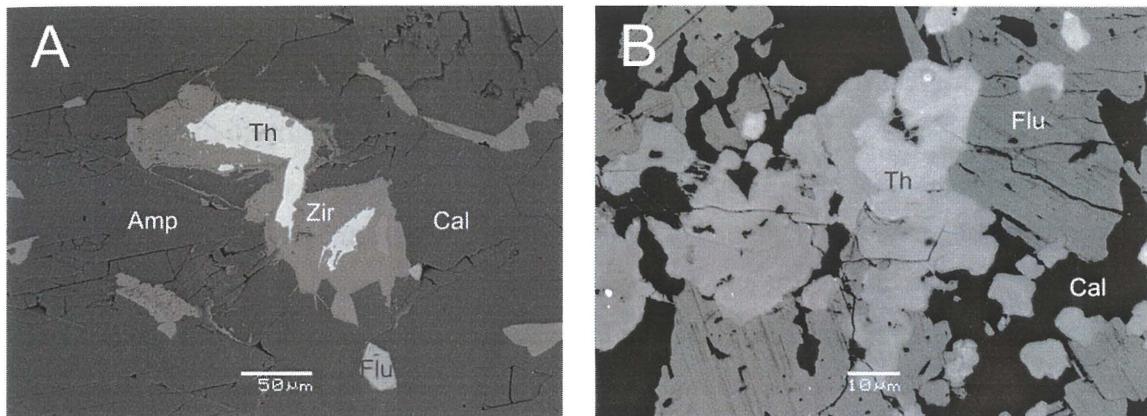
FIGURE 4.54: BSE-images of thorite (Th). A is thorite mantled by zircon (Zir) and surrounded by amphibole (Amp) and calcite (Cal). B is highly metamict thorite and fluorocarbonates (Flu) with a calcite groundmass. Fluorocarbonates are replacement minerals representing either REE silicates or phosphates.
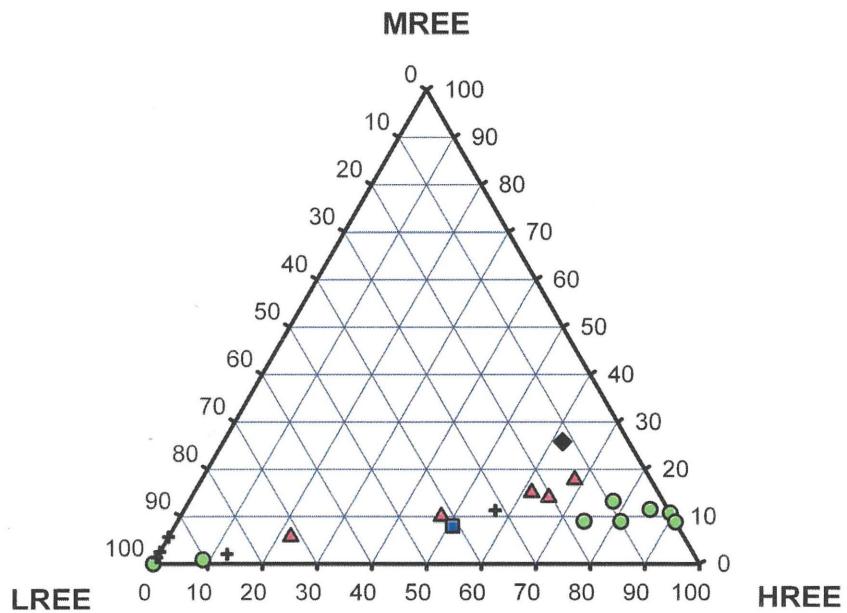
FIGURE 4.55: Thorite MREE (Sm-Ho) – LREE (La-Nd) – HREE (Y,Er-Lu) ternary plot (apfu).

Relative amounts of uranium versus thorium and REEs are shown in Figure 4.56. Uranium is a minor component in Coldwell thorite, with a maximum value of 10.76 wt. % UO_2, but averaging 2.42 wt. % UO_2. Other ions included in Coldwell thorite are phosphorus (0-2.83

wt. % P_2O_5), niobium (0-1.18 wt. % Nb_2O_5), zirconium (0-1.86 wt. % ZrO_2), aluminum (0-1.32 wt. % Al_2O_3), calcium (0-4.46 wt. % CaO), manganese (0-0.46 wt. % MnO), iron 0-4.98 wt. % FeO), and lead (0-0.98 wt. % PbO).

The monoclinic polymorph huttonite may occur in place of thorite. Mazeina et al. (2005) have determined that the phase transition from thorite to huttonite from an oxide melt occurs at approximately 800 ˚C, thus, in Coldwell pegmatites, the thorite structure likely prevails.

Thorite is a common inclusion in zircon. Lei et al. (2005) have proposed that the thorite inclusions are a product of "wet" dissolution of thorium from the zircon host and then reprecipitation of primary Th-poor zircon and thorite:

$$(Zr_{1-x}Th_x)SiO_4 \rightarrow (1-x)ZrSiO_4 + xThSiO_4$$
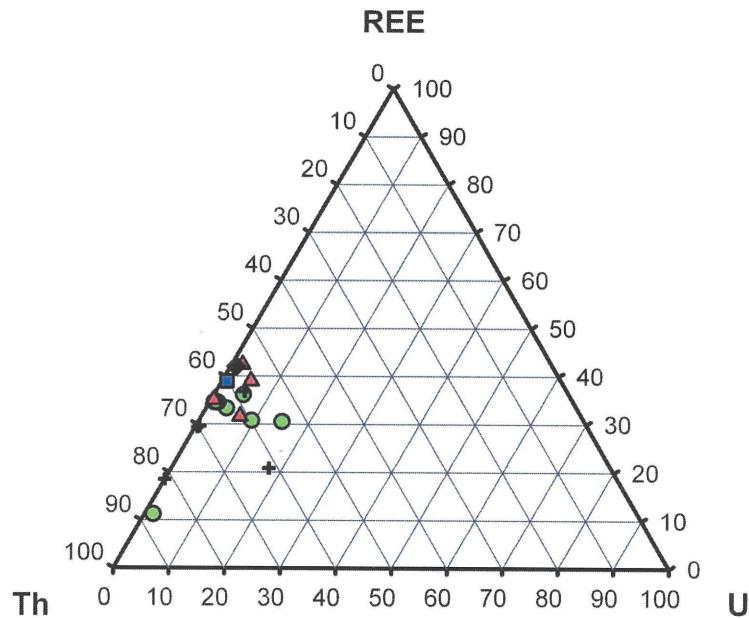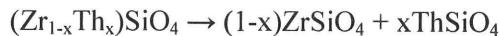
FIGURE 4.56: Thorite REE – thorium (Th) – uranium (U) ternary diagram (apfu). The contribution from uranium in the Coldwell thorite is small, instead the mineral is enriched in REEs.

Substitution mechanisms for thorite are difficult to illustrate as metamictization destroys the crystal structure, leaving short range ordering of ions. Correlations are then difficult to constrain as valency and ionic radii do not necessarily govern which ions are able to enter the short range thorite structure.

TABLE 4.25: Representative compositions of thorite.

	Border Gabbro[1]	Railway[2]	Upper Marathon Shore[3]	Black[4]	Center Three[5]	Granitic Peg.[6]	Altered Syenite[7]
P_2O_5	-	2.83	0.79	0.96	-	0.9	0.48
SiO_2	23.35	18.56	20.27	19.14	19.21	18.0	17.82
ZrO_2	-	-	-	-	-	0.1	-
ThO_2	52.35	52.09	50.03	46.21	48.33	64.4	53.19
UO_2	0.92	0.56	5.75	0.77	0.72	6.7	1.59
Al_2O_3	1.32	0.20	0.35	0.23	0.38	-	0.24
Y_2O_3	-	-	2.37	8.09	6.18	4.0	1.36
La_2O_3	0.99	5.58	1.20	0.06	0.64	0.1	0.33
Ce_2O_3	2.01	6.06	6.21	0.58	3.41	0.2	6.65
Pr_2O_3	0.35	0.77	0.87	0.39	0.92	-	0.78
Nd_2O_3	0.90	1.15	3.27	1.55	3.10	0.4	4.28
Sm_2O_3	-	0.21	0.20	1.12	0.74	0.4	0.84
Eu_2O_3	-	-	-	0.70	-	-	-
Gd_2O_3	-	-	0.21	1.69	0.26	0.3	0.84
Tb_2O_3	-	-	-	0.29	-	-	-
Dy_2O_3	-	-	0.54	1.48	0.66	0.2	-
Ho_2O_3	-	-	-	0.75	-	-	-
Er_2O_3	-	-	0.10	0.64	0.86	0.2	-
Tm_2O_3	-	-	-	0.39	-	-	-
Yb_2O_3	-	-	-	0.48	0.21	0.1	-
Lu_2O_3	-	-	-	0.10	-	-	-
CaO	4.46	1.07	1.01	0.76	1.18	0.7	2.96
FeO	2.06	4.02	-	2.24	0.71	-	0.48
ZnO	-	-	-	-	-	-	0.80
PbO	-	0.35	-	-	-	0.5	-
Na_2O	-	-	-	-	-	-	0.22
Total	**88.71**	**93.45**	**93.17**	**88.62**	**87.51**	**97.2**	**92.86**

[1] Border Gabbro pegmatite (4 analyses of sample MAS002) from the Coldwell complex.

[2] Railway pegmatite (4 analyses of sample MAS016) from the Coldwell complex.

[3] Upper Marathon Shore pegmatite (6 analyses of sample MAS019) from the Coldwell complex.

[4] Black pegmatite (3 analyses of sample MAS029) from the Coldwell complex.

[5] Center Three pegmatite (2 analyses of sample MAS037) from the Coldwell complex.

[6] Granitic pegmatite (second intermediate zone sample) from the Amelia district, Virginia (Lumpkin 1998).

[7] Altered syenite (sample PT67) from Thor Lake complex, Canada (Pinckston and Smith 1995).

4.24 Titanite

Titanite is a trace mineral in the Border Gabbro, Railway and Center Three pegmatites. Titanite is associated with amphibole, and its decomposition products, i.e. chlorite and quartz (Fig. 4.57A). Initial-forming minerals, i.e. magnetite, are common inclusions in titanite crystals (Fig. 4.57B). All grains analyzed contain minor to trace amounts of aluminum, iron and niobium (Table 4.25 and Appendix III.XIV).

Only one grain of titanite is present in the Border Gabbro samples. This grain, shown in Figure 4.57A, has corroded edges, and occurs with chlorite. The grain has minor aluminum (3.69 wt. % Al_2O_3), iron (3.33 wt. % Fe_2O_3) and niobium (0.60 wt. % Nb_2O_5).

In the Railway pegmatites, titanite occurs twice in one sample, one of which is shown in Figure 4.57B. These grains enclosed small magnetite crystals, and grew interstitially between the cumulous-forming feldspar. The Railway pegmatite titanite grains contains slightly more aluminum (4.87-6.02 wt. % Al_2O_3), similar niobium (0.54-1.82 wt. % Nb_2O_5) and lower iron (2.11-3.11 wt. % Fe_2O_3) than the Border Gabbro titanite.
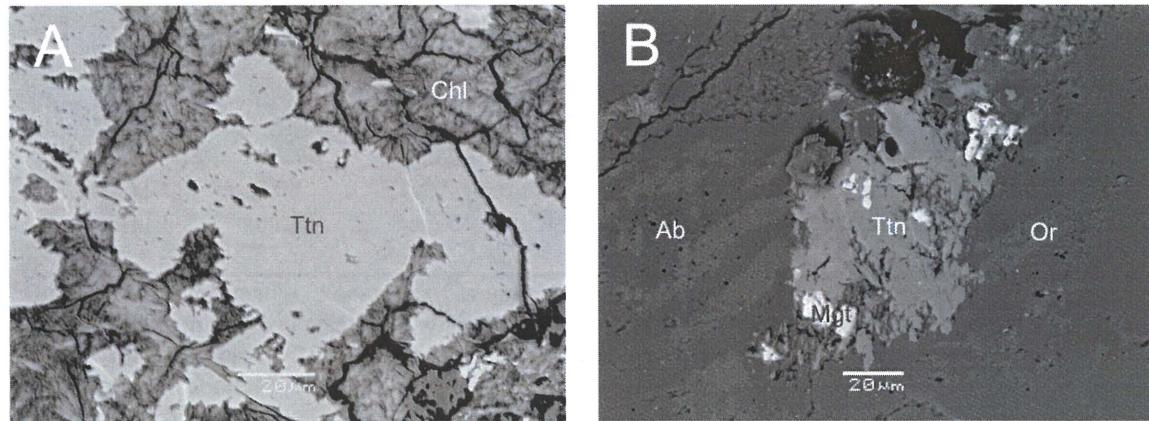
FIGURE 4.57: BSE-images of titanite (Ttn). A is interstitial titanite in albite (Ab) and orthoclase (Or) with magnetite (Mgt) inclusions. B is titanite surrounded by chlorite (Chl).

There are two samples in Center Three pegmatites which contain titanite. In both cases, titanite occurs with taramite amphibole, magnetite and chlorite. These two titanite grains contain low-to-high niobium (0.34-3.46 wt. % Nb_2O_5), minor amounts of aluminum (2.70-3.22 wt. % Al_2O_3) and iron (2.59-5.22 wt. % Fe_2O_3). One of the samples also contains detectable zirconium (1.00 wt % ZrO_2).

TABLE 4.26: Representative compositions of titanite.

	Border Gabbro[1]	Railway[2]	Center Three[3]	Granitic Pegmatite[4]	Per-alkaline Granite[5]	Aluminous Granite[6]
Ta_2O_5	-	-	-	0.72	0.11	-
Nb_2O_5	0.60	0.54	3.46	1.51	0.35	0.27
SiO_2	31.75	31.40	31.04	30.03	25.83	27.66
TiO_2	32.16	30.81	30.72	34.39	35.83	33.00
SnO_2	-	-	-	0.23	-	-
ZrO_2	-	-	1.00	-	-	-
Al_2O_3	3.69	6.02	2.70	1.92	1.91	8.51
Y_2O_3	-	-	-	1.13	1.34	-
La_2O_3	-	-	-	-	0.32	-
Ce_2O_3	-	-	-	0.90	1.53	0.11
Pr_2O_3	-	-	-	0.23	-	-
Nd_2O_3	-	-	-	0.77	0.39	-
Sm_2O_3	-	-	-	0.24	-	-
Gd_2O_3	-	-	-	0.23	-	-
Dy_2O_3	-	-	-	0.17	-	-
Yb_2O_3	-	-	-	0.14	-	-
Fe_2O_3	3.33	2.11	3.12	0.47	3.55	0.82
CaO	28.73	28.64	26.58	26.13	23.97	27.67
MnO	-	-	-	-	0.63	0.14
Total	**100.26**	**99.52**	**98.62**	**99.21**	**95.76**	**98.18**
H_2O_C	0.08	0.07	0.47	0.21	0.05	0.04
Total	**100.34**	**99.59**	**99.09**	**99.42**	**95.81**	**98.22**

[1] Border Gabbro pegmatite (5 analysis of sample MAS003) from the Coldwell complex.
[2] Upper Marathon Shore pegmatite (4 analyses of sample MAS024) from the Coldwell complex.
[3] Center Three pegmatite (3 analyses of sample MAS036) from the Coldwell complex.
[4] Granitic pegmatite (1st Val p. sample) from the Vladislav-Pazderníkův mlýn pluton, Czech Republic (Škoda et al. 2006).
[5] Peralkaline granite (sample 3) from the Kuiqi intrusive, China (Xie et al. 2006).
[6] Aluminous Granite (sample 7) from the Putuoshan intrusive, China (Xie et al. 2006).

Titanite compositions from other A-type intrusives, i.e. NYF-pegmatites, peralkaline granites and aluminous granites, differ from Coldwell titanites in a number of ways (Table 4.25). The NYF pegmatites of the Vladislav-Pazderníkův mlýn pluton, Czech Republic (Škoda et al. 2006) are REE- and tantalum-rich, and aluminum- and iron-poor relative to Coldwell titanite. Peralkaline granites from Kuiqi intrusive, China (Xie et al. 2006) have similar iron, high REEs and manganese, and are relatively deficient in aluminum. Aluminous granite from the Putuoshan intrusive, China (Xie et al. 2006), contain higher aluminum, similar REEs and lower iron.

Aluminum varies considerably among units, and may reflect source rather than crystallochemical controls. As such, using titanite compositions alone may infer source composition, e.g. Coldwell pegmatites are peralkaline and aluminous.

Titanite, $CaTiSiO_5$, is an orthosilicate with corner sharing kinked TiO_6 octahedra parallel to the c-axis and cross-linked by SiO_4 tetrahedra. In Coldwell titanite, the calcium site accommodates Al^{3+} and Fe^{3+}; the titanium site accommodates Al^{3+}, Fe^{3+}, Si^{4+}, Nb^{5+}, and Zr^{4+}; and the bridging O(1) anion site contains OH^- and possibly F^- in some of the analyses. Balanced simple substitutions include zirconium into the titanium site:

$$Zr^{4+} \rightarrow Ti^{4+}$$ Liferovich and Mitchell (2005b)

Trivalent ions enter the calcium and titanium structural sites by two-site substitution:

$$2(Fe,Al)^{3+} \rightarrow Ca^{2+} + Ti^{4+}$$ Hoskin et al. (2000)

All titanites analyzed contain niobium. Liferovich and Mitchell (2005a) have documented a two-site replacement from the Khibina, Russia complex, that is:

$$Na^+ + Nb^{5+} \rightarrow Ca^{2+} + Ti^{4+}$$ Liferovich and Mitchell (2006b)

As there are no monovalent ions in Coldwell titanite, the coupled substitution of niobium and hydroxyl for titanium and oxygen occurs:

$$Nb^{5+} + (F,OH)^- \rightarrow Ti^{4+} + O^{2-}$$ Clark (1974)

As such, all formula recalculations include hydroxyl in equal proportions to niobium, as listed in Table 4.25 and Appendix III.XIV.

4.25 Xenotime

Yttrium phosphate (YPO_4), or xenotime, occurs as an accessory phase in many rock types, such as granite, granitic pegmatite, granodiorite, migmatites, a range of metamorphic rocks, and syenites. Xenotime is rare in Coldwell pegmatites, and present in six of 40 samples examined. Of the six occurrences, three are from the Upper Marathon Shore, one from the Railway, and the remainder from Center Three pegmatites. Xenotime has an extremely high relief, colourless (Fig.4.58A), and high third order birefringence (Fig. 4.58B). In all cases, xenotime forms in the initial stage of crystallization, and is usually intergrown with zircon (Fig. 4.59). Xenotime crystals are euhedral-to-subhedral and generally smaller than 70 μm. Compositions are similar in all samples, as listed in Table 4.26 and Appendix III.XV.
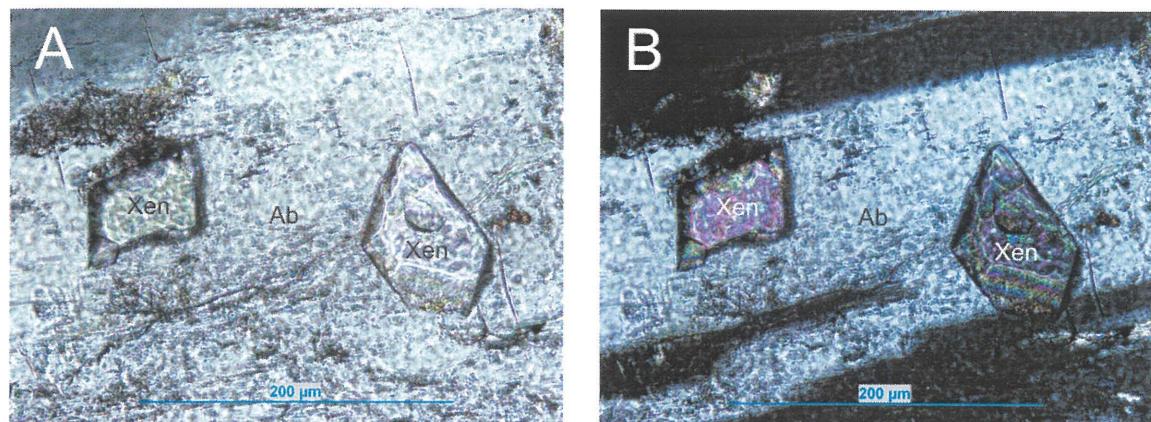
FIGURE 4.58: Photomicrographs of xenotime (Xen) in albite (Ab). A is plane-polarized, B is cross-polarized.
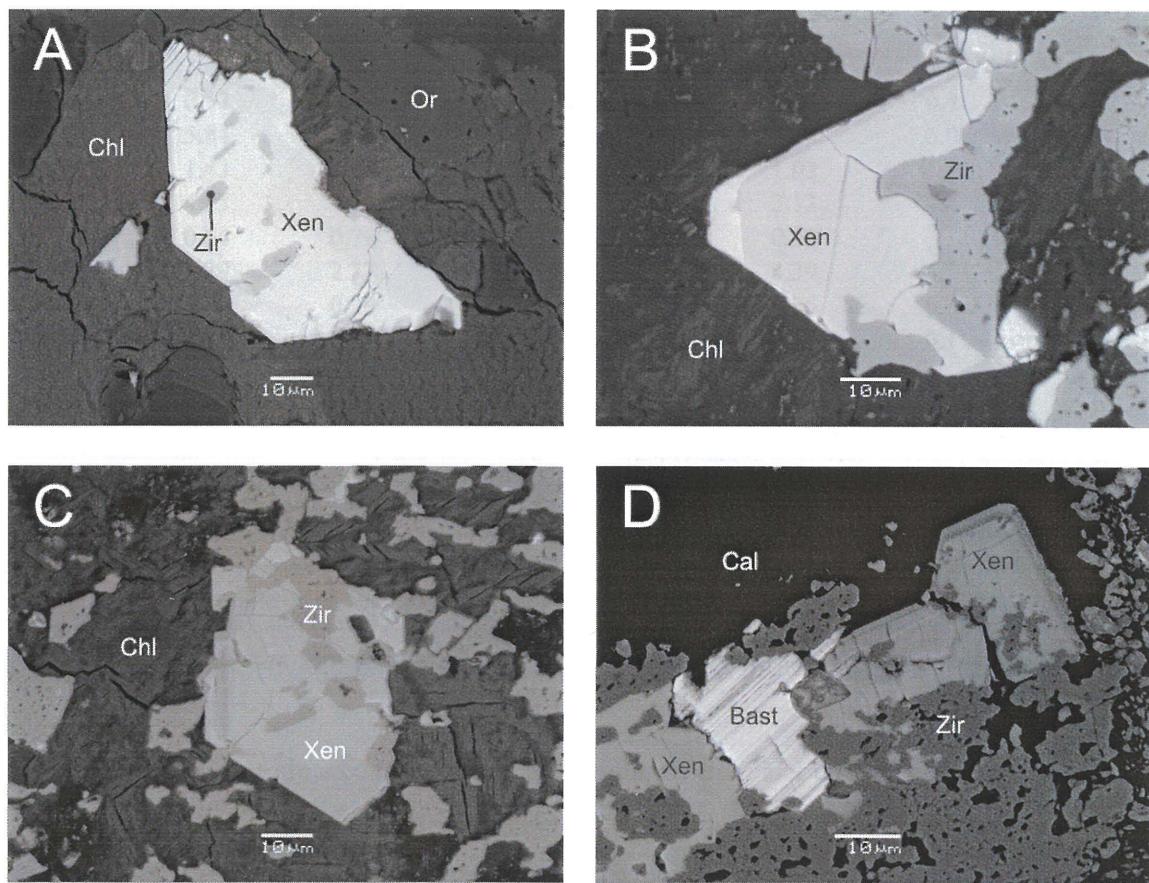
FIGURE 4.59: BSE-images of xenotime (Xen). A is xenotime with zircon (Zir) inclusions in chlorite (Chl) and orthoclase (Or). B and C are xenotime intergrown with zircon in chlorite. The lighter area in B contains 1.85 wt. % ThO$_2$. D is zoned xenotime intergrown with zircon and surrounded by bastnaesite (Bast) and calcite (Cal).

TABLE 4.27: Representative compositions of xenotime.

	Railway[1]	Upper Marathon Shore[2]	Center Three[3]	Pegma-tite[4]	Biotite Granite[5]	Granitic Pegma-tite[6]	NYF-Pegma-tite[7]
P_2O_5	35.20	34.24	35.25	34.4	32.0	34.0	33.25
SiO_2	0.98	0.50	0.02	-	1.53	-	0.09
ThO_2	1.14	0.30	0.45	0.4	2.85	0.3	0.22
UO_2	0.21	0.12	0.14	3.7	3.92	1.2	0.42
Al_2O_3	-	-	0.53	-	-	-	-
Y_2O_3	45.53	44.36	40.21	40.9	36.6	45.2	41.79
La_2O_3	-	0.14	-	-	-	-	-
Ce_2O_3	-	0.30	-	-	0.33	-	-
Pr_3O_3	-	0.17	-	-	0.11	-	-
Nd_2O_3	0.14	0.20	-	-	1.00	-	0.34
Sm_2O_3	-	0.47	-	-	1.26	-	0.63
Eu_2O_3	-	-	0.03	0.1	-	-	-
Gd_2O_3	1.66	2.86	3.27	2.2	3.60	2.3	2.25
Tb_2O_3	0.53	0.62	1.05	0.6	0.70	0.7	-
Dy_2O_3	5.84	6.69	7.46	5.5	4.84	6.0	5.93
Ho_2O_3	1.43	1.45	1.55	1.2	1.03	1.1	-
Er_2O_3	4.23	4.10	4.04	4.0	3.13	4.4	4.27
Tm_2O_3	0.64	0.78	1.14	-	0.57	-	-
Yb_2O_3	2.29	2.17	3.99	4.7	4.39	4.3	4.55
Lu_2O_3	0.16	0.29	0.23	0.6	0.56	0.5	-
CaO	0.35	-	0.10	0.4	0.17	0.1	-
PbO	-	-	-	-	0.18	-	0.33
Total	**100.32**	**99.76**	**99.46**	**98.8**	**98.8**	**100.1**	**94.07**

[1] Railway pegmatite (4 analyses of sample MAS026) from the Coldwell complex.
[2] Upper Marathon Shore pegmatite (4 analyses of sample MAS018) from the Coldwell complex.
[3] Center Three pegmatite (2 analyses of sample MAS040) from the Coldwell complex.
[4] Pegmatite (sample 4) from Val Codera (DeMartin et al. 1991).
[5] Biotite Granite (sample GOT Gb-71) from Ergebirge-Fichtelgebirge region, Germany (Förster 1998b).
[6] Granitic pegmatite (sample 1) from Ca'Mondei, Montescheno (DeMartin et al. 1991).
[7] NYF-pegmatite (1st Kra xenotime sample) from the Kracovice intrusion, Czech Republic (Škoda et al. 2006).

Coldwell xenotime contains minor aluminum, thorium and uranium, and are enriched in MREE and HREEs, specifically Y>Dy>Er>Gd>Yb>Ho (Table 4.26). Although in trace amounts, xenotime (together with fergusonite) is the main HREE sink. The ternary plot in Figure 4.60 shows that all xenotimes are enriched in HREE relative to LREE and MREE, which is typical of anorgenic A-type suites, i.e. A-type granites of the Ergebirge-Fichtelgebirge region, Germany (Förster 1998), granitic pegmatites from Ca'Mondei, Montescheno (DeMartin et al.

1991), and NYF pegmatites from the Kracovice intrusion, Czech Republic (Škoda et al. 2006). The low analytical total in the Kracovice intrusion may be related to the absence of Tb, Ho, Tm, and Lu in the analyses. Since the other HREEs from Kracovice are very similar to Coldwell xenotimes, it is likely that the Tb, Ho, Tm, and Lu were not analyzed.
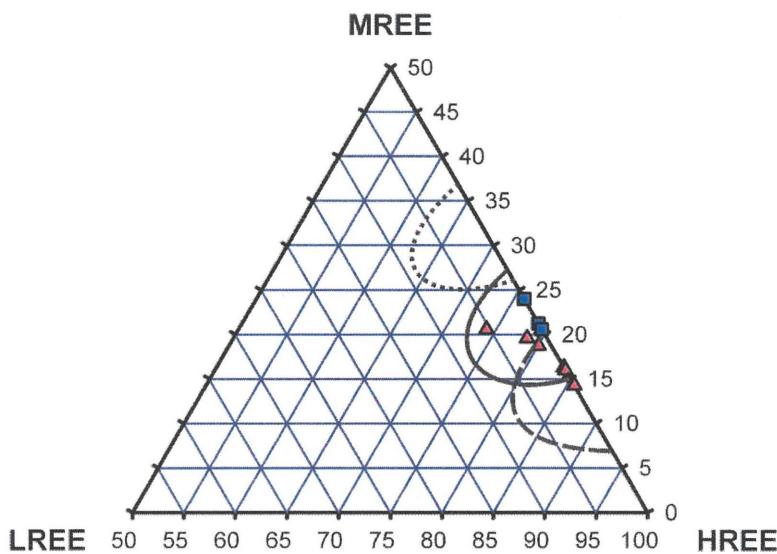
FIGURE 4.60: Xenotime MREE (Sm-Ho) – LREE (La-Nd) – HREE (Er-Lu+Y) ternary plot with MREE and LREE reduced to 50 %. Solid line encloses various igneous xenotimes (Kositcin et al. 2003). Close spaced dashed line encloses hydrothermal xenotimes (Kositcin et al. 2003). Long dashed line is from A-type granites (Förster 1998b).

The study of Kositcin et al. (2003) analyzed xenotime from igneous, digenetic and hydrothermal origin within the Archean Witwatersrand Basin, South Africa, and determined, without the use of textural evidence, that REE, Th and U contents can be effectively used to characterize the origin. According to Kositcin et al. (2003), igneous xenotime is characterized by lower europium, dysprosium, gadolinium, and Gd/Yb ratio than diagenic and hydrothermal xenotime. In addition to REE differences, uranium and thorium in hydrothermal xenotime is characteristically lower than igneous and diagenic varieties (Kositcin et al. 2003). Coldwell xenotimes contain low to not detectable europium content, an average Gd/Yb ratio of 1/1.35, and uranium and thorium values between 0 to 0.21 wt. % UO_2 and 0 to 1.85 wt. % ThO_2. These features are seen in Coldwell xenotime. In addition, Figure 4.60 contains ranges of compositions from igneous detrital Kositcin et al. (2003), hydrothermal (Kositcin et al. 2003) and A-type

granite (Förster 1998a) xenotimes. Apart from low uranium values, Coldwell xenotimes resemble the igneous xenotime described by Kositcin et al. (2003).

Xenotime adopts the tetragonal $I4_1/amd$ space group (Ni et al. 1995). Common ions substituted into the Coldwell xenotime structure include Al^{3+}, Ca^{2+}, REE^{3+}, Th^{4+}, and U^{4+} into the Y-site, and Si^{4+} into the P-site. In common with monazite, there are solid solutions between xenotime, apatite ($CaPO_4$) and britholite [$LREE_5(Si,P)_3O_{12}(OH,F)$]. Tetravalent ions may enter the LREE and phosphorus (Fig. 4.61A):

$$(Th,U)^{4+} + Si^{4+} \rightarrow LREE^{3+} + P^{5+} \qquad \text{Gramaccioli and Segalstad (1978)}$$
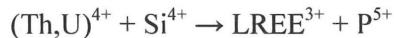
$$(Th,U)^{4+} + (Ca,Sr)^{2+} \rightarrow 2REE^{3+} \qquad \text{Gramaccioli and Segalstad (1978)}$$
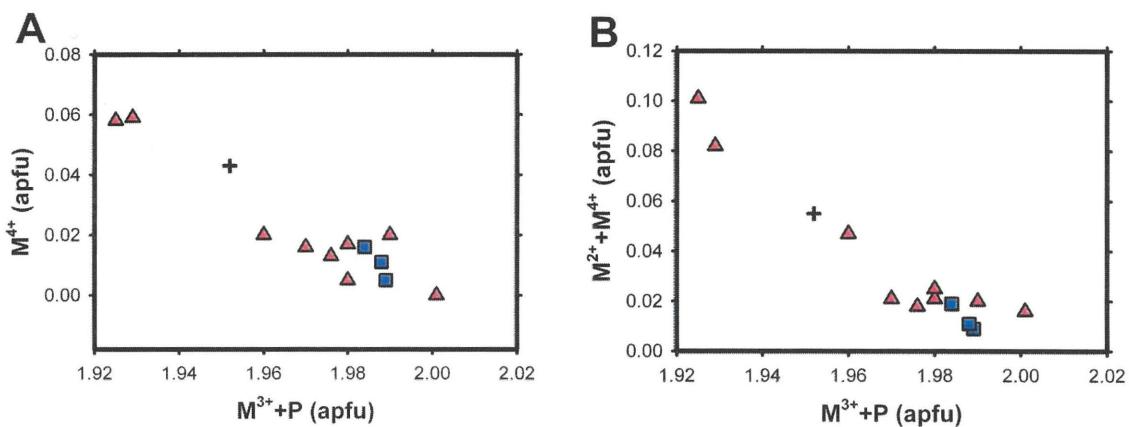
FIGURE 4.61: A- and B-site substitution in xenotime. A is tetravalent (M^{4+}) ions versus trivalent (M^{3+}) ions plus phosphorus (P). B is tetra- and di-valent (M^{2+}) ions versus trivalent ion and phosphorus. Red triangles and blue squares are Upper Marathon Shore and Center Three pegmatites, respectively.

The presence of divalent ions indicates that some of the tetravalent ions are used to charge balance the crystal lattice.

The combination of divalent and tetravalent ions plotted against all trivalent ions and P_2O_5, as shown in Figure 4.61B, gives a more reasonable correlation ($r^2 = 0.913$) than that of the tetravalent ions ($r^2 = 0.897$).

In common with the isostructural minerals thorite and zircon, xenotime may be able to incorporate hydroxyl ions into the structure:
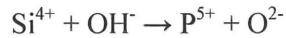
$$Si^{4+} + OH^- \rightarrow P^{5+} + O^{2-} \qquad \text{van Emden et al. (1997)}$$
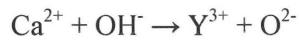
$$Ca^{2+} + OH^- \rightarrow Y^{3+} + O^{2-} \qquad \text{Gorshkov et al. (1998)}$$

4.26 Zircon

Zircon is the main zirconium-bearing phase, and is present in all units. Zircon has a high relief, is colourless, and first order grey birefringence (Fig. 4.62). Where metamict or hydrated, the birefringence increases to upper third and fourth interference colours. In the Coldwell pegmatites, zircon occurs in the initial stage of precipitation. The mineral has euhedral-to-anhedral habit (Fig. 4.63), and is commonly altered along grain boundaries and fractures, some of which are partially absorbed, leaving behind skeletal/corrosional textures (Fig. 4.63B).
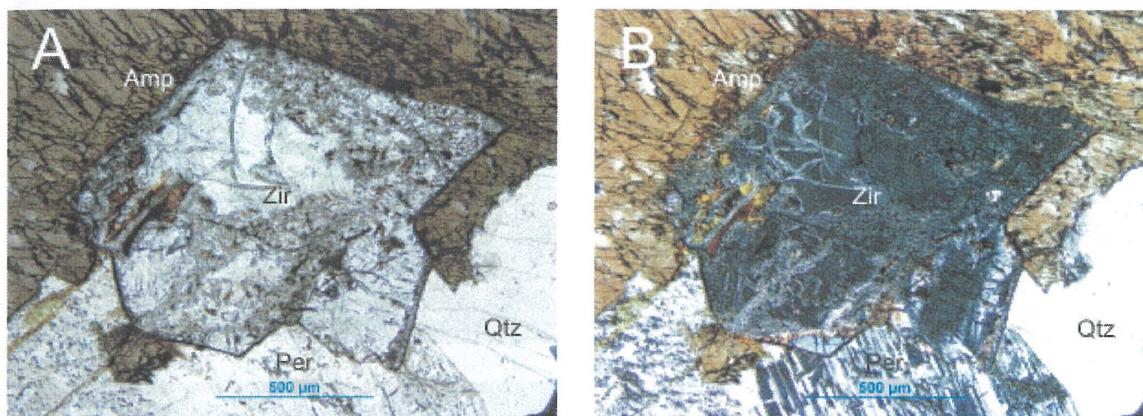
FIGURE 4.62: Photomicrographs of zircon (Zir) surrounded by amphibole (Amp), perthite (Per) and quartz (Qtz). A is under plane-polarized, B is cross-polarized light.

Zircon associations are generally similar between units. In all units, zircon is associated with pyrochlore and thorite. Atypical zircon associations occur in Center Three, as baddeleyite overgrows, instead of intergrowing zircon; and with xenotime/zircon intergrowths occurring in the Railway, Upper Marathon Shore and Center Three pegmatites.

Zircon compositions commonly include iron, calcium, thorium, uranium, and hafnium (Table 4.27 and Appendix III.XVII). No compositional difference is observed between initially- and interstitially-forming zircon. Coldwell zircons are similar in composition to zircons from the Kuiqi peralkaline granites (Xie et al. 2006), with hafnium oxide values between not detectable and 2.51 wt. % and variable thorium. Alternatively, Coldwell zircons have higher uranium and iron than the peralkaline granites from Kuiqi. Aluminous granites from Putuoshan (Xie et al. 2006) have higher hafnium (2.03-5.92 wt. % HfO_2) and yttrium, but similar high uranium values.

Zircon is an orthosilicate with the formula $ZrSiO_4$. The tetragonal $I4_1/amd$ structure consists of independent SiO_4 tetrahedra joined to distorted ZrO_8 cubes. Common ions found

substituting into Coldwell zircon include: Al^{3+}, Ca^{2+}, Fe^{2+}, Fe^{3+}, Mg^{2+}, Mn^{2+}, Nb^{3+}, Th^{4+}, U^{4+}, Hf^{4+}, REE^{3+}, and Ta^{4+} at the zirconium site; and P at the silicon site. Thorite ($ThSiO_4$), coffinite ($USiO_4$), and hafnon ($HfSiO_4$) are isomorphs of zircon and their cations can easily enter the zircon structure by simple substitution:
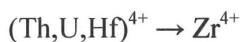
$$(Th,U,Hf)^{4+} \rightarrow Zr^{4+} \qquad\qquad\qquad\qquad \text{Krasnobaev et al. (1988)}$$
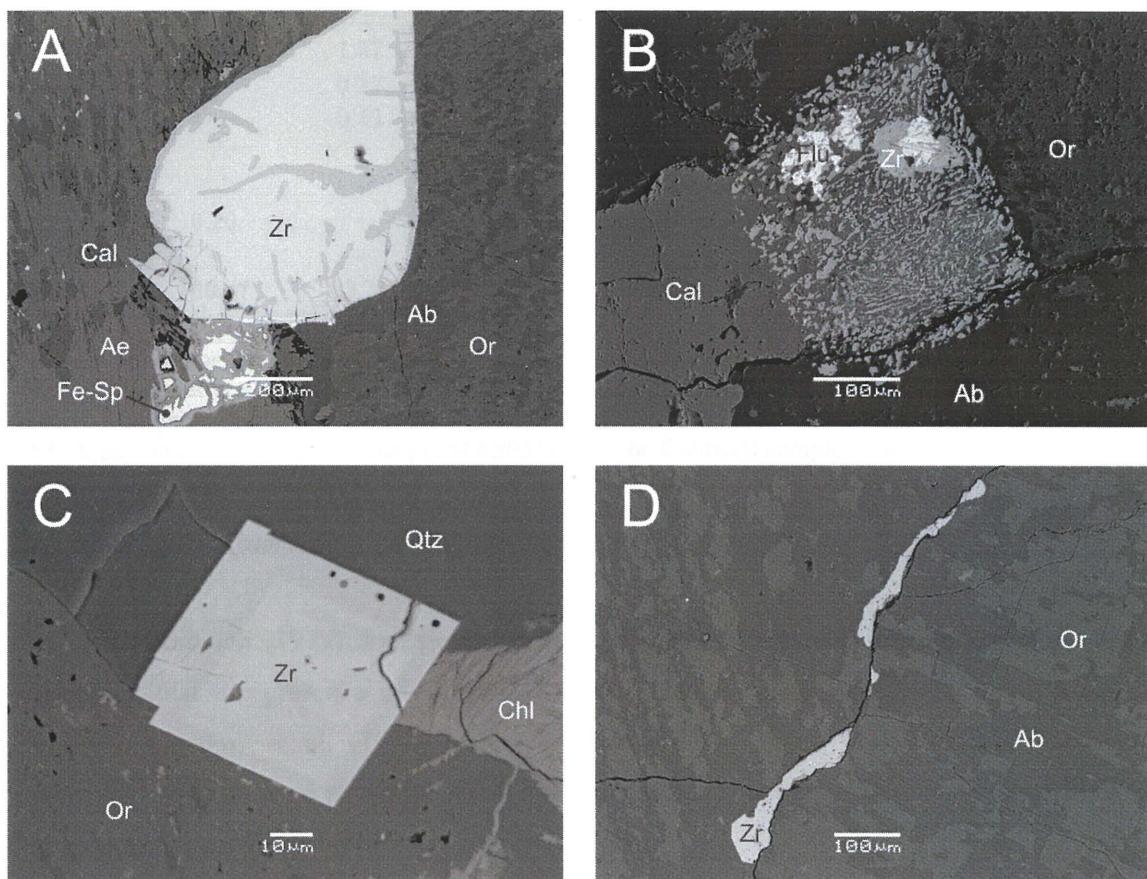
Figure 4.63: BSE-images of zircon. A is primary zircon with the darker zones being hydrated zircon and is surrounded by albite (Ab), orthoclase (Or), calcite (cal), aegirine (Ae) and Fe-sphalerite (Fe-Sp). B is a primary zircon that was partially reabsorbed, in this case it is surrounded by fluorocarbonates (Flu), calcite (Cal), albite and orthoclase. C is a zoned euhedral zircon surrounded by orthoclase, quartz (Qtz), and chlorite (Chl). D is anhedral zircon surrounded by albite and orthoclase.

Coupled substitutions, namely the solid solution between zircon and monazite ($REEPO_4$), xenotime (YPO_4) and fergusonite ($YNbO_4$) commonly occur in Coldwell zircon:

$$(Y,REE)^{3+} + P^{5+} \rightarrow Zr^{4+} + Si^{4+} \qquad\qquad \text{Speer (1982)}$$

$$(Y,REE)^{3+} + (Nb,Ta)^{5+} \rightarrow 2Zr^{4+} \qquad\qquad \text{Es'kova (1959)}$$

TABLE 4.28: Representative compositions of zircon.

	Border Gabbro[1]	Railway[2]	Upper Marathon Shore[3]	Black[4]	Center Three[5]	Per-alkaline Granite[6]	Alumi-nous Granite[7]
P_2O_5	-	-	-	-	-	-	0.30
SiO_2	33.08	32.40	32.55	32.87	33.32	32.79	30.40
ZrO_2	66.24	65.02	65.72	65.43	64.91	62.54	53.42
HfO_2	0.95	1.47	1.12	1.38	1.10	1.93	3.16
ThO_2	-	0.37	-	-	-	-	2.55
UO_2	-	0.13	-	-	-	0.15	4.34
Al_2O_3	-	-	-	0.21	0.44	-	-
Y_2O_3	-	-	-	-	-	0.14	2.70
FeO	0.20	-	-	0.21	0.72	-	-
PbO	-	-	-	-	-	-	0.10
Total	**100.47**	**99.39**	**99.39**	**100.10**	**100.49**	**97.55**	**96.97**

[1] Border Gabbro pegmatite (3 analyses of sample MAS001) from the Coldwell complex.
[2] Railway pegmatite (3 analyses of sample MAS016) form the Coldwell complex.
[3] Upper Marathon Shore pegmatite (4 analyses of sample MAS020) from the Coldwell complex.
[4] Black pegmatite (3 analyses of sample MAS031) from the Coldwell complex.
[5] Center Three pegmatite (3 analyses of sample MAS038) from the Coldwell complex.
[6] Peralkaline granite (sample 22) from the Kuiqi intrusive, China (Xie et al. 2006).
[7] Aluminous granite (sample 23) from the Putuoshan intrusive, China (Xie et al. 2006).

Lyakhovich (1979) documented a direct correlation between yttrium and phosphorus suggesting that the presence of extremely small inclusions may account for their presence. Similarly, Gorskov et al. (1998) concluded that REE in zircon are a result of xenotime inclusions. As there is no phosphorus in Coldwell zircons, xenotime and monazite inclusions do not account for the REEs present in Coldwell zircons.

The occurrence of REE not in proportion to PO_4 indicates that other cations, such as Al^{3+}, Fe^{2+}, Fe^{3+}, and Mg^{2+} accommodate for charge balance in the crystal lattice. As such, there are interstitial sites that can accommodate a multitude of ions allowing for the low levels of HFSEs and REEs (Finch and Harchar 2003):

$$[(Mg,Fe)^{2+}]_{inter} + 3(Y,REE)^{3+} + P^{5+} \rightarrow 3Zr^{4+} + Si^{4+} \qquad \text{Hoskin et al. (2000)}$$

$$[(Al,Fe)^{3+}]_{inter} + 4(Y,REE)^{3+} + P^{5+} \rightarrow 4Zr^{4+} + Si^{4+} \qquad \text{Hoskin et al. (2000)}$$
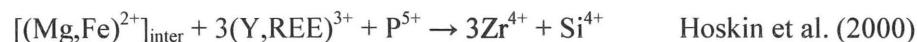
Hydrated zircon (Fig. 4.63), $\{[(Zr_{1-x},Ca_x)Si[O_{1-2x},(OH)_{2x}]_4\}$, commonly occurs throughout the Coldwell pegmatites (Table 4.28), and is marked by the addition of aluminum, yttrium, REEs, calcium, manganese, iron, and sodium. The alteration of zircon into its hydrated

variety occurs in the secondary stage of crystallization, and prevails along microfractures, inclusions and grain boundaries (Fig. 4.64B). Hydrated zircon may form by decomposition via metamictization and dissolution/reprecipitation reactions:

$$Ca^{2+} + 2(OH)^- + 2H_2O \rightarrow Zr^{4+} + (SiO_4)^{4-} \qquad \text{Gorshkov et al. (1998)}$$
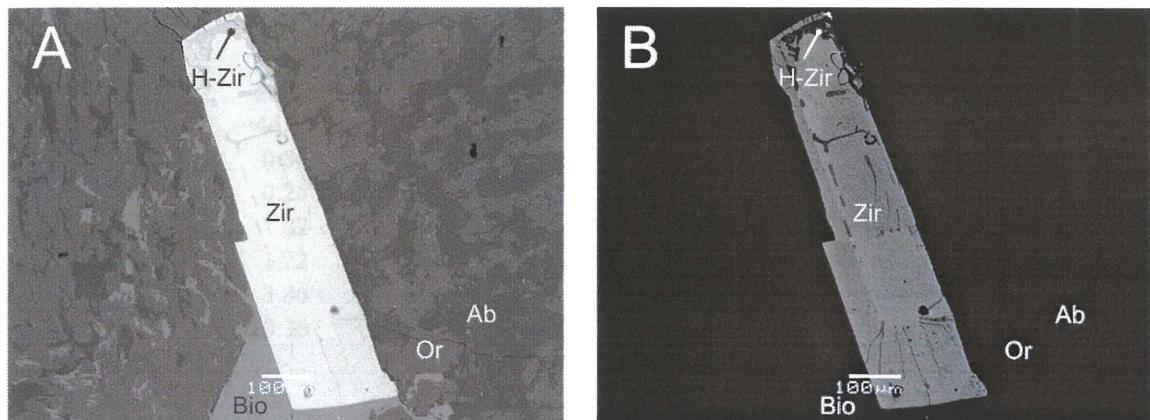
FIGURE 4.64: Zircon (Zir) and hydrated variety (H-Zir) surrounded by albite (Ab), orthoclase (Or) and biotite (Bio). A is normal contrast, B is high contrast. All dark areas in the zircon grain are the hydrous variety.

Dissolution of zircon is relatively uncommon, as it is stable during most hydrothermal episodes. Despite this, the occurrence of the hydrated zircon species and skeletal zircon grains indicate that zirconium was dissolved and recrystalized later to form the hydrous variety or other zirconium-bearing minerals, i.e. Fe-zircophyllite. Similar to Coldwell pegmatites, late stage zircon varieties can be found in other alkali, F-rich igneous suites (Rubin et al. 1993). Initial zircon occurs, at least in the case of the Coldwell pegmatites, because of differentiation and solubility. As the pegmatitic melt evolved, the absence of fluorine compatible minerals enriched the melt in fluorine, and stabilizes Zr-F complexes. It has been shown by Keppler (1993) that the solubility of zirconium increases dramatically with higher amounts of fluorine. So while zircon formed in the initial stages of crystalization, an increase in fluorine permitted zirconium to remain stable in the melt.

TABLE 4.29: Representative compositions of hydrous zircon.

	Border Gabbro[1]	Railway[2]	Upper Marathon Shore[3]	Black[4]	Center Three[5]	Altered Syenite[6]
P_2O_5	-	-	-	-	-	0.13
Nb_2O_5	-	-	-	-	-	2.71
Ta_2O_5	-	-	-	-	-	0.18
SiO_2	26.71	28.72	31.61	28.30	27.52	26.27
ZrO_2	46.99	54.58	62.26	55.47	48.43	54.17
HfO_2	0.80	1.65	1.33	0.83	-	1.02
ThO_2	0.25	0.81	0.42	1.05	-	-
UO_2	1.02	-	0.21	-	-	-
Al_2O_3	1.22	0.30	0.36	0.27	0.80	0.15
Y_2O_3	3.86	-	-	-	-	1.95
Ce_2O_3	0.36	-	0.35	-	-	-
Pr_2O_3	-	-	-	-	-	-
Nd_2O_3	-	-	0.12	-	-	-
Sm_2O_3	-	-	-	-	-	0.21
Gd_2O_3	0.43	-	-	-	-	0.52
Tb_2O_3	-	-	-	-	-	-
Dy_2O_3	0.53	-	.	-	0.91	0.73
Ho_2O_3	-	-	-	-	0.32	-
Er_2O_3	0.82	-	-	-	0.63	0.23
Tm_2O_3		-	-	-	-	-
Yb_2O_3	0.66	-	-	-	0.83	-
CaO	1.74	1.61	0.45	1.27	1.64	0.14
MnO	-	0.14	-	-	-	-
FeO	1.19	0.99	0.35	1.44	1.05	0.86
Na_2O	0.63	0.49	-	0.43	0.33	-
Total	**87.21**	**89.29**	**97.46**	**89.06**	**82.43**	**89.27**

[1] Border Gabbro pegmatite (5 analyses of sample MAS007) from the Coldwell complex.
[2] Railway pegmatite (3 analyses of sample MAS024) from the Coldwell complex.
[3] Upper Marathon Shore pegmatite (3 analyses of sample MAS018) from the Coldwell complex.
[4] Black pegmatite (2 analyses of sample MAS032) from the Coldwell complex.
[5] Center Three syenite pegmatite (2 analyses of sample MAS033) from the Coldwell complex.
[6] Altered syenite (sample PT5) from the Lake Zone, Thor Lake, N.W.T., Canada (Pinckston and Smith 1995).

4.27 Zirconolite

Zirconolite, $CaZrTi_2O_7$, is a common trace mineral in alkaline intrusives, carbonatites, kimberlites, and metasomatic/metamorphic rocks. In Coldwell pegmatites, the mineral is present in three Border Gabbro and two Railway pegmatite samples. In these units, zirconolite has a

high relief, red/brown pleochroism, and anomalous birefringence (Fig. 4.65). The mineral forms elongate subhedral-to-anhedral crystals with tapered terminations, and range in size from 2 μm to 1 mm. All crystals form in the initial stage of crystallization, and are associated with other early-initial stage minerals, i.e. apatite, baddeleyite, pyrochlore, and zircon (Fig. 4.66).

In the Border Gabbro pegmatites, zirconolite compositions are diverse (Table 4.30 and Appendix III.XVII). High HREEs, yttrium and silicon are accompanied by low iron and calcium. One of the crystals is isolated; one is intergrown with zircon; and the other intergrown with baddeleyite.
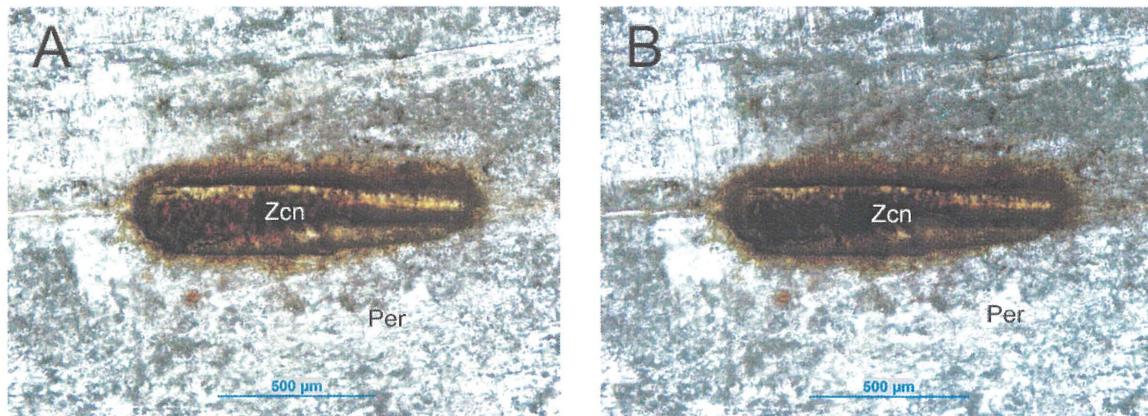
FIGURE 4.65: Photomicrograph of zirconolite (Zcn) in perthite (Per). The lighter outer zone seen in the crystal is enriched in titanium and REEs relative to the interior. A is plane-polarized, B is cross-polarized.
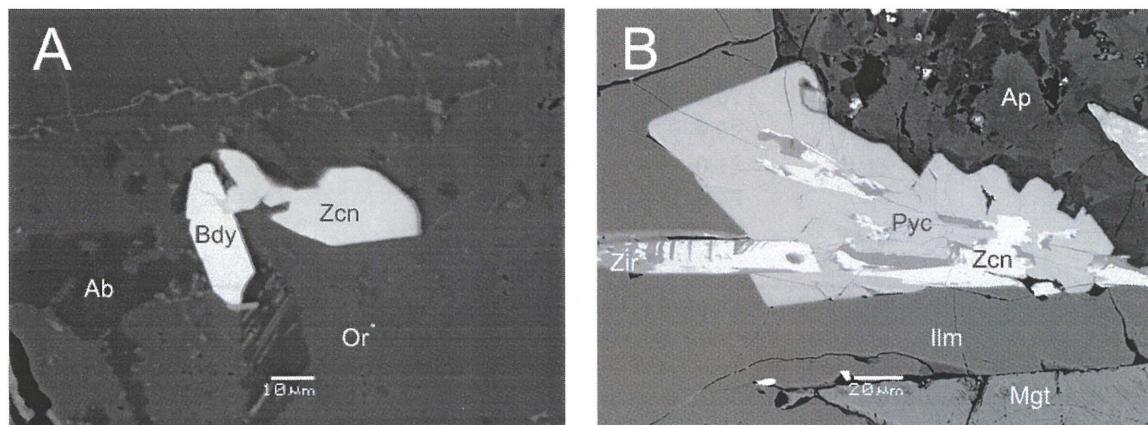
FIGURE 4.66: BSE-images of zirconolite (Zcn). A is zirconolite associated with baddeleyite (Bdy) in a albite (Ab) and orthoclase (Or). B is subhedral elongate zirconolite intergrown with zircon (Zir) and surrounded by pyrochlore (Pyc), ilmenite (Ilm) and apatite (Ap).

TABLE 4.30: Representative compositions of zirconolite.

	Border Gabbro[1]	Railway[2]	Syenite[3]	Syenite Pegma-tite[4]
WO_3	0.26	-	-	-
Nb_2O_5	10.54	17.58	2.71	19.72
Ta_2O_5	1.90	0.91	0.26	1.08
SiO_2	0.79	-	0.29	-
TiO_2	20.58	18.18	28.80	21.50
ZrO_2	27.20	30.40	31.35	29.83
HfO_2	0.44	0.54	0.31	0.68
ThO_2	3.09	0.16	8.22	0.20
UO_2	1.14	-	2.86	0.11
Al_2O_3	0.26	0.20	0.27	0.27
Y_2O_3	1.77	1.78	0.67	0.30
La_2O_3	2.24	2.54	0.91	0.95
Ce_2O_3	6.37	7.11	3.25	2.31
Pr_2O_3	1.54	1.10	0.28	0.20
Nd_2O_3	4.10	3.67	1.29	0.53
Sm_2O_3	0.79	0.55	0.28	-
$Eu2O3$	-	-	0.15	-
Gd_2O_3	0.14	-	0.10	-
Tb_2O_3	0.32	-	-	-
Dy_2O_3	0.84	-	-	-
Ho_2O_3	0.39	-	-	-
Er_2O_3	0.31	-	-	-
Tm_2O_3	0.40	-	-	-
Yb_2O_3	0.37	-	-	-
Lu_2O_3	0.25	-	-	-
Fe_2O_3	1.84	-	-	-
FeO	6.84	9.13	7.70	7.84
MgO	-	-	0.07	0.07
CaO	6.11	6.98	9.05	12.60
MnO	-	-	0.15	0.43
PbO	-	-	0.29	-
Total	**100.76**	**100.83**	**99.26**	**98.62**

[1] Border Gabbro pegmatite (5 analyses of sample MAS001) from the Coldwell complex.
[2] Railway pegmatite (3 analyses of sample MAS023) form the Coldwell complex.
[3] Syenite (sample 42781) from Glen Dessarry, Scotland (Fowler and Williams 1986).
[4] Coarse-grained syenite pegmatite (sample S6) from Langesundfjord, Norway (Williams and Gieré 1996).

The Railway zirconolites (Fig. 4.66B), are intergrown with zircon and surrounded by the early-initial-forming minerals pyrochlore, ilmenite and apatite. One grain of zirconolite is

present in sample MAS015. This crystal is associated with baddeleyite and enclosed by amphibole. Here the crystal is small (~ 2 μm) and no accurate analyses could be undertaken.

As shown in Table 4.29, the Coldwell zirconolites are high in REEs (13.62-22.84 wt. % REE_2O_3), when compared to syenites (6.93 wt. % REE_2O_3) from Glen Dessarry, Scotland (Fowler and Williams 1986) and syenite pegmatite (4.33 wt. % REE_2O_3) from Langesund fjord, Norway (Williams and Gieré 1996). As REEs substitute into the calcium site, calcium is low compared to other localities (Table 4.29). The calcium – titanium – zirconium plot in Figure 4.67 shows all Coldwell zirconolites plotting with high zirconium relative to the ideal stoichiometry. As the zirconium site is relatively constant, variation, illustrated in Figure 4.67, is dependant on calcium and titanium substitution, and indicates that Coldwell zirconolites are more evolved, as they are enriched in REEs, than zirconolite from other rock types, i.e. carbonatites, syenites, and nepheline syenites.
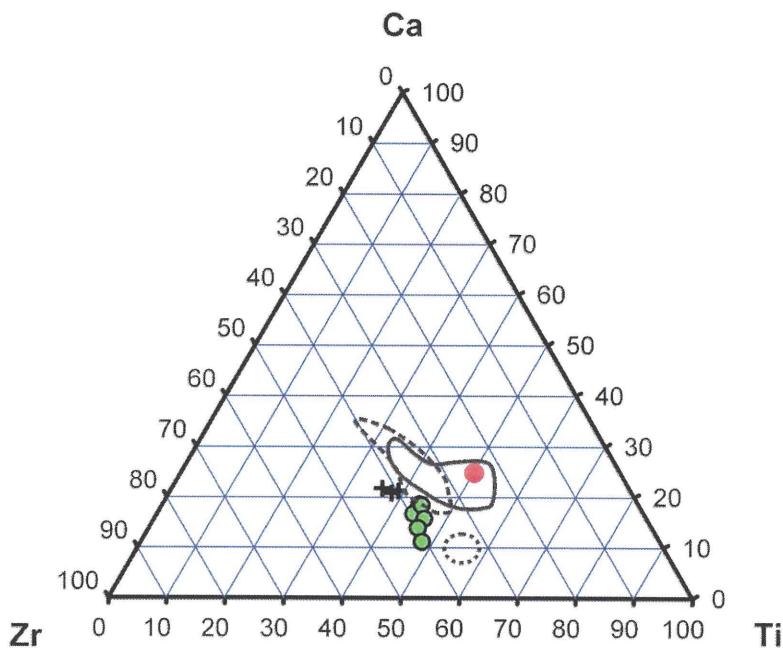
FIGURE 4.67: Calcium (Ca) – zirconium (Zr) – titanium (Ti) in apfu ternary plot. Green circles and black crosses are the Border Gabbro and Railway pegmatites, respectively. Red dot is stoichiometric zirconolite. Solid line, intermediate dashed and close-spaced dashed encompass metasomatic, carbonatites and syenites/ nepheline syenite rocks, respectively (Williams and Gieré 1996).

The REE – ACT – M^{5+} ternary diagram in Figure 4.68 shows that the Coldwell zirconolites are ACT-poor, the Border Gabbro pegmatites are REE-rich, and the Railway pegmatites are relatively M^{5+}-rich. The trend from M^{5+} to REE is similar to Schryburt Lake, Ontario and Araxà, Brazil carbonatites (Gieré et al. 1998).

Zirconolite has a monoclinic crystal structure that consists of 5-coordinated Ti atoms surrounded by six-membered corner-sharing TiO_6 octahedra and interlayering chains of CaO_8 cubes and ZrO_7 polyhedra (Gieré et al. 1998). Zirconolite polytypes include monoclinic "typical" zirconolite-2M (White et al. 1984), the trigonal zirconolite-3T, or "zirkelite" (Mazzi and Munro 1983), orthorhombic zirconolite-3O (Bayliss et al. 1989), and the monoclinic zirconolite-4M (Coelho et al. 1997).
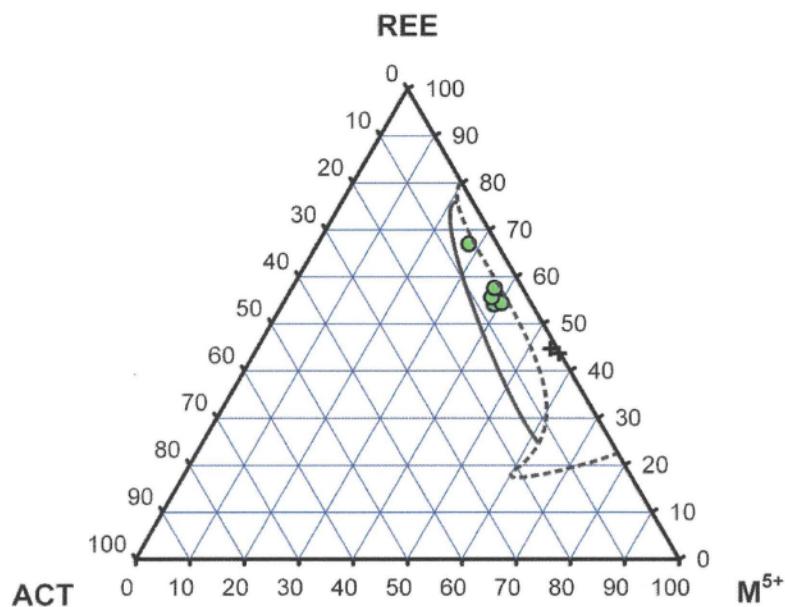
FIGURE 4.68: Zirconolite REE – ACT – M^{5+} ternary diagram. Both units are ACT-poor. The Border Gabbro (green circles) being REE-enriched, the Railway (black crosses) being M^{5+}-enriched. The solid line represents where the Araxà, Brazil carbonatites plot; dashed line is where Schryburt Lake, Ontario carbonatites plot (Gieré et al. 1998).

The composition of Coldwell zirconolite includes Y^{3+}, REE^{3+}, Th^{4+}, U^{4+}, Fe^{2+}, Mg^{2+}, and Mn^{2+} in the Ca-site; $HREE^{3+}$, Hf^{4+}, U^{4+}, Ca^{2+}, and Ti^{3+} in the Zr-site; and Nb^{5+}, Fe^{2+}, Fe^{3+}, Zr^{4+}, Mg^{2+}, and Ta^{5+} in the Ti-site. A list of possible mechanisms, suggested by Gieré et al. (1998), is shown in Table 4.30. In Coldwell zirconolites, titanium versus the M^{5+} ions (niobium and tantalum) gives a good negative correlation with an r^2 value of 0.947 (Fig. 4.69).
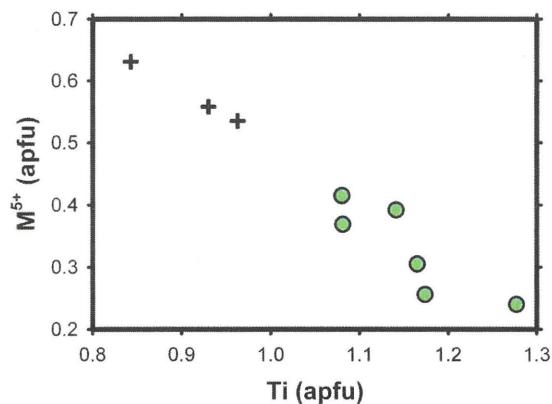
FIGURE 4.69: Zirconolite M^{5+}-site vs. titanium (Ti) in apfu. The r^2 value is 0.947.

TABLE 4.31: Substitution mechanisms found in zirconolite (Gieré et al. 1998).

Mechanism	Sites involved
$Zr^{4+} \rightarrow Ti^{4+}$	M5,6
$M^{5+} + M^{3+} \rightarrow 2Ti^{4+}$	M5,6
$W^{6+} + M^{2+} \rightarrow 2Ti^{4+}$	M5,6
$2M^{3+} \rightarrow Ti^{4+} + M^{2+}$	M5,6
$M^{5+} + M^{2+} \rightarrow Ti^{4+} + M^{3+}$	M5,6
$Ti^{4+} \rightarrow Zr^{4+}$	M7
$Hf^{4+} \rightarrow Zr^{4+}$	M7
$ACT^{4+} \rightarrow Zr^{4+}$	M7
$REE^{3+} + M^{5+} \rightarrow Zr^{4+} + Ti^{4+}$	M5,6/M7
$REE^{3+} + Ti^{4+} \rightarrow Zr^{4+} + M^{3+}$	M5,6/M7
$REE^{3+} + 2Ti^{4+} \rightarrow Zr^{4+} + M^{5+} + M^{2+}$	M5,6/M7
$ACT^{4+} + M^{2+} \rightarrow Ca^{2+} + Ti^{4+}$	M5,6/M8
$ACT^{4+} + 2M^{3+} \rightarrow Ca^{2+} + 2Ti^{4+}$	M5,6/M8
$ACT^{4+} + M^{3+} \rightarrow Ca^{2+} + M^{5+}$	M5,6/M8
$ACT^{4+} + M^{3+} \rightarrow REE^{3+} + Ti^{4+}$	M5,6/M8
$ACT^{4+} + M^{2+} \rightarrow REE^{3+} + M^{3+}$	M5,6/M8
$ACT^{4+} + Ti^{4+} \rightarrow REE^{3+} + M^{5+}$	M5,6/M8
$ACT^{4+} + Ti^{4+} + M^{2+} \rightarrow Ca^{2+} + M^{5+} + M^{3+}$	M5,6/M8
$ACT^{4+} + 2M^{3+} \rightarrow REE^{3+} + M^{5+} + M^{2+}$	M5,6/M8
$REE^{3+} + M^{3+} \rightarrow Ca^{2+} + Ti^{4+}$	M5,6/M8
$REE^{3+} + M^{5+} + M^{2+} \rightarrow Ca^{2+} + 2Ti^{4+}$	M5,6/M8
$REE^{3+} + Ti^{4+} \rightarrow Ca^{2+} + M^{5+}$	M5,6/M8
$REE^{3+} + M^{2+} \rightarrow Ca^{2+} + M^{3+}$	M5,6/M8
$2REE^{3+} \rightarrow Ca^{2+} + Zr^{4+}$	M7/M8

In acidic environments and temperatures above 500°C, the degradation of zirconolite can lead to the formation of rutile and anatase; while in basic environments and variable temperatures, zirconolite can break down to perovskite and calzirtite (Malmstroem et al. 2000). Pan (1997) suggests that zirconolite decomposes into rutile + titanite + zircon. As neither of these two assemblages, or any other assemblage which may be indicative of zirconolite decomposition, is present, subsequent reheating or pressure could not have been intense enough to breakdown Coldwell zirconolite. Due to the lack of corrosional or alteration textures present in Coldwell pegmatites, it is unlikely that any dissolution occurs.

CHAPTER FIVE
PETROGENESIS

5.1 Introduction

Age relations of the western and central/eastern areas of the Coldwell complex have been constrained using uranium-lead geochronology to 1108±1 and 1118±1 Ma, respectively (Heaman and Machado 1992). The North American Midcontinent Rift System has been constrained to 1114.7±1.1 Ma and 1091.1±4.5 Ma (Heaman et al. 2007; Hollings et al. 2007), thus that the Coldwell complex was emplaced early in the development of the rift.

Overall, the North American Midcontinent Rift System is a product of mantle plume generated extensional tectonism, and the Coldwell rocks, specifically the syenites, exhibit anorogenic (A-type) characteristics (Mitchell et al. 1993), i.e. peralkaline, aluminous with fluorine, HFSE, and LREE enrichment. These characteristics are similar to other A-type intrusive complexes, e.g. Thor Lake (Pinckston and Smith 1995), Strange Lake (Salvi and Williams-Jones 1996), A-type granites of southeast coastal China (Xie et al. 2006), and many others (Abdel-Rahman 2006; Srivastava et al. 2007; Xie et al. 2005). The genesis of A-type syenites/granites is possibly the result of partial melting of metasomatized lower crust during extension (Martin 2005). Degassing, which is associated with decompression, within the mantle allows for normally incompatible ions to be swept up by hydrothermal and/or carbothermal fluids (Bailey 1980). As these fluids are buoyant, the normally incompatible ions rise towards the crust. Consequently, Coldwell syenites and related rocks are enriched in iron, fluorine, LREEs, ACTs, and HFSEs.

There are many examples of REEs precipitating in hydrothermal and carbothermal environments (Gieré 1996; Rubin et al. 1993; Della Ventura et al. 1999), as they are able to complex with sulphate, chloride, fluoride, hydroxide, carbonate, bicarbonate, nitrate, and orthophosphate (Haas et al. 1995). Studies have shown that REE complexes prefer low pH solutions (Michard 1989), which are saline (Banks et al. 1994) and relatively hot (Banks et al. 1994). In common with HFSEs, REEs are able to partition into the Coldwell syenites/related rocks because of their elevated fluorine content (Keppler 1993); the same can be assumed for the ACTs.

In Coldwell syenites, pegmatite-forming residua represent the last stage of syenitic melt evolution. As the initial syenitic melts were enriched in immobile elements, the evolved residua are even more enriched in iron, fluorine, silica, LREEs, ACTs, and HFSEs. Similarly, as

fractionation progresses, the volatile contents increase, and, consequently, the late-crystallizing residua are coarse-grained and contain many forms of hydrous (allanite, amphibole, chevkinite, etc.), carbonated (calcite, kainosite, fluorocarbonates), and fluorinated (amphiboles, apatite, fluorite etc.) minerals. Pegmatites formed in anorgenic conditions and enriched in the elements/minerals mentioned above are classified as NYF-pegmatites (Černý 1992).

5.2 Melt/Fluid Evolution

The evolution of Coldwell syenite residua occurs in four main textural stages. The first stage consists of the crystallization of euhedral-to-anhedral grains of apatite/britholite, baddeleyite, chevkinite, fergusonite, ilmenite, magnetite, monazite, olivine, pyrochlore, pyroxene, thorite, xenotime, zircon, and zirconolite.

It has been shown by Mitchell and Platt (1978) that baddeleyite-zircon stability can be used to constrain silica activity. Baddeleyite-zircon intergrowths indicate that the initial environment is very close to the baddeleyite-zircon stability line. The silica activity is constrained to approximately $10^{-0.75}$ (Fig. 5.1). As quartz reaches saturation in the interstitial stage, silica activity increases with differentiation (shown by the red arrow in Figure 5.1).
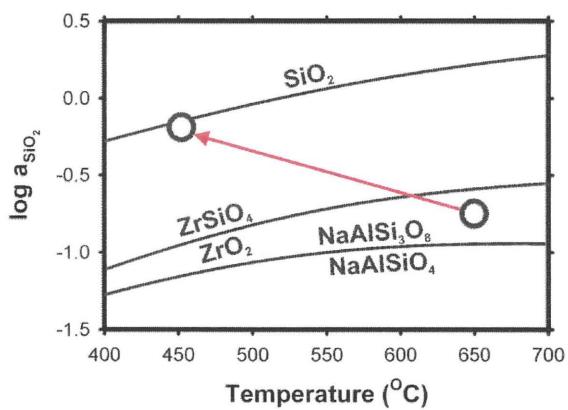
FIGURE 5.1: Baddeleyite-zircon stability diagram in respect to temperature and silica activity (log a_{SiO2}). Red arrow is the general trend taken by the melt as silica increases. Green circles, black crosses, red triangles, black diamonds, and blue squares are the Border Gabbro, Railway, Upper Marathon Shore, Black, and Center Three pegmatites.

As the melt evolved, the alkalis and aluminum were precipitated as cryptoperthitic alkali feldspars. According to James and Hamilton (1969), at 1 kbar pH$_2$O and normative SiO$_2$ less

than 15 %, a complete solid solution between albite and orthoclase $(Ab-Or-Q_{15})_{97}An_3$ exists at liquidus temperatures (approximately 730 °C). Below 730 °C and/or above 15 % normative SiO_2, a miscibility gap forms and, with decreasing temperature and/or increasing SiO_2, expands. Cryptoperthitic textures indicate that normative SiO_2 % was low (<15 %), the feldspar compositions were approximately $Ab_{85}Or_{15}$ – $Ab_{15}Or_{85}$ and subsolidus cooling time was short, as microcline would have formed at approximately 450 °C (Martin 2005). As such, the magnetite-ilmenite equilibration temperatures (531-633 °C) and oxygen fugacities ($10^{-16.5}$-$10^{-22.9}$ bars) are near the initial crystallization conditions, volatile proportions (volatile-enriched minerals and vesicles that occur in the Upper Marathon Shore pegmatites) are common, and a slow cooling regime above the solidus temperature cannot account for the coarse-grained textures.

Cryptoperthitic texture in feldspar can, according to Waldron and Parsons (1992), be used to infer equilibration temperatures. Lee et al. (1997) and Waldron and Parsons (1992) have used TEM to describe the Center One ferroaugite syenites (host rock of the Upper Marathon Shore pegmatites) feldspars. Waldron and Parsons (1992) determined that the periodicities of the microtextures increase slightly inwards from the contact and upwards in the stratigraphy of the Marathon Shore layered syenites. Similarly, Brown et al. (1983) have documented the same trend from the Klokken, Greenland layered syenite. Microtextures within Center One ferroaugite syenites include ripples (Lee et al. 1997), parallel-sided pleats (Lee et al. 1997), regular straight, wavy, lozenge (Waldron and Parsons 1992), and albite banding (Waldron and Parsons 1992). Bulk compositions of the ripple microtextures measured by Waldron and Parsons (1992) give a solvus temperature of approximately 500 to 550 °C, that is, the Center One ferroaugite syenites cooled to approximately 525 °C and were then affected by a fluid influx thermal event. As Center One ferroaugite syenites are host to the Upper Marathon Shore pegmatites, the lack of zoning and graded contacts suggests that the Upper Marathon Shore pegmatites intruded while the host syenite was still relatively hot, and, thus, represent the fluid influx event described by Waldron and Parsons (1992).

The ulvöspinel component in magnetite, hematite component in ilmenite, and the exsolution of these two minerals is controlled by oxygen fugacity (f_{O_2}) and temperature (Buddington and Lindsley 1964). The QUILF program (Andersen et al 1993) is used to calculate X'Usp and X'Ilm (Fig. 5.2), and the geothermometer program of Nasir (1994) to determine temperatures and oxygen fugacity. The range of temperatures and oxygen fugacities are 531 to 633 °C and $10^{-16.5}$ to $10^{-22.9}$ bars, respectively. Temperatures and oxygen fugacities of each unit are shown in Figure 5.3, and indicate that as temperatures increase oxygen fugacities also
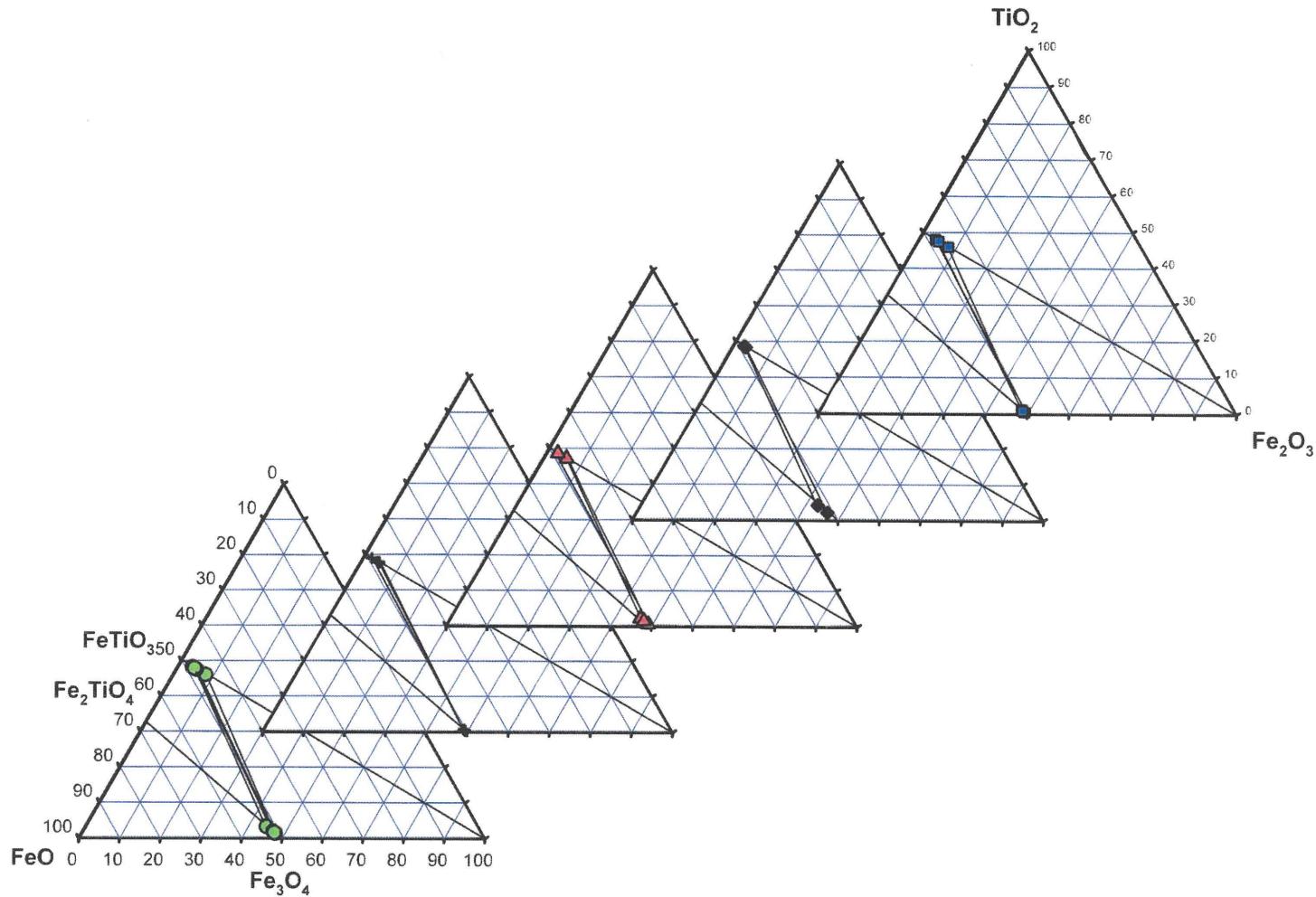
FIGURE 5.2: Magnetite and ilmenite TiO₂ − FeO − Fe₂O₃ ternary plot. Exsolution pairs are connected with tie lines. Green circles, black crosses, red triangles, black diamonds and blue squares are the Border Gabbro, Railway, Upper Marathon Shore, Black, and Center Three pegmatites, respectively.

increase. As shown in Figure 5.3, no real difference in oxygen fugacity and temperature is observed between units.
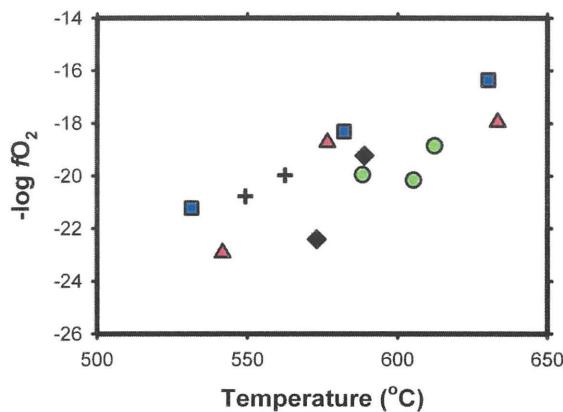
FIGURE 5.3: Magnetite-ilmenite temperature vs. oxygen fugacity (log fO_2). Green circles, black crosses, red triangles, black diamonds, and blue squares are the Border Gabbro, Railway, Upper Marathon Shore, Black, and Center Three pegmatites.

Apart from colour, feldspar compositions and textures and associations are similar in every other aspect. Hofmeister and Rossman (1985) attribute the green colour of alkali feldspars, as found in the Border Gabbro unit, to trace lead and water substituting for potassium. Red feldspars in the Upper Marathon Shore and Center Three units reflect oxidation of iron and indicates that most, if not all, feldspar iron is in the ferric state, as opposed to ferric/ferrous iron accounting for black feldspars in the Railway and Black units. The oxidation state of iron in feldspar can be either related to primary or secondary mechanisms.

In addition to differences in iron oxidation, the presence of lead, as inferred by their green colour, in the Border Gabbro feldspars indicates that these pegmatites are possibly derived from a different batch of magma than the other pegmatites.

Subsequent to the formation of the framework feldspars, the precipitation of intercumulous minerals occurred. These include amphiboles, astrophyllite, sulphides, sulphates, quartz, and calcite. In contrast to Center Three pegmatites, which only contain amphibole (taramite) in the initial stage, amphibole can be used to constrain temperature and oxygen fugacity.

The presence of magmatic riebeckite in Upper Marathon Shore pegmatites indicates that the melt had a relatively high oxygen fugacity, otherwise arfvedsonite would have formed (Ernst

1962; Evans 2007). The breakdown of riebeckite, with a composition of 5% ferrorichterite, 5% grunerite, and 90% riebeckite, occurs at 359 °C at 2 kbar on the hematite-magnetite (HM) buffer (Owen 1985). The experimental work of Evans (2007) suggest that endmember riebeckite can stably exist below 450 °C at 2 kbar midway between the HM and fayalite-magnetite-quartz (FMQ) buffers. As riebeckite has a limited stability, it can be used to constrain oxygen fugacity and temperature based on its composition, specifically, its arfvedsonitic component (Ernst 1962) and fluorine content (Owen 1985). Coldwell riebeckites have approximately 5 to 10 % arfvedsonite component. Stability of riebeckite with 10 % arfvedsonite at 2 kbar is shown in Figure 5.4. As the pegmatites were intruded at approximately 1 kbar and the minimum subsolidus temperatures are greater than 450 °C, the stability for riebeckite might expand (not shown in Figure 5.4).
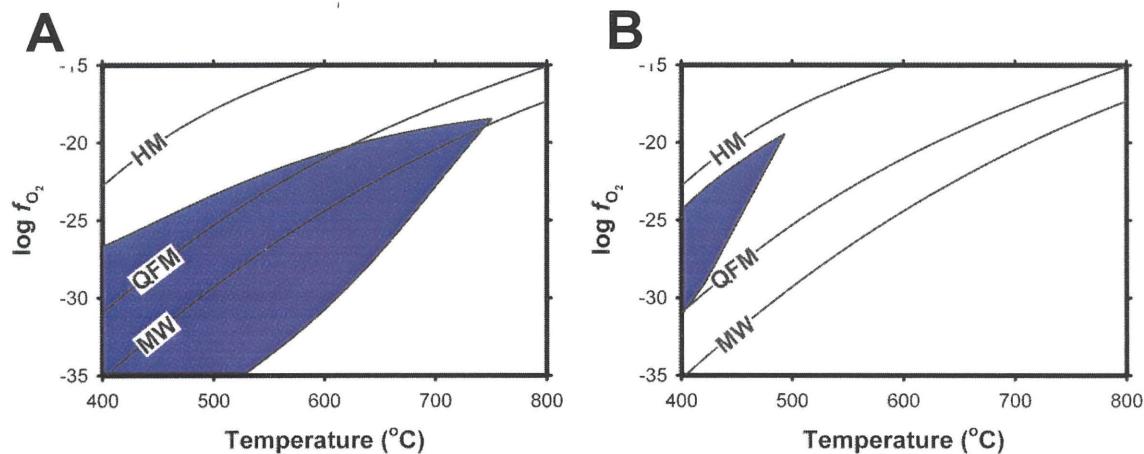
FIGURE 5.4: Ferrorichterite (A) and riebeckite (B) stability fields in relation to temperature and oxygen fugacity [Log $f(O_2)$] at 1 and 2 kbar respectively. Ferrorichterite is from Charles (1975). The riebeckite contains 10% arfvedsonite component (Evans 2007). HM = hematite-magnetite buffer; FMQ = fayalite-magnetite-quartz buffer; MW = magnetite-wüstite buffer.

Apart from Center Three, all pegmatites contain ferrorichterite amphiboles. According to Charles (1975), ferrorichterite decomposes into fayalite, magnetite, quartz, and vapor at 525 °C, 1 kbar (QFM buffer). The stability field of ferrorichterite with respect to temperature and oxygen fugacity is shown in Figure 5.5A. As the Upper Marathon Shore pegmatites contain both ferrorichterite and riebeckite, the temperature must have decreased with oxygen fugacity (Fig. 5.5).

Amphibole in Center Three pegmatites forms in the initial stage of crystallization and, unlike other units, is the main mafic silicate. This feature is also present in the host syenite, and indicates that the pegmatites represent the host syenite residua.
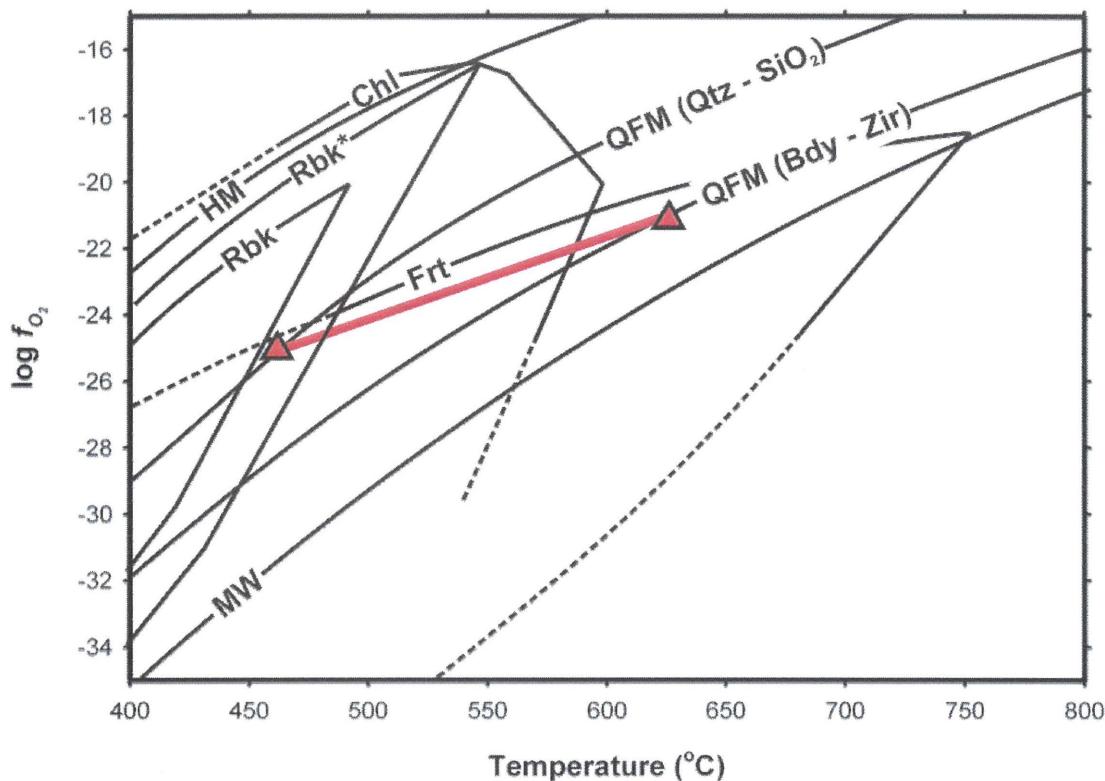
FIGURE 5.5: The primary magmatic trend of the Upper Marathon Shore pegmatites as the melt evolved in respect to temperature and oxygen fugacity (log fo_2). See text for explanation.

Ferroactinolite is a common mineral forming after all other amphiboles in Center One upper ferroaugite syenites, but is not observed in the pegmatites. Similar amphiboles, e.g. ferroedenite, are present and indicate that the Border Gabbro pegmatites are enriched in calcium relative to the Center One ferroaugite syenites. Aenigmatite is another mineral absent in the residua but present in the host rock. As titanium preferentially partitions into magnetite early in the paragenesis, no aenigmatite is observed.

Subsequent to the final magmatic stage, fluids saturated in iron, REEs, fluorine and carbonate infiltrated the pegmatites along fractures, grain boundaries and inclusions. These fluids selectively altered and recrystallized LREE silicates and phosphates into fluorocarbonates

and other products, i.e. quartz, calcite, and magnetite. Using fluid inclusions, Salvi and Williams-Jones (1996) have determined that REEs are mobile at low temperatures (< 200 °C). These temperatures might correspond to those of the Coldwell alteration fluids and, in common with the Strange Lake peralkaline complex (Salvi and Williams-Jones 1996), these fluids precipitated fluorocarbonates once saturation was reached. Unlike LREE minerals, HREE minerals were stable during the secondary stage of crystallization. This is related to the relative insolubility of HREEs in hydrothermal solutions (Wood 1990) and the stability of HREE bearing minerals, i.e. fergusonite, zirconolite and xenotime.

In addition to fluorocarbonates, chamosite (Fe-chlorite) forms in the secondary stage. In Coldwell rocks, chamosite commonly replaces amphibole, muscovite and Fe-biotite (annite). The large stability field of chlorite with respect to temperature and oxygen fugacity is shown in Figure 5.5 (Chernosky et al. 1988). Geothermometry and geobarometry has been attempted using chlorite-amphibole interactions (Laird 1982), but as Fe^{2+}/Fe^{3+} and substitution calculations are not accurate, no useful information can be extracted (Laird 1988). As feldspar textures suggest a short subsolidus cooling interval, amphibole, muscovite and biotite disequilibrium likely occurred at the same time as the REE silicate and phosphate recrystallization.

5.3 Conclusion

The objective of this thesis is to document the character, paragenesis and petrogenesis of Coldwell pegmatites. Rock-forming and accessory mineralization indicates: that Coldwell pegmatites are of the NYF-type; there is a direct compositional link between Coldwell syenites and pegmatites; with the different pegmatites being derived from differing batches of magma. The paragenesis can be divided into three magmatic stages and one secondary stage. The initial stage is characterized by REE and HFSE minerals. The cumulus stage is dominated by alkali feldspars that form in framework-type textures. The interstitial stage is composed of sodic, sodic-calcic and calcic amphiboles, quartz and calcite. And, the final crystallization stage recrystallizes REMs and REE-bearing minerals with fluorocarbonates and amphiboles, biotite and muscovite with chlorite.

Cryptoperthitic feldspar textures and the absence of microcline indicate that the feldspars began to crystallize slightly above 730 °C and that the pegmatites underwent a short cooling history (were essentially quenched or held at high temp during Center Two and Three emplacement and then rapidly cooled). As such, magnetite-ilmenite exsolution pairs indicate that subsolidus temperatures were 531 to 633 °C and oxygen fugacities were $10^{-16.5}$ to $10^{-22.9}$ bars. In

the initial stages, zircon-baddeleyite textures indicate that initial silica activities were approximately $10^{-0.75}$ and, as quartz precipitated in the interstitial stage, silica activity increased. The presence of riebeckite in the interstitial stage indicates that the stability field expands, as riebeckite forms above 450 °C, and before quartz. A possible riebeckite stability field at 1 kbar is shown in Figure 5.5 (Rbk*).

In the case of Coldwell pegmatites, there is evidence of REEs and HFSEs minerals being precipitated magmatically and hydrothermally. In both cases carbo- and hydro-thermal fluids made it possible for a significant proportion of REEs, specifically LREEs, and HFSEs to remain mobile throughout the crystallization process. The majority of primary REE and HFSE minerals form in the initial stage of crystallization, but saturation of HFSEs, in the form of astrophyllite and pyrochlore, also occurs in the interstitial stage. Final low temperature (< 200 °C) fluids saturated in calcium, fluorine, and water migrated along grain boundaries, fractures and inclusions. These fluids replaced REMs, i.e. allanite, chevkinite, kainosite, and REE-bearing minerals, i.e. apatite, with fluorocarbonates, and replaced hydrous silicates, i.e. amphibole, biotite, and muscovite, with Fe-chlorite (chamosite).

REFERENCES

Adams JW, Staatz MH and Havens RG (1964) Cenosite from Porthill, Idaho. American Mineralogist 49: 1736-1741

Abdel-Rahman AM (2006) Petrogenesis of anorogenic peralkaline granitic complexes from eastern Egypt. Mineralogical Magazine 70: 27-50

Andersen DJ, Lindsley DH and Davidson PM (1993) Quilf: a pascal program to assess equilibria among Fe-Mg-Ti oxides, pyroxenes, olivine, and quartz. Computers and Geosciences 19: 1333-1350

Bailey DK (1980) Volcanism, Earth degassing, and replenished lithosphere mantle. Philosophical Transactions, Royal Society of London A297: 309-322

Bailey SW (1988) Chlorites: Structures and crystal chemistry. *In* Hydrous Phyllosilicates (eds. Bailey SW). Mineralogical Society of America – Reviews in Mineralogy 19: 347-403

Banks DA, Yardley BWD, Campbell AR, and Jarvis KE (1994) REE composition of an aqueous magmatic fluid: a fluid inclusion study from the Capitan Pluton, New Mexico. Chemical Geology 113: 259-272

Bayliss P (1975) Nomenclature of the trioctahedral chlorites. The Canadian Mineralogist 13: 178-180

Bayliss P, Mazzi F, Munno R, and White TJ (1989) Mineral nomenclature: zirconolite. Mineralogical Magazine 53: 565-569

Bea F (1996) Residence of REE, Y, Th and U in granites and crustal protoliths; implications for the chemistry of crustal melts. Journal of Petrology 37: 521-552

Behrendt JC, Green AG, Cannon WF, Hutchinson DR, Lee MW, Milkereit B, Agena WF, and Spencer C (1988) Crustal structure of the Midcontinental rift system: Results from GLIMPCE deep seismic reflection profiles. Geology 16: 81-85

Bell K, Blenkinsop J and Watkinson DH (1979) Rb/Sr geochronology of alkalic complexes, Ontario. Ontario Geologic Survey, Miscellaneous Paper 87: 69-78

Bell K and Blenkinsop J (1980) Ages and initial ^{87}Sr-^{86}Sr ratios from alkalic complexes of Ontario. Ontario Geologic Survey, Miscellaneous Paper 93: 16-23

Brown WL, Becker SM and Parsons I (1983) Cryptoperthites and cooling rate in a layered syenite pluton: a chemical and TEM study. Contributions to Mineralogy and Petrology 82:13-25

Brown WL and Parsons I (1984a) Exsolution and coarsening mechanisms and kinetics in an ordered cryptoperthite series. Contributions to Mineralogy and Petrology 86:3-18

Brown WL and Parsons I (1984b) The nature of potassium feldspar, exsolution microtextures and development of dislocations as a function of composition in perthitic alkali feldspars. Contributions to Mineralogy and Petrology 86:335-341

Buddington AF and Lindsley DH (1964) Iron-titanium oxide minerals and synthetic equivalents. Journal of Petrology 5: 310-357

Calvo C and Faggiani R (1974) A re-investigation of the crystal structure of chevkinite and perrierite. American Mineralogist 59: 1277-1285

Cannon WF (1992) The Midcontinent rift in the Lake Superior region with emphasis on its geodynamic evolution. Tectonophysics 213: 41-48

Cannon WF, Green AG, Hutchinson DR, Lee M, Milkereit B, Behrendt JC, Halls HC, Green JC, Dickas AB, Morey GB, Suttcliffe R, and Spencer C (1989) The North American Midcontinent rift beneath Lake Superior from GLIMPCE seismic reflection profiling. Tectonics 8: 305-332

Cannon WF and Hinze WJ (1992) Speculations on the origin of the North American Midcontinent rift. Tectonophysics 213: 49-55

Card KD, Church WR, Franklin JM, Frarey MJ, Robertson JA, West GF, and Young GM (1972) The Southern Province, in Variations in Tectonic Styles of Canada (Price RA and Douglas RJ, eds) Geological Association of Canada, Special Paper 11: 335-380

Černý P (1991) Rare-element granitic pegmatites. I. Anatomy and internal evolution of pegmatite deposits. Geosciences Canada 18: 49-67

Černý P (1992) Geochemical and petrogenetic features of mineralization in rare-element granitic pegmatites in the light of current research. Applied Geochemistry. 7: 393-416

Černý P and Ercit TS (1989) Mineralogy of niobium and tantalum: crystal chemical relationships, paragenetic aspects and their economic implications. *In* Lanthinides, Tantalum and Niobium (Moller P, Cerny P and Saupe F, eds) Springer-Verlag, Heidelberg, Germany 27-79

Charles RW (1975) The phase equilibria of richterite and ferrorichterite. American Mineralogist 60: 367-374

Chaudhuri S, Brookins DG and Fenton MD (1971) Rubidium-strontium whole rock and mineral ages of the Coldwell, Ontario, syenites. Geological Society of America, North-central Meeting, Lincoln, NE, Abstracts with Programs 225

Chernosky JV, Berman RG and Bryndzia LT (1988) Stability, phase relations, and thermodynamic properties of chlorite and serpentine group minerals. *In* Hydrous Phyllosilicates (exclusive of micas) (Bailey ed). Reviews in Mineralogy 19: 294-346

Clark AM (1974) A tantalum-rich variety of sphene. Mineralogical Magazine 39: 605-607

Coelho AA, Cheary RW and Smith KL (1997) Analysis and structural determination of the Nd-substituted zirconolite-4M. Journal of Solid State Chemistry. 129: 346-359

Collins WJ, Beams SD, White AJR, and Chappell BW (1982) Nature and origin of A-type granites with particular reference to southeastern Australia. Contributions to Mineralogy and Petrology 80: 189-200

Congdon RD and Nash WP (1991) Eruptive pegmatite magma: rhyolite of the Honeycomb Hills. Utah. American Mineralogist 76:1261-1278

Currie KL (1976) The alkaline rocks of Canada. Geological Survey of Canada, Bulletin 239

Currie KL (1980) A contribution to the petrology of the Coldwell alkaline complex, Northern Ontario. Geological Survey of Canada, Bulletin 287

Dahl R, Watkinson DH and McGoran JW (1987) Two Duck Lake intrusion, Coldwell Alkaline Complex, Ontario 1. Geology and Structure. *Abstract* Lake Superior Institute Meeting, Wawa

Davis DW and Paces JB (1990) Time resolution of geologic events on the Keweenawan Peninsula and implications for development of the Midcontinental Rift System. Earth Planet Science Letters 97: 54-64

Davis DW and Sutcliffe RH (1985) U-Pb ages from the Nipigon plate and northern Lake Superior. Geologic Society of America Bulletin 96: 1572-1579

De Hoog JCM and van Bergen MJ (2000) Volatile-induced transport of HFSE, REE, Th and U in arc magmas: evidence from zirconolite-bearing vesicles in potassic lavas of Lewotolo volcano (Indonesia). Contributions to Mineralogy and Petrology 139: 485-502

De Vito C, Pezzotta F, Ferrini V, and Aurisicchio C (2006) Nb-Ti-Ta oxides in the gem-mineralized and "hybrid" Anjanabonoina granite pegmatite, central Madagascar: a record of magmatic and postmagmatic events. The Canadian Mineralogist 44:87-103

Deer WA, Howie RA and Zussman J (2001) Rock Forming Minerals: Framework Silicates, Feldspars, Second Edition. The Geological Society 4A: 3, 117 -139

Della Ventura G, Willians CT, Cabella R, Oberti R, Caprilli E, and Bellatreccia F (1999) Britholite-hellandite intergrowths and associated REE-minerals from the alkali-syenitic ejecta of the Voci volcanic complex (Latium, Italy): petrological implications bearing on REE mobility in volcanic systems. European Journal of Mineralogy 11: 843-854

DeMartin F, Pilati T, Diella V, Donzelli S, Gentile P, and Gramaccioli M (1991) The chemical composition of xenotime from fissures and pegmatites in the Apls. Canadian Mineralogist 29:69-75

Donnay G and Donnay JDH (1953) The crystallography of bastnaesite, parisite, röentgenite, and synchysite. American Mineralogist 38: 932-963

Droop GTR (1987) A general equation for estimating Fe^{3+} concentrations in ferromagnesian silicates and oxides from microprobe analyses, using stoichiometric criteria. Mineralogical Magazine 51: 431-435

Ercit TS (2002) The mess that is "allanite". The Canadian Mineralogist 40: 1411-1419

Ercit TS (2005) Identification and alteration trends of granitic-pegmatite-hosted (Y,REE,U,Th)-(Nb,Ta,Ti) oxide minerals: a statistical approach. The Canadian Mineralogist 43: 1291-1303

Ernst WG (1962) Synthesis, stability relations, and occurrence of riebeckite and riebeckite-arfvedsonite solid solutions. The Journal of Geology 70: 91-121

Es'kova EM (1959) Geochemistry of Nb and Ta in the nepheline syenite massifs of the Vishnevyie Mountains. Geokhimiya 2: 130-139

Evans BW (2007) The synthesis and stability of some end-member amphiboles. *In* Amphiboles: Crystal Chemistry, Occurrence, and Health Issues (eds. Hawthorne FC, Oberti R, Della Ventura G, and Mottana A). Reviews in Mineralogy and Geochemistry 67: 261-286

Finch RJ and Harchar JM (2003) Structure and chemistry of zircon and zircon-group minerals. Reviews in Mineralogy and Geochemistry 53: 1-25

Fleischer MW (1965) Some aspects of the geochemistry of yttrium and the lanthanides. Geochimica et Cosmochimica Acta 29:755-772

Fleischer MW and Altschuler ZS (1969) The relationship of the rare-earth composition of minerals to geological environment. Geochimica et Cosmochimica Acta 33: 725-732

Förster HJ (1998a) The chemical composition of REE-Y-Th-U-rich accessory minerals in peraluminous granites of the Erzgebirge-Fichtelgebirge region, Germany. Part I. The monazite-(Ce)-brabantite solid solution series. American Mineralogist 83: 259-272

Förster HJ (1998b) The chemical composition of REE-Y-Th-U-rich accessory minerals in peraluminous granites of the Erzgebirge-Fichtelgebirge region, Germany. Part II. The xenotime. American Mineralogist 83: 1302-1315

Fowler M and Williams CT (1986) Zirconolite from the Glen Dessarry syenite; a comparison with other Scottish zirconolites. Mineralogical Magazine 50: 326-328

Gaite JM and Michoulier J (1970) Application de la resonance paramagnétique electronique de l'ion Fe^{3+} à l'étude de la structure des feldspaths. Bulletin de la Société Chimique de France 93: 341-356

Gieré R (1996) Formation of rare earth minerals in hydrothermal systems. *In* Rare Earth Minerals: Chemistry, Origin and Ore Deposits (eds. Jones AP, Wall F and Williams CT) Chapman and Hall, London 105-150

Gieré R, Williams CT and Lumpkin GR (1998) Chemical characteristics of natural zirconolite. Schweizerische Mineralogische und Petrographische Mitteilungen 78: 433-459

Gorshkov AI, Sidorenko GA, Lapina MI, Naumova IS, and Sivtsov AV (1998) The structural relationship between zircon and xenotime in regular intergrowths. Lithology and Mineral Resources 33:395-400

Gramaccioli CM and Segalstad TV (1978) A uranium- and thorium-rich monazite from a south-alpine pegmatite at Piona, Italy. American Mineralogist 63: 757-761

Green JC (1983) Geologic and geochemical evidence for the nature and development of the Middle Proterozoic (Keweenawan) Midcontinental Rift of North America. Tectonophysics 94: 413-437

Green JC, Davis DW, Easton RM, Miller JD, Vervoort JD, and Zartman RE (2005) Geochronology of the igneous rocks of the midcontinental rift system; a review. Geological Society of America 37, 5: 73

Haas JR, Shock EL and Sassani DC (1995) Rare earth elements in hydrothermal systems: Estimates of standard partial modal thermodynamic properties of aqueous complexes or the rare earth elements at high pressures and temperatures. Geochimica et Cosmochimica Acta 59: 4329-4350

Halls HC and Pesonen LJ (1982) Paleomagnetism of Keeweenaw rocks. *In* Geology and Tectonics of the Lake Superior Basin (eds. Wold RJ and Hinze WJ) Geologic Society of America Memoirs 156: 173-202

Hammer VMF and Beran A (1991) Variations in the OH concentration of rutiles from different geological environments. Mineralogy and Petrology 45: 1-9

Hanor JS (2000) Barite-celectine geochemistry and environments of formation. *In* Sulphate minerals: Crystallography, geochemistry, and environmental significance (eds. Alpers CN, Jambor JL and Nordstrom DK) Reviews in Mineralogy and Geochemistry 40: 193-275

Haskin LA (1990) PREEconceptions pREEvent pREEcise pREEdictions. Geochimica et Cosmochimica Acta 54: 2353-2361.

Hawthorne FC and Oberti R (2006) On the classification of amphiboles. The Canadian Mineralogist 44:1-21

Hay S (2003) Nb mineralization of the Oka carbonatite complex, Quebec. Unpublished M.Sc. thesis, Lakehead University, Thunder Bay

Heaman LM and Machado N (1992) Timing and origin of midcontinent rift alkaline magmatism, North America: Evidence from the Coldwell Complex. Contributions to Mineralogy and Petrology 110: 289-303

Heaman LM, Easton RM, Hart TR, Hollings P, MacDonald CA, and Smyk M (2007) Mesoproterozoic magmatism, Lake Nipigon region, Ontario. Canadian Journal of Earth Sciences 44: 1055-1086

Henderson P (1996) The rare earth elements: introduction and review. *In* Rare Earth Minerals: Chemistry, Origin and Ore Deposits (eds. Jones AP, Wall F and Williams CT) Chapman and Hall, London 1-19

Hewitt DA and Abrecht J (1986) Limitations on the interpretation of biotite substitutions from chemical analyses of natural samples. American Mineralogist 71: 1126-1128

Hill GJ (1968) The effect of hydrogen on the electrical properties of rutile. British Journal of Applied Physics 1: 1151-1162

Hoche T, Moisescu C, Avramov I, Russel C, and Heerdegen WD (2001a) Microstructure of $SiO_2-Al_2O_3-CaO-P_2O_5-K_2O-F-$ glass ceramics. 1. Neddlelike versus isometric morphology of apatite crystals. Chemistry of Materials 13: 1312-1219

Hoche T, Moisescu C, Avramov I, Russel C, Heerdegen WD, and Jäger C (2001b) Microstructure of $SiO_2-Al_2O_3-CaO-P_2O_5-K_2O-F-$ glass ceramics. 2. Time dependence of apatite crystal growth Chemistry of Materials 13:1320-1325

Hofmeister AM and Rossman GR (1985) A spectroscopic study of irradiation coloring of amazonite: structurally hydrous, Pb-bearing feldspar. American Mineralogist 70: 794-804

Hogarth DD (1977) Classification and nomenclature of the pyrochlore group. American Mineralogist 62:403-410

Hogarth DD (1989) Pyrochlore, Apatite and Amphibole: Distinctive Minerals in Carbonatite. Carbonatites: Genesis and Evolution (Bell K, ed) Chapman and Hall, London 105-148

Holland T, Baker J and Powell R (1998) Mixing properties and activity-composition relationships of chlorites in the system $MgO-FeO-Al_2O_3-SiO_2-H_2O$. European Journal of Mineralogy 10: 395-406

Hollings P, Hart T, Richardson A, and MacDonald CA (2007) Geochemistry of the Mesoproterozoic intrusive rocks of the Nipigon Embayment, northwestern Ontario: evaluating the earliest phases of rift development. Canadian Journal of Earth Science 44: 1087-1110

Hoshino M, Kimata M, Shimizu M, Nishida N, and Fujiwara T (2006) Allanite-(Ce) in granitic rocks from Japan: genetic implications of patterns of REE and Mn enrichment. The Canadian Mineralogist 44:45-62

Hoskin PWO, Kinny PD, Wyborn D, and Chappell BW (2000) Identifying accessory mineral saturation during differentiation in granitoid magmas: and integrated approach. Journal of Petrology 41: 1365-1396

Hsu LC (1992) Synthesis and stability of bastnaesites in a part of the system (Ce, La)-F-H-C-O. Mineralogy and Petrology 47:87-101

Hughson MR and Sen Gupta JG (1964) A thorian intermediate member of the britholite-apatite series. The American Mineralogist 49: 937-951

Hutchinson DR, White RS, Cannon WF and Schulz KJ (1990) Keweenaw hot spot: Geophysical evidence for a 1.1 Ga mantle plume beneath the Midcontinent Rift System. Journal of Geophysical Research 87: 10869-10884

Imaoka T and Nakashima K (1994) Chevkinite in syenites from Cape Ashizuri, Shikoku Island, Japan. Neues Jahrbuch Mineralogie Monatshefte 8: 358-366

James RS and Hamilton DL (1969) Phase relations in the system $NaAlSi_3O_8$-$KAlSi_3O_8$-$CaAl_2Si_2O_8$-SiO_2 at 1 kilobar water vapour pressure. Contributions to Mineralogy and Petrology 21: 111-141

James RS, Turnock AC and Fawcett JJ (1976) The stability and phase relations of iron chlorite below 8.5 kb P_{H2O}. Contributions to Mineralogy and Petrology 56: 1-25

Jiang N (2006) Hydrothermal alteration of chevkinite-(Ce) in the Shuiquangou syenitic intrusion, northern China. Chemical Geology 227:100-112

Kalsbeek N, Larsen S, Rönsbo JD (1990) Crystal structure of rare earth elements rich apatite analogues. Zeitschrift für Kristallographie 191: 249-263

Kapustin YuL (1973) Zircophyllite, the zirconium analogue of astrophyllite. International Geology Review 15: 621-625

Kawasaki T (1999) Thermodynamic analysis of partitioning of Ca, Fe and Mg between olivine and clinopyroxene. Geochemical Journal 33: 33-58

Keppler H (1993) Influence of fluorine on the enrichment of high field strength trace elements in granitic rocks. Contribution to Mineral Petrology 114: 479-488

Klasner JS, Cannon WF and van Schmus WR (1982) The pre-Keweenawan tectonic history of southern Canadian shield and its influence on formation of the Midcontinent rift. Geological Society of America, Memoir 156, Geology and Tectonics of the Lake Superior Basin. 27-46

Klein C (2002) Manual of Mineral Science, New York, John Wiley and Sons Inc.

Komkov AI (1959) Struktura prirodnogo fergusonite I ego polimorfioi modifikacii. Crystallography 4: 836-841

Kositcin N, McNaughton NJ, Griffin BJ, Fletcher IR, Groves DI, and Rasmussen B (2003) Textural and geochemical discrimination between xenotime of different origin in the Archean Witwatersrand Basin, South Africa. Geochimica et Cosmochimica Acta 67: 709-731

Krasnobaev AA, Votyakov SL and Krokhalev VYa (1988) Zircon spectroscopy: properties and geological applications. Moscow: Nauka

Laird J (1982) Amphiboles in metamorphosed basaltic rocks: greenschist to amphibolite facies and blueschist-greenschist-eclogite relations. *In* Amphiboles: Petrology and Experimental Phase Relations (Veblen DR and Ribbe PH eds) Rev. Mineral. 9B: 113-159

Laird J (1988) Chlorites: metamorphic petrology. Hydrous Phyllosilicates (exclusive of micas) (Bailey SW ed). Reviews in Mineralogy 19: 405-453

Larsen L M (1976) Clinopyroxenes and coexisting mafic minerals from the alkaline Ilímaussaq intrusion, south Greenland. Journal of Petrology 17: 258-290

Leake BE, Woolley AR, Arps CES, Birch WD, Gilbert MC, Grice JD, Hawthorne FC, Kato A, Kisch HJ, Krivovichev VG, Linthout K, Laird J, Mandarino JA, Maresch WV, Nickel EH, Rock NMS, Schumacher JC, Smith DC, Stephenson NCN, Ungaretti L, Whittaker EJW, and Youzhi G. (1997) Nomenclature of amphiboles: report of the subcommittee on amphiboles of the International Mineralogical Association, Commission on New Minerals and Mineral Names. The Canadian Mineralogist 35: 219-246

Leake BE, Woolley AR, Birch WD, Ferraris G, Grice JD, Hawthorne FC, Kisch HJ, Krivovichev VG, Schumacher JC, Stephenson NCN, and Whittaker EJW (2003) Nomenclature of amphiboles: additions and revisions to the International Mineralogical Association's amphibole nomenclature. The Canadian Mineralogist 41: 1355-1370

LeCheminant AN and Heaman LM (1989) Mackenzie igneous events, Canada: Middle Proterozoic hotspot magmatism associated with ocean opening. Earth Planetary Science Letters 96: 38-48

Lee MR, Waldron KA, Parsons I, and Brown WL (1997) Feldspar-fluid interaction in braid microperthites: pleated rims and vein microperthites. Contributions to Mineralogy and Petrology 127: 291-304

Lie X, Rucheng W, Xiaoming C, Jianshenf O, Dezi W (2005) Th-rich zircon from peralkaline A-type granite: Mineralogical features and petrological implications. Chinese Science Bulletin 50: 809-817

Liferovich RP and Mitchell RH (2005a) Composition and genesis of Na-, Nb- and Zr-bearing titanite from Khibina, Russia, and crystal-structure data for synthetic analogues. The Canadian Mineralogist 43:795-812

Liferovich RP and Mitchell RH (2005b) Crystal chemistry of titanite-structured compounds: the $CaTi_{1-x}Zr_xOSiO_4$ (x ≤ 0.5) series. Physics and Chemistry of Minerals 32: 40-51

Liferovich RP and Mitchell RH (2006b) Apatite-group minerals from nepheline syenite, Pilansberg alkaline complex, South Africa. Mineralogical Magazine 70: 463-484

Liferovich RP and Mitchell RH (2006b) Solid solutions of niobium in synthetic titanite. The Canadian Mineralogist 44:1089-1097

Lilley FEM (1964) An analysis of the magnetic features of the Port Coldwell intrusive. Unpublished M.Sc. thesis, University of Western Ontario, London

Lima-de-Faria J (1962) Heat treatment of chevkinite and perrierite. Mineralogical Magazine 33:42-47

Lumpkin GP (1998) Rare-element mineralogy and internal evolution of the Rutherford #2 pegmatite, Amelia county, Virginia: a classic locality revisited. The Canadian Mineralogist 36: 339-353

Lumpkin GR and Ewing RC (1995) Geochemical alteration of pyrochlore group minerals: pyrochlore subgroup. American Mineralogist 80: 732-743

Lyakhovich VV (1979) Genesis of accessory moissanite. Izvestiya Akademii Nauk SSSR. Seriya Geologicheskaya 4:63-74

Macdonald R and Belkin HE (2002) Compositional variation in minerals of the chevkinite group. Mineralogical Magazine 66(6): 1075-1098

Macdonald R, Karup-Møller S and Rose-Hansen J (2007) Astrophyllite-group minerals from the Ilímaussaq complex, South Greenland (contribution to the mineralogy of Ilímaussaq no. 123). Mineralogical magazine 71: 1-16

Macdonald R and Saunders MJ (1973) Chemical variation in minerals of the astrophyllite group. Mineralogical Magazine 39: 97-111

Malmstroem JC (2007) Zirconolite: Experiments on the stability in hydrothermal fluids. Doctoral Dissertation. Swiss Federal Institute of Technology Zürich.

Malmstroem JC, Reusser E and Giere R ( ) Zirconolite experiments on the stability in hydrothermal fluids. Ninth International Symposium on Experimental Mineralogy, Petrology and Geochemistry 67-68

Markl G, Marks M, Schwinn G, and Sommer H (2001) Phase equilibrium constraints on Intensive crystallization parameters of the Ilimaussaq complex, south Greenland. Journal of Petrology 42: 2231-2258

Martin RF (2007) Amphiboles in the Igneous environment. *In* Amphiboles: Crystal chemistry, Occurrence, and Health Issues (eds. Hawthorne FC, Oberti R, Della Ventura G, and Mottana A) Reviews in Mineralogy and Geochemistry 67: 323-358

Martin RF and De Vito C (2005) The patterns of enrichment in felsic pegmatites ultimately depend on tectonic setting. The Canadian Mineralogist 43: 2027-2048

Martin RF, De Vito C and Pezzotta F (2008) Why is amazonitic K-feldspar an earmark of NYF-type granitic pegmatites? Clues from hybrid pegmatites in Madagascar. American Mineralogist 93: 263-269

Mazeina L, Ushakov SV, Navrotsky A, and Boatner LA (2005) Formation enthalpy of $ThSiO_4$ and enthalpy of the thorite $\rightarrow$ huttonite phase transition. Geochimica et Cosmochimica Acta 69: 4675-4683

Mazzi F and Munro R (1983) Caciobetafite (new mineral of the pyrochlore group) and related minerals from Campi Flegrei, Italy: crystal structures of polymignite and zirkelite, comparison with pyrochlore and zirconolite. The American Mineralogist 68: 262-276

McDowell SD (1979) Chevkinite from the Little Chief Granite porphyry stock, California. The American Mineralogist 64: 721-727

McLaughlin RM and Mitchell RH (1989) Rare metal mineralization in the Coldwell alkaline complex, northwestern Ontario. Geologic Association of Canada – Mineralogical Association of Canada, Program with Abstracts 14: A1

McLaughlin RM (1990) Accessory rare metal mineralization in the Coldwell complex, northwestern Ontario. M.Sc. Thesis. Lakehead University

Michard A (1989) Rare earth element systematics in hydrothermal fluids. Geochimica et Cosmochimica Acta 53: 745-750

Mitchell RH (1990) A review of the compositional variation of amphiboles in alkaline plutonic complexes. Lithos 26: 135-156

Mitchell RH and Platt RG (1977) Field guide to aspects of the geology of the Coldwell alkaline complex. 23rd Annual Mtg. Inst. Lake Superior Geology, Thunder Bay Ontario

Mitchell RH and Platt RG (1978) Mafic mineralogy of ferroaugite syenite from the Coldwell alkaline complex, Ontario, Canada. Journal of Petrology 19: 627-651

Mitchell RH and Platt RG (1982) Mineralogy and petrology of nepheline syenites from the Coldwell alkaline complex, Ontario, Canada. Journal of Petrology 23: 186-214

Mitchell RH, Platt RG and Cheadle SP (1983) A gravity study of the Coldwell complex, Northwestern Ontario and its Petrological Significance. Canadian Journal of Earth Sciences 20, 11: 1631-1638

Mitchell RH, Platt RG, Downey M, and Laderoute DG (1991) Petrology of alkaline lamprophyres from the Coldwell alkaline complex, northwestern Ontario. Canadian Journal of Earth Science 28: 1653-1663

Mitchell RH, Platt RG, Lukosius-Sanders, J, Artist-Downey M, and Moogk-Pickard S (1993) Petrology of syenites from center III of the Coldwell alkaline complex, northwestern Ontario, Canada. Canadian Journal of Earth Sciences 30: 145-158

Mitchell RS (1966) Virginia metamict minerals: perrierite and chevkinite. American Mineralogist 51: 1394 - 1405

Monchoux P, Fontan F, De Parseval P, Martin RF, and Wang RC (2006) Igneous albitite dikes in orogenic lherzolites, western Pyrenees, France: a possible source for corundum and alkali feldspar xenocrysts in basaltic terranes. I. Mineralogical associations. The Canadian Mineralogist 44:817-842

Morimoto N, Fabries J, Ferguson AK, Ginzburg IV, Ross M, Seifert FA, Zussman J, Aoki K, and Gottardi G (1989) Nomenclature of pyroxenes. The Canadian Mineralogist 27: 143-156

Mulja T and Mitchell RH (1990) Platinum-group minerals and tellurides from the Geordie Lake intrusion, Coldwell complex, northwestern Ontario. Canadian Mineralogist 28: 489-501

Nasir S (1994) PTOXY: Software package for the calculation of pressure-temperature-oxygen fugacity using a selection of metamorphic geothermobarometers. Computers and Geosciences 20: 1297-1320

Nasraoui M and Bilal E (2000) Pyrochlores from the Lueshe carbonatite complex (Democratic Republic of Congo): a geochemical record of different alteration stages. Journal of Asian Earth Sciences 18: 237-251

Nasraoui M and Waerenborgh JC (2001) Fe speciation in weathered pyrochlore-group minerals from the Lueshe and Araxá (Barreiro) carbonatites by ^{57}Fe Mössbauer spectroscopy. The Canadian Mineralogist 39: 1073-1080

Ni Y, Hughes JM and Mariano AN (1995) Crystal chemistry of the monazite and xenotime structures. American Mineralogist 80: 21-26

Nicol DN (1990) Assimilation of basic xenoliths within center III syenites of the Coldwell alkaline complex, Ontario. M.Sc. thesis, Lakehead University, Thunder Bay, Ontario

Oberti R, Ottolini L, Ventura GD, and Parodi GC (2001) On the symmetry and the crystal chemistry of britholite: New structural and microanalytical data. American Mineralogist 86: 1066-1071

Ohnenstetter D, Watkinson DH and Dahl R (1991) Zoned Hollingworthite from the Two Duck Lake intrusion, Coldwell complex, Ontario. American Mineralogist 76:1694-1700

Owen C (1985) Constraints on the stability of riebeckite. EOS Transitions of the American Geophysical Union 66: 1230

Palmer HC and Davis DW (1987) Paloemagnetism and U-Pb geochronology of volcanic rocks from Michipicoten Island, Lake Superior: Precise calibration of the Keweenawan polar wander track. Precambrian Research 37: 157-171

Pan Y (1997) Zircon- and monazite-forming metamorphic reactions at Manitouwadge, Ontario. The Canadian mineralogist 35: 105-118

Parodi GC, Della Ventura G, Montana A, and Raudsepp M (1994) Zr-rich non metamict perrierite-(Ce) from holocrystalline ejecta in the Sabatini volcanic complex (Latium, Italy). Mineralogical Magazine 58: 607,613

Parsons I (1978) Feldspars and fluids in cooling plutons. Mineralogical Magazine 42: 1-17

Parsons I and Lee MR (2005) Minerals are not just chemical compounds. The Canadian Mineralogist 43: 1959-1992

Perhac RM and Heinrich EW (1964) Fluorite-bastnaesite deposits of the Gallinas Mountains, New Mexico and bastnaesite paragenesis. Economic Geology 59: 226-239

Piccoli PM and Candela PA (2002) Apatite in igneous systems. Reviews in Mineralogy and Geochemistry 48: 255-292

Piilonen PC, Lalonde AE, McDonald AM, and Gault RA (2000) Niobokupletskite, a new astrophyllite-group mineral from Mount Saint-Hilaire, Québec: description and crystal structure. The Canadian Mineralogist 38: 627-639

Piilonen PC, Lalonde AE, McDonald AM, and Larsen AO (2003) Insights into astrophyllite-group minerals. I. Nomenclature, composition and development of a standardized general formula. The Canadian Mineralogist 41: 1-26

Pinckston DR and Smith DGW (1995) Mineralogy of the Lake zone, Thor Lake rare-metals deposit, N.W.T., Canada. Canadian Journal of Earth Sciences 32: 516-532

Platt RG (1996) Nepheline syenite complexes – An overview. *In* Undersaturated alkaline rocks: Mineralogy, petrogenesis, and economic potential (Mitchell RH, ed). Mineralogical Association of Canada Short Course Series 24: 63-99

Platt RG and Mitchell RH (1979) The Marathon Dikes. I: Zirconium-rich titanian garnets and manganoan magnesian ulvospinel-magnetite spinels. American Mineralogist 64: 546-550

Platt RG and Mitchell RH (1982a) The Marathon dikes: ultrabasic lamprophyres from the vicinity of McKellar Harbour, N.W. Ontario. American Mineralogist 67: 907-916

Platt RG and Mitchell RH (1982b) Rb-Sr geochronology of the Coldwell complex, northwestern Ontario, Canada. Canadian Journal of Earth Sciences 19: 1796-1801

Platt RG, Wall F, Williams CT, and Woolley AR (1987) Zirconolite, chevkenite and other rare earth minerals from nepheline syenites and peralkaline granites and syenites of the Chilwa Alkaline Province, Malawi. Mineralogical Magazine 51: 253-63.

Pouliot G, Maxwell JA and Robinson SC (1964) Cenosite from Bancroft, Ontario. Canadian Mineralogist 8: 1-10

Puskas FP (1967) The geology of the Port Coldwell area. Ontario Department of Mines Open File Report 5104

Rieder M, Cavazzini G, D'Yakonov YS, Frank-Kamenetskii VA, Gottardi G, Guggenheim S, Koval PV, Müller G, Neiva AMR, Radoslovich EW, Robert JL, Sassi FP, Takeda H, Weiss Z, and Wones DR (1998) Nomenclature of the micas. The Canadian Mineralogist 36: x-xx

Rizvanova NG, Levchenko OA, Belous OA, Bezman NI, Maslennikov AV, Komarov AN, MakeevAF, and Levisky LK (2000) Zircon reaction and stability of the U-Pb isotope system during interaction with carbonate fluid: experimental hydrothermal study. Contributions to Mineralogy and Petrology 139:101-114

Rodolfi F, Renzulli A, Santi P, and Upton BGJ (2003) Elvolutionary stages of crystallization of weakly peralkaline syenites: evidence from ejecta in the plinian deposits of Agua de Pau volcano (São Miguel, Azores Islands). Mineralogical Magazine 67: 749-767

Rønsbo JG (1989) Coupled substitution involving REEs and Na and Si in apatite in alkaline rocks from the Illimanaussaq intrusion, South Greenland, and the petrologic implications. American Mineralogist 74: 869-901

Rubin JN, Henry CD and Price JD (1993) The mobility of zirconium and other "immobile" elements during hydrothermal alteration. Chemical Geology 110: 29-47

Rule AC and Bailey SW (1987) Refinement of the crystal structure of a monoclinic ferroan clinochlore. Clays and Clay Minerals 35: 129-138

Sage RP (1982) Mineralization in diatreme structures north of Lake Superior. Ontario Geological Survey Study, Ontario Ministry of Natural Resources 27: 57

Salvi S and Williams-Jones AE (1996) The role of hydrothermal processes in concentrating high-field strength elements in the Strange Lake peralkaline complex, northeasthern Canada 60: 1917-1932

Shaw CSJ (1997) The petrology of the layered gabbro intrusion, eastern gabbro, Coldwell alkaline complex, Northwestern Ontario, Canada: evidence for multiple phases in a ring dyke. Lithos 40: 243-259

Škoda R, Novák M and Stanislav H (2006) Granitic NYF pegmatites of the Třebíč pluton (Czech Republic). Acta Mus. Moraviae Sci. Geol. LXXXXXI: 129-176

Smith JV and Brown WL (1988) Feldspar Minerals: Crystal Structure, Physical, Chemical and Microtextural Properties 2nd edition. Springer, New York

Smith MP, Henderson P and Campbell LS (2000) Fractionation of the REE during hydrothermal processes: constraints from the Bayan Obo Fe-REE-Nb deposit, Inner Mongolia, China 64: 3141-3160

Smith WL, Stone J, Ross DR, and Levine H (1960) Doverute, a possible new yttrium fluorocarbonate from Dover, Morris County, New Jersey. The American Mineralogist 45: 92-98

Smyk MC and Franklin JM (2007) A synopsis of mineral deposits in the Archean and Proterozoic rocks of the Lake Nipigon Region, Thunder Bay District, Ontario. Canadian Journal of Earth Science 44: 1041-1053

Soffer BH (1961) Studies of the optical and infrared absorption spectra of rutile single crystals. Journal of Chemical Physics 35: 940-945

Sokolova E, Hawthorne F, Della Ventura, and Kartashov PM (2004) Chevkinite-(Ce): crystal structure and the effect of moderate radiation-induced damage on site-occupancy refinement. The Canadian Mineralogist 42: 1013-1025

Song R, Ding K and Li Z (1999) Site occupancies of iron in saimaite and chevkinite. Chinese Science Bulletin 44: 2224-2276

Speer JA (1982) Zircon. Reviews in Mineralogy and Geochemistry 5, 2nd edn 67-112

Srivastava PK, Gupta YP and Qazi A (2007) Geochemistry of rare metal bearing A-type Dhanota granite, Mahendragarh District, Haryana. Journal Geological Society of India 70: 265-272

Stephenson D (1972) Alkali clinopyroxenes from the nepheline syenites of the South Oôroq center, south Greenland. Lithos 7: 35-41

Stull RJ (1973) Calcic and alkali amphiboles from the Golden Horn Batholith, North Cascades, Washington. American Mineralogist 58: 873-878

Thompson JB and Hovis GL (1978) Triclinic feldspars: angular relations and the representations of feldspar series. American Mineralogist 63: 981-990

Thompson RN (1976) Alkali amphiboles in the Eocene high-level granites of Skye, Scotland. Mineralogical Magazine 40:891-893

Tomašić N, Gajović A, Bermanec V, Su DS, Rajić Linarić M, Ntaflos T, and Schlögl R (2006) Recrystallization mechanisms of fergusonite from metamict mineral precursors. Physics and Chemistry of Minerals 33: 145-159

Uher P, Cerny P, Chapman R, Hatar J, and Miko O (1998) Evolution of Nb, Ta-oxide minerals in the Prasiva granitic pegmatites, Slovakia. II. External hydrothermal Pb, Sb overprint. The Canadian Mineralogist 36: 535-545

Van Emden B, Thornber MR, Graham J, and Lincoln FJ (1997) The incorporation of the actinides in monazite and xenotime from placer deposits in western Australia. Canadian Mineralogist 35: 95-104

Van Landuyk and Amelinckx (1975) Multiple beam imaging of new mixed-layer compounds of the bastnaesite-synchysite series. The American Mineralogist 60: 351-358

Van Schmus WR and Hinze WJ (1985) The Midcontinental Rift system. Annual Reviews of Earth and Planetary Science 13: 345-383

Vlach SRF and Gualda GAR (2007) Allanite and chevkinite in A-type granites and syenites of the Graciosa Province, southern Brazil. Lithos 97: 98-121

Vlassopoulos D, Rossman GR and Haggerty SE (1993) Coupled substitution of H and minor elements in rutile and the implications of high OH contents in Nb- and Cr-rich rutile from the upper mantle. American Mineralogist 78: 1181-1191

Waldron KA and Parsons I (1992) Feldspar microtextures and multistage thermal history of syenites from the Coldwell Complex, Ontario. Contributions to Mineralogy and Petrology 111: 222-234

Walker JWB (1967) Geology of the Jackfish-Middleton area. Ontario Department of Mines Geological Report 50: 3

Wang RC, Fontan F, Chen XM, Hu H, Liu CS, XU SJ, and De Parseval P (2003) Accessory minerals in the Xihuashan Y-enriched granitic complex, southern China: a record of magmatic and hydrothermal stages of evolution. The Canadian Mineralogist 41: 727-748

Watson Eb and Capobianco CJ (1981) Phosphorus and the rare earth elements in felsic magmas: an assessment of the role of apatite. Geochimica et Cosmochimica Acta 45: 2349-2358

Weiliang G (1991) Chemistry and evolution of fergusonite-group minerals, Bayan Obo, Inner Mongolia. Chinese Journal of Geochemistry 10: 266-276

Weitzel H and Schröcke H (1980) Kristallstruktuverfeinerungen von euxenit, $Y(Nb_{0.5}Ti_{0.5})_2O_6$, und M-fergusonit, $YNbO_4$. Zeitschrift für Kristallographie 52: 69-82

White JS and Nelen JE (1987) Monazite and calcioancylite from the Foote mine, North Carolina, U.S.A. Chemical Geology 110: 49-67

White TJ, Segali RL, Hutchison JL, and Barry JC (1984) Polytypic behavior of zirconolite. Proceedings of the Royal Society, London A392: 343-358

Willaime C and Brown WL (1974) A coherent elastic model for determination of the orientation of exsolution boundaries: application to the feldspars. Acta Crystallographica A30:316-331

Williams CT and Gieré R (1996) Zirconolite: a review of localities worldwide, and a compilation of its chemical compositions. Bulletin of the Natural History Museum (Geology Series) 52(1): 1-24

Williams-Jones A and Wood SA (1992) A preliminary petrogenetic grid for REE fluorocarbonates and associated minerals. Geochimica et Cosmochimica Acta 56: 725-738

Wood SA (1990) The aqueous geochemistry of the rare-earth elements and yttrium: 2. Theoretical prediction of speciation in hydrothermal solutions to 350 °C at saturation water pressure. Chemical Geology 88:99-125

Worden RH, Walker FDL, Parsons I, and Brown WL (1990) Development of microporocity, diffusion channel and deuteric coarsening in perthitic alkali feldspars. Contributions to Mineralogy and Petrology 104: 507-515

Wright TL (1968) X-ray and optical study of alkali feldspar: II. An X-ray method for determining the composition and structural state from measurement of 2θ values for three reflections. The American Mineralogist 53: 88-104

Wright TL and Stewart DB (1968) X-ray and optical study of alkali feldspar: I. Determination of composition and structural state from refined unit cell parameters and 2V. The American Mineralogist 53: 38-87

Wyllie PJ, Cox KG and Biggar GM (1962) The habit of apatite in synthetic systems and igneous rocks. Journal of Petrology 3: 238-242

Xie L, Wang RC, Wang DZ, and Qiu JS (2006) A survey of accessory mineral assemblages in peralkaline and more aluminous A-type granites of the southeast coastal area of China. Mineralogical Magazine 70:709-729

Xueming Y, Peishan Z, and Kejie T (1993) Studies of phase transition of partly metamict fergusonite at high temperature. Chinese Science Bulletin 38: 1626-1631

Yakovenchuk VN, Ivanyuk G, Pakhomovsky Ya, Men'shikov Yu (2005) Khibiny. Laplandia Minerals, Khibiny, Russia

Yang Z, Fleck M, Smith M, Tao K, Song R, and Zhang P (2002) The crystal structure of natural Fe-rich chevkinite-(Ce). European Journal of Mineralogy 14: 969-975

Yund Ra (1984) Alkali feldspar exsolution: kinetics and dependence on alkali interdiffusion. In Feldspars and Feldspatiods (Brown, ed) Reidel, Dordrecht 281-315

Zaitsev AN, Wall F and Le Bas MJ (1998) REE-Sr-Ba mineral from the Khibina carbonatites, Kola Peninsula, Russia: their mineralogy, paragenesis and evolution. Mineralogical Magazine 62(2): 225-250

APPENDIX I
SYMBOLS FOR SELECTED MINERALS

Ae	aegirine		Ilm	ilmenite
Aln	allanite		Knz	kainosite
Ab	albite		Llg	löllingite
Amp	amphibole		Mgt	magnetite
An	anorthite		Mlb	molybdenite
Ap	apatite		Mon	monazite
Astro	astrophyllite		Ms	muscovite
Bdy	baddeleyite		Or	orthoclase
Bast	bastnaesite		Prs	parisite
Bt	biotite		Per	perthite
Cal	calcite		Pyc	pyrochlore
Ccp	chalcopyrite		Py	pyrite
Chv	chevkinite		Qtz	quartz
Chl	chlorite		Rbp	rhabdophane
Fa	fayalite		Rt	rutile
Fe-Sp	Fe-sphalerite		Sp	sphalerite
Fe-Zcp	Fe-zircophyllite		Syn	synchysite
Fgs	Fergusonite		Ttn	titanite
Fl	fluorite		Th	thorite
Flu	fluorocarbonate		Xen	xenotime
Gn	galena		Zir	zircon
Hd	hedenbergite		Zcn	zirconolite
Hem	hematite			

APPENDIX II
COMPOSITIONS OF ROCK FORMING AND MINOR MINERALS

Microprobe analyses and various recalculations for each of the rock forming and minor minerals are listed in the following tables. Sample numbers for each unit are:

Border Gabbro pegmatites:	MAS001-MAS013
Railway pegmatites:	MAS014-MAS017; MAS023-MAS028
Upper Marathon Shore pegmatites	MAS018-MAS022
Black pegmatites	MAS029-MAS032
Center Three pegmatites	MAS033-MAS040

II.I Feldspar: Albite-orthoclase exsolution pairs

	MAS001 N = 6	MAS001 N = 5	MAS001 N = 3	MAS002 N = 4	MAS002 N = 4	MAS002 N = 6	MAS002 N = 2	MAS003 N = 5	MAS003 N = 6	MAS004 N = 5	MAS004 N = 9	MAS004 N = 11
Na_2O	10.67	0.72	0.50	11.58	10.39	0.63	0.96	11.47	0.26	11.53	11.07	0.29
Al_2O_3	20.27	18.51	18.71	20.01	21.41	18.75	18.62	19.17	18.57	18.76	18.99	17.98
SiO_2	66.89	64.51	64.90	67.44	65.11	64.38	64.07	68.54	64.91	68.52	68.75	64.52
K_2O	0.20	15.47	15.70	0.40	0.59	15.43	18.28	0.11	16.04	0.15	0.36	15.76
CaO	1.03	-	-	0.48	2.31	-	-	-	-	-	-	-
Fe_2O_3	0.35	0.38	0.03	-	-	-	-	0.47	0.10	0.42	0.71	1.07
BaO	-	-	0.51	-	-	0.77	0.31	-	-	-	-	0.07
Total	**99.41**	**99.59**	**100.35**	**99.91**	**99.81**	**99.96**	**99.23**	**99.76**	**99.88**	**99.38**	**99.87**	**99.69**

	MAS005 N = 6	MAS005 N = 6	MAS006 N = 4	MAS006 N = 4	MAS007 N = 4	MAS007 N = 3	MAS008 N = 6	MAS008 N = 6	MAS009 N = 7	MAS009 N = 6	MAS010 N = 5	MAS010 N = 5
Na_2O	11.25	0.79	11.39	0.28	12.31	0.28	11.31	0.26	12.00	0.30	11.52	0.26
Al_2O_3	19.04	18.28	18.99	18.30	19.33	18.41	19.04	18.54	19.08	18.48	19.45	18.30
SiO_2	68.45	64.89	69.26	65.2	68.66	64.86	68.76	65.46	68.84	65.16	68.84	65.50
K_2O	0.12	15.56	0.16	15.99	0.16	16.56	0.14	16.09	0.13	15.98	0.20	15.79
CaO	-	-	-	-	-	-	-	-	-	-	-	-
Fe_2O_3	0.50	0.38	0.68	0.65	0.30	0.17	0.60	0.24	0.59	0.20	-	-
BaO	-	-	-	-	-	-	-	-	-	-	-	-
Total	**99.36**	**99.91**	**100.47**	**100.41**	**100.76**	**100.43**	**99.85**	**100.59**	**100.62**	**100.11**	**100.02**	**100.18**

	MAS011 N = 5	MAS011 N = 4	MAS012 N = 5	MAS012 N = 3	MAS012 N = 4	MAS013 N = 8	MAS013 N = 6	MAS014 N = 5	MAS014 N = 6	MAS015 N = 3	MAS015 N = 3	MAS015 N = 3
Na_2O	11.58	0.28	11.82	0.26	0.18	11.83	0.35	11.42	0.40	11.53	11.50	0.50
Al_2O_3	19.28	18.50	19.26	18.47	18.23	19.44	18.36	19.49	18.48	20.53	20.78	19.19
SiO_2	69.07	65.50	68.27	64.56	64.18	68.34	64.52	69.00	65.02	67.69	67.30	64.02
K_2O	0.16	15.79	0.15	16.38	16.16	0.09	16.04	0.14	16.12	0.34	0.23	15.90
CaO	-	-	-	-	-	-	-	-	-	-	0.49	-
Fe_2O_3	-	-	0.75	0.13	0.53	0.48	0.57	0.47	0.33	0.03	0.05	0.03
BaO	-	-	-	-	-	-	-	-	-	-	-	-
Total	100.09	100.18	100.25	99.78	99.29	100.18	99.83	100.52	100.35	100.35	100.35	99.64

	MAS015 N = 3	MAS016 N = 4	MAS016 N = 2	MAS016 N = 5	MAS017 N = 6	MAS017 N = 6	MAS018 N = 6	MAS018 N = 7	MAS019 N = 6	MAS019 N = 6	MAS020 N = 6	MAS020 N = 6
Na_2O	0.65	11.02	11.52	0.32	11.70	0.27	11.83	0.45	11.83	0.68	11.33	0.73
Al_2O_3	19.07	20.77	20.28	19.22	19.55	18.72	19.32	18.29	19.74	18.57	20.27	18.73
SiO_2	64.55	66.55	67.53	63.81	68.36	64.41	68.74	65.05	68.47	65.13	68.40	65.15
K_2O	15.27	0.21	0.19	16.03	0.17	16.52	0.07	16.08	0.11	15.91	0.09	15.73
CaO	-	0.79	0.07	-	-	-	-	-	-	-	0.38	-
Fe_2O_3	0.12	0.03	0.05	0.12	0.35	0.03	-	0.08	0.15	0.18	0.05	0.12
BaO	-	-	-	-	-	-	-	-	-	-	-	-
Total	100.01	99.36	99.62	99.39	100.13	99.94	99.97	99.96	100.46	100.47	100.51	100.44

	MAS021 N = 6	MAS021 N = 6	MAS022 N = 6	MAS022 N = 7	MAS023 N = 3	MAS023 N = 3	MAS023 N = 6	MAS024 N = 4	MAS024 N = 4	MAS025 N = 4	MAS025 N = 5	MAS026 N = 6
Na_2O	11.95	0.42	11.97	0.51	11.48	11.50	0.73	11.92	0.60	11.77	0.33	11.89
Al_2O_3	19.39	18.57	19.39	18.38	19.89	20.27	18.77	19.55	18.31	19.20	18.59	19.49
SiO_2	67.95	64.48	68.57	64.99	67.95	68.13	64.84	68.43	64.54	69.03	65.31	68.38
K_2O	0.14	15.66	0.18	15.91	0.17	0.09	15.78	0.18	15.82	0.08	16.27	0.15
CaO	-	-	-	-	0.14	0.37	-	-	-	-	-	-
Fe_2O_3	0.13	0.20	-	-	0.10	0.12	0.15	0.02	-	0.49	0.36	0.51
BaO	-	-	-	-	-	-	-	-	-	-	-	-
Total	**99.55**	**99.32**	**100.10**	**99.80**	**99.73**	**100.48**	**100.29**	**100.09**	**99.29**	**100.55**	**100.74**	**100.42**

	MAS026 N = 5	MAS027 N = 6	MAS027 N = 5	MAS028 N = 3	MAS028 N = 3	MAS028 N = 6	MAS029 N = 6	MAS029 N = 5	MAS030 N = 6	MAS030 N = 6	MAS031 N = 6	MAS031 N = 6
Na_2O	0.40	11.54	0.40	11.33	11.63	0.39	11.90	0.21	11.73	0.58	11.69	0.26
Al_2O_3	18.48	19.80	18.69	20.12	19.86	18.79	20.40	18.86	20.38	18.51	19.55	18.68
SiO_2	64.86	68.20	64.42	68.24	68.79	64.71	66.85	63.70	67.07	64.94	68.54	64.83
K_2O	15.78	0.24	16.32	0.22	0.28	16.26	0.14	16.60	0.23	15.74	0.13	16.18
CaO	-	-	-	0.19	-	-	-	-	0.25	-	-	-
Fe_2O_3	0.52	0.38	0.50	0.17	0.17	0.42	0.15	0.43	0.13	0.58	0.61	0.36
BaO	-	-	-	-	-	-	-	-	-	-	-	-
Total	**100.03**	**100.15**	**100.33**	**100.27**	**100.73**	**100.56**	**99.43**	**99.80**	**99.79**	**100.34**	**100.52**	**100.30**

	MAS032 N = 4	MAS032 N = 6	MAS033 N = 4	MAS033 N = 3	MAS033 N = 6	MAS034 N = 6	MAS034 N = 5	MAS035 N = 6	MAS035 N = 6	MAS036 N = 6	MAS036 N = 3	MAS037 N = 6
Na_2O	11.98	0.33	11.96	11.96	0.52	11.26	1.40	10.85	0.95	11.67	0.62	10.84
Al_2O_3	19.63	18.30	19.76	19.59	18.43	20.49	18.63	20.20	18.62	19.83	18.67	20.68
SiO_2	68.38	64.64	68.44	67.84	64.76	67.56	66.01	67.85	64.62	68.14	64.50	67.04
K_2O	0.17	16.37	0.14	0.09	15.71	0.15	14.54	0.22	15.34	0.13	14.98	0.24
CaO	-	-	0.12	0.03	-	0.68	-	0.55	-	0.47	-	1.10
Fe_2O_3	0.29	0.44	0.25	0.25	0.23	0.14	0.10	0.08	0.20	0.13	0.16	0.10
BaO	-	-	-	-	-	-	-	-	-	-	-	-
Total	100.45	100.07	100.65	99.77	99.63	100.27	100.68	99.76	99.72	100.37	99.26	99.99

	MAS037 N = 7	MAS038 N = 6	MAS038 N = 6	MAS039 N = 6	MAS039 N = 6	MAS040 N = 5	MAS040 N = 6
Na_2O	0.28	11.86	0.57	11.74	0.37	12.17	0.55
Al_2O_3	18.82	20.14	18.87	19.92	18.71	20.41	19.01
SiO_2	64.73	67.21	63.91	68.43	65.25	66.81	63.73
K_2O	16.32	0.14	16.03	0.13	16.20	0.12	16.38
CaO	-	-	-	-	-	-	-
Fe_2O_3	0.15	0.14	0.20	0.09	0.07	0.06	0.17
BaO	-	-	-	-	-	-	-
Total	100.30	99.48	99.58	100.31	100.59	99.57	99.81

II.II Pyroxene (Na combined with Fe^{3+})

	MAS001 N = 4	MAS001 N = 4	MAS002 N = 3	MAS003 N = 2	MAS003 N = 2	MAS003 N = 1	MAS004 N = 8
Wt. %							
SiO_2	48.21	48.23	49.71	50.66	50.25	50.22	49.22
TiO_2	0.70	0.89	0.83	0.18	0.33	0.42	0.37
Al_2O_3	1.03	1.06	1.40	0.33	0.75	0.24	0.57
Fe_2O_3	1.19	1.19	1.39	7.78	6.85	12.26	7.50
FeO	25.31	23.78	18.87	17.95	29.02	16.16	21.60
MnO	0.96	0.79	0.71	0.79	1.10	0.78	0.83
MgO	2.28	3.30	6.67	2.93	0.88	1.25	1.20
CaO	20.64	20.96	20.70	16.76	7.45	14.24	16.51
Na_2O	0.46	0.46	0.54	3.02	2.66	4.76	2.91
Total	**100.78**	**100.66**	**100.82**	**100.40**	**99.29**	**100.33**	**100.71**
Structural formulae calculated on the basis of 4 cations							
Si	1.947	1.937	1.940	2.001	2.044	1.992	1.972
Al(IV)	0.049	0.050	0.060	0.000	0.000	0.008	0.027
Al(VI)	0.004	0.013	0.005	0.016	0.080	0.003	0.001
Ti	0.021	0.027	0.024	0.005	0.010	0.013	0.011
Fe^{3+}	0.032	0.023	0.041	0.231	0.210	0.366	0.225
Fe^{2+}	0.855	0.799	0.616	0.593	0.987	0.536	0.724
Mn	0.033	0.027	0.034	0.026	0.038	0.026	0.028
Mg	0.137	0.198	0.388	0.173	0.053	0.074	0.072
Ca	0.893	0.902	0.866	0.709	0.325	0.605	0.709
Na	0.036	0.036	0.041	0.231	0.210	0.366	0.226
Total	**4.007**	**4.012**	**4.015**	**3.985**	**3.957**	**3.989**	**3.995**
Mol % endmembers							
Ae	3.96	3.93	4.66	24.58	37.69	37.85	24.45
Hd	82.75	77.02	58.48	58.42	59.11	54.62	68.75
Di	13.29	19.05	36.86	17.00	3.20	7.53	6.80

Ae = aegirine, Hd = hedenbergite and Di = diopside.

	MAS004 N = 3	MAS004 N = 5	MAS006 N = 5	MAS006 N = 5	MAS007 N = 7	MAS009 N = 5	MAS010 N = 14
Wt. %							
SiO_2	49.17	50.19	48.43	51.70	50.01	49.90	48.44
TiO_2	1.36	-	1.32	0.34	0.07	0.16	1.67
Al_2O_3	2.77	0.14	1.72	0.53	0.37	0.32	1.82
Fe_2O_3	11.54	0.00	11.54	16.80	7.27	7.88	11.23
FeO	13.96	29.01	25.38	22.61	21.34	20.88	24.13
MnO	0.66	0.83	0.92	0.15	0.79	0.99	0.93
MgO	8.29	1.09	0.55	0.57	1.17	1.06	0.76
CaO	8.13	18.79	5.54	0.15	17.14	16.46	5.78
Na_2O	4.48	-	4.48	5.52	2.81	3.06	4.36
Total	**100.36**	**100.05**	**99.88**	**98.37**	**100.97**	**100.71**	**99.12**
Structural formulae calculated on the basis of 4 cations							
Si	1.887	2.044	1.954	2.064	1.996	1.996	1.946
Al(IV)	0.113	0.000	0.046	0.000	0.004	0.004	0.054
Al(VI)	0.012	0.051	0.036	0.089	0.014	0.011	0.032
Ti	0.039	-	0.040	0.010	0.002	0.005	0.050
Fe^{3+}	0.333	0.000	0.351	0.505	0.218	0.237	0.340
Fe^{2+}	0.448	0.988	0.857	0.755	0.712	0.698	0.811
Mn	0.022	0.029	0.031	0.005	0.027	0.034	0.032
Mg	0.474	0.066	0.033	0.034	0.070	0.063	0.046
Ca	0.334	0.820	0.240	0.006	0.733	0.706	0.249
Na	0.333	-	0.351	0.505	0.218	0.237	0.340
Total	**3.995**	**3.998**	**3.939**	**3.973**	**3.994**	**3.991**	**3.900**
Mol % endmembers							
Ae	54.11	0.00	61.81	92.92	22.99	25.22	60.50
Hd	22.31	93.72	36.77	6.78	70.15	68.57	37.48
Di	23.58	6.28	1.42	0.30	6.86	6.21	2.02

	MAS013 N = 5	MAS013 N = 3	MAS013 N = 7	MAS014 N = 4	MAS015 N = 4	MAS016 N = 6	MAS017 N = 6
Wt. %							
SiO_2	50.11	48.22	49.06	49.04	49.08	48.23	49.62
TiO_2	-	1.25	0.48	0.42	0.17	0.60	0.32
Al_2O_3	0.74	2.18	0.71	0.37	0.45	0.55	0.43
Fe_2O_3	4.66	10.82	2.22	3.56	6.47	2.06	3.74
FeO	31.74	24.57	23.97	25.57	22.45	26.33	23.79
MnO	1.52	0.88	0.86	0.79	0.77	0.96	0.94
MgO	0.77	1.21	2.60	0.84	0.38	1.00	1.53
CaO	8.44	6.05	19.63	18.89	17.55	19.63	18.84
Na_2O	1.81	4.20	0.86	1.38	2.51	0.80	1.45
Total	**99.79**	**99.38**	**100.39**	**100.86**	**99.83**	**100.16**	**100.66**

Structural formulae calculated on the basis of 4 cations

Si	2.047	1.945	1.974	1.985	1.993	1.971	1.995
Al(IV)	0.000	0.055	0.026	0.015	0.007	0.027	0.005
Al(VI)	0.083	0.049	0.008	0.002	0.015	0.002	0.015
Ti		0.038	0.015	0.013	0.005	0.018	0.010
Fe^{3+}	0.143	0.329	0.067	0.108	0.198	0.061	0.113
Fe^{2+}	1.085	0.829	0.807	0.865	0.763	0.900	0.800
Mn	0.053	0.030	0.029	0.027	0.027	0.033	0.032
Mg	0.047	0.073	0.156	0.051	0.023	0.061	0.092
Ca	0.370	0.262	0.846	0.819	0.764	0.860	0.811
Na	0.143	0.329	0.067	0.108	0.198	0.063	0.113
Total	**3.971**	**3.939**	**3.995**	**3.993**	**3.993**	**3.996**	**9.986**

Mol % endmembers

Ae	26.72	58.38	7.45	11.78	20.64	6.97	12.26
Hd	70.24	38.26	77.55	83.34	77.04	87.13	78.71
Di	3.04	3.36	15.00	4.88	2.32	5.90	9.03

	MAS022 N = 2	MAS022 N = 1	MAS023 N = 3	MAS024 N = 4	MAS025 N = 7	MAS027 N = 7	MAS029 N = 5
Wt. %							
SiO_2	50.25	49.97	49.73	48.51	48.93	49.27	48.57
TiO_2	-	0.36	0.31	0.19	0.46	0.28	0.66
Al_2O_3	1.25	0.77	0.85	0.73	0.44	0.35	0.71
Fe_2O_3	4.97	3.99	4.77	2.55	3.14	5.08	1.8
FeO	16.22	20.40	19.97	23.73	25.81	24.32	26.8
MnO	0.85	0.97	0.82	0.95	0.80	0.76	0.93
MgO	5.31	2.85	3.08	2.88	0.80	0.59	0.94
CaO	19.72	20.06	19.29	20.06	19.19	18.34	19.83
Na_2O	1.93	1.55	1.85	0.99	1.22	1.97	0.70
Total	**100.50**	**100.92**	**100.67**	**100.59**	**100.79**	**100.96**	**100.94**
Structural formulae calculated on the basis of 4 cations							
Si	1.964	1.979	1.973	1.955	1.983	1.988	1.970
Al(IV)	0.036	0.021	0.027	0.035	0.017	0.012	0.030
Al(VI)	0.022	0.015	0.012	0.010	0.004	0.004	0.004
Ti	-	0.011	0.009	0.006	0.014	0.009	0.020
Fe^{3+}	0.146	0.119	0.142	0.067	0.096	0.154	0.055
Fe^{2+}	0.53	0.676	0.663	0.800	0.785	0.821	0.909
Mn	0.028	0.033	0.028	0.032	0.028	0.026	0.032
Mg	0.309	0.168	0.182	0.173	0.048	0.036	0.057
Ca	0.826	0.851	0.820	0.866	0.833	0.793	0.862
Na	0.146	0.119	0.142	0.077	0.096	0.154	0.055
Total	**4.007**	**3.992**	**3.998**	**4.021**	**3.904**	**3.997**	**3.994**
Mol % endmembers							
Ae	15.39	12.40	15.07	8.25	10.42	16.38	6.10
Hd	53.42	70.13	66.61	75.43	84.89	80.15	88.37
Di	31.19	17.47	18.32	16.32	4.69	3.47	5.53

	MAS030 N = 6	MAS031 N = 4	MAS033 N = 4	MAS037 N = 5
Wt. %				
SiO_2	49.35	48.76	50.39	50.54
TiO_2	0.54	0.55	0.18	0.14
Al_2O_3	0.47	0.48	1.04	1.05
Fe_2O_3	4.51	3.32	16.41	11.49
FeO	23.80	25.73	9.62	13.13
MnO	0.79	0.81	1.83	1.80
MgO	0.73	0.70	2.10	2.46
CaO	18.98	19.08	12.01	15.06
Na_2O	1.75	1.29	6.37	4.46
Total	**100.92**	**100.72**	**99.95**	**100.13**

Structural formulae calculated on the basis of 4 cations

Si	1.984	1.978	1.974	1.985
Al(IV)	0.016	0.022	0.026	0.015
Al(VI)	0.007	0.001	0.022	0.034
Ti	0.016	0.017	0.005	0.004
Fe^{3+}	0.136	0.102	0.484	0.340
Fe^{2+}	0.804	0.873	0.315	0.431
Mn	0.027	0.028	0.061	0.060
Mg	0.044	0.042	0.153	0.144
Ca	0.818	0.829	0.504	0.634
Na	0.136	0.102	0.484	0.340
Total	**3.988**	**3.994**	**4.028**	**3.987**

Mol % endmembers

Ae	14.42	11.03	4.83	37.12
Hd	81.16	84.85	81.47	47.71
Di	4.42	4.12	13.70	15.74

II.III Amphibole [recalculation follows the methodology of Leake et al. (1997)]

	MAS002 N = 3	MAS004 N = 7	MAS006 N = 5	MAS007 N = 10	MAS009 N = 7	MAS009 N = 2	MAS009 N = 4
Wt. %							
SiO_2	45.81	44.40	47.99	47.11	48.54	47.20	50.05
TiO_2	0.41	0.71	1.16	1.62	1.29	1.65	0.16
Al_2O_3	3.24	8.09	1.69	3.36	1.51	2.19	0.90
Fe_2O_3	6.18	0.71	2.54	3.19	2.71	0.90	3.72
FeO	29.14	15.27	31.63	30.68	31.12	32.49	31.77
MnO	0.64	0.28	0.94	0.72	0.96	0.87	0.89
MgO	1.47	12.45	0.61	1.16	0.38	0.75	0.27
CaO	9.92	12.03	5.93	6.25	5.00	6.18	7.16
Na_2O	1.44	3.61	4.52	4.50	4.81	4.84	2.94
K_2O	0.74	0.37	1.10	1.13	1.04	1.12	0.42
Total	**98.99**	**97.92**	**98.11**	**99.72**	**97.36**	**98.19**	**98.28**
OH_C	1.88	2.00	1.87	1.88	1.86	1.86	1.89
Total	**100.89**	**99.91**	**99.98**	**100.60**	**99.22**	**100.05**	**100.17**
Structural formulae calculated on the basis of 23 oxygen							
Si	7.289	6.667	7.709	7.514	7.816	7.601	7.958
Ti	0.608	1.333	0.291	0.444	0.184	0.399	0.042
Al (iv)	-	0.099	0.029	-	0.102	0.017	0.127
Al (vi)	0.049	0.080	0.140	0.194	0.156	0.200	0.019
Fe^{3+}	0.740	0.080	0.307	0.382	0.329	0.109	0.445
Fe^{2+}	3.879	1.918	4.250	4.093	4.171	4.376	4.225
Mn	0.086	0.036	0.128	0.097	0.131	0.119	0.120
Mg	0.349	2.787	0.146	0.276	0.091	0.180	0.064
Ca	1.691	1.935	1.021	1.068	0.863	1.066	1.220
Na	0.444	1.051	1.408	1.392	1.502	1.511	0.906
K	0.150	0.071	0.225	0.230	0.214	0.23	0.085
OH	2.000	2.000	2.000	2.000	2.000	2.000	2.000
Total	**17.285**	**18.057**	**17.654**	**17.690**	**17.758**	**17.808**	**17.484**

	MAS009 N = 7	MAS012 N = 4	MAS012 N = 3	MAS013 N = 3	MAS017 N = 7	MAS019 N = 4	MAS020 N = 4
Wt. %							
SiO_2	48.95	46.24	47.97	50.15	47.45	50.15	39.32
TiO_2	0.36	1.80	0.25	0.07	1.79	-	1.20
Al_2O_3	0.71	2.19	0.88	0.77	2.22	0.97	9.72
Fe_2O_3	8.15	4.59	6.28	4.37	2.57	11.80	5.89
FeO	28.63	30.07	30.84	30.34	30.84	20.65	24.55
MnO	0.46	0.77	0.91	1.32	0.79	2.19	0.98
MgO	0.61	1.03	0.24	0.95	0.95	3.05	2.54
CaO	4.02	6.06	8.58	8.45	5.84	2.97	9.29
Na_2O	5.58	4.62	1.71	1.78	4.58	5.63	3.46
K_2O	0.34	1.09	0.46	0.37	1.12	1.09	1.62
Total	**97.81**	**98.46**	**98.12**	**98.57**	**98.15**	**98.50**	**98.57**
OH_C	1.88	1.87	1.86	1.90	1.87	1.93	1.87
Total	**99.68**	**100.33**	**99.98**	**100.48**	**100.03**	**100.44**	**100.44**

Structural formulae calculated on the basis of 23 oxygen

Si	7.815	7.425	7.714	7.920	7.594	7.776	6.291
Ti	0.134	0.414	0.030	0.080	0.215	-	0.144
Al (iv)	-	-	0.167	0.064	0.406	0.177	1.709
Al (vi)	0.043	0.217	-	0.008	0.013	-	0.123
Fe^{3+}	0.979	0.555	0.760	0.520	0.310	1.377	0.709
Fe^{2+}	3.822	4.037	4.147	4.008	4.128	2.678	3.285
Mn	0.062	0.105	0.124	0.177	0.107	0.288	0.133
Mg	0.145	0.247	0.058	0.224	0.227	0.705	0.606
Ca	0.688	1.043	1.478	1.430	1.001	0.493	1.592
Na	1.727	1.438	0.533	0.545	1.421	1.692	1.073
K	0.069	0.223	0.094	0.075	0.229	0.216	0.331
OH	2.000	2.000	2.000	2.000	2.000	2.000	2.000
Total	**17.484**	**17.704**	**17.106**	**17.049**	**17.651**	**17.401**	**17.996**

	MAS020 N = 4	MAS026 N = 8	MAS027 N = 5	MAS029 N = 5	MAS031 N = 4	MAS032 N = 4	MAS032 N = 3
Wt. %							
SiO_2	40.77	48.15	45.98	48.08	43.79	45.27	47.16
TiO_2	0.89	0.81	2.45	1.52	2.63	1.43	1.15
Al_2O_3	8.56	1.54	2.51	1.71	4.13	3.96	2.44
Fe_2O_3	8.59	1.24	2.04	2.69	0.20	2.92	4.49
FeO	21.53	32.25	31.99	31.75	32.96	30.65	29.70
MnO	1.20	1.03	0.81	0.72	0.54	1.31	0.87
MgO	3.22	0.28	0.48	0.39	0.58	0.19	1.02
CaO	7.24	5.31	5.98	4.92	7.65	5.69	5.56
Na_2O	4.60	4.86	4.65	5.00	4.01	5.05	4.73
K_2O	1.57	1.29	1.44	1.49	1.45	1.49	1.41
Total	**98.17**	**96.76**	**98.33**	**98.27**	**97.94**	**97.96**	**98.53**
OH_C	1.89	1.84	1.86	1.87	1.84	1.85	1.88
Total	**100.06**	**98.59**	**100.19**	**100.14**	**99.78**	**99.81**	**100.41**
Structural formulae calculated on the basis of 23 oxygen							
Si	6.478	7.848	7.428	7.716	7.145	7.335	7.534
Ti	0.106	0.099	0.298	0.183	0.323	0.174	0.138
Al (iv)	1.522	0.152	0.478	0.284	0.794	0.665	0.459
Al (vi)	0.081	0.143	-	0.039	-	0.091	-
Fe^{3+}	1.027	0.152	0.248	0.325	0.025	0.356	0.540
Fe^{2+}	2.861	4.395	4.322	4.261	4.497	4.153	3.967
Mn	0.162	0.142	0.111	0.098	0.075	0.180	0.118
Mg	0.763	0.068	0.116	0.093	0.141	0.046	0.243
Ca	1.233	0.927	1.035	0.846	1.337	0.988	0.952
Na	1.417	1.536	1.456	1.556	1.269	1.586	1.465
K	0.318	0.268	0.297	0.305	0.302	0.308	0.287
OH	2.000	2.000	2.000	2.000	2.000	2.000	2.000
Total	**17.968**	**17.731**	**17.788**	**17.707**	**17.908**	**17.882**	**17.704**

	MAS035 N = 3	MAS036 N = 11	MAS037 N = 3
Wt. %			
SiO$_2$	38.95	39.36	39.57
TiO$_2$	1.31	1.69	3.07
Al$_2$O$_3$	9.96	8.92	9.10
Fe$_2$O$_3$	4.50	4.18	1.61
FeO	27.07	27.45	26.20
MnO	1.09	1.09	0.72
MgO	1.18	1.45	3.05
CaO	9.86	9.76	10.32
Na$_2$O	2.85	3.01	2.49
K$_2$O	1.58	1.50	1.41
Total	**98.35**	**98.41**	**97.54**
OH$_C$	1.85	1.85	1.87
Total	**100.20**	**100.26**	**99.41**

Structural formulae calculated on the basis of 23 oxygen

	MAS035	MAS036	MAS037
Si	6.299	6.370	6.360
Ti	0.159	0.206	0.371
Al (iv)	1.701	1.630	1.640
Al (vi)	0.198	0.071	0.084
Fe^{3+}	0.547	0.509	0.195
Fe^{2+}	3.662	3.715	3.521
Mn	0.149	0.149	0.098
Mg	0.284	0.350	0.731
Ca	1.709	1.692	1.777
Na	0.894	0.944	0.776
K	0.326	0.310	0.289
OH	2.000	2.000	2.000
Total	**17.928**	**17.946**	**17.842**

II.IV Chlorite [Fe^{3+} recalculated using Droop method (1987)]

	MAS001 N = 4	MAS002 N = 4	MAS004 N = 3	MAS005 N = 4	MAS005 N = 3	MAS006 N = 3	MAS008 N = 7
Wt. %							
SiO_2	35.14	34.96	35.14	32.29	33.91	36.39	35.87
TiO_2	-	0.54	-	0.10	0.04	-	-
Al_2O_3	5.66	7.18	7.52	10.23	6.63	8.43	9.00
Fe_2O_3	3.15	3.77	5.34	2.89	2.38	4.09	6.68
FeO	36.38	36.15	35.73	34.53	38.22	34.38	33.20
MnO	1.31	1.84	0.82	0.51	1.75	0.44	0.25
MgO	3.68	3.02	2.82	6.64	3.18	1.32	1.01
CaO	2.05	0.83	0.85	0.94	1.65	1.97	1.66
Na_2O	0.65	0.53	0.26	0.23	0.83	1.89	0.50
K_2O	0.58	1.01	-	0.19	0.42	0.62	0.14
Total	**88.60**	**89.83**	**88.49**	**88.55**	**89.02**	**89.53**	**88.31**
OH_C	10.53	10.67	10.58	10.76	10.49	10.81	10.67
Total	**99.12**	**100.50**	**99.07**	**99.30**	**99.51**	**100.34**	**98.97**
Structural formulae calculated on the basis of 28 oxygen							
Si	7.868	7.697	7.821	7.120	7.632	7.840	7.871
Al (iv)	0.132	0.303	0.179	0.880	0.368	0.160	0.129
Al (vi)	1.388	1.599	1.830	1.809	1.420	2.045	2.257
Ti	-	0.089	-	0.017	0.007	-	-
Fe^{3+}	0.531	0.625	0.895	0.480	0.403	0.662	1.103
Fe^{2+}	6.812	6.655	6.651	6.367	7.195	6.195	6.093
Mn	0.248	0.343	0.155	0.095	0.334	0.080	0.046
Mg	1.228	0.991	0.936	2.183	1.067	0.424	0.330
Ca	0.492	0.196	0.203	0.222	0.398	0.455	0.390
Na	0.564	0.453	0.224	0.197	0.724	1.579	0.425
K	0.331	0.567	-	0.107	0.247	0.341	0.078
OH	16.000	16.000	16.000	16.000	16.000	16.000	16.000
Total	**35.594**	**35.518**	**34.893**	**35.476**	**35.794**	**35.782**	**34.723**

	MAS009 N = 5	MAS010 N = 4	MAS012 N= 4	MAS015 N = 6	MAS016 N = 5	MAS018 N = 4	MAS018 N = 1
Wt. %							
SiO_2	32.33	31.64	24.42	35.66	35.74	25.47	30.90
TiO_2	-	-	-	0.11	0.04	-	-
Al_2O_3	7.29	8.22	20.26	6.21	5.87	17.19	13.23
Fe_2O_3	1.92	3.28	0.73	4.72	4.96	-	1.26
FeO	43.46	45.44	38.37	36.30	39.74	40.59	24.03
MnO	-	-	1.29	0.20	0.98	1.33	0.86
MgO	2.80	-	4.04	2.72	2.54	4.75	16.51
CaO	0.08	0.73	0.17	2.90	0.35	0.04	0.43
Na_2O	0.79	-	0.17	0.38	0.08	0.21	-
K_2O	0.03	-	-	0.04	-	0.16	0.03
Total	**88.70**	**89.31**	**89.45**	**89.24**	**90.31**	**89.74**	**87.25**
OH_C	10.31	10.20	10.69	10.63	10.62	10.61	11.31
Total	**99.01**	**99.51**	**100.14**	**99.87**	**100.93**	**100.35**	**98.56**
Structural formulae calculated on the basis of 28 oxygen							
Si	7.426	7.364	5.461	7.907	7.948	5.741	6.528
Al (iv)	0.574	0.636	2.539	0.093	0.052	2.259	1.472
Al (vi)	1.425	1.643	2.820	1.559	1.511	2.322	1.834
Ti	-	-	-	0.018	0.007	-	-
Fe^{3+}	0.332	0.576	0.123	0.787	0.830	-	0.200
Fe^{2+}	8.350	8.846	7.177	6.733	7.392	7.671	4.245
Mn	-	-	0.244	0.038	0.185	0.254	0.154
Mg	0.959	-	1.347	0.899	0.842	1.596	5.199
Ca	0.020	0.182	0.041	0.689	0.083	0.010	0.097
Na	0.704	-	0.147	0.327	0.069	0.184	-
K	0.018	-	-	0.023	-	0.092	0.016
OH	16.000	16.000	16.000	16.000	16.000	16.000	16.000
Total	**35.806**	**35.244**	**35.900**	**35.072**	**34.919**	**36.128**	**35.746**

	MAS020 N = 5	MAS022 N = 7	MAS022 N = 5	MAS029 N = 4	MAS029 N = 4	MAS029 N = 3	MAS032 N = 5
Wt. %							
SiO_2	29.11	32.81	30.37	34.77	35.84	31.97	30.71
TiO_2	-	0.02	1.40	0.10	0.11	-	-
Al_2O_3	17.44	14.37	13.24	7.91	4.79	5.13	8.64
Fe_2O_3	3.19	4.10	2.25	3.00	3.85	0.66	-
FeO	32.77	27.29	33.69	34.91	37.77	47.53	43.02
MnO	1.00	0.25	0.40	1.04	0.68	0.91	0.75
MgO	5.84	9.48	5.90	4.29	4.09	2.68	4.82
CaO	0.16	0.76	0.32	1.55	0.60	0.27	0.45
Na_2O	0.20	0.09	-	1.31	0.72	0.48	0.59
K_2O	-	0.42	2.01	0.21	0.07	0.12	0.61
Total	**89.71**	**89.59**	**89.58**	**89.09**	**88.53**	**89.75**	**89.59**
OH_C	11.03	11.35	10.87	10.75	10.52	10.18	10.45
Total	**100.74**	**100.94**	**100.44**	**99.84**	**99.05**	**99.93**	**100.04**
Structural formulae calculated on the basis of 28 oxygen							
Si	6.261	6.837	6.592	7.606	8.025	7.482	6.997
Al (iv)	1.739	1.163	1.408	0.394	-	0.518	1.003
Al (vi)	2.731	2.416	2.036	1.686	1.287	0.907	1.335
Ti	-	0.003	0.229	0.016	0.019	-	-
Fe^{3+}	0.516	0.643	0.367	0.493	0.649	0.116	-
Fe^{2+}	5.895	4.755	6.115	6.387	7.073	9.303	8.197
Mn	0.182	0.044	0.074	0.193	0.129	0.180	0.145
Mg	1.873	2.945	1.909	1.399	1.365	0.935	1.637
Ca	0.037	0.170	0.074	0.363	0.144	0.068	0.110
Na	0.167	0.073	-	1.111	0.625	0.436	0.521
K	-	0.223	1.113	0.117	0.040	0.072	0.355
OH	16.000	16.000	16.000	16.000	16.000	16.000	16.000
Total	**35.401**	**35.273**	**35.916**	**35.767**	**35.355**	**36.016**	**36.299**

	MAS035 N = 5	MAS036 N = 5	MAS037 N = 4	MAS038 N = 7	MAS039 N = 4	MAS040 N = 5
Wt. %						
SiO_2	36.44	29.32	23.80	33.03	25.67	30.19
TiO_2	1.12	-	0.16	-	-	-
Al_2O_3	9.29	13.02	19.28	12.26	18.56	11.47
Fe_2O_3	3.01	1.34	0.31	2.81	0.59	-
FeO	23.50	36.69	42.42	28.15	35.44	30.38
MnO	0.87	0.89	0.49	0.38	0.76	0.33
MgO	1.19	7.44	2.33	11.80	7.84	10.99
CaO	8.67	0.48	0.13	0.82	-	5.68
Na_2O	2.95	0.06	0.23	0.22	-	0.25
K_2O	1.44	-	-	0.12	-	0.14
Total	**88.48**	**89.26**	**89.15**	**89.59**	**88.86**	**89.43**
OH_C	11.01	10.78	10.44	11.35	10.84	11.06
Total	**99.49**	**100.04**	**99.59**	**100.94**	**99.70**	**100.49**
Structural formulae calculated on the basis of 28 oxygen						
Si	7.648	6.496	5.452	6.911	5.669	6.514
Al (iv)	0.352	1.504	2.548	1.089	2.331	1.486
Al (vi)	2.035	1.919	2.672	1.965	2.507	1.446
Ti	0.177	-	0.028	-	-	-
Fe^{3+}	0.476	0.223	0.054	0.443	0.098	-
Fe^{2+}	4.125	6.798	8.127	4.926	6.545	5.543
Mn	0.155	0.167	0.095	0.067	0.142	0.060
Mg	0.372	2.457	0.796	3.680	2.581	3.535
Ca	1.950	0.114	0.032	0.184	-	1.313
Na	2.401	0.052	0.204	0.179	-	0.209
K	0.771	-	-	0.064	-	0.077
OH	16.000	16.000	16.000	16.000	16.000	16.000
Total	**36.462**	**35.730**	**36.007**	**35.508**	**35.875**	**36.184**

II.V Olivine

	MAS001 N = 4	MAS014 N = 5	MAS016 N = 3	MAS025 N = 4	MAS026 N = 4	MAS028 N = 5
Wt. %						
SiO_2	30.15	29.94	29.50	29.76	29.68	29.69
FeO	66.19	67.24	66.26	67.13	66.49	66.73
MnO	2.40	3.08	3.01	2.61	2.54	2.63
MgO	1.19	0.22	0.61	0.36	0.47	0.46
CaO	0.39	0.29	0.40	0.39	0.36	0.47
Total	**100.32**	**100.77**	**99.78**	**100.25**	**99.54**	**99.98**
Structural formulae calculated on the basis of 4 oxygen						
Si	1.006	1.003	0.997	1.002	1.004	1.001
Fe^{2+}	1.847	1.884	1.874	1.890	1.882	1.882
Mn	0.068	0.087	0.086	0.074	0.073	0.075
Mg	0.059	0.011	0.031	0.018	0.024	0.023
Ca	0.014	0.010	0.014	0.014	0.013	0.017
Total	**2.994**	**2.997**	**3.003**	**2.998**	**2.996**	**2.999**

II.VI Biotite

	MAS001 N = 4	MAS001 N = 3	MAS002 N = 4	MAS003 N = 5	MAS005 N = 5	MAS012 N = 6	MAS015 N = 4
Wt. %							
SiO_2	35.46	34.54	33.03	39.11	37.32	35.81	35.03
TiO_2	0.72	1.44	4.63	0.06	0.16	2.39	3.25
Al_2O_3	10.25	10.52	11.95	6.21	7.57	8.04	8.32
FeO	39.23	39.76	35.94	37.98	41.28	39.92	39.58
MnO	0.57	0.49	0.22	1.61	0.65	0.54	0.28
MgO	0.99	0.20	1.35	1.29	0.31	0.26	0.35
CaO	0.01	0.19	0.09	0.32	-	-	-
Na_2O	0.67	0.31	0.42	0.61	0.55	0.58	0.52
K_2O	8.35	8.63	8.59	8.11	8.48	8.43	8.50
Cl	-	-	0.17	-	0.58	1.03	0.45
O = Cl	-	-	0.04	-	0.13	0.23	0.10
Total	**96.25**	**96.08**	**96.35**	**95.30**	**96.77**	**96.77**	**96.18**
H_2O_C	3.57	3.54	3.56	3.56	3.39	3.27	3.41
Total	**99.82**	**99.62**	**99.92**	**98.86**	**100.16**	**100.04**	**99.59**
Structural formulae calculated on the basis of 22 oxygen							
Si	5.961	5.863	5.489	6.596	6.328	6.079	5.954
Al (iv)	2.031	2.101	2.341	1.234	1.513	1.609	1.667
Al (vi)	-	-	-	-	-	-	-
Ti	0.091	0.184	0.579	0.008	0.020	0.305	0.415
Fe^{2+}	5.515	5.635	4.995	5.357	5.854	5.667	5.626
Mn	0.081	0.070	0.031	0.230	0.093	0.078	0.040
Mg	0.248	0.051	0.334	0.324	0.078	0.066	0.089
Ca	0.002	0.035	0.016	0.058	-	-	-
Na	0.218	0.102	0.135	0.199	0.181	0.191	0.171
K	1.790	1.865	1.821	1.745	1.834	1.825	1.843
Cl	-	-	0.048	-	0.167	0.296	0.130
OH	4.000	4.000	3.952	4.000	3.833	3.704	3.870
Total	**19.937**	**19.896**	**19.740**	**19.751**	**19.902**	**19.820**	**19.805**

	MAS015 N = 4	MAS023 N = 4	MAS025 N = 4	MAS026 N = 3	MAS027 N = 4	MAS028 N = 5	MAS030 N = 7
Wt. %							
SiO_2	37.35	35.67	35.81	36.47	36.31	35.60	33.95
TiO_2	0.05	4.04	-	0.38	-	-	3.68
Al_2O_3	7.54	10.35	7.45	6.43	6.45	8.11	9.67
FeO	41.24	30.99	42.55	43.31	43.43	42.07	39.90
MnO	0.96	0.49	0.69	0.19	0.88	0.77	0.26
MgO	0.27	5.34	0.42	0.76	0.40	0.36	0.25
CaO	0.15	-	-	-	-	-	-
Na_2O	0.88	0.22	0.59	0.32	0.57	0.42	0.47
K_2O	7.78	9.39	8.24	8.70	8.21	8.42	8.54
Cl	0.10	0.08	0.45	0.44	0.87	0.59	-
O = Cl	0.02	0.02	0.10	0.10	0.20	0.13	-
Total	**96.30**	**96.55**	**96.10**	**96.90**	**96.92**	**96.21**	**96.72**
H_2O_C	3.51	3.69	3.36	3.38	3.25	3.33	3.55
Total	**99.81**	**100.24**	**99.46**	**100.28**	**100.18**	**99.54**	**100.27**

Structural formulae calculated on the basis of 22 oxygen

	MAS015	MAS023	MAS025	MAS026	MAS027	MAS028	MAS030
Si	6.331	5.761	6.183	6.253	6.266	6.134	5.728
Al (iv)	1.506	1.970	1.516	1.300	1.312	1.647	1.923
Al (vi)	-	-	-	-	-	-	-
Ti	0.006	0.491	-	0.049	-	-	0.467
Fe^{2+}	5.846	4.186	6.144	6.213	6.268	6.062	5.630
Mn	0.138	0.067	0.101	0.028	0.129	0.112	0.037
Mg	0.068	1.286	0.108	0.194	0.103	0.092	0.063
Ca	0.027	-	-	-	-	-	-
Na	0.289	0.069	0.198	0.106	0.191	0.140	0.154
K	1.682	1.934	1.815	1.904	1.807	1.850	1.838
Cl	0.029	0.022	0.132	0.128	0.255	0.172	-
OH	3.971	3.978	3.868	3.872	3.745	3.828	4.000
Total	**19.895**	**19.765**	**20.065**	**20.050**	**20.077**	**20.038**	**19.839**

	MAS031 N = 4

Wt. %

SiO_2	34.08
TiO_2	0.63
Al_2O_3	8.45
FeO	43.33
MnO	0.40
MgO	0.49
CaO	-
Na_2O	0.79
K_2O	7.89
Cl	0.35
O = Cl	0.08
Total	**96.33**
H_2O_C	3.38
Total	**99.71**

Structural formulae calculated on the basis of 22 oxygen

Si	5.897
Al (iv)	1.723
Al (vi)	-
Ti	0.082
Fe^{2+}	6.270
Mn	0.059
Mg	0.126
Ca	-
Na	0.265
K	1.741
Cl	0.103
OH	3.897
Total	**20.163**

II.VII Muscovite

	MAS019 N = 4	MAS021 N = 3	MAS033 N = 4	MAS033 N = 1	MAS039 N = 3	MAS039 N = 2	MAS040 N = 3	MAS040 N = 3
Wt. %								
SiO_2	47.41	45.42	44.58	43.29	44.11	43.85	45.78	45.24
TiO_2	0.39	-	0.18	-	0.04	0.07	0.24	0.16
Al_2O_3	33.68	37.84	35.78	37.31	38.47	39.07	36.55	36.58
FeO	3.73	0.88	3.51	2.54	1.16	0.44	1.31	1.82
MgO	-	-	0.52	0.33	-	-	-	-
Na_2O	0.10	-	0.25	0.17	0.17	0.27	0.19	0.16
K_2O	11.11	11.59	10.99	11.25	10.85	11.22	11.38	10.89
H_2O	4.50	4.52	4.46	4.43	4.48	4.54	4.50	4.47
Total	**100.92**	**100.25**	**100.27**	**99.32**	**99.28**	**99.46**	**99.95**	**99.32**
Structural formulae calculated on the basis of 12 oxygen								
Si	3.156	3.012	2.997	2.930	2.952	2.960	3.051	3.034
Al (iv)	0.844	0.988	1.003	1.070	1.048	1.040	0.949	0.966
Al (vi)	1.799	1.970	1.831	1.907	1.987	2.000	1.921	1.926
Ti	0.020	-	0.009	-	0.002	0.003	0.012	0.008
Fe^{3+}	-	-	-	-	-	-	-	-
Fe^{2+}	0.208	0.049	0.197	0.144	0.065	0.024	0.073	0.102
Mg	-	-	0.052	0.033	-	-	-	-
Na	0.013	-	0.033	0.022	0.022	0.035	0.025	0.021
K	0.944	0.981	0.942	0.972	0.926	0.945	0.967	0.932
OH	1.998	2.000	2.000	2.000	2.000	1.999	2.000	2.000
Total	**8.980**	**8.999**	**9.064**	**9.078**	**9.003**	**9.006**	**8.998**	**8.988**

APPENDIX III
COMPOSITIONS OF ACCESSORY MINERALS

Minerals are listed alphabetically. Sample numbers for each unit are:

Border Gabbro pegmatites:	MAS001-MAS013
Railway pegmatites:	MAS014-MAS017; MAS023-MAS028
Upper Marathon Shore pegmatites	MAS018-MAS022
Black pegmatites	MAS029-MAS032
Center Three pegmatites	MAS033-MAS040

III.I Allanite [Fe^{3+} recalculated using method 10 of Ercit (2002)]

	MAS001 N = 2	MAS001 N = 1	MAS001 N = 1	MAS002 N = 5	MAS018 N = 4	MAS018 N = 1	MAS023 N = 5
Wt. %							
SiO_2	30.83	30.31	30.09	30.89	32.12	34.89	30.84
TiO_2	3.09	2.63	3.02	1.46	1.14	2.49	-
Al_2O_3	9.59	9.99	9.67	11.61	16.02	19.15	8.39
Y_2O_3	0.23	-	-	-	-	-	-
La_2O_3	8.31	8.23	8.48	3.90	7.37	2.86	7.15
Ce_2O_3	12.27	11.95	13.50	9.10	12.17	5.91	12.94
Pr_2O_3	1.09	1.04	1.16	1.26	0.95	0.24	1.27
Nd_2O_3	3.01	3.84	2.85	5.57	2.40	2.17	4.47
Sm_2O_3	0.35	0.18	0.33	1.24	0.29	0.02	0.56
Fe_2O_3	-	-	-	-	-	-	15.69
FeO	18.72	18.68	19.25	20.27	12.09	12.09	6.57
MgO	-	-	-	-	-	-	-
CaO	9.17	9.21	9.01	10.75	11.69	16.18	9.07
MnO	0.29	0.19	0.18	0.52	0.60	0.51	0.26
H_2O_C	3.07	3.04	3.05	3.12	3.25	3.53	3.10
Total	**100.02**	**99.29**	**100.59**	**99.69**	**100.09**	**100.04**	**100.31**
Structural formulae calculated on the basis of 13 oxygens							
Si	3.011	2.989	2.956	2.969	2.962	2.962	2.983
Ti	0.229	0.195	0.223	0.106	0.079	0.159	-
Al	1.104	1.161	1.120	1.315	1.741	1.916	0.956
Y	0.012	-	-	-	-	-	-
La	0.299	0.299	0.307	0.138	0.251	0.090	0.255
Ce	0.439	0.431	0.486	0.320	0.411	0.184	0.458
Pr	0.039	0.037	0.042	0.044	0.032	0.007	0.045
Nd	0.104	0.134	0.099	0.190	0.078	0.065	0.153
Sm	0.012	0.006	0.011	0.041	0.009	0.001	0.019
Fe^{3+}	-	-	-	-	-	-	1.142
Fe^{2+}	1.529	1.540	1.582	1.629	0.932	0.858	0.532
Mg	-	-	-	-	-	-	-
Ca	0.959	0.973	0.948	1.107	1.155	1.472	0.940
Mn	0.024	0.016	0.015	0.042	0.047	0.037	0.021
OH	1.000	1.000	0.999	1.000	1.000	0.999	1.000
Total	**8.759**	**8.782**	**8.788**	**8.901**	**8.698**	**8.749**	**8.503**

	MAS024 N = 3	MAS024 N = 1	MAS024 N = 1	MAS025 N = 4	MAS028 N = 2	MAS028 N = 2	MAS038 N = 2
Wt. %							
SiO_2	31.08	31.25	30.89	29.62	29.55	29.54	32.69
TiO_2	0.89	0.14	0.32	-	0.36	-	-
Al_2O_3	11.86	12.96	12.38	7.74	6.60	6.37	12.45
Y_2O_3	-	-	-	-	0.54	0.32	-
La_2O_3	7.73	7.65	8.27	6.07	7.41	7.59	7.11
Ce_2O_3	12.73	13.34	12.45	12.30	11.66	12.83	11.93
Pr_2O_3	0.71	1.15	0.98	1.53	1.33	1.15	1.30
Nd_2O_3	1.55	2.23	2.14	3.55	4.26	3.98	1.65
Sm_2O_3	0.32	0.44	0.12	0.52	0.49	0.33	0.14
Fe_2O_3	-	-	0.28	20.34	20.65	22.24	-
FeO	17.47	16.47	16.22	5.36	5.86	4.36	17.60
MgO	0.92	-	-	-	-	-	-
CaO	10.30	10.93	10.82	9.15	8.94	8.84	11.14
MnO	0.51	0.41	0.59	-	-	0.35	-
H_2O_C	3.11	3.12	3.08	3.08	3.08	3.08	3.15
Total	**99.18**	**100.09**	**98.54**	**99.26**	**100.73**	**100.98**	**99.16**

Structural formulae calculated on the basis of 13 oxygens

Si	2.994	2.999	3.007	2.883	2.877	2.876	3.109
Ti	0.064	0.010	0.023	-	0.026	-	-
Al	1.347	1.466	1.420	0.888	0.757	0.731	1.395
Y	-	-	-	-	0.028	0.017	-
La	0.275	0.271	0.297	0.218	0.266	0.273	0.249
Ce	0.449	0.469	0.444	0.438	0.416	0.457	0.415
Pr	0.025	0.040	0.035	0.054	0.047	0.041	0.045
Nd	0.053	0.076	0.074	0.122	0.147	0.137	0.056
Sm	0.011	0.015	0.004	0.017	0.016	0.011	0.005
Fe^{3+}	-	-	0.021	1.490	1.513	1.629	-
Fe^{2+}	1.408	1.322	1.320	0.436	0.477	0.355	1.400
Mg	0.132	-	-	-	-	-	-
Ca	1.063	1.124	1.129	0.954	0.932	0.922	1.135
Mn	0.042	0.033	0.049	-	-	0.029	-
OH	0.999	0.999	1.000	1.000	1.000	1.000	0.999
Total	**8.862**	**8.823**	**8.822**	**8.502**	**8.502**	**8.477**	**8.808**

III.II Apatite-britholite (the halogen site is assumed to be occupied by fluorine)

	MAS001 N = 2	MAS001 N = 1	MAS002 N = 1	MAS002 N = 3	MAS002 N = 4	MAS004 N = 2	MAS004 N = 2
Wt. %							
P_2O_5	29.55	27.03	3.45	3.29	4.29	40.03	37.98
SiO_2	7.08	8.88	21.2	20.32	20.50	1.37	3.11
ThO_2	-	-	-	1.82	2.55	-	-
UO_2	-	-	-	0.30	0.62	-	-
Y_2O_3	-	-	2.69	2.99	2.93	-	-
La_2O_3	4.22	5.99	15.01	16.15	14.97	0.48	0.68
Ce_2O_3	8.50	11.06	26.39	26.39	24.89	1.59	3.21
Pr_2O_3	0.50	1.17	1.60	1.60	0.94	0.23	0.42
Nd_2O_3	3.44	3.49	7.96	7.96	7.21	1.79	2.02
Sm_2O_3	0.55	0.28	0.83	1.11	0.42	0.11	0.46
CaO	42.18	38.77	16.09	15.57	16.50	52.88	49.67
FeO	0.58	0.22	0.23	0.47	0.44	-	-
SrO	0.36	0.36	0.40	0.20	0.39	-	-
Na_2O	0.03	-	-	-	-	0.21	0.22
Total	**96.99**	**97.25**	**95.85**	**98.17**	**96.65**	**98.69**	**97.77**
F_C	3.35	3.27	2.51	2.47	2.50	3.72	3.65
O=F	1.41	1.38	1.06	1.04	1.05	1.57	1.54
Total	**98.93**	**99.14**	**97.30**	**99.60**	**98.10**	**100.84**	**99.88**

Structural formulae calculated on the basis of 13 anions (O,F)

P	2.362	2.212	0.368	0.357	0.459	2.884	2.787
Si	0.668	0.858	2.670	2.601	2.591	0.117	0.270
Th	-	-	0.051	0.053	0.073	-	-
U	-	-	0.005	0.009	0.017	-	-
Y	-	-	0.180	0.204	0.197	-	-
La	0.147	0.214	0.697	0.762	0.698	0.015	0.022
Ce	0.294	0.391	1.217	1.237	1.152	0.050	0.102
Pr	0.017	0.041	0.073	0.075	0.043	0.007	0.013
Nd	0.116	0.120	0.358	0.364	0.326	0.054	0.063
Sm	0.018	0.009	0.036	0.049	0.018	0.003	0.014
Ca	4.266	4.015	2.171	2.135	2.235	4.822	4.612
Fe	0.046	0.018	0.024	0.050	0.047	-	-
Sr	0.020	0.020	0.029	0.015	0.029	-	-
Na	0.006	-	-	-	-	0.035	0.038
F	1.000	1.000	1.000	1.000	0.999	1.001	1.000
Total	**8.984**	**8.923**	**8.921**	**8.942**	**8.903**	**9.003**	**8.949**

	MAS006 N = 5	MAS006 N = 3	MAS007 N = 5	MAS009 N = 5	MAS012 N = 4	MAS012 N = 3	MAS014 N = 2
Wt. %							
P_2O_5	35.36	41.23	30.07	32.74	40.63	35.20	38.92
SiO_2	3.72	0.51	6.79	5.29	0.98	3.72	1.93
ThO_2	-	-	-	-	-	-	-
UO_2	-	-	-	-	-	-	-
Y_2O_3	-	-	-	-	-	-	-
La_2O_3	2.06	0.58	3.42	3.08	0.83	2.69	1.26
Ce_2O_3	5.06	1.11	8.01	6.89	1.53	5.35	2.53
Pr_2O_3	0.45	0.13	2.16	0.64	0.05	0.44	0.26
Nd_2O_3	2.42	0.71	5.98	3.41	0.66	2.43	1.09
Sm_2O_3	0.33	-	1.06	0.42	0.07	0.30	0.19
CaO	47.57	54.53	39.84	44.82	52.77	47.13	51.28
FeO	-	-	0.31	0.39	0.23	0.39	0.19
SrO	-	-	-	-	-	-	-
Na_2O	-	-	0.34	-	0.25	0.25	-
Total	**96.97**	**98.80**	**97.98**	**97.68**	**98.00**	**97.90**	**97.65**
F_C	3.51	3.75	3.34	3.44	3.72	3.52	3.65
O=F	1.48	1.58	1.41	1.45	1.57	1.48	1.54
Total	**99.00**	**100.97**	**99.91**	**99.67**	**100.15**	**99.94**	**99.76**

Structural formulae calculated on the basis of 13 anions (O,F)

	MAS006 N = 5	MAS006 N = 3	MAS007 N = 5	MAS009 N = 5	MAS012 N = 4	MAS012 N = 3	MAS014 N = 2
P	2.693	2.946	2.410	2.546	2.926	2.675	2.850
Si	0.335	0.043	0.643	0.486	0.083	0.334	0.167
Th	-	-	-	-	-	-	-
U	-	-	-	-	-	-	-
Y	-	-	-	-	-	-	-
La	0.068	0.018	0.119	0.104	0.026	0.089	0.040
Ce	0.167	0.034	0.278	0.232	0.048	0.176	0.080
Pr	0.015	0.004	0.074	0.021	0.002	0.014	0.008
Nd	0.078	0.021	0.202	0.112	0.020	0.078	0.034
Sm	0.010	-	0.035	0.013	0.002	0.009	0.006
Ca	4.585	4.931	4.040	4.411	4.809	4.533	4.753
Fe	-	-	0.025	0.030	0.016	0.029	0.014
Sr	-	-	-	-	-	-	-
Na	-	-	0.063	-	0.042	0.044	-
F	0.999	1.001	1.000	0.999	1.001	0.999	0.999
Total	**8.954**	**8.999**	**8.910**	**8.954**	**8.992**	**8.988**	**8.965**

	MAS014 N = 2	MAS014 N = 2	MAS014 N = 2	MAS015 N = 3	MAS015 N = 2	MAS015 N = 2	MAS016 N = 2
Wt. %							
P_2O_5	32.89	7.24	9.08	40.85	35.77	25.31	40.01
SiO_2	4.81	18.22	17.10	1.06	3.81	9.33	0.95
ThO_2	-	1.08	0.49	-	-	-	-
UO_2	-	-	-	-	-	-	-
Y_2O_3	-	-	-	-	-	-	-
La_2O_3	4.20	14.26	12.41	0.78	2.22	6.64	0.88
Ce_2O_3	7.96	24.33	23.56	1.33	4.77	12.54	2.09
Pr_2O_3	1.52	2.09	2.41	0.04	0.35	1.64	0.24
Nd_2O_3	3.34	8.34	8.50	0.77	1.94	5.23	0.86
Sm_2O_3	0.89	0.87	1.08	0.16	0.49	1.03	0.19
CaO	42.16	17.90	19.62	51.96	46.93	35.64	51.44
FeO	0.09	0.48	0.78	0.20	0.45	0.61	0.17
SrO	-	-	-	-	-	-	-
Na_2O	-	-	-	0.29	0.20	0.31	-
Total	**97.86**	**94.81**	**95.03**	**97.44**	**96.93**	**98.28**	**96.83**
F_C	3.40	2.52	2.58	3.71	3.53	3.19	3.65
O=F	1.43	1.06	1.09	1.56	1.49	1.34	1.54
Total	**99.83**	**96.27**	**96.52**	**99.59**	**98.97**	**100.13**	**98.94**

Structural formulae calculated on the basis of 13 anions (O,F)

P	2.588	0.771	0.943	2.948	2.709	2.122	2.932
Si	0.447	2.291	2.098	0.090	0.341	0.924	0.082
Th	-	0.031	0.014	-	-	-	-
U	-	-	-	-	-	-	-
Y	-	-	-	-	-	-	-
La	0.144	0.661	0.561	0.025	0.073	0.242	0.028
Ce	0.271	1.120	1.058	0.042	0.156	0.455	0.066
Pr	0.051	0.096	0.108	0.001	0.011	0.059	0.008
Nd	0.111	0.374	0.372	0.023	0.062	0.185	0.027
Sm	0.029	0.038	0.046	0.005	0.015	0.035	0.006
Ca	4.199	2.411	2.579	4.746	4.497	3.781	4.771
Fe	0.007	0.050	0.080	0.014	0.034	0.051	0.012
Sr	-	-	-	-	-	-	-
Na	-	-	-	0.049	0.035	0.060	-
F	0.999	1.002	1.001	1.000	0.999	0.999	0.999
Total	**8.860**	**8.868**	**8.888**	**8.957**	**8.947**	**8.928**	**8.945**

	MAS016 N = 1	MAS016 N = 2	MAS017 N = 3	MAS017 N = 2	MAS017 N = 1	MAS017 N = 1	MAS018 N = 2
Wt. %							
P_2O_5	37.74	34.75	35.37	35.59	40.33	32.20	41.49
SiO_2	2.19	4.09	3.44	3.30	1.11	5.23	-
ThO_2	-	-	-	-	-	0.29	-
UO_2	-	-	-	-	-	-	-
Y_2O_3	-	-	-	-	-	-	-
La_2O_3	1.74	2.85	2.27	2.39	0.64	3.33	0.13
Ce_2O_3	3.64	5.94	4.97	5.22	0.89	7.04	0.70
Pr_2O_3	0.57	0.98	1.02	0.67	0.29	1.07	-
Nd_2O_3	1.62	2.68	3.86	2.63	0.68	3.59	0.43
Sm_2O_3	0.32	0.36	0.64	0.29	0.12	0.86	-
CaO	48.58	44.72	46.06	46.52	52.37	42.44	53.89
FeO	0.55	0.64	0.26	0.17	0.25	0.31	-
SrO	-	-	-	-	-	-	-
Na_2O	-	-	-	-	-	-	0.48
Total	**96.95**	**97.01**	**97.89**	**96.78**	**96.68**	**96.36**	**97.12**
F_C	3.57	3.48	3.50	3.50	3.69	3.38	3.71
O=F	1.50	1.47	1.47	1.47	1.55	1.42	1.56
Total	**99.02**	**99.02**	**99.92**	**98.81**	**98.82**	**98.32**	**99.27**

Structural formulae calculated on the basis of 13 anions (O,F)

P	2.826	2.676	2.702	2.720	2.927	2.554	2.993
Si	0.194	0.372	0.310	0.298	0.095	0.490	-
Th	-	-	-	-	-	0.006	-
U	-	-	-	-	-	-	-
Y	-	-	-	-	-	-	-
La	0.057	0.096	0.076	0.080	0.020	0.115	0.004
Ce	0.118	0.198	0.164	0.173	0.028	0.241	0.022
Pr	0.018	0.032	0.034	0.022	0.009	0.037	-
Nd	0.051	0.087	0.124	0.085	0.021	0.120	0.013
Sm	0.010	0.011	0.020	0.009	0.004	0.028	-
Ca	4.604	4.358	4.453	4.500	4.810	4.260	4.920
Fe	0.041	0.049	0.020	0.013	0.018	0.024	-
Sr	-	-	-	-	-	-	-
Na	-	-	-	-	-	-	0.081
F	0.999	1.001	0.999	0.999	1.000	1.001	1.000
Total	**8.932**	**8.895**	**8.919**	**8.924**	**8.960**	**8.894**	**9.032**

	MAS018 N = 2	MAS022 N = 1	MAS022 N = 2	MAS022 N = 1	MAS023 N = 4	MAS023 N = 4	MAS024 N = 4
Wt. %							
P_2O_5	40.97	38.46	40.14	42.09	35.26	30.23	33.45
SiO_2	-	2.29	1.38	0.36	3.92	6.34	4.90
ThO_2	-	-	-	-	-	-	-
UO_2	-	-	-	-	-	-	-
Y_2O_3	-	-	-	-	-	-	-
La_2O_3	0.58	1.79	1.16	-	2.23	4.29	2.86
Ce_2O_3	1.57	3.19	2.06	-	4.87	8.01	5.81
Pr_2O_3	0.16	0.48	0.38	-	0.38	1.24	0.58
Nd_2O_3	0.88	1.11	1.26	-	2.09	3.59	2.50
Sm_2O_3	0.13	0.14	0.18	-	0.20	0.38	0.42
CaO	52.12	49.42	50.12	54.15	47.93	43.89	46.24
FeO	-	-	-	-	-	-	0.17
SrO	-	-	-	-	-	-	-
Na_2O	0.97	0.31	0.54	0.09	-	-	-
Total	**97.38**	**97.19**	**97.22**	**96.69**	**96.88**	**97.97**	**96.93**
F_C	3.68	3.62	3.67	3.76	3.53	3.38	3.47
O=F	1.55	1.52	1.55	1.58	1.49	1.42	1.46
Total	**99.51**	**99.29**	**99.34**	**98.87**	**98.92**	**99.93**	**98.94**

Structural formulae calculated on the basis of 13 anions (O,F)

P	2.983	2.841	2.927	2.998	2.675	2.396	2.577
Si	-	0.200	0.119	0.030	0.351	0.594	0.446
Th	-	-	-	-	-	-	-
U	-	-	-	-	-	-	-
Y	-	-	-	-	-	-	-
La	0.018	0.058	0.037	-	0.074	0.148	0.096
Ce	0.049	0.102	0.065	-	0.160	0.275	0.194
Pr	0.005	0.015	0.012	-	0.012	0.042	0.019
Nd	0.027	0.035	0.039	-	0.067	0.120	0.081
Sm	0.004	0.004	0.005	-	0.006	0.012	0.013
Ca	4.803	4.530	4.625	4.881	4.603	4.403	4.509
Fe	-	-	-	-	-	-	0.013
Sr	-	-	-	-	-	-	-
Na	0.164	0.053	0.092	0.015	-	-	-
F	1.001	0.999	1.000	1.000	1.001	1.001	0.999
Total	**9.056**	**8.948**	**8.945**	**8.962**	**8.967**	**9.006**	**8.973**

	MAS024 N = 2	MAS025 N = 4	MAS025 N = 2	MAS025 N = 2	MAS026 N = 3	MAS026 N = 2	MAS026 N = 2
Wt. %							
P_2O_5	38.67	38.91	35.80	34.93	39.51	35.55	24.89
SiO_2	1.87	2.21	3.47	5.20	1.83	3.97	9.43
ThO_2	-	-	-	-	-	-	-
UO_2	-	-	-	-	-	-	-
Y_2O_3	-	-	-	-	-	-	-
La_2O_3	1.21	1.02	1.79	2.86	0.93	1.94	5.84
Ce_2O_3	2.09	2.49	4.59	6.67	2.17	4.90	12.68
Pr_2O_3	0.09	0.23	0.62	0.94	0.20	0.62	1.34
Nd_2O_3	0.70	1.16	2.02	2.74	0.97	2.23	5.69
Sm_2O_3	0.15	-	0.45	0.45	-	-	0.78
CaO	51.79	51.17	48.33	44.36	53.17	48.51	37.17
FeO	0.11	-	-	-	-	-	-
SrO	-	-	-	-	-	-	-
Na_2O	-	-	-	-	-	-	-
Total	**96.68**	**97.19**	**97.07**	**98.15**	**98.78**	**97.72**	**97.82**
F_C	3.64	3.65	3.53	3.52	3.71	2.66	3.18
O=F	1.53	1.54	1.49	1.48	1.56	1.49	1.34
Total	**98.79**	**99.30**	**99.11**	**100.19**	**100.93**	**98.89**	**99.66**

Structural formulae calculated on the basis of 13 anions (O,F)

	MAS024	MAS025	MAS025	MAS025	MAS026	MAS026	MAS026
P	2.844	2.854	2.713	2.653	2.852	2.679	2.095
Si	0.162	0.191	0.311	0.467	0.156	0.353	0.937
Th	-	-	-	-	-	-	-
U	-	-	-	-	-	-	-
Y	-	-	-	-	-	-	-
La	0.039	0.033	0.059	0.095	0.029	0.064	0.214
Ce	0.066	0.079	0.150	0.219	0.068	0.160	0.462
Pr	0.003	0.007	0.020	0.031	0.006	0.020	0.049
Nd	0.022	0.036	0.065	0.088	0.030	0.071	0.202
Sm	0.004	-	0.014	0.014	-	-	0.027
Ca	4.820	4.750	4.635	4.265	4.858	4.626	3.959
Fe	0.008	-	-	-	-	-	-
Sr	-	-	-	-	-	-	-
Na	-	-	-	-	-	-	-
F	1.000	1.000	0.999	0.999	1.001	0.999	1.000
Total	**8.993**	**8.950**	**8.966**	**8.830**	**8.999**	**8.971**	**8.944**

	MAS027 N = 4	MAS027 N = 3	MAS028 N = 3	MAS028 N = 2	MAS028 N = 3	MAS028 N = 2	MAS029 N = 2
Wt. %							
P_2O_5	39.13	26.91	12.89	14.69	26.93	34.23	12.60
SiO_2	2.17	8.07	16.29	14.64	8.50	4.53	15.12
ThO_2	-	-	0.60	0.38	.0.3	-	16.99
UO_2	-	-	-	-	-	-	-
Y_2O_3	1.01	1.75	11.19	-	1.41	0.83	-
La_2O_3	0.84	5.50	21.64	9.52	5.35	2.63	5.03
Ce_2O_3	2.30	10.84	2.19	19.12	10.96	5.48	10.93
Pr_2O_3	0.41	1.17	7.87	2.09	1.33	0.32	1.29
Nd_2O_3	1.09	4.06	0.98	7.07	4.55	2.35	3.46
Sm_2O_3	0.22	0.44	0.60	0.91	0.54	0.31	0.57
CaO	50.25	37.21	22.66	27.23	38.25	46.11	6.65
FeO	0.50	1.24	0.64	0.35	0.57	0.31	10.96
SrO	-	-	-	-	-	-	0.68
Na_2O	-	-	-	-	-	-	-
Total	**97.92**	**97.19**	**97.55**	**96.00**	**98.39**	**97.10**	**88.82**
F_C	3.67	3.23	2.85	2.83	3.27	3.50	2.41
O=F	1.55	1.36	1.20	1.19	1.38	1.47	1.01
Total	**100.04**	**99.06**	**99.20**	**97.64**	**100.28**	**99.13**	**87.05**

Structural formulae calculated on the basis of 13 anions (O,F)

	MAS027 N = 4	MAS027 N = 3	MAS028 N = 3	MAS028 N = 2	MAS028 N = 3	MAS028 N = 2	MAS029 N = 2
P	2.854	2.230	1.213	1.392	2.203	2.618	1.398
Si	0.187	0.790	1.811	1.639	0.821	0.409	1.982
Th	-	-	0.015	0.010	0.001	-	0.507
U	-	-	-	-	-	-	-
Y	0.046	0.091	0.662	-	0.073	0.040	-
La	0.027	0.199	0.887	0.393	0.919	0.088	0.243
Ce	0.073	0.388	0.089	0.784	0.388	0.181	0.524
Pr	0.013	0.042	0.319	0.085	0.047	0.011	0.062
Nd	0.034	0.142	0.039	0.283	0.157	0.076	0.162
Sm	0.007	0.015	0.023	0.035	0.018	0.010	0.162
Ca	4.639	3.903	2.698	3.266	3.960	4.464	0.026
Fe	0.036	0.102	0.059	0.033	0.046	0.023	1.201
Sr	-	-	-	-	-	-	0.052
Na	-	-	-	-	-	-	-
F	1.000	1.000	1.002	1.002	0.999	1.000	0.999
Total	**8.927**	**8.918**	**8.837**	**8.957**	**8.926**	**8.947**	**8.300**

	MAS031 N = 4	MAS032 N = 6	MAS033 N = 6	MAS034 N = 3	MAS037 N = 4	MAS038 N = 4	MAS038 N = 1
Wt. %							
P_2O_5	40.35	36.54	33.63	35.56	32.98	37.31	42.62
SiO_2	1.63	3.21	4.61	4.02	4.98	2.65	0.29
ThO_2	-	-	-	-	0.27	-	-
UO_2	-	-	-	-	-	-	-
Y_2O_3	0.89	0.77	1.28	-	-	-	-
La_2O_3	1.89	1.70	3.30	2.28	3.56	0.74	0.03
Ce_2O_3	0.10	3.81	6.58	4.88	6.55	2.51	0.43
Pr_2O_3	0.69	0.46	0.58	0.59	0.73	0.35	0.07
Nd_2O_3	0.23	1.71	2.36	1.75	2.43	1.65	0.32
Sm_2O_3	-	0.27	0.31	0.34	0.41	0.31	0.17
CaO	52.11	49.16	43.88	48.07	45.31	50.78	54.22
FeO	0.17	0.38	0.40	0.12	0.43	0.21	0.07
SrO	-	-	-	-	-	-	-
Na_2O	-	0.15	0.40	-	-	0.38	0.06
Total	**98.06**	**98.16**	**97.33**	**97.61**	**97.65**	**96.89**	**98.28**
F_C	3.73	3.60	3.46	3.56	3.46	3.61	3.79
O=F	1.57	1.52	1.46	1.50	1.46	1.52	1.60
Total	**100.22**	**100.24**	**99.33**	**99.67**	**99.65**	**98.98**	**100.47**

Structural formulae calculated on the basis of 13 anions (O,F)

	MAS031	MAS032	MAS033	MAS034	MAS037	MAS038	MAS038
P	2.900	2.720	2.694	2.677	2.555	2.770	3.010
Si	0.138	0.282	0.422	0.358	0.456	0.232	0.024
Th	-	-	-	-	0.006	-	-
U	-	-	-	-	-	-	-
Y	0.040	0.036	0.062	-	-	-	-
La	0.059	0.055	0.111	0.075	0.120	0.024	0.001
Ce	0.003	0.123	0.220	0.159	0.219	0.081	0.013
Pr	0.021	0.015	0.019	0.019	0.024	0.011	0.002
Nd	0.007	0.054	0.077	0.056	0.079	0.052	0.010
Sm	-	0.008	0.010	0.010	0.013	0.009	0.005
Ca	4.739	4.632	4.301	4.580	4.442	4.771	4.846
Fe	0.012	0.028	0.031	0.009	0.033	0.015	0.005
Sr	-	-	-	-	-	-	-
Na	-	0.026	0.072	-	-	0.066	0.010
F	1.001	1.001	1.001	1.001	1.001	1.001	1.000
Total	**8.939**	**8.997**	**8.949**	**8.960**	**8.969**	**9.049**	**8.942**

III.III Astrophyllite (fluorine and hydroxyl set to 1 and 4 ions, respectively)

	MAS005 N = 5	MAS015 N = 4	MAS015 N = 1	MAS015 N = 2	MAS026 N = 4	MAS026 N = 1	MAS026 N = 1
Wt. %							
Nb_2O_5	3.76	3.09	5.33	5.07	2.48	2.23	4.06
SiO_2	32.32	34.27	34.47	34.94	34.31	34.06	34.73
TiO_2	2.35	8.25	6.33	6.70	3.94	3.68	6.88
ZrO_2	10.48	1.00	3.24	2.69	9.73	9.74	4.47
Al_2O_3	1.39	1.50	1.31	1.18	1.29	1.07	1.46
FeO	34.48	35.82	34.70	35.89	34.69	34.57	34.47
MnO	0.95	1.03	1.08	0.95	2.23	2.34	2.45
MgO	-	-	0.14	0.11	0.01	0.14	0.03
CaO	1.24	2.17	1.78	1.60	1.41	1.03	1.34
Na_2O	1.62	1.57	1.68	1.86	1.71	2.07	2.05
K_2O	5.05	5.32	4.99	5.26	5.10	5.28	5.44
Total	**93.64**	**94.02**	**95.05**	**96.25**	**96.90**	**96.21**	**97.38**
H_2O_C	2.62	2.65	2.67	2.70	2.65	2.63	2.72
F_C	1.38	1.40	1.41	1.42	1.40	1.39	1.43
O=F	0.58	0.59	0.59	0.60	0.59	0.59	0.60
Total	**98.86**	**97.48**	**98.54**	**99.77**	**100.45**	**99.64**	**100.93**
Structural formulae calculated on the basis of 31 anions (O,OH,F)							
Nb	0.401	0.316	0.541	0.509	0.253	0.230	0.405
Si	7.633	7.744	7.746	7.764	7.727	7.757	7.662
Ti	0.417	1.402	1.070	1.120	0.667	0.630	1.142
Zr	1.184	0.110	0.355	0.291	1.069	1.082	0.481
Al	0.387	0.399	0.347	0.309	0.342	0.287	0.380
Fe	6.810	6.769	6.521	6.670	6.534	6.584	6.360
Mn	0.190	0.197	0.206	0.179	0.425	0.451	0.458
Mg	-	-	0.047	0.036	0.034	0.048	0.010
Ca	0.314	0.525	0.429	0.381	0.340	0.251	0.317
Na	0.742	0.688	0.732	0.801	0.747	0.914	0.877
K	1.522	1.534	1.430	1.491	1.465	1.534	1.531
OH	4.001	3.994	4.002	4.002	3.995	2.995	4.003
F	1.001	1.000	1.002	0.998	0.997	1.001	0.998
Total	**24.603**	**24.679**	**24.427**	**24.552**	**24.591**	**24.765**	**24.622**

	MAS032 N = 2	MAS032 N = 1
Wt. %		
Nb_2O_5	1.76	2.45
SiO_2	33.35	34.81
TiO_2	2.51	2.67
ZrO_2	12.97	12.84
Al_2O_3	1.06	0.78
FeO	33.33	33.65
MnO	3.69	3.28
MgO	-	0.37
CaO	2.05	2.27
Na_2O	1.23	1.23
K_2O	4.70	2.53
Total	**96.65**	**96.88**
H_2O_C	2.62	2.67
F_C	1.38	1.41
O=F	0.58	0.59
Total	**100.07**	**100.37**

Structural formulae calculated on the basis of 31 anions (O,OH,F)

Si	7.642	7.811
Ti	0.433	0.451
Al	0.286	0.206
Fe	6.387	6.315
Mn	0.716	0.623
Mg	-	0.124
Ca	0.503	0.546
Na	0.546	0.535
K	1.374	0.724
Zr	1.449	1.405
Nb	0.182	0.249
OH	4.004	3.996
F	1.000	1.001
Total	**24.523**	**23.986**

III.IV Baddeleyite

	MAS005 N = 3	MAS006 N = 4	MAS015 N = 5	MAS016 N = 3	MAS017 N = 5	MAS017 N = 3	MAS018 N = 3	MAS026 N = 4	MAS030 N = 3	MAS031 N = 4	MAS036 N = 5
Wt. %											
Ta_2O_5	-	-	-	-	0.70	0.48	0.61	-	-	-	-
SiO_2	-	0.41	0.23	-	-	-	-	0.12	0.11	0.16	-
TiO_2	0.26	-	-	-	0.47	0.20	0.18	-	-	-	-
ZrO_2	98.08	97.63	97.22	98.84	97.66	98.03	95.89	98.37	98.57	98.26	98.55
HfO_2	0.98	1.91	1.49	0.81	1.62	1.08	1.87	1.40	0.90	1.06	1.26
CaO	-	-	0.20	-	-	-	-	-	-	-	-
FeO	0.18	0.41	0.94	1.02	-	0.53	0.55	0.40	0.66	0.53	0.39
Total	**99.50**	**100.36**	**100.08**	**100.67**	**100.45**	**100.32**	**99.10**	**100.29**	**100.24**	**100.01**	**100.20**
Structural formulae calculated on the basis of 2 oxygens											
Ta	-	-	-	-	0.004	0.003	0.003	-	-	-	-
Si	-	0.008	0.005	-	-	-	-	0.002	0.002	0.003	-
Ti	0.004	-	-	-	0.007	0.003	0.003	-	-	-	-
Zr	0.990	0.970	0.961	0.970	0.986	0.977	0.970	0.979	0.976	0.977	0.983
Hf	0.006	0.011	0.009	0.005	0.010	0.006	0.011	0.008	0.005	0.006	0.007
Ca	-	-	0.004	-	-	-	-	-	-	-	-
Fe	0.009	0.021	0.049	0.051	-	0.027	0.029	0.020	0.034	0.027	0.020
Total	**1.009**	**1.010**	**1.026**	**1.026**	**1.006**	**1.016**	**1.016**	**1.010**	**1.017**	**1.014**	**1.010**

III.V Barite

	MAS012 N = 4	MAS018 N = 4	MAS023 N = 3	MAS037 N = 4
Wt. %				
SO_3	35.11	34.94	34.29	34.72
CaO	-	-	-	0.65
SrO	0.62	1.18	1.71	0.29
BaO	63.89	64.15	63.59	64.41
Total	**99.62**	**100.27**	**99.59**	**100.07**
Structural formulae calculated on the basis of 4 oxygens				
S	1.009	0.995	0.998	0.992
Ca	-	-	-	0.027
Sr	0.014	0.026	0.038	0.006
Ba	0.959	0.954	0.967	0.961
Total	**1.982**	**1.975**	**2.003**	**1.986**

III.VI Chevkinite [Fe^{3+} recalculated using the method of Droop (1987)]

	MAS001 N = 1	MAS001 N = 3	MAS001 N = 3	MAS003 N = 5	MAS003 N = 7	MAS005 N = 2	MAS005 N = 3
Wt. %							
Nb_2O_5	-	-	-	3.96	5.43	1.91	4.38
SiO_2	20.55	20.80	21.22	19.55	19.18	21.03	21.33
TiO_2	19.28	19.75	25.68	16.05	13.60	17.08	19.47
ZrO_2	-	-	-	1.20	0.50	1.02	0.73
ThO_2	1.87	1.70	3.51	1.08	1.77	0.30	1.00
UO_2	0.04	0.37	0.17	-	-	0.06	0.14
Al_2O_3	0.53	0.67	0.48	0.33	0.21	0.74	1.21
Y_2O_3	-	-	-	-	-	-	-
La_2O_3	10.25	11.27	7.73	11.80	11.56	6.41	5.47
Ce_2O_3	17.96	19.21	15.20	20.83	22.32	19.63	15.44
Pr_2O_3	1.59	2.23	1.40	1.62	1.94	2.98	1.81
Nd_2O_3	4.63	4.93	4.48	5.26	5.49	10.58	4.19
Sm_2O_3	0.13	0.44	0.51	-	-	1.35	0.65
Fe_2O_3	-	-	-	3.41	3.84	-	-
FeO	8.13	8.24	3.14	8.24	8.74	10.57	5.22
MnO	0.61	0.66	0.71	-	-	-	-
CaO	3.78	3.81	2.76	4.49	3.62	2.63	4.40
Na_2O	-	-	-	-	-	-	-
Total	**89.35**	**94.08**	**86.99**	**97.82**	**98.19**	**98.29**	**85.44**
Structural formulae calculated on the basis of 22 oxygens							
Nb	-	-	-	0.367	0.515	0.179	0.417
Si	4.423	4.324	4.411	4.012	4.026	4.350	4.494
Ti	3.121	3.088	4.015	2.477	2.147	2.657	3.085
Zr	-	-	-	0.120	0.051	0.103	0.075
Th	0.092	0.080	0.166	0.050	0.085	0.014	0.048
U	0.002	0.017	0.008	-	-	0.003	0.007
Al	0.134	0.164	0.118	0.080	0.052	0.180	0.300
Y	-	-	-	-	-	-	-
La	0.814	0.864	0.593	0.893	0.895	0.489	0.425
Ce	1.415	1.462	1.157	1.565	1.715	1.487	1.191
Pr	0.125	0.169	0.106	0.121	0.148	0.225	0.139
Nd	0.356	0.366	0.333	0.385	0.412	0.782	0.315
Sm	0.010	0.032	0.037	-	-	0.096	0.047
Fe3+	-	-	-	0.534	0.615	-	-
Fe	1.463	1.432	0.546	1.431	1.555	1.828	0.920
Mn	0.111	0.116	0.125	-	-	-	-
Ca	0.872	0.849	0.615	0.987	0.814	0.583	0.993
Na	-	-	-	-	-	-	-
Total	**12.936**	**12.963**	**12.228**	**13.024**	**13.030**	**12.976**	**12.457**

	MAS005 N = 5	MAS007 N = 3	MAS007 N = 3	MAS009 N = 3	MAS009 N = 2	MAS012 N = 4	MAS014 N = 2
Wt. %							
Nb_2O_5	1.15	0.86	0.32	4.74	3.66	6.08	1.25
SiO_2	19.49	18.94	20.77	17.99	20.33	20.00	18.88
TiO_2	16.93	17.13	23.25	20.77	17.43	21.72	15.77
ZrO_2	1.28	1.85	0.24	-	-	1.67	0.74
ThO_2	-	-	-	1.13	0.90	0.90	1.12
UO_2	-	-	0.73	0.06	0.02	-	0.24
Al_2O_3	0.55	0.22	0.71	0.38	0.30	0.58	0.60
Y_2O_3	-	-	-	-	-	-	1.06
La_2O_3	6.30	4.92	9.09	10.47	12.36	5.63	10.85
Ce_2O_3	21.15	20.00	18.69	18.44	20.98	14.18	22.65
Pr_2O_3	3.24	3.28	2.48	1.68	2.55	1.73	2.19
Nd_2O_3	12.12	13.18	6.15	4.62	5.01	4.73	6.88
Sm_2O_3	2.05	1.93	0.23	0.42	0.26	0.62	0.68
Fe_2O_3	4.16	3.46	-	-	-	-	3.50
FeO	7.99	7.77	6.50	3.34	8.64	4.46	8.74
MnO	-	-	0.23	-	-	0.44	-
CaO	2.79	3.14	3.12	1.89	3.12	3.67	1.74
Na_2O	-	-	-	-	-	-	-
Total	**99.20**	**96.69**	**92.51**	**85.93**	**95.56**	**86.41**	**96.89**

Structural formulae calculated on the basis of 22 oxygens

Nb	0.107	0.082	0.030	0.480	0.346	0.574	0.212
Si	4.015	4.000	4.242	4.033	4.255	4.177	4.034
Ti	2.624	2.721	3.571	3.502	2.744	3.412	2.535
Zr	0.129	0.191	0.024	-	-	0.170	0.077
Th	-	-	-	0.058	0.043	0.043	0.054
U	-	-	0.033	0.003	0.001	-	0.011
Al	0.134	0.055	0.171	0.100	0.074	0.143	0.151
Y	-	-	-	-	-	-	0.121
La	0.479	0.383	0.685	0.866	0.954	0.434	0.855
Ce	1.595	1.547	1.397	1.513	1.608	1.084	1.772
Pr	0.243	0.252	0.185	0.137	0.194	0.132	0.171
Nd	0.892	0.994	0.449	0.370	0.375	0.353	0.525
Sm	0.146	0.140	0.016	0.032	0.019	0.045	0.050
Fe^{3+}	0.655	0.558	-	-	-	-	0.570
Fe	1.397	1.391	1.110	0.626	1.512	0.779	1.583
Mn	-	-	0.040	-	-	0.078	-
Ca	0.616	0.711	0.683	0.454	0.700	0.821	0.398
Na	-	-	-	-	-	-	-
Total	**13.031**	**13.025**	**12.634**	**12.175**	**12.825**	**12.243**	**13.028**

	MAS014 N = 1	MAS014 N = 2	MAS014 N = 2	MAS015 N = 4	MAS015 N = 3	MAS015 N = 2	MAS015 N = 2
Wt. %							
Nb_2O_5	1.36	1.18	1.33	2.40	3.16	2.96	3.05
SiO_2	19.10	20.04	20.10	19.41	15.72	19.57	20.02
TiO_2	14.63	18.19	19.71	16.61	18.42	21.79	17.53
ZrO_2	0.39	-	0.33	0.02	-	-	1.99
ThO_2	0.98	0.58	0.51	2.86	3.17	3.24	1.17
UO_2	0.25	-	-	-	-	0.31	0.59
Al_2O_3	1.18	0.48	0.67	0.18	0.27	0.26	0.25
Y_2O_3	0.39	-	-	-	-	0.94	0.07
La_2O_3	10.36	11.06	10.03	15.99	15.04	7.01	12.44
Ce_2O_3	24.01	20.88	20.25	21.81	21.16	16.36	20.69
Pr_2O_3	2.93	2.50	2.58	1.84	1.84	1.77	2.01
Nd_2O_3	7.25	6.47	6.52	4.60	4.48	4.47	5.55
Sm_2O_3	0.42	0.42	0.35	0.44	0.31	0.70	0.37
Fe_2O_3	3.50	-	-	2.16	-	-	0.95
FeO	8.84	8.90	8.36	10.16	3.88	3.10	10.05
MnO	-	0.36	0.25	0.10	0.26	1.88	-
CaO	1.12	2.44	2.87	1.97	0.51	0.69	3.84
Na_2O	-	-	-	-	-	-	-
Total	96.71	93.50	93.86	100.56	88.22	85.05	100.56

Structural formulae calculated on the basis of 22 oxygens

Nb	0.132	0.114	0.126	0.226	0.341	0.296	0.278
Si	4.109	4.285	4.206	4.035	3.753	4.323	4.034
Ti	2.367	2.926	3.103	2.597	3.307	3.620	2.657
Zr	0.041	-	0.034	0.002	-	-	0.196
Th	0.048	0.028	0.024	0.135	0.172	0.163	0.054
U	0.012	-	-	-	-	0.015	0.026
Al	0.299	0.121	0.165	0.044	0.076	0.068	0.059
Y	0.045	-	-	-	-	0.110	0.008
La	0.822	0.872	0.774	1.226	1.324	0.571	0.925
Ce	1.891	1.635	1.552	1.660	1.849	1.323	1.526
Pr	0.230	0.195	0.197	0.139	0.160	0.142	0.148
Nd	0.557	0.494	0.487	0.342	0.382	0.353	0.399
Sm	0.031	0.031	0.025	0.032	0.026	0.053	0.026
Fe^{3+}	0.573	-	-	0.341	-	-	0.144
Fe	1.612	1.591	1.463	1.781	0.775	0.573	1.699
Mn	-	0.065	0.044	0.018	0.053	0.352	-
Ca	0.258	0.559	0.644	0.439	0.130	0.163	0.829
Na	-	-	-	-	-	-	-
Total	13.028	12.916	12.844	13.016	12.348	12.125	13.006

	MAS016 N = 1	MAS016 N = 6	MAS016 N = 2	MAS017 N = 4	MAS017 N = 4	MAS025 N = 3	MAS025 N = 1
Wt. %							
Nb_2O_5	5.97	1.52	1.91	4.72	7.54	3.31	4.25
SiO_2	19.75	19.37	14.79	19.79	16.72	19.25	19.21
TiO_2	12.64	18.22	25.64	17.14	29.41	13.05	13.37
ZrO_2	1.02	0.26	0.39	0.77	1.52	-	-
ThO_2	-	0.70	1.46	0.85	1.48	-	-
UO_2	-	0.14	0.28	0.14	0.01	-	-
Al_2O_3	0.46	0.25	0.33	0.58	0.47	0.44	0.49
Y_2O_3	-	-	0.78	-	-	-	-
La_2O_3	9.32	13.57	7.19	9.68	3.01	12.28	11.84
Ce_2O_3	21.37	23.05	17.67	19.02	9.87	22.91	21.27
Pr_2O_3	3.02	2.06	2.13	2.08	1.29	2.41	1.27
Nd_2O_3	8.68	5.88	5.84	5.37	2.91	6.78	5.72
Sm_2O_3	0.92	0.75	0.82	0.59	0.26	0.83	1.13
Fe_2O_3	4.22	1.63	-	-	-	3.98	1.72
FeO	9.62	10.09	2.97	7.47	2.91	9.62	11.03
MnO	-	-	-	0.45	0.57	-	-
CaO	2.75	2.04	0.79	3.30	3.85	1.02	1.24
Na_2O	-	-	-	-	-	-	-
Total	**99.74**	**99.53**	**82.99**	**91.95**	**81.82**	**95.88**	**92.54**
Structural formulae calculated on the basis of 22 oxygens							
Nb	0.557	0.142	0.201	0.455	0.709	0.326	0.426
Si	4.079	4.011	3.446	4.218	3.479	4.191	4.257
Ti	1.964	2.838	4.494	2.748	4.603	2.137	2.229
Zr	0.103	0.026	0.044	0.080	0.154	-	-
Th	-	0.033	0.077	0.041	0.070	-	-
U	-	0.006	0.015	0.007	-	-	-
Al	0.112	0.061	0.091	0.146	0.115	0.113	0.128
Y	-	-	0.097	-	-	-	-
La	0.710	1.036	0.618	0.761	0.231	0.986	0.968
Ce	1.616	1.747	1.507	1.484	0.752	1.826	1.726
Pr	0.227	0.155	0.181	0.162	0.098	0.191	0.103
Nd	0.640	0.435	0.486	0.409	0.216	0.527	0.453
Sm	0.065	0.054	0.066	0.043	0.019	0.062	0.086
Fe^{3+}	0.666	0.255	-	-	-	0.662	0.289
Fe	1.687	1.758	0.579	1.332	0.506	1.778	2.058
Mn	-	-	-	0.081	0.100	-	-
Ca	0.609	0.453	0.197	0.754	0.858	0.238	0.294
Na	-	-	-	-	-	-	-
Total	**13.036**	**13.012**	**12.099**	**12.721**	**11.913**	**13.037**	**13.015**

	MAS028 N = 3	MAS028 N = 2
Wt. %		
Nb_2O_5	-	-
SiO_2	19.79	19.10
TiO_2	16.72	16.28
ZrO_2	-	0.52
ThO_2	0.08	-
UO_2	-	-
Al_2O_3	0.20	0.43
Y_2O_3	-	0.58
La_2O_3	8.89	9.32
Ce_2O_3	23.89	23.16
Pr_2O_3	3.44	3.13
Nd_2O_3	11.05	11.09
Sm_2O_3	1.32	1.51
Fe_2O_3	4.94	6.84
FeO	8.26	6.48
MnO	-	0.92
CaO	1.42	1.32
Na_2O	-	-
Total	**100.00**	**100.67**

Structural formulae calculated on the basis of 22 oxygens

Nb	-	-
Si	4.120	3.960
Ti	2.618	2.539
Zr	-	0.053
Th	0.004	-
U	-	-
Al	0.049	0.105
Y	-	0.064
La	0.683	0.713
Ce	1.821	1.758
Pr	0.261	0.236
Nd	0.821	0.821
Sm	0.095	0.108
Fe3+	0.788	1.094
Fe	1.465	1.152
Mn	-	0.162
Ca	0.317	0.293
Na	-	-
Total	**13.040**	**13.056**

III.VII Fergusonite

	MAS006 N = 2	MAS006 N = 1	MAS006 N = 1	MAS006 N = 2	MAS006 N = 2	MAS009 N = 1	MAS009 N = 3
Wt. %							
WO_3	5.30	2.48	3.95	4.15	2.95	4.44	2.92
Nb_2O_5	44.63	44.05	41.85	42.80	43.95	46.64	49.21
Ta_2O_5	1.14	1.66	1.94	2.11	2.50	-	-
SiO_2	0.42	0.04	-	-	-	-	-
TiO_2	0.88	0.71	1.05	0.58	0.59	-	-
ThO_2	1.21	2.90	0.96	1.79	2.75	-	-
UO_2	1.34	2.81	2.59	1.44	1.70	-	-
Y_2O_3	21.82	22.41	22.24	19.80	20.06	17.38	20.71
La_2O_3	-	-	0.15	0.18	0.33	0.82	0.16
Ce_2O_3	1.36	1.20	1.16	1.92	1.63	7.95	5.74
Pr_2O_3	0.59	0.66	0.70	0.66	0.67	2.12	1.30
Nd_2O_3	4.47	4.02	4.39	5.41	4.90	9.14	7.68
Sm_2O_3	2.64	2.32	0.57	2.64	2.62	2.17	1.83
Eu_2O_3	-	-	0.45	0.36	0.70	-	-
Gd_2O_3	3.64	3.91	3.49	3.51	4.20	1.27	1.68
Tb_2O_3	0.89	0.67	0.71	0.71	0.68	0.01	0.55
Dy_2O_3	2.96	4.78	4.82	4.39	3.95	2.48	2.88
Ho_2O_3	-	-	1.24	0.86	0.56	0.86	0.41
Er_2O_3	2.00	0.95	2.86	2.02	2.39	1.17	1.01
Tm_2O_3	-	-	1.00	0.77	0.82	0.28	0.38
Yb_2O_3	2.29	2.18	2.58	2.03	1.23	1.55	1.96
Lu_2O_3	-	-	0.40	0.50	0.25	-	-
CaO	0.70	0.54	0.58	0.69	0.69	1.99	1.34
MnO	0.09	0.16	-	-	-	-	-
FeO	0.52	0.64	0.35	0.50	0.77	0.51	0.64
Total	**98.89**	**99.09**	**100.03**	**99.82**	**100.89**	**100.78**	**100.40**

	MAS006 N = 2	MAS006 N = 1	MAS006 N = 1	MAS006 N = 2	MAS006 N = 2	MAS009 N = 1	MAS009 N = 3
Structural formulae calculated on the basis of 4 oxygens							
W	0.062	0.029	0.047	0.050	0.035	0.052	0.033
Nb	0.910	0.914	0.877	0.898	0.905	0.947	0.981
Ta	0.014	0.021	0.024	0.027	0.031	-	-
Si	0.019	0.002	-	-	-	-	-
Ti	0.030	0.025	0.037	0.020	0.020	-	-
Th	0.012	0.030	0.010	0.019	0.029	-	-
U	0.013	0.029	0.027	0.015	0.017	-	-
Y	0.524	0.547	0.549	0.489	0.486	0.415	0.486
La	-	-	0.003	0.003	0.006	0.014	0.003
Ce	0.022	0.020	0.020	0.033	0.027	0.131	0.093
Pr	0.010	0.011	0.012	0.011	0.011	0.035	0.021
Nd	0.072	0.066	0.073	0.090	0.080	0.147	0.121
Sm	0.041	0.037	0.009	0.042	0.041	0.034	0.028
Eu	-	-	0.007	0.006	0.011	-	-
Gd	0.054	0.059	0.054	0.054	0.063	0.019	0.025
Tb	0.013	0.010	0.011	0.011	0.010	0.000	0.008
Dy	0.043	0.071	0.072	0.066	0.058	0.036	0.041
Ho	-	-	0.018	0.013	0.008	0.012	0.006
Er	0.028	0.014	0.042	0.029	0.034	0.017	0.014
Tm	-	-	0.014	0.011	0.012	0.004	0.005
Yb	0.031	0.031	0.036	0.029	0.017	0.021	0.026
Lu	-	-	0.006	0.007	0.003	-	-
Ca	0.034	0.027	0.029	0.034	0.034	0.096	0.063
Mn	0.003	0.006	-	-	-	-	-
Fe	0.059	0.074	0.041	0.058	0.088	0.057	0.071
Total	**1.994**	**2.021**	**2.017**	**2.013**	**2.026**	**2.035**	**2.024**

	MAS012 N = 2	MAS012 N = 1	MAS012 N = 1	MAS026 N = 2	MAS026 N = 1	MAS026 N = 1
Wt. %						
WO_3	4.75	4.60	6.22	3.82	2.79	3.71
Nb_2O_5	45.35	44.92	44.11	45.18	45.69	44.54
Ta_2O_5	-	-	-	0.72	1.00	1.07
SiO_2	1.84	2.08	1.89	-	-	-
TiO_2	0.59	0.87	0.96	0.45	0.48	0.14
ThO_2	0.23	0.19	0.11	4.49	5.25	5.26
UO_2	0.13	0.03	0.05	1.66	1.51	0.77
Y_2O_3	14.27	18.47	21.42	20.23	18.22	15.65
La_2O_3	-	0.19	0.08	0.26	0.64	0.54
Ce_2O_3	5.00	2.99	1.56	2.55	3.14	3.97
Pr_2O_3	1.44	0.58	0.48	0.78	0.73	0.83
Nd_2O_3	10.68	5.66	4.50	5.02	5.51	6.91
Sm_2O_3	3.54	2.65	2.76	2.56	2.15	2.81
Eu_2O_3	1.00	-	0.79	-	-	-
Gd_2O_3	3.40	4.18	3.92	3.56	-3.60	3.79
Tb_2O_3	0.43	1.27	1.48	0.44	0.34	0.47
Dy_2O_3	2.41	4.52	3.82	4.00	4.45	3.84
Ho_2O_3	0.12	0.78	0.26	-	-	-
Er_2O_3	1.34	1.72	1.71	1.94	2.09	1.58
Tm_2O_3	0.57	0.15	1.07	-	-	-
Yb_2O_3	0.73	1.26	1.04	1.10	0.92	1.32
Lu_2O_3	0.22	0.32	0.10	-	-	-
CaO	0.49	0.56	0.43	1.21	1.32	1.58
MnO	0.08	0.42	0.29	0.19	0.16	0.09
FeO	0.92	1.83	1.20	0.02	0.12	0.28
Total	**99.53**	**100.24**	**100.25**	**100.18**	**100.11**	**99.15**

	MAS012 N = 2	MAS012 N = 1	MAS012 N = 1	MAS026 N = 2	MAS026 N = 1	MAS026 N = 1
Structural formulae calculated on the basis of 4 oxygens						
W	0.055	0.051	0.070	0.046	0.033	0.045
Nb	0.911	0.868	0.861	0.940	0.953	0.945
Ta	-	-	-	0.009	0.013	0.014
Si	0.082	0.089	0.082	-	-	-
Ti	0.020	0.028	0.031	0.016	0.017	0.005
Th	0.002	0.002	0.001	0.047	0.055	0.056
U	0.001	0.000	-	0.017	0.015	0.008
Y	0.337	0.420	0.492	0.495	0.447	0.391
La	-	0.003	0.001	0.004	0.011	0.009
Ce	0.081	0.047	0.025	0.043	0.053	0.068
Pr	0.023	0.009	0.008	0.013	0.012	0.014
Nd	0.169	0.086	0.069	0.082	0.091	0.116
Sm	0.054	0.039	0.041	0.041	0.034	0.045
Eu	0.015	-	0.012	-	-	-
Gd	0.050	0.059	0.056	0.054	0.055	0.059
Tb	0.006	0.018	0.021	0.007	0.005	0.007
Dy	0.034	0.062	0.053	0.059	0.066	0.058
Ho	0.002	0.011	0.004	-	-	-
Er	0.019	0.023	0.023	0.028	0.030	0.023
Tm	0.008	0.002	0.014	-	-	-
Yb	0.010	0.016	0.014	0.015	0.013	0.019
Lu	0.003	0.004	0.001	-	-	-
Ca	0.023	0.026	0.020	0.060	0.065	0.079
Mn	0.003	0.015	0.011	0.007	0.006	0.004
Fe	0.103	0.196	0.130	0.002	0.014	0.033
Total	**2.013**	**2.076**	**2.039**	**1.985**	**1.989**	**1.998**

III.VIII Fluorocarbonates (fluorine and carbon calculated assuming full occupancy)

	MAS004 N = 2	MAS004 N = 3	MAS005 N = 4	MAS006 N = 3	MAS006 N = 3	MAS006 N = 3	MAS007 N = 2	MAS007 N = 3	MAS009 N = 2	MAS011 N = 5	MAS012 N = 4
Wt. %											
SO_3	-	-	1.58	-	-	-	-	-	-	-	-
SiO_2	1.80	0.36	1.62	0.32	0.39	0.92	0.68	0.53	1.22	-	0.53
ThO_2	3.00	0.96	1.35	-	0.41	1.27	2.87	1.82	3.91	1.07	0.90
Y_2O_3	2.03	1.17	1.59	0.56	-	1.01	1.01	0.65	1.01	-	0.70
La_2O_3	7.64	15.42	14.57	11.41	20.59	9.03	7.93	15.63	18.22	15.03	8.98
Ce_2O_3	19.03	34.15	27.59	27.98	37.26	22.86	22.49	35.05	31.28	36.82	25.49
Pr_2O_3	2.70	3.50	3.01	4.02	4.02	2.76	3.16	3.69	3.51	4.59	3.20
Nd_2O_3	9.89	11.98	9.97	12.97	9.83	10.55	10.23	12.27	8.54	12.88	11.66
Sm_2O_3	1.90	1.49	0.76	1.35	1.03	1.59	1.37	1.41	1.02	1.65	1.72
Gd_2O_3	-	-	-	-	-	-	-	-	-	-	-
Dy_2O_3	0.25	0.25	0.11	-	-	-	-	-	-	-	-
Er_2O_3	0.11	-	-	-	-	-	-	-	-	-	-
Fe_2O_3	1.37	0.42	4.78	0.41	0.18	3.18	5.22	0.29	2.30	0.61	1.02
CaO	16.91	1.57	0.44	10.40	0.09	15.58	12.90	1.12	1.43	0.23	14.23
SrO	0.73	0.91	0.41	-	-	-	0.59	0.65	1.42	0.21	0.39
Total	**66.36**	**72.18**	**68.01**	**69.68**	**74.13**	**68.97**	**68.67**	**73.28**	**73.86**	**73.09**	**69.03**
F_C	6.21	8.71	9.36	7.06	8.78	6.18	7.09	8.81	9.31	8.51	6.84
$O=F$	2.61	3.67	3.94	2.97	3.7	2.60	2.99	3.71	3.92	3.58	2.88
CO_{2C}	28.75	20.18	21.69	24.54	20.34	28.65	27.38	20.40	21.57	19.72	26.40
Total	**99.71**	**97.40**	**95.12**	**98.31**	**99.55**	**101.20**	**100.15**	**98.78**	**100.82**	**97.74**	**99.39**

	MAS004	MAS004	MAS005	MAS006	MAS006	MAS006	MAS007	MAS007	MAS009	MAS011	MAS012
	N = 2	N = 3	N = 4	N = 3	N = 3	N = 3	N = 2	N = 3	N = 2	N = 5	N = 4

Structural formulae calculated on the # of ions in each respected mineral type (bastnaesite = 4; synchysite = 7; parisite = 11; röentgenite = 18)

	MAS004	MAS004	MAS005	MAS006	MAS006	MAS006	MAS007	MAS007	MAS009	MAS011	MAS012
S	-	-	0.040	-	-	-	-	-	-	-	-
Si	0.092	0.013	0.055	0.029	0.014	0.047	0.091	0.019	0.041	-	0.074
Th	0.029	0.008	0.010	-	0.003	0.015	0.087	0.015	0.030	0.009	0.028
Y	0.055	0.023	0.029	0.027	-	0.027	0.072	0.012	0.018	-	0.052
La	0.144	0.207	0.183	0.377	0.273	0.170	0.391	0.207	0.228	0.206	0.459
Ce	0.355	0.454	0.344	0.917	0.491	0.409	1.101	0.461	0.389	0.501	1.294
Pr	0.050	0.046	0.037	0.131	0.053	0.051	0.154	0.048	0.043	0.062	0.162
Nd	0.180	0.155	0.121	0.415	0.126	0.193	0.489	0.157	0.104	0.171	0.578
Sm	0.033	0.019	0.009	0.042	0.013	0.028	0.064	0.017	0.012	0.021	0.082
Gd	-	-	-	-	-	-	-	-	-	-	-
Dy	0.004	0.003	0.001	-	-	-	-	-	-	-	-
Er	0.002	-	-	-	-	-	-	-	-	-	-
Fe^{3+}	0.017	0.002	0.022	0.010	0.001	0.040	0.204	0.001	0.006	0.003	0.041
Ca	0.923	0.061	0.016	0.998	0.003	0.854	1.849	0.043	0.084	0.009	2.115
Sr	0.022	0.019	0.008	-	-	-	0.046	0.014	0.028	0.005	0.031
F	1.001	1.000	1.000	1.999	1.000	1.000	3.000	1.000	1.000	1.000	3.000
CO_2	2.000	1.000	0.960	3.000	1.000	2.000	5.000	1.000	1.000	1.000	4.999
Total	**4.907**	**3.010**	**2.844**	**7.972**	**2.991**	**4.847**	**12.583**	**3.001**	**2.983**	**2.987**	**12.949**

	MAS012 N = 5	MAS012 N = 4	MAS012 N = 5	MAS012 N = 4	MAS013 N = 5	MAS013 N = 4	MAS013 N = 4	MAS013 N = 4	MAS014 N = 3	MAS014 N = 3	MAS014 N = 3
Wt. %											
SO_3	-	-	-	-	-	1.70	-	-	-	3.87	1.86
SiO_2	0.40	0.41	1.68	0.63	2.38	0.85	0.99	0.39	0.50	0.75	0.94
ThO_2	0.10	-	1.66	1.66	4.61	1.64	0.54	0.13	0.23	0.54	-
Y_2O_3	0.68	0.31	1.69	6.55	0.61	1.16	1.42	2.35	0.17	0.66	0.17
La_2O_3	11.68	19.31	12.55	8.46	10.11	13.48	15.83	10.60	21.17	15.45	13.30
Ce_2O_3	24.24	35.27	22.01	18.59	18.79	27.03	33.58	23.25	35.07	28.35	24.19
Pr_2O_3	3.03	3.40	2.25	2.02	2.30	2.84	3.54	2.53	3.38	2.75	2.51
Nd_2O_3	9.70	10.92	8.32	8.64	9.02	12.31	13.05	9.46	9.69	9.23	7.88
Sm_2O_3	0.89	1.00	0.96	1.35	1.36	1.45	1.50	1.05	0.70	1.02	0.78
Gd_2O_3	-	-	-	1.08	-	-	-	-	-	-	-
Dy_2O_3	-	-	-	1.36	-	-	-	-	-	-	-
Er_2O_3	-	-	-	0.73	-	-	-	-	-	-	-
Fe_2O_3	0.03	0.18	0.23	0.36	0.89	0.46	1.64	0.71	2.14	4.59	2.52
CaO	16.78	1.38	16.00	16.28	16.71	3.97	0.83	17.04	0.28	4.32	13.64
SrO	1.03	1.05	0.69	0.43	0.54	0.23	0.80	0.47	0.29	0.16	0.08
Total	**68.74**	**73.39**	**68.27**	**68.14**	**67.32**	**67.69**	**73.95**	**68.11**	**73.68**	**71.98**	**68.07**
F_C	5.99	8.84	6.19	6.10	6.23	6.09	9.26	6.06	8.99	9.86	7.00
$O=F$	2.52	3.72	2.61	2.57	2.62	2.56	3.90	2.55	3.79	4.15	2.95
CO_{2C}	27.78	20.47	28.68	28.23	28.86	22.59	21.45	28.06	20.82	20.72	26.03
Total	**99.99**	**98.98**	**100.53**	**99.90**	**99.79**	**93.81**	**100.76**	**99.68**	**99.70**	**98.41**	**98.15**

	MAS012 N = 5	MAS012 N = 4	MAS012 N = 5	MAS012 N = 4	MAS013 N = 5	MAS013 N = 4	MAS013 N = 4	MAS013 N = 4	MAS014 N = 3	MAS014 N = 3	MAS014 N = 3

Structural formulae calculated on the # of ions in each respected mineral type (bastnaesite = 4; synchysite = 7; parisite = 11; röentgenite = 18)

	MAS012 N = 5	MAS012 N = 4	MAS012 N = 5	MAS012 N = 4	MAS013 N = 5	MAS013 N = 4	MAS013 N = 4	MAS013 N = 4	MAS014 N = 3	MAS014 N = 3	MAS014 N = 3
S	-	-	-	-	-	0.199	-	-	-	0.093	0.189
Si	0.021	0.015	0.086	0.033	0.121	0.132	0.034	0.020	0.018	0.024	0.127
Th	0.001	-	0.019	0.020	0.053	0.058	0.004	0.002	0.002	0.004	-
Y	0.019	0.006	0.046	0.181	0.016	0.096	0.026	0.065	0.003	0.011	0.012
La	0.227	0.255	0.236	0.162	0.189	0.774	0.199	0.204	0.275	0.183	0.665
Ce	0.468	0.462	0.412	0.353	0.349	1.541	0.420	0.444	0.452	0.333	1.200
Pr	0.058	0.044	0.042	0.038	0.043	0.161	0.044	0.048	0.043	0.032	0.124
Nd	0.183	0.140	0.152	0.160	0.163	0.684	0.159	0.176	0.122	0.106	0.381
Sm	0.016	0.012	0.017	0.024	0.024	0.078	0.018	0.019	0.008	0.011	0.036
Gd	-	-	-	0.011	-	-	-	-	-	-	-
Dy	-	-	-	0.023	-	-	-	-	-	-	-
Er	-	-	-	0.012	-	-	-	-	-	-	-
Fe^{3+}	0.000	0.001	0.003	0.004	0.011	0.021	0.009	0.009	0.009	0.019	0.100
Ca	0.948	0.053	0.876	0.905	0.909	0.662	0.030	0.953	0.011	0.148	1.980
Sr	0.031	0.022	0.020	0.013	0.016	0.021	0.015	0.014	0.006	0.003	0.006
F	0.999	1.000	1.000	1.001	1.000	2.998	1.000	1.000	1.000	1.000	3.000
CO_2	2.000	1.000	2.000	2.000	2.000	4.801	1.000	2.000	1.000	0.907	4.815
Total	**4.982**	**3.017**	**4.921**	**4.940**	**4.894**	**12.331**	**2.967**	**4.962**	**2.951**	**2.884**	**12.667**

	MAS014 N = 4	MAS017 N = 3	MAS017 N = 3	MAS019 N = 3	MAS019 N = 4	MAS021 N = 2	MAS022 N = 3	MAS022 N = 17	MAS022 N = 5	MAS023 N = 3	MAS023 N = 4
Wt. %											
SO_3	-	-	-	-	-	-	-	-	-	-	0.83
SiO_2	0.39	0.95	0.44	0.38	0.39	0.62	1.44	0.32	0.52	0.48	0.76
ThO_2	0.18	0.90	0.56	-	-	-	2.24	0.21	0.69	0.22	2.24
Y_2O_3	0.13	1.84	1.02	-	0.94	0.65	0.43	-	0.12	-	0.76
La_2O_3	15.36	12.39	13.56	25.20	13.51	22.10	11.20	21.89	15.37	23.89	19.65
Ce_2O_3	28.49	24.38	25.99	36.46	28.13	35.55	19.32	37.37	26.59	34.65	32.07
Pr_2O_3	2.93	2.55	3.01	2.59	3.14	4.02	1.61	3.02	2.01	3.24	3.15
Nd_2O_3	8.69	8.40	8.22	7.80	10.99	9.81	5.26	8.79	6.28	9.03	10.45
Sm_2O_3	0.72	0.51	0.78	1.02	1.05	1.40	0.25	0.51	0.98	0.67	0.59
Gd_2O_3	-	-	-	-	-	-	-	-	-	-	
Dy_2O_3	-	-	-	-	-	-	-	-	-	-	
Er_2O_3	-	-	-	-	-	-	-	-	-	-	
Fe_2O_3	0.77	6.83	1.59	0.17	1.33	-	11.98	-	5.82	0.78	0.53
CaO	11.11	8.83	13.71	0.38	10.20	0.43	13.22	0.72	10.62	0.68	1.75
SrO	0.11	0.71	0.66	0.14	0.18	-	-	-	-	-	0.53
Total	**69.16**	**68.72**	**69.85**	**74.51**	**70.21**	**74.79**	**67.01**	**72.96**	**69.00**	**73.64**	**66.67**
F_C	7.13	7.68	6.94	8.88	7.23	8.97	7.69	8.65	7.51	8.83	9.26
$O=F$	3.00	3.23	2.92	3.74	3.04	3.78	3.24	3.64	3.16	3.72	3.90
CO_{2C}	24.78	26.68	26.81	20.57	25.12	20.78	29.68	20.04	26.10	20.45	21.45
Total	**98.07**	**99.85**	**100.68**	**100.22**	**99.52**	**100.76**	**101.14**	**98.01**	**99.45**	**99.20**	**100.02**

	MAS014 N = 4	MAS017 N = 3	MAS017 N = 3	MAS019 N = 3	MAS019 N = 4	MAS021 N = 2	MAS022 N = 3	MAS022 N = 17	MAS022 N = 5	MAS023 N = 3	MAS023 N = 4

Structural formulae calculated on the # of ions in each respected mineral type (bastnaesite = 4; synchysite = 7; parisite = 11; röentgenite = 18)

	MAS014 N = 4	MAS017 N = 3	MAS017 N = 3	MAS019 N = 3	MAS019 N = 4	MAS021 N = 2	MAS022 N = 3	MAS022 N = 17	MAS022 N = 5	MAS023 N = 3	MAS023 N = 4
S	-	-	-	-	-	-	-	-	-	-	0.021
Si	0.035	0.078	0.060	0.014	0.034	0.022	0.178	0.012	0.044	0.017	0.026
Th	0.004	0.017	0.017	-	-	-	0.063	0.002	0.013	0.002	0.017
Y	0.006	0.081	0.074	-	0.044	0.012	0.028	-	0.005	-	0.014
La	0.502	0.376	0.683	0.331	0.436	0.287	0.510	0.295	0.477	0.316	0.248
Ce	0.925	0.735	1.300	0.475	0.898	0.459	0.873	0.500	0.820	0.454	0.401
Pr	0.095	0.077	0.150	0.034	0.100	0.052	0.072	0.040	0.062	0.042	0.039
Nd	0.275	0.247	0.401	0.099	0.343	0.124	0.232	0.115	0.189	0.116	0.127
Sm	0.022	0.014	0.037	0.013	0.032	0.017	0.011	0.006	0.028	0.008	0.007
Gd	-	-	-	-	-	-	-	-	-	-	-
Dy	-	-	-	-	-	-	-	-	-	-	-
Er	-	-	-	-	-	-	-	-	-	-	-
Fe^{3+}	0.019	0.154	0.064	0.001	0.032	-	0.433	-	0.135	0.003	0.002
Ca	1.056	0.779	2.007	0.014	0.956	0.016	1.748	0.028	0.958	0.026	0.064
Sr	0.006	0.034	0.052	0.003	0.009	-	-	-	-	-	0.009
F	2.000	2.000	2.998	1.000	2.000	1.000	3.001	1.000	2.000	1.000	1.000
CO_2	3.000	3.000	5.000	1.000	3.000	1.000	5.000	1.000	3.000	1.000	1.000
Total	**7.971**	**7.630**	**12.893**	**3.000**	**7.917**	**2.998**	**12.158**	**3.004**	**7.731**	**2.984**	**2.976**

	MAS025 N = 3	MAS026 N = 3	MAS026 N = 3	MAS028 N = 3	MAS028 N = 3	MAS032 N = 4	MAS032 N = 4	MAS033 N = 2	MAS033 N = 2	MAS034 N = 2	MAS034 N = 2
Wt. %											
SO_3	-	-	-	-	-	-	-	-	-	-	-
SiO_2	0.22	0.51	0.30	0.35	2.10	1.70	0.81	0.97	1.99	1.05	1.25
ThO_2	2.24	-	0.40	0.41	4.70	-	-	2.01	4.29	1.07	2.11
Y_2O_3	-	0.51	-	-	2.19	2.68	0.33	0.59	0.46	0.53	0.54
La_2O_3	15.99	12.55	18.48	21.65	11.98	9.19	19.81	18.99	17.50	20.59	17.50
Ce_2O_3	31.18	24.03	36.09	36.21	24.36	19.74	36.11	31.54	27.69	30.37	29.21
Pr_2O_3	2.87	2.67	3.84	2.58	2.61	2.64	3.29	2.76	1.99	3.83	3.18
Nd_2O_3	10.73	8.02	11.10	11.77	9.73	8.97	11.12	7.53	6.59	9.90	8.52
Sm_2O_3	0.64	0.63	1.41	0.85	1.09	1.03	1.29	0.85	0.55	0.67	0.84
Gd_2O_3	-	-	-	-	-	-	-	-	-	-	-
Dy_2O_3	-	-	-	-	-	-	-	-	-	-	-
Er_2O_3	-	-	-	-	-	-	-	-	-	-	-
Fe_2O_3	-	1.40	0.30	0.18	8.79	0.70	0.36	3.80	5.61	2.19	1.89
CaO	7.97	17.93	0.44	0.25	2.96	18.00	0.46	2.35	4.06	1.53	6.08
SrO	-	-	-	-	0.35	0.18	0.12	0.40	0.30	0.53	0.71
Total	**71.84**	**68.50**	**72.65**	**74.25**	**70.86**	**65.37**	**73.98**	**72.03**	**71.39**	**72.26**	**71.83**
F_C	6.90	6.18	8.63	8.72	10.25	6.24	8.98	9.41	10.02	9.11	9.58
$O=F$	2.91	2.60	3.63	3.67	4.32	2.63	3.78	3.96	4.22	3.84	4.03
CO_{2C}	23.97	28.63	20.00	20.19	23.75	28.94	20.80	21.80	23.21	21.10	22.20
Total	**99.80**	**100.71**	**97.65**	**99.49**	**100.54**	**97.92**	**99.98**	**99.28**	**100.40**	**98.63**	**99.58**

	MAS025 N = 3	MAS026 N = 3	MAS026 N = 3	MAS028 N = 3	MAS028 N = 3	MAS032 N = 4	MAS032 N = 4	MAS033 N = 2	MAS033 N = 2	MAS034 N = 2	MAS034 N = 2

Structural formulae calculated on the # of ions in each respected mineral type (bastnaesite = 4; synchysite = 7; parisite = 11; röentgenite = 18)

	MAS025	MAS026	MAS026	MAS028	MAS028	MAS032	MAS032	MAS033	MAS033	MAS034	MAS034
S	-	-	-	-	-	-	-	-	-	-	-
Si	0.020	0.026	0.011	0.013	0.065	0.086	0.029	0.033	0.063	0.036	0.041
Th	0.047	-	0.003	0.003	0.033	-	-	0.015	0.031	0.008	0.016
Y	-	0.014	-	-	0.036	0.072	0.006	0.011	0.008	0.010	0.009
La	0.541	0.237	0.250	0.290	0.136	0.172	0.257	0.235	0.204	0.264	0.213
Ce	1.047	0.450	0.484	0.481	0.275	0.366	0.466	0.388	0.320	0.386	0.353
Pr	0.096	0.050	0.051	0.034	0.029	0.049	0.042	0.034	0.023	0.048	0.038
Nd	0.351	0.147	0.145	0.152	0.107	0.162	0.140	0.090	0.074	0.123	0.100
Sm	0.020	0.011	0.018	0.011	0.012	0.018	0.016	0.010	0.006	0.008	0.010
Gd	-	-	-	-	-	-	-	-	-	-	-
Dy	-	-	-	-	-	-	-	-	-	-	-
Er	-	-	-	-	-	-	-	-	-	-	-
Fe^{3+}	-	0.018	0.001	0.001	0.037	0.009	0.001	0.016	0.023	0.009	0.008
Ca	0.783	0.983	0.017	0.010	0.098	0.976	0.017	0.085	0.137	0.057	0.215
Sr	-	-	-	-	0.006	0.005	0.002	0.008	0.005	0.011	0.014
F	2.001	1.000	1.000	1.000	1.000	0.999	1.000	1.000	1.000	1.000	1.000
CO_2	3.000	2.000	1.000	1.000	1.000	2.000	1.000	1.000	1.000	1.000	1.000
Total	**7.906**	**4.951**	**2.993**	**2.995**	**2.835**	**4.946**	**2.988**	**2.935**	**2.907**	**2.960**	**3.018**

	MAS034 N = 2	MAS035 N = 3	MAS035 N = 2	MAS036 N = 2	MAS036 N = 3	MAS037 N = 4	MAS040 N = 4	MAS040 N = 5
Wt. %								
SO_3	-	-	-	-	-	-	-	-
SiO_2	0.72	0.73	0.62	0.89	1.00	0.42	0.37	0.27
ThO_2	1.19	1.97	0.51	0.88	0.87	0.29	-	-
Y_2O_3	1.03	0.85	0.45	0.46	0.69	-	-	-
La_2O_3	16.83	10.22	16.27	11.56	10.70	24.67	26.02	16.92
Ce_2O_3	27.68	17.71	25.63	19.93	20.70	35.78	37.20	31.57
Pr_2O_3	2.71	1.65	3.16	2.43	2.81	3.11	2.94	2.92
Nd_2O_3	8.07	6.02	8.25	6.62	8.82	7.37	7.88	9.57
Sm_2O_3	0.70	0.72	0.70	0.50	1.17	0.34	0.29	0.81
Gd_2O_3	-	-	-	-	-	-	-	-
Dy_2O_3	-	-	-	-	-	-	-	-
Er_2O_3	-	-	-	-	-	-	-	-
Fe_2O_3	1.89	8.35	4.06	9.43	4.68	-	-	-
CaO	9.00	17.21	9.68	13.55	15.53	0.34	0.14	8.84
SrO	0.55	0.26	0.21	-	-	-	0.26	0.18
Total	**70.37**	**66.09**	**69.86**	**66.75**	**67.14**	**73.01**	**75.10**	**71.08**
F_C	7.21	6.54	7.53	7.46	7.20	8.81	8.81	6.95
$O=F$	3.04	2.75	3.17	3.14	3.03	3.71	3.71	2.93
CO_{2C}	25.05	30.28	26.15	28.82	27.79	20.40	20.41	24.15
Total	**99.59**	**100.16**	**100.37**	**99.89**	**99.10**	**98.51**	**100.61**	**99.25**

	MAS034 N = 2	MAS035 N = 3	MAS035 N = 2	MAS036 N = 2	MAS036 N = 3	MAS037 N = 4	MAS040 N = 4	MAS040 N = 5

Structural formulae calculated on the # of ions in each respected mineral type (bastnaesite = 4; synchysite = 7; parisite = 11; röentgenite = 18)

	MAS034	MAS035	MAS035	MAS036	MAS036	MAS037	MAS040	MAS040
S	-	-	-	-	-	-	-	-
Si	0.063	0.035	0.052	0.113	0.132	0.015	0.013	0.025
Th	0.024	0.022	0.010	0.025	0.026	0.002	-	-
Y	0.048	0.022	0.020	0.031	0.048	-	-	-
La	0.545	0.182	0.504	0.542	0.520	0.327	0.344	0.568
Ce	0.889	0.314	0.788	0.927	0.999	0.470	0.489	1.052
Pr	0.087	0.029	0.097	0.113	0.135	0.041	0.038	0.097
Nd	0.253	0.104	0.248	0.300	0.415	0.094	0.101	0.311
Sm	0.021	0.012	0.020	0.022	0.053	0.004	0.004	0.025
Gd	-	-	-	-	-	-	-	-
Dy	-	-	-	-	-	-	-	-
Er	-	-	-	-	-	-	-	-
Fe^{3+}	0.045	0.105	0.104	0.351	0.180	-	-	-
Ca	0.846	0.892	0.871	1.845	2.193	0.013	0.005	0.862
Sr	0.028	0.007	0.010	-	-	-	0.005	0.009
F	2.001	1.000	2.001	2.998	3.001	1.000	1.000	2.000
CO_2	3.000	2.000	3.000	5.000	5.000	1.000	1.000	3.000
Total	**7.850**	**4.743**	**7.753**	**12.330**	**12.728**	**2.990**	**2.999**	**7.949**

III.IX Kainosite and altered variety (carbon and hydrogen calculated assuming full occupancy)

	MAS003 N = 2	MAS014 N = 3	MAS014 N = 2	MAS024 N = 3	MAS024 N = 2	MAS032 N = 4
Wt. %						
SiO_2	21.24	21.53	19.07	16.04	19.59	22.28
Al2O3	0.33	0.15	-	0.10	-	1.15
Y_2O_3	-	2.58	2.20	6.09	5.88	7.29
La_2O_3	13.53	10.09	10.42	13.19	13.22	12.98
Ce_2O_3	29.72	27.25	26.39	24.12	24.29	24.28
Pr_2O_3	3.45	3.51	2.41	2.16	2.36	2.02
Nd_2O_3	11.20	11.59	9.57	7.24	7.54	6.40
Sm_2O_3	1.41	1.54	1.21	0.76	1.04	0.99
Gd_2O_3	-	-	-	0.59	0.22	0.56
Tb_2O_3	-	-	-	0.11	-	0.22
Dy_2O_3	-	-	-	0.49	0.15	0.45
Ho_2O_3	-	-	-	-	-	-
Er_2O_3	-	-	-	0.26	-	0.31
Yb_2O_3	-	-	-	0.31	0.31	0.47
CaO	11.70	10.99	13.20	3.56	4.24	3.96
FeO*	0.85	0.60	0.91	1.88	1.96	0.86
Total**	**93.43**	**89.83**	**85.38**	**76.90**	**80.80**	**84.22**
CO_{2C}	5.00	4.90	4.62	3.90	4.33	4.73
H_2O_C	2.05	2.01	1.89	1.60	1.77	1.93
Total	**100.48**	**96.74**	**91.89**	**82.40**	**86.90**	**90.88**

III.X Magnetite and ilmenite [Fe^{2+}/Fe^{3+} recalculated using the method of Carmichael (1967)]

	MAS001 N = 4	MAS001 N = 3	MAS007 N = 3	MAS007 N = 3	MAS009 N = 5	MAS009 N = 5	MAS013 N = 3	MAS013 N = 4
Wt. %								
Nb_2O_5	-	-	-	0.38	-	2.97	-	-
SiO_2	0.38	0.32	0.30	0.28	0.41	0.32	0.37	0.30
TiO_2	3.82	50.49	2.04	50.27	1.62	47.27	2.29	49.78
Al_2O_3	0.46	0.10	0.19	0.04	-	-	0.18	0.19
Fe_2O_3	60.42	3.42	63.38	3.26	64.52	7.16	63.72	4.42
FeO	35.29	43.82	32.99	44.06	32.92	40.11	33.80	42.14
MnO	-	1.96	0.04	1.48	-	2.76	-	2.96
CaO	-	-	-	-	-	-	-	-
Total	**100.37**	**100.11**	**98.94**	**99.77**	**99.47**	**100.59**	**100.36**	**99.79**

Structural formulae calculated on the basis of 4 (magnetite) and 3 (ilmenite) oxygens

Nb	-	-	-	0.005	-	0.039	-	-
Si	0.014	0.008	0.012	0.007	0.016	0.008	0.014	0.008
Ti	0.109	0.958	0.060	0.959	0.047	0.904	0.066	0.947
Al	0.021	0.003	0.009	0.001	-	-	0.008	0.006
Fe^{3+}	1.732	0.065	1.849	0.062	1.874	0.137	1.832	0.084
Fe^{2+}	1.124	0.924	1.070	0.934	1.063	0.853	1.080	0.892
MnO	-	0.042	0.001	0.032	-	0.059	-	0.063
Ca	-	-	-	-	-	-	-	-
Total	**3.000**	**2.000**	**3.001**	**2.000**	**3.000**	**2.000**	**3.000**	**2.000**

Magnetite ternary values (Andersen 1998)

FeO	52.24		51.20		50.96		51.34	
TiO_2	3.37		1.80		1.43		2.01	
Fe_2O_3	44.39		47.00		47.61		46.65	

Ilmenite ternary values (Andersen 1998)

FeO		48.09		48.20		46.05		47.54
TiO_2		48.09		48.20		46.05		47.54
Fe_2O_3		3.82		3.60		7.90		4.92

	MAS013 N = 3	MAS013 N = 4	MAS017 N = 5	MAS017 N = 3	MAS018 N = 3	MAS018 N = 3	MAS019 N = 4	MAS019 N = 3
Wt. %								
Nb_2O_5	-	-	-	0.31	-	-	-	1.38
SiO_2	0.37	0.35	-	0.30	0.35	0.33	0.37	0.33
TiO_2	1.91	50.12	0.49	50.95	0.86	49.17	2.65	49.17
Al_2O_3	0.53	0.16	0.11	0.09	0.04	-	0.07	-
Fe_2O_3	64.05	3.71	67.66	2.50	66.27	5.07	62.97	5.07
FeO	33.51	42.93	31.12	40.34	32.01	42.20	34.03	42.20
MnO	-	2.54	-	4.88	0.21	2.40	-	2.40
CaO	-	-	0.22	0.71	-	-	-	-
Total	**100.37**	**99.81**	**99.60**	**100.08**	**99.74**	**99.17**	**100.09**	**100.55**

Structural formulae calculated on the basis of 4 (magnetite) and 3 (ilmenite) oxygens

Nb	-	-	-	0.004	-	-	-	0.018
Si	0.014	0.009	-	0.008	0.013	0.008	0.014	0.008
Ti	0.055	0.953	0.014	0.965	0.025	0.943	0.076	0.934
Al	0.024	0.005	0.005	0.003	0.002	-	0.003	-
Fe^{3+}	1.838	0.071	1.967	0.047	1.921	0.097	1.816	0.096
Fe^{2+}	1.069	0.908	1.005	0.850	1.032	0.90	1.091	0.891
MnO	-	0.054	-	0.104	0.007	0.052	-	0.051
Ca	-	-	0.009	0.019	-	-	-	-
Total	**3.000**	**2.000**	**3.000**	**2.000**	**3.000**	**2.000**	**3.000**	**1.998**

Magnetite ternary values (Andersen 1998)

FeO	51.12		50.29		50.44		51.55	
TiO_2	1.69		0.42		0.66		2.33	
Fe_2O_3	47.19		49.29		48.90		46.12	

Ilmenite ternary values (Andersen 1998)

FeO		47.89		48.98		47.20		47.20
TiO_2		47.89		48.98		47.20		47.20
Fe_2O_3		4.22		2.04		5.60		5.60

	MAS022 N = 3	MAS022 N = 5	MAS023 N =3	MAS023 N = 4	MAS024 N = 4	MAS024 N = 4	MAS030 N = 3	MAS030 N = 3
Wt. %								
Nb_2O_5	-	-	-	0.72	-	0.92	-	0.50
SiO_2	0.27	0.20	0.46	0.29	0.39	0.26	0.30	0.25
TiO_2	1.91	51.28	0.86	49.87	0.87	50.10	4.95	50.77
Al_2O_3	0.32	0.16	0.15	0.04	-	0.13	0.18	0.13
Fe_2O_3	64.34	2.26	65.75	3.99	66.36	2.55	58.96	2.34
FeO	33.09	50.62	32.34	41.64	32.28	31.11	36.14	43.81
MnO	0.16	5.68	-	3.52	0.07	14.09	0.14	2.13
CaO	-	-	-	-	-	-	-	-
Total	**100.09**	**100.20**	**99.56**	**100.07**	**99.97**	**99.16**	**100.67**	**99.93**

Structural formulae calculated on the basis of 4 (magnetite) and 3 (ilmenite) oxygens

	MAS022 N = 3	MAS022 N = 5	MAS023 N =3	MAS023 N = 4	MAS024 N = 4	MAS024 N = 4	MAS030 N = 3	MAS030 N = 3
Nb	-	-	-	0.009	-	0.012	-	0.009
Si	0.010	0.005	0.018	0.007	0.015	0.007	0.011	0.007
Ti	0.055	0.971	0.025	0.494	0.025	0.961	0.142	0.962
Al	0.014	0.005	0.007	0.001	-	0.004	0.008	-
Fe^{3+}	1.855	0.043	1.908	0.076	1.920	0.049	1.686	0.054
Fe^{2+}	1.060	0.855	1.043	0.881	1.038	0.663	1.148	0.927
MnO	0.005	0.121	-	0.075	0.002	0.304	0.005	0.042
Ca	-	-	-	-	-	-	-	-
Total	**2.999**	**2.000**	**3.001**	**2.000**	**3.000**	**2.000**	**3.000**	**2.001**

Magnetite ternary values (Andersen 1998)

	MAS022 N = 3	MAS022 N = 5	MAS023 N =3	MAS023 N = 4	MAS024 N = 4	MAS024 N = 4	MAS030 N = 3	MAS030 N = 3
FeO	51.07		50.51		50.49		51.50	
TiO_2	1.61		0.76		0.73		2.24	
Fe_2O_3	47.32		48.73		48.78		46.26	

Ilmenite ternary values (Andersen 1998)

	MAS022 N = 3	MAS022 N = 5	MAS023 N =3	MAS023 N = 4	MAS024 N = 4	MAS024 N = 4	MAS030 N = 3	MAS030 N = 3
FeO		48.63		47.73		47.98		48.41
TiO_2		48.63		47.73		47.98		48.41
Fe_2O_3		2.74		4.54		4.04		3.18

	MAS032 N = 3	MAS032 N = 3	MAS033 N = 3	MAS033 N = 5	MAS036 N = 5	MAS036 N = 3	MAS037 N = 3	MAS037 N = 3
Wt. %								
Nb_2O_5	-	0.75	-	0.75	-	1.57	-	0.62
SiO_2	0.30	0.32	0.36	0.34	0.27	0.29	0.41	0.38
TiO_2	1.44	50.10	0.66	50.67	1.14	48.54	0.84	49.55
Al_2O_3	0.20	-	0.26	-	0.50	0.12	0.38	0.14
Fe_2O_3	65.68	3.62	65.86	3.25	65.17	5.91	65.75	4.29
FeO	32.86	31.76	31.60	41.19	32.28	32.94	32.12	34.19
MnO	0.13	13.14	0.17	4.74	0.09	10.93	0.22	10.70
CaO	-	0.30	0.07	-	-	-	-	-
Total	**100.61**	**99.99**	**98.98**	**100.94**	**99.45**	**100.30**	**99.72**	**99.87**

Structural formulae calculated on the basis of 4 (magnetite) and 3 (ilmenite) oxygens

Nb	-	0.007	-	0.010	-	0.010	-	0.020
Si	0.011	0.006	0.014	0.008	0.010	0.009	0.016	0.007
Ti	0.041	0.966	0.019	0.953	0.033	0.956	0.024	0.924
Al	0.009	0.004	0.012	-	0.023	-	0.017	0.004
Fe^{3+}	1.885	0.045	1.922	0.069	1.890	0.061	1.903	0.113
Fe^{2+}	1.049	0.927	1.025	0.671	1.041	0.864	1.033	0.697
MnO	0.004	0.046	0.006	0.281	0.003	0.101	0.007	0.234
Ca	-	-	0.003	0.008	-	-	-	-
Total	**2.999**	**2.001**	**3.001**	**2.000**	**3.000**	**2.001**	**3.000**	**1.999**

Magnetite ternary values (Andersen 1998)

FeO	52.84		50.80		50.34		50.65	
TiO_2	4.25		1.20		0.51		0.98	
Fe_2O_3	42.91		48.00		49.15		48.37	

Ilmenite ternary values (Andersen 1998)

FeO		48.66		47.56		48.04		46.01
TiO_2		48.66		47.56		48.04		46.01
Fe_2O_3		2.68		4.88		3.92		7.98

III.XI Monazite and rhabdophane

	MAS003 N = 1	MAS003 N = 1	MAS004 N = 2	MAS004 N = 2	MAS004 N = 2	MAS005 N = 3	MAS005 N = 3
Wt. %							
SO_3	-	-	-	-	-	0.82	-
P_2O_5	28.42	29.82	30.48	30.35	29.61	20.70	28.12
SiO_2	2.14	0.89	0.93	0.97	1.27	5.92	1.85
ThO_2	0.78	-	0.95	0.31	1.83	0.30	0.65
Al_2O_3	0.36	0.39	-	-	-	0.37	0.35
Fe_2O_3	-	0.63	-	-	-	0.73	0.25
Y_2O_3	-	-	0.20	0.56	0.80	0.33	1.40
La_2O_3	14.98	15.86	11.86	10.70	10.29	16.74	14.58
Ce_2O_3	36.60	34.39	31.96	31.92	30.36	32.75	31.78
Pr_2O_3	3.27	3.95	3.74	4.25	4.24	2.41	3.45
Nd_2O_3	9.89	11.57	15.11	16.05	15.55	7.14	13.09
Sm_2O_3	1.13	1.32	2.59	2.78	3.01	0.30	1.23
Gd_2O_3	-	-	-	-	-	-	-
Dy_2O_3	-	-	-	-	-	-	-
CaO	0.93	0.55	0.60	0.73	1.07	2.86	1.86
SrO	0.60	0.26	0.63	0.66	0.55	0.81	0.55
Total	**99.10**	**99.63**	**99.05**	**99.28**	**98.58**	**92.18**	**99.16**
Structural formulae calculated on the basis of 4 oxygen							
S	-	-	-	-	-	0.025	-
P	0.936	0.973	0.997	0.991	0.976	0.734	0.925
Si	0.083	0.034	0.036	0.037	0.049	0.248	0.072
Th	0.007	-	0.008	0.003	0.016	0.003	0.006
Al	0.017	0.018	-	-	-	0.018	0.016
Fe	-	0.018	-	-	-	0.026	0.007
Y	-	-	0.004	0.011	0.017	0.007	0.029
La	0.215	0.226	0.169	0.152	0.148	0.259	0.209
Ce	0.521	0.486	0.452	0.451	0.433	0.502	0.452
Pr	0.046	0.055	0.053	0.060	0.060	0.037	0.049
Nd	0.137	0.159	0.208	0.221	0.216	0.107	0.182
Sm	0.015	0.018	0.034	0.037	0.040	0.004	0.016
Gd	-	-	-	-	-	-	-
Dy	-	-	-	-	-	-	-
Ca	0.039	0.023	0.025	0.030	0.045	0.128	0.077
Sr	0.014	0.006	0.014	0.015	0.012	0.020	0.012
Total	**2.030**	**2.016**	**2.000**	**2.008**	**2.013**	**2.118**	**2.054**

	MAS009 N = 5	MAS009 N = 3	MAS010 N = 5	MAS011 N = 2	MAS011 N = 2	MAS011 N = 2	MAS014 N = 4
Wt. %							
SO_3	-	-	-	-	-	-	-
P_2O_5	28.68	29.55	30.98	30.51	30.54	29.31	27.34
SiO_2	0.97	1.44	1.67	0.92	1.06	1.48	1.97
ThO_2	0.25	0.33	0.62	0.23	0.48	1.23	2.00
Al_2O_3	0.49	-	-	-	-	-	0.28
Fe_2O_3	0.37	-	0.25	-	-	-	0.26
Y_2O_3	0.99	1.48	-	-	-	-	0.53
La_2O_3	15.42	14.31	10.60	12.51	10.02	11.57	21.38
Ce_2O_3	32.68	31.97	30.99	33.58	32.09	33.29	34.26
Pr_2O_3	3.78	3.92	3.58	3.76	4.19	3.87	2.65
Nd_2O_3	13.19	13.43	14.21	15.13	17.65	14.49	8.44
Sm_2O_3	1.34	0.40	1.89	1.86	2.81	1.64	0.28
Gd_2O_3	-	-	-	-	-	-	-
Dy_2O_3	-	-	-	-	-	-	-
CaO	0.63	2.84	4.14	0.38	0.25	0.66	0.03
SrO	0.39	0.62	0.41	0.38	0.60	0.54	0.41
Total	**99.18**	**100.29**	**99.34**	**99.26**	**99.69**	**98.08**	**99.83**
Structural formulae calculated on the basis of 4 oxygen							
S	-	-	-	-	-	-	-
P	0.952	0.951	0.975	0.997	0.995	0.973	0.917
Si	0.038	0.055	0.062	0.036	0.041	0.058	0.078
Th	0.002	0.003	0.005	0.002	0.004	0.011	0.018
Al	0.023	-	-	-	-	-	0.013
Fe	0.011	-	0.007	-	-	-	0.008
Y	0.021	0.030	-	-	-	-	0.011
La	0.223	0.201	0.145	0.178	0.142	0.167	0.312
Ce	0.469	0.445	0.422	0.475	0.452	0.478	0.497
Pr	0.054	0.054	0.049	0.053	0.059	0.055	0.038
Nd	0.185	0.182	0.189	0.209	0.243	0.203	0.119
Sm	0.018	0.005	0.024	0.025	0.037	0.022	0.004
Gd	-	-	-	-	-	-	-
Dy	-	-	-	-	-	-	-
Ca	0.026	0.116	0.165	0.016	0.010	0.028	0.001
Sr	0.009	0.014	0.009	0.009	0.013	0.012	0.009
Total	**2.030**	**2.056**	**2.052**	**1.998**	**1.996**	**2.008**	**2.027**

	MAS018 N = 4	MAS022 N = 4	MAS023 N = 4	MAS024 N = 3	MAS024 N = 1	MAS025 N = 2	MAS025 N = 2
Wt. %							
SO_3	-	-	-	-	-	-	5.41
P_2O_5	29.73	29.16	29.46	28.30	28.18	28.46	25.06
SiO_2	0.63	0.87	0.32	2.14	1.87	2.05	0.49
ThO_2	0.78	1.18	0.99	4.19	4.50	2.71	0.52
Al_2O_3	0.38	0.32	0.64	-	-	-	0.85
Fe_2O_3	-	-	-	-	-	-	3.23
Y_2O_3	-	0.35	0.10	-	-	-	2.78
La_2O_3	12.48	24.53	17.55	18.55	25.46	14.23	9.61
Ce_2O_3	34.52	32.71	33.42	34.28	31.48	34.26	23.20
Pr_2O_3	4.18	2.38	3.27	2.74	2.60	3.40	2.87
Nd_2O_3	13.55	6.64	10.29	8.04	4.56	12.33	9.98
Sm_2O_3	2.57	0.62	1.17	0.54	0.21	1.56	0.84
Gd_2O_3	1.48	0.61	1.17	-	-	-	-
Dy_2O_3	0.27	0.12	-	-	-	-	-
CaO	-	0.16	0.64	1.05	1.47	0.18	4.44
SrO	-	-	-	-	-	-	-
Total	**100.57**	**99.65**	**100.31**	**99.83**	**100.33**	**99.18**	**89.28**
Structural formulae calculated on the basis of 4 oxygen							
S	-	-	-	-	-	-	0.150
P	0.979	0.966	0.968	0.936	0.932	0.947	0.817
Si	0.025	0.034	0.038	0.084	0.073	0.081	0.019
Th	0.007	0.011	0.017	0.037	0.040	0.024	0.005
Al	0.017	0.015	0.015	-	-	-	0.039
Fe	-	-	-	-	-	-	0.104
Y	-	0.007	0.002	-	-	-	0.057
La	0.179	0.354	0.251	0.267	0.367	0.206	0.136
Ce	0.492	0.469	0.475	0.490	0.450	0.493	0.327
Pr	0.059	0.034	0.046	0.039	0.037	0.049	0.040
Nd	0.188	0.093	0.143	0.112	0.064	0.173	0.137
Sm	0.034	0.008	0.016	0.007	0.003	0.021	0.011
Gd	0.019	0.008	0.015	-	-	-	-
Dy	0.003	0.002	-	-	-	-	-
Ca	-	0.007	0.027	0.044	0.062	0.008	0.183
Sr	-	-	-	-	-	-	-
Total	**2.003**	**2.008**	**2.012**	**2.017**	**2.028**	**2.003**	**2.025**

	MAS025 N = 2	MAS025 N = 2	MAS029 N = 5	MAS036 N = 4
Wt. %				
SO$_3$	10.09	15.82	-	-
P$_2$O$_5$	22.23	20.13	28.54	28.86
SiO$_2$	0.65	1.60	1.09	1.07
ThO$_2$	0.38	1.03	0.81	0.68
Al$_2$O$_3$	1.26	0.54	-	0.30
Fe$_2$O$_3$	6.30	1.94	0.38	0.47
Y$_2$O$_3$	1.87	-	1.58	1.10
La$_2$O$_3$	8.68	11.58	16.86	13.20
Ce$_2$O$_3$	21.31	27.89	33.98	33.76
Pr$_2$O$_3$	2.46	2.62	3.21	3.91
Nd$_2$O$_3$	9.02	9.87	11.07	14.33
Sm$_2$O$_3$	0.91	1.23	1.37	1.41
Gd$_2$O$_3$	-	-	-	-
Dy$_2$O$_3$	-	-	-	-
CaO	4.87	1.49	0.21	0.63
SrO	-	-	-	-
Total	**90.03**	**95.74**	**99.10**	**99.72**
Structural formulae calculated on the basis of 4 oxygen				
S	0.263	0.398	-	-
P	0.682	0.595	0.955	0.953
Si	0.024	0.056	0.043	0.042
Th	0.003	0.008	0.007	0.006
Al	0.054	0.022	-	0.014
Fe	0.191	0.057	0.011	0.014
Y	0.036	-	0.033	0.023
La	0.116	0.149	0.246	0.190
Ce	0.283	0.357	0.491	0.482
Pr	0.033	0.033	0.046	0.056
Nd	0.117	0.123	0.156	0.200
Sm	0.011	0.015	0.019	0.019
Gd	-	-	-	-
Dy	-	-	-	-
Ca	0.189	0.056	0.009	0.026
Sr	-	-	-	-
Total	**2.002**	**1.869**	**2.017**	**2.024**

III.XII Pyrochlore

	MAS003 N = 3	MAS003 N = 3	MAS003 N = 8	MAS006 N = 2	MAS006 N = 3	MAS008 N = 1	MAS008 N = 1
Wt. %							
WO_3	1.13	1.66	1.61	1.59	3.73	2.11	1.00
Nb_2O_5	48.23	46.41	53.83	48.59	54.92	53.21	50.98
Ta_2O_5	4.23	3.17	3.69	3.56	4.76	4.94	2.87
SiO_2	-	2.70	-	3.67	1.32	2.35	3.77
TiO_2	7.16	3.53	5.51	6.74	6.39	4.66	5.54
ZrO_2	-	-	-	-	-	-	-
ThO_2	1.22	1.35	1.19	0.52	0.96	0.71	0.88
UO_2	12.01	4.02	5.44	5.10	3.53	1.75	2.17
Al_2O_3	-	-	-	0.33	0.26	0.68	0.52
Y_2O_3	-	0.91	0.08	2.38	0.48	2.55	1.41
La_2O_3	0.08	1.18	0.09	0.54	-	0.77	1.44
Ce_2O_3	2.22	6.47	1.74	5.00	1.65	2.59	2.98
Pr_2O_3	0.39	1.11	0.32	0.88	0.25	-	-
Nd_2O_3	0.86	5.11	0.82	3.60	0.85	4.94	2.87
Sm_2O_3	0.39	1.26	0.21	0.80	0.11	-	-
Fe_2O_3	2.28	3.46	4.97	4.41	4.01	4.58	4.69
MnO	-	-	-	0.37	0.55	-	0.50
CaO	15.42	10.33	17.75	6.44	12.64	9.61	10.46
SrO	-	0.28	0.08	-	-	-	-
Na_2O	0.18	-	0.20	-	-	-	-
Total	**95.80**	**92.95**	**97.53**	**94.52**	**96.41**	**96.45**	**92.08**

	MAS003 N = 3	MAS003 N = 3	MAS003 N = 8	MAS006 N = 2	MAS006 N = 3	MAS008 N = 1	MAS008 N = 1

Structural formulae calculated on the basis of 2 anions (O,F)

	MAS003 N=3	MAS003 N=3	MAS003 N=8	MAS006 N=2	MAS006 N=3	MAS008 N=1	MAS008 N=1
W	0.019	0.029	0.025	0.023	0.054	0.031	0.014
Nb	1.451	1.408	1.465	1.242	1.396	1.355	1.284
Ta	0.077	0.058	0.060	0.055	0.073	0.076	0.043
Si	-	0.181	-	0.207	0.074	0.132	0.210
Ti	0.358	0.178	0.249	0.287	0.270	0.197	0.232
Zr	-	-	-	-	-	-	-
Th	0.018	0.021	0.016	0.007	0.012	0.009	0.011
U	0.178	0.060	0.073	0.064	0.044	0.022	0.027
Al	-	-	-	0.022	0.017	0.045	0.034
Y	-	0.032	0.003	0.072	0.014	0.076	0.042
La	0.002	0.029	0.002	0.011	-	0.016	0.030
Ce	0.054	0.159	0.038	0.103	0.034	0.053	0.061
Pr	0.009	0.027	0.007	0.018	0.005	-	-
Nd	0.020	0.123	0.018	0.073	0.017	0.099	0.057
Sm	0.009	0.029	0.004	0.016	0.002	-	-
Fe^{3+}	0.114	0.175	0.225	0.188	0.170	0.194	0.197
Mn	-	-	-	0.018	0.026	-	0.024
Ca	1.099	0.743	1.145	0.390	0.761	0.580	0.624
Sr	-	0.011	0.003	-	-	-	-
Na	0.023	-	0.023	-	-	-	-
Total	**3.431**	**3.263**	**3.356**	**2.796**	**2.969**	**2.885**	**2.890**

Mol %

	MAS003 N=3	MAS003 N=3	MAS003 N=8	MAS006 N=2	MAS006 N=3	MAS008 N=1	MAS008 N=1
Na + Ca	58.93	46.72	60.67	23.08	40.05	33.45	35.39
U + Th	10.30	5.06	4.64	4.20	2.97	1.79	2.16
A-def.	30.77	48.22	34.69	72.72	56.98	64.76	62.45

Mol %

	MAS003 N=3	MAS003 N=3	MAS003 N=8	MAS006 N=2	MAS006 N=3	MAS008 N=1	MAS008 N=1
Nb	76.94	85.65	82.51	78.44	80.28	83.23	82.33
Ta	4.06	3.52	3.44	3.46	4.18	4.65	2.79
Ti	19.00	10.84	14.05	18.10	15.54	12.12	14.88

	MAS008 N = 1	MAS008 N = 1	MAS009 N =3	MAS009 N =2	MAS009 N =5	MAS010 N = 2	MAS010 N = 1
Wt. %							
WO_3	2.16	1.59	-	-	1.61	-	-
Nb_2O_5	45.58	40.97	52.00	59.03	53.25	40.74	41.91
Ta_2O_5	3.78	3.29	1.66	0.09	2.51	1.27	1.35
SiO_2	3.38	3.62	5.06	1.34	3.21	12.51	15.29
TiO_2	5.26	7.12	6.56	6.76	6.72	5.25	5.29
ZrO_2	-	-	-	-	-	-	-
ThO_2	.81	0.84	1.33	0.54	0.89	1.14	0.03
UO_2	4.8	7.23	0.96	-	3.99	6.28	6.13
Al_2O_3	.39	0.32	0.22	-	0.13	-	-
Y_2O_3	3.66	3.75	-	-	-	0.64	0.03
La_2O_3	0.81	0.91	0.64	0.79	0.24	0.34	-
Ce_2O_3	3.66	3.02	2.89	2.47	1.85	3.53	1.78
Pr_2O_3	-	-	0.30	0.45	-	0.44	0.35
Nd_2O_3	2.48	3.29	1.14	1.29	0.77	0.90	0.43
Sm_2O_3	-	-	0.12	0.22	-	0.24	0.14
Fe_2O_3	4.34	4.61	8.41	1.45	4.31	1.56	1.46
MnO	0.48	0.15	0.67	0.15	0.58	-	-
CaO	5.12	5.86	6.83	14.40	7.85	6.30	5.89
SrO	-	-	-	-	-	0.01	0.77
Na_2O	-	-	-	4.03	-	0.11	0.02
Total	**86.71**	**86.57**	**88.79**	**93.01**	**87.91**	**81.26**	**80.87**

	MAS008 N = 1	MAS008 N = 1	MAS009 N =3	MAS009 N =2	MAS009 N =5	MAS010 N = 2	MAS010 N = 1
Structural formulae calculated on the basis of 2 anions (O,F)							
W	0.034	0.026	-	-	0.023	-	-
Nb	1.261	1.149	1.150	1.559	1.322	1.012	0.955
Ta	0.063	0.056	0.022	0.001	0.037	0.019	0.019
Si	0.207	0.225	0.250	0.078	0.176	0.687	0.771
Ti	0.242	0.332	0.243	0.297	0.278	0.217	0.201
Zr	-	-	-	-	-	-	-
Th	0.011	0.012	0.015	0.007	0.011	0.014	-
U	0.065	0.100	0.011	-	0.049	0.077	0.069
Al	0.028	0.023	0.013	-	0.008	-	-
Y	0.119	0.124	-	-	-	0.019	0.001
La	0.018	0.021	0.012	0.017	0.005	0.007	-
Ce	0.082	0.069	0.052	0.053	0.037	0.071	0.033
Pr	-	-	0.005	0.010	-	0.009	0.006
Nd	0.054	0.073	0.020	0.027	0.015	0.018	0.008
Sm	-	-	0.002	0.004	-	0.005	0.002
Fe^{3+}	0.200	0.215	0.312	0.064	0.178	0.065	0.055
Mn	0.025	0.008	0.028	0.007	0.027	-	-
Ca	0.336	0.390	0.361	0.902	0.462	0.371	0.318
Sr	-	-	-	-	-	-	0.023
Na	-	-	-	0.457	-	0.012	0.002
Total	**2.745**	**2.821**	**2.506**	**3.484**	**2.629**	**2.602**	**2.463**
Mol %							
Na + Ca	19.72	22.83	19.20	72.17	24.11	20.44	16.61
U + Th	4.50	6.55	1.35	0.38	3.13	4.86	3.59
A-def.	75.78	70.62	79.45	27.45	72.76	74.70	79.80
Mol %							
Nb	80.53	74.77	81.36	83.93	80.76	81.10	81.34
Ta	4.01	3.62	1.57	0.08	2.29	1.52	1.58
Ti	15.46	21.61	17.07	15.99	16.95	17.38	17.08

	MAS010 N = 1	MAS010 N = 2	MAS010 N = 2	MAS011 N = 6	MAS011 N = 3	MAS012 N = 1	MAS016 N = 1
Wt. %							
WO_3	-	-	1.09	0.90	1.31	-	-
Nb_2O_5	56.13	54.16	58.19	48.57	45.08	54.20	50.01
Ta_2O_5	1.13	2.87	3.05	7.91	11.82	2.65	2.70
SiO_2	5.44	3.21	0.61	4.94	4.75	5.51	2.58
TiO_2	6.09	7.15	5.40	6.55	7.22	4.73	5.37
ZrO_2	-	-	-	-	-	0.64	-
ThO_2	0.69	1.14	0.99	0.83	0.73	0.88	0.63
UO_2	1.91	2.21	1.54	4.61	5.94	4.14	2.96
Al_2O_3	-	-	-	-	-	0.64	0.18
Y_2O_3	0.65	0.29	0.04	3.30	3.77	-	-
La_2O_3	0.76	-	0.07	0.39	0.43	0.44	1.25
Ce_2O_3	3.19	1.78	1.58	3.53	3.62	2.19	2.34
Pr_2O_3	0.10	0.28	0.23	0.55	0.26	-	0.33
Nd_2O_3	1.10	0.47	0.35	2.26	2.36	0.33	0.67
Sm_2O_3	0.39	-	0.38	0.41	0.42	-	0.03
Fe_2O_3	3.92	1.67	3.72	5.23	3.98	8.38	25.50
MnO	-	-	-	0.43	0.44	1.39	1.68
CaO	10.78	5.79	13.89	7.48	5.61	7.88	0.93
SrO	0.53	1.51	1.66	-	-	.63	-
Na_2O	0.22	0.37	2.92	-	-	0.10	0.15
Total	**93.03**	**82.90**	**95.71**	**97.89**	**97.74**	**94.73**	**97.31**

	MAS010 N = 1	MAS010 N = 2	MAS010 N = 2	MAS011 N = 6	MAS011 N = 3	MAS012 N = 1	MAS016 N = 1
Structural formulae calculated on the basis of 2 anions (O,F)							
W	-	-	0.016	0.012	0.018	-	-
Nb	1.313	1.395	1.520	1.158	1.109	1.176	0.916
Ta	0.016	0.044	0.048	0.113	0.175	0.035	0.030
Si	0.281	0.183	0.035	0.261	0.258	0.264	0.105
Ti	0.237	0.306	0.235	0.260	0.295	0.171	0.164
Zr	-	-	-	-	-	0.015	-
Th	0.008	0.015	0.013	0.010	0.009	0.010	0.006
U	0.022	0.028	0.020	0.054	0.072	0.044	0.027
Al	-	-	-	-	-	0.036	0.009
Y	0.018	0.009	0.001	0.093	0.109	-	-
La	0.015	-	0.001	0.008	0.009	0.008	0.019
Ce	0.060	0.037	0.033	0.068	0.072	0.038	0.035
Pr	0.002	0.006	0.005	0.011	0.005	-	0.005
Nd	0.020	0.010	0.007	0.043	0.046	0.006	0.010
Sm	0.007	-	0.008	0.007	0.008	-	-
Fe^{3+}	0.153	0.072	0.162	0.208	0.163	0.303	0.777
Mn	-	-	-	0.019	0.020	0.057	0.058
Ca	0.598	0.353	0.860	0.423	0.327	0.405	0.040
Sr	0.016	0.050	0.056	-	-	0.018	-
Na	0.022	0.041	0.327	-	-	0.009	0.012
Total	**2.788**	**2.549**	**3.347**	**2.748**	**2.695**	**2.595**	**2.213**
Mol %							
Na + Ca	33.28	20.75	62.04	24.14	18.89	22.12	2.78
U + Th	1.62	2.25	1.71	3.66	4.67	2.88	1.74
A-def.	65.1	77.00	36.25	72.20	76.44	75.00	95.48
Mol %							
Nb	83.85	79.90	84.32	75.63	70.22	85.14	82.57
Ta	1.02	2.55	2.66	7.41	11.07	2.50	2.68
Ti	15.13	17.55	13.02	16.96	18.71	12.36	14.75

	MAS016 N = 2	MAS018 N = 1	MAS018 N = 1	MAS018 N = 1	MAS018 N = 1	MAS018 N = 2	MAS019 N = 3
Wt. %							
WO_3	-	-	0.80	1.94	0.97	0.26	-
Nb_2O_5	51.30	38.51	39.71	53.88	43.14	51.50	25.49
Ta_2O_5	2.67	1.86	3.60	3.70	1.69	0.72	3.66
SiO_2	3.22	13.01	11.44	2.35	8.52	5.02	17.48
TiO_2	5.70	6.66	5.70	6.80	7.68	4.82	6.89
ZrO_2	-	1.25	1.21	-	-	-	-
ThO_2	0.56	0.27	-	0.78	0.60	0.64	1.55
UO_2	3.35	-	1.31	0.81	1.13	5.77	10.61
Al_2O_3	0.04	0.85	0.81	0.38	1.57	-	0.75
Y_2O_3	-	-	-	1.38	1.37	1.63	-
La_2O_3	0.79	0.33	-	1.13	0.49	-	0.60
Ce_2O_3	2.08	5.50	5.23	9.96	8.73	4.40	3.23
Pr_2O_3	0.09	-	-	1.60	1.59	0.80	-
Nd_2O_3	0.42	0.48	0.71	5.33	5.39	2.61	0.81
Sm_2O_3	0.09	-	-	0.61	0.89	0.15	-
Fe_2O_3	24.07	2.66	2.02	2.57	2.98	2.57	3.17
MnO	1.75	-	-	-	-	1.49	-
CaO	1.46	8.52	8.56	6.15	4.24	4.07	7.24
SrO	-	-	-	-	-	-	-
Na_2O	0.19	0.35	0.47	-	0.85	-	0.23
Total	**97.78**	**80.25**	**81.57**	**99.37**	**91.83**	**86.45**	**81.71**

	MAS016 N = 2	MAS018 N = 1	MAS018 N = 1	MAS018 N = 1	MAS018 N = 1	MAS018 N = 2	MAS019 N = 3
Structural formulae calculated on the basis of 2 oxygens							
W	-	-	0.011	0.029	0.013	0.004	-
Nb	0.935	0.881	0.952	1.384	1.017	1.367	0.599
Ta	0.028	0.026	0.052	0.057	0.024	0.011	0.052
Si	0.130	0.658	0.606	0.133	0.444	0.295	0.909
Ti	0.173	0.253	0.227	0.290	0.301	0.213	0.270
Zr	-	0.031	0.031	-	-	-	-
Th	0.005	0.003	-	0.010	0.007	0.009	0.018
U	0.030	-	0.015	0.010	0.013	0.075	0.123
Al	0.002	0.051	0.051	0.025	0.096	-	0.046
Y	-	-	-	0.042	0.038	0.051	-
La	0.012	0.006	-	0.024	0.009	-	0.012
Ce	0.031	0.102	0.102	0.207	0.167	0.095	0.062
Pr	0.001	-	-	0.033	0.030	0.017	-
Nd	0.006	0.009	0.013	0.108	0.100	0.055	0.015
Sm	0.001	-	-	0.012	0.016	0.003	-
Fe^{3+}	0.731	0.101	0.081	0.110	0.117	0.114	0.124
Mn	0.060	-	-	-	-	0.074	-
Ca	0.063	0.462	0.486	0.374	0.237	0.256	0.404
Sr	-	-	-	-	-	-	-
Na	0.015	0.034	0.048	-	0.086	-	0.023
Total	**2.223**	**2.617**	**2.675**	**2.848**	**2.715**	**2.639**	**2.657**
Mol %							
Na + Ca	4.13	26.34	28.36	23.77	19.70	15.02	22.32
U + Th	1.86	0.16	0.82	1.30	1.23	4.92	7.38
A-def.	94.01	73.50	70.82	74.93	79.07	80.06	70.30
Mol %							
Nb	82.23	75.95	77.32	79.92	75.78	85.90	65.11
Ta	2.57	2.21	4.22	3.30	1.79	0.73	5.62
Ti	15.20	21.84	18.46	16.78	22.43	13.37	29.27

	MAS020 N = 4	MAS020 N = 3	MAS020 N = 3	MAS021 N = 7	MAS021 N = 3	MAS021 N = 2	MAS022 N = 3
Wt. %							
WO_3	0.68	0.47	-	-	-	-	1.09
Nb_2O_5	55.98	62.52	63.02	33.01	38.13	41.30	64.50
Ta_2O_5	1.40	0.99	0.88	5.49	3.75	2.77	1.33
SiO_2	2.17	0.32	0.67	15.66	11.50	11.29	-
TiO_2	1.42	1.70	5.09	7.12	6.62	5.93	4.73
ZrO_2	-	-	-	2.36	0.81	2.40	-
ThO_2	-	-	-	0.60	0.34	0.48	1.33
UO_2	0.93	-	-	16.10	14.54	9.53	1.09
Al_2O_3	0.18	0.15	0.05	0.51	0.27	0.17	0.15
Y_2O_3	-	-	-	-	-	-	-
La_2O_3	1.96	1.56	0.23	-	-	-	-
Ce_2O_3	6.08	3.59	1.42	2.78	3.42	4.00	0.49
Pr_2O_3	0.67	0.38	0.31	-	-	-	-
Nd_2O_3	2.11	1.09	0.62	0.49	0.99	0.97	0.29
Sm_2O_3	0.28	-	-	-	-	-	-
Fe_2O_3	5.31	0.59	0.27	2.04	1.08	1.26	1.60
MnO	-	0.04	-	-	-	-	-
CaO	9.14	12.45	16.91	6.67	5.40	4.78	18.20
SrO	-	-	-	-	-	-	-
Na_2O	0.03	7.36	7.16	-	-	-	6.48
Total	**88.34**	**93.21**	**96.63**	**92.83**	**86.85**	**84.88**	**101.28**

	MAS020 N = 4	MAS020 N = 3	MAS020 N = 3	MAS021 N = 7	MAS021 N = 3	MAS021 N = 2	MAS022 N = 3
Structural formulae calculated on the basis of 2 oxygens							
W	0.011	0.008	-	-	-	-	0.016
Nb	1.528	1.838	1.701	0.733	0.951	0.996	1.692
Ta	0.023	0.018	0.014	0.073	0.056	0.040	0.021
Si	0.131	0.021	0.040	0.769	0.634	0.602	-
Ti	0.064	0.083	0.229	0.263	0.275	0.238	0.206
Zr	-	-	-	0.057	0.022	0.062	-
Th	-	-	-	0.007	0.004	0.006	0.018
U	0.012	-	-	0.176	0.178	0.113	0.014
Al	0.013	0.011	0.004	0.030	0.018	0.011	0.010
Y	-	-	-	-	-	-	-
La	0.044	0.037	0.005	-	-	-	-
Ce	0.134	0.085	0.031	0.050	0.069	0.078	0.010
Pr	0.015	0.009	0.007	-	-	-	-
Nd	0.045	0.025	0.013	0.009	0.020	0.018	0.006
Sm	0.006	-	-	-	-	-	-
Fe^{3+}	0.241	0.029	0.012	0.075	0.045	0.051	0.070
Mn	-	0.002	-	-	-	-	-
Ca	0.591	0.867	1.082	0.351	0.319	0.273	1.132
Sr	-	-	-	-	-	-	-
Na	0.004	0.928	0.829	-	-	-	0.729
Total	**2.862**	**3.961**	**3.967**	**2.593**	**2.591**	**2.488**	**3.924**
Mol %							
Na + Ca	33.86	97.55	98.30	18.08	16.69	14.33	93.82
U + Th	0.71	-	-	9.41	9.56	6.25	1.60
A-def.	65.43	2.45	1.70	72.51	73.75	79.42	4.58
Mol %							
Nb	94.59	94.81	87.51	68.55	74.19	78.18	88.15
Ta	1.42	0.90	0.73	6.86	4.39	3.15	1.10
Ti	3.99	4.29	11.76	24.59	21.42	18.67	10.75

	MAS023 N = 1	MAS023 N = 2	MAS023 N = 2	MAS023 N = 4	MAS023 N = 1	MAS023 N = 1	MAS024 N = 3
Wt. %							
WO_3	-	-	-	-	-	-	0.91
Nb_2O_5	59.40	40.08	54.06	59.97	58.83	54.97	40.45
Ta_2O_5	1.57	-	-	1.26	1.91	1.20	1.71
SiO_2	0.67	4.44	3.65	1.71	5.02	6.59	5.02
TiO_2	6.39	10.87	9.95	7.00	7.37	8.03	5.30
ZrO_2	-	-	-	-	-	-	1.95
ThO_2	-	1.57	2.66	-	1.88	-	1.18
UO_2	-	0.60	-	0.67	0.67	3.51	2.08
Al_2O_3	-	-	0.13	-	-	-	0.26
Y_2O_3	-	2.77	0.35	-	-	-	1.57
La_2O_3	1.38	1.17	1.06	0.85	0.94	0.05	0.88
Ce_2O_3	2.53	7.03	4.63	1.79	2.13	1.29	6.97
Pr_2O_3	-	1.52	0.98	0.35	0.25	0.33	1.44
Nd_2O_3	0.78	6.72	1.84	0.65	0.47	0.68	7.41
Sm_2O_3	-	2.10	0.43	0.43	-	-	2.32
Fe_2O_3	0.18	5.00	3.78	2.92	4.26	7.09	5.67
MnO	-	-	-	0.66	0.73	0.85	-
CaO	17.73	4.94	9.45	16.87	12.77	7.88	3.70
SrO	-	-	-	-	-	-	-
Na_2O	6.10	-	-	2.27	0.16	0.42	-
Total	**96.73**	**88.81**	**92.97**	**97.40**	**97.39**	**92.89**	**88.82**

	MAS023 N = 1	MAS023 N = 2	MAS023 N = 2	MAS023 N = 4	MAS023 N = 1	MAS023 N = 1	MAS024 N = 3
Structural formulae calculated on the basis of 2 oxygens							
W	-	-	-	-	-	-	0.014
Nb	1.633	1.051	1.267	1.481	1.301	1.152	1.099
Ta	0.026	-	-	0.019	0.025	0.015	0.028
Si	0.041	0.257	0.189	0.093	0.246	0.305	0.302
Ti	0.292	0.474	0.388	0.287	0.271	0.280	0.240
Zr	-	-	-	-	-	-	0.057
Th	-	0.021	0.031	-	0.021	-	0.016
U	-	0.008	-	0.008	0.007	0.036	0.028
Al	-	-	0.008	-	-	-	0.018
Y	-	0.085	0.010	-	-	-	0.050
La	0.031	0.025	0.020	0.017	0.017	0.001	0.020
Ce	0.056	0.149	0.088	0.036	0.038	0.022	0.153
Pr	-	0.032	0.019	0.007	0.004	0.006	0.032
Nd	0.017	0.129	0.034	0.013	0.008	0.011	0.159
Sm	-	0.042	0.008	0.008	-	-	0.048
Fe^{3+}	0.008	0.218	0.147	0.120	0.157	0.247	0.256
Mn	-	-	-	0.031	0.030	0.033	-
Ca	1.155	0.307	0.525	0.987	0.669	0.391	0.238
Sr	-	-	-	-	-	-	-
Na	0.719	-	-	0.240	0.015	0.038	-
Total	**3.978**	**2.798**	**2.734**	**3.347**	**2.809**	**2.537**	**2.758**
Mol %							
Na + Ca	98.86	20.09	28.82	64.98	35.99	22.27	15.49
U + Th	-	1.87	1.72	0.43	1.48	1.88	2.86
A-def.	1.14	78.04	69.46	34.59	62.53	75.85	81.65
Mol %							
Nb	83.69	68.91	76.56	82.86	81.44	79.61	80.43
Ta	1.33	-	-	1.05	1.60	1.05	2.05
Ti	14.98	31.09	23.44	16.09	16.87	19.34	17.52

	MAS025 N = 1	MAS025 N = 1	MAS025 N = 3	MAS026 N = 2	MAS026 N = 1	MAS026 N = 2	MAS026 N = 1
Wt. %							
WO_3	1.46	-	-	0.60	1.24	1.62	0.16
Nb_2O_5	51.12	56.36	55.48	51.85	51.62	63.11	60.02
Ta_2O_5	2.63	2.11	1.99	3.41	4.23	3.37	2.57
SiO_2	2.29	3.59	3.92	2.73	2.53	-	-
TiO_2	7.09	5.00	2.98	4.85	6.33	4.88	4.94
ZrO_2	-	-	-	-	-	-	-
ThO_2	1.23	0.62	0.24	-	-	0.26	2.23
UO_2	2.70	3.54	2.80	2.42	4.28	1.03	-
Al_2O_3	0.37	-	-	0.18	0.20	0.29	0.42
Y_2O_3	-	-	-	-	-	-	-
La_2O_3	0.16	-	0.22	0.96	0.47	0.27	-
Ce_2O_3	1.12	1.43	1.11	1.80	1.04	1.38	1.30
Pr_2O_3	0.39	0.44	0.24	0.07	-	-	-
Nd_2O_3	0.44	0.33	0.65	0.47	0.47	0.23	-
Sm_2O_3	0.02	0.03	0.06	-	-	-	-
Fe_2O_3	25.62	14.40	20.74	21.24	20.13	5.91	13.38
MnO	1.54	1.49	2.02	2.62	2.69	1.22	1.49
CaO	0.88	8.13	3.80	3.05	1.99	15.93	8,67
SrO	-	-	-	-	-	-	-
Na_2O	0.33	0.24	0.20	-	-	0.68	-
Total	**99.39**	**97.71**	**97.45**	**96.25**	**97.22**	**100.18**	**86.51**

	MAS025 N = 1	MAS025 N = 1	MAS025 N = 3	MAS026 N = 2	MAS026 N = 1	MAS026 N = 2	MAS026 N = 1
Structural formulae calculated on the basis of 2 oxygens							
W	0.015	-	-	0.007	0.014	0.022	0.002
Nb	0.903	1.152	1.042	0.999	0.990	1.505	1.289
Ta	0.028	0.026	0.022	0.040	0.049	0.048	0.033
Si	0.090	0.162	0.163	0.116	0.107	-	-
Ti	0.208	0.170	0.124	0.155	0.202	0.194	0.176
Zr	-	-	-	-	-	-	-
Th	0.011	0.006	0.002	-	-	0.003	0.024
U	0.023	0.036	0.026	0.023	0.040	0.012	-
Al	0.017	-	-	0.009	0.010	0.018	0.024
Y	-	-	-	-	-	-	-
La	0.002	-	0.003	0.015	0.007	0.005	-
Ce	0.016	0.024	0.017	0.028	0.016	0.027	0.023
Pr	0.006	0.007	0.004	0.001	-	-	-
Nd	0.006	0.005	0.010	0.007	0.007	0.004	-
Sm	-	-	0.001	-	-	-	-
Fe^{3+}	0.754	0.490	0.648	0.681	0.642	0.235	0.478
Mn	0.051	0.057	0.071	0.095	0.097	0.055	0.060
Ca	0.037	0.394	0.169	0.139	0.090	0.900	0.441
Sr	-	-	-	-	-	0	-
Na	0.025	0.021	0.016	-	-	0.070	-
Total	**2.192**	**2.550**	**2.318**	**2.315**	**2.271**	**3.098**	**2.550**
Mol %							
Na + Ca	3.22	21.76	9.78	7.51	4.83	50.81	23.01
U + Th	1.80	2.20	1.49	1.24	2.16	0.80	1.26
A-def.	94.98	76.04	88.73	91.25	93.01	48.39	75.73
Mol %							
Nb	79.26	85.46	87.65	83.67	79.79	86.15	86.01
Ta	2.45	1.93	1.89	3.31	3.93	2.77	2.22
Ti	18.29	12.61	10.46	13.02	16.28	11.08	11.77

	MAS027 N = 2	MAS027 N = 2	MAS028 N = 4	MAS028 N = 1	MAS028 N = 1	MAS029 N = 1	MAS029 N = 3
Wt. %							
WO_3	0.92	0.64	0.76	0.82	0.03	0.50	0.56
Nb_2O_5	45.04	45.29	50.0	48.21	48.21	51.02	49.54
Ta_2O_5	4.68	4.06	3.48	4.55	3.33	0.76	0.73
SiO_2	4.97	4.58	2.46	2.71	3.18	2.26	2.72
TiO_2	8.43	8.33	8.01	7.90	7.52	0.15	0.19
ZrO_2	-	-	-	-	-	-	-
ThO_2	1.13	0.92	0.98	0.79	1.05	6.10	4.46
UO_2	6.93	6.79	4.38	5.72	5.30	0.32	1.08
Al_2O_3	0.35	0.38	0.33	0.51	0.27	-	-
Y_2O_3	-	-	0.03	0.12	-	1.97	1.97
La_2O_3	1.53	1.47	0.85	1.01	0.65	0.56	0.59
Ce_2O_3	5.06	5.98	1.91	2.26	2.20	5.24	4.86
Pr_2O_3	0.58	0.66	0.26	0.08	0.71	1.19	1.17
Nd_2O_3	1.82	2.52	0.86	0.88	0.45	6.40	6.46
Sm_2O_3	0.39	0.29	-	-	-	2.14	1.90
Fe_2O_3	8.90	7.19	15.90	16.65	20.93	6.80	7.24
MnO	1.48	1.35	1.4	1.46	1.59	0.26	0.04
CaO	4.09	4.91	5.66	5.89	3.67	4.66	4.61
SrO	-	-	-	-	-	-	-
Na_2O	0.06	-	0.09	0.29	0.01	-	-
Total	**96.36**	**95.36**	**97.36**	**99.85**	**99.10**	**90.33**	**88.12**

	MAS027 N = 2	MAS027 N = 2	MAS028 N = 4	MAS028 N = 1	MAS028 N = 1	MAS029 N = 1	MAS029 N = 3
Structural formulae calculated on the basis of 2 oxygens							
W	0.012	0.009	0.009	0.009	-	0.008	0.009
Nb	1.017	1.070	0.996	0.973	0.916	1.500	1.449
Ta	0.064	0.058	0.042	0.055	0.038	0.013	0.013
Si	0.248	0.239	0.152	0.121	0.134	0.147	0.176
Ti	0.317	0.327	0.265	0.265	0.238	0.007	0.009
Zr	-	-	-	-	-	-	-
Th	0.013	0.011	0.010	0.008	0.010	0.090	0.066
U	0.077	0.079	0.043	0.057	0.050	0.005	0.016
Al	0.021	0.023	0.017	0.027	0.013	-	-
Y	-	-	0.001	0.003	-	0.068	0.068
La	0.029	0.028	0.014	0.017	0.010	0.016	0.014
Ce	0.093	0.114	0.031	0.037	0.034	0.125	0.115
Pr	0.011	0.013	0.004	0.001	0.011	0.028	0.028
Nd	0.032	0.047	0.014	0.014	0.007	0.149	0.149
Sm	0.007	0.005	-	-	-	0.048	0.042
Fe^{3+}	0.334	0.283	0.527	0.559	0.662	0.333	0.353
Mn	0.063	0.060	0.054	0.055	0.057	0.014	0.002
Ca	0.219	0.275	0.267	0.282	0.165	0.325	0.320
Sr	-	-	-	-	-	-	-
Na	0.006	-	0.008	0.025	0.001	-	-
Total	**2.563**	**2.641**	**2.454**	**2.508**	**2.346**	**2.876**	**2.829**
Mol %							
Na + Ca	12.71	15.86	14.60	16.38	8.82	20.91	20.21
U + Th	5.09	5.19	2.80	3.46	3.17	6.11	5.14
A-def.	82.20	78.95	82.60	80.16	88.01	72.98	74.65
Mol %							
Nb	72.79	73.54	76.44	75.23	76.86	98.63	98.50
Ta	4.55	3.97	3.20	4.27	3.20	0.88	0.87
Ti	22.66	22.49	20.36	20.50	19.94	0.48	0.63

	MAS029 N = 3	MAS029 N = 1	MAS032 N = 2	MAS032 N = 2	MAS033 N = 1	MAS033 N = 2	MAS035 N = 2
Wt. %							
WO_3	1.19	1.39	0.96	1.90	1.87	3.13	-
Nb_2O_5	58.39	50.58	63.62	59.98	61.24	60.24	27.04
Ta_2O_5	0.40	0.56	3.60	4.44	2.84	4.10	0.76
SiO_2	6.96	5.84	0.10	4.15	-	-	9.12
TiO_2	1.02	0.32	0.79	1.12	5.50	5.43	11.96
ZrO_2	-	-	-	-	1.68	2.34	-
ThO_2	3.29	3.62	-	-	-	0.78	17.03
UO_2	1.02	1.73	1.15	1.80	-	0.29	5.16
Al_2O_3	0.52	0.56	0.10	0.20	0.15	0.26	0.50
Y_2O_3	0.15	-	-	-	-	-	1.54
La_2O_3	-	0.20	1.93	0.39	0.78	0.46	1.55
Ce_2O_3	2.09	1.43	2.70	1.87	2.56	2.31	4.18
Pr_2O_3	0.25	0.29	-	-	0.55	0.32	0.76
Nd_2O_3	0.61	0.34	0.42	0.51	0.54	0.47	3.49
Sm_2O_3	0.10	0.02	0.40	-	0.12	-	1.19
Fe_2O_3	3.55	9.59	7.86	9.17	1.84	2.87	3.97
MnO	0.62	0.67	0.98	1.40	0.57	0.63	-
CaO	5.57	5.16	13.74	4.90	14.67	12.64	4.49
SrO	-	-	-	-	-	-	-
Na_2O	-	-	0.37	0.17	3.28	2.04	-
Total	**85.73**	**82.30**	**98.72**	**92.00**	**98.19**	**98.31**	**92.74**

	MAS029 N = 3	MAS029 N = 1	MAS032 N = 2	MAS032 N = 2	MAS033 N = 1	MAS033 N = 2	MAS035 N = 2
Structural formulae calculated on the basis of 2 oxygens							
W	0.016	0.019	0.014	0.024	0.028	0.045	-
Nb	1.407	1.237	1.577	1.341	1.577	1.511	0.717
Ta	0.006	0.008	0.054	0.060	0.044	0.062	0.012
Si	0.371	0.316	0.005	0.205	-	-	0.535
Ti	0.041	0.013	0.033	0.042	0.236	0.227	0.527
Zr	-	-	-	-	0.047	0.063	-
Th	0.040	0.045	-	-	-	0.010	0.227
U	0.012	0.021	0.014	0.020	-	0.004	0.067
Al	0.033	0.036	0.006	0.012	0.010	0.017	0.035
Y	0.004	-	-	-	-	-	0.048
La	-	0.004	0.039	0.007	0.016	0.009	0.034
Ce	0.041	0.028	0.054	0.034	0.053	0.047	0.090
Pr	0.005	0.006	-	-	0.011	0.006	0.016
Nd	0.012	0.007	0.008	0.009	0.011	0.009	0.073
Sm	0.002	-	0.008	-	0.002	-	0.024
Fe^{3+}	0.142	0.390	0.324	0.341	0.086	0.120	0.175
Mn	0.028	0.031	0.046	0.059	0.028	0.030	-
Ca	0.318	0.299	0.807	0.260	0.895	0.752	0.282
Sr	-	-	-	-	-	-	-
Na	-	-	0.039	0.016	0.362	0.219	-
Total	**2.478**	**2.460**	**3.028**	**2.430**	**3.406**	**3.131**	**2.862**
Mol %							
Na + Ca	16.67	15.54	45.88	14.58	66.98	51.41	16.37
U + Th	2.72	3.40	0.76	1.05	-	0.71	17.10
A-def.	80.61	81.06	53.36	84.37	33.02	47.88	66.53
Mol %							
Nb	96.79	98.31	94.81	92.97	84.94	83.97	57.06
Ta	0.40	0.65	3.23	4.14	2.37	3.44	0.96
Ti	2.81	1.03	1.96	2.89	12.69	12.59	41.98

	MAS037 N = 3	MAS038 N = 5	MAS040 N = 4	MAS040 N = 3
Wt. %				
WO_3	4.44	0.39	0.63	1.65
Nb_2O_5	61.66	64.15	54.96	37.11
Ta_2O_5	3.23	2.34	0.47	4.71
SiO_2	1.08	0.30	2.30	14.66
TiO_2	5.72	5.11	6.62	3.60
ZrO_2	1.56	-	-	2.01
ThO_2	0.64	-	-	0.25
UO_2	1.08	-	-	6.81
Al_2O_3	0.25	0.11	0.37	1.18
Y_2O_3	-	-	1.77	-
La_2O_3	0.26	0.09	0.57	0.44
Ce_2O_3	2.84	0.83	6.68	3.24
Pr_2O_3	0.24	-	1.43	0.26
Nd_2O_3	0.49	0.39	6.39	0.32
Sm_2O_3	0.07	-	0.97	-
Fe_2O_3	2.67	0.74	4.46	2.87
MnO	0.89	-	0.27	-
CaO	9.49	17.28	6.69	9.33
SrO	-	-	-	-
Na_2O	0.45	6.72	-	0.61
Total	**97.06**	**98.45**	**94.58**	**89.05**

	MAS037 N = 3	MAS038 N = 5	MAS040 N = 4	MAS040 N = 3

Structural formulae calculated on the basis of 2 oxygens

W	0.062	0.006	0.009	0.021
Nb	1.499	1.683	1.379	0.840
Ta	0.047	0.037	0.007	0.064
Si	0.058	0.017	0.128	0.734
Ti	0.231	0.223	0.276	0.136
Zr	0.041	-	-	0.049
Th	0.008	-	-	0.003
U	0.013	-	-	0.076
Al	0.016	0.008	0.024	0.070
Y	-	-	0.052	-
La	0.005	0.002	0.012	0.008
Ce	0.056	0.018	0.136	0.059
Pr	0.005	-	0.029	0.005
Nd	0.009	0.008	0.127	0.006
Sm	0.001	-	0.019	-
Fe^{3+}	0.108	0.032	0.186	0.108
Mn	0.041	-	0.013	-
Ca	0.547	1.074	0.398	0.500
Sr	-	-	-	-
Na	0.047	0.756	-	0.059
Total	**2.794**	**3.864**	**2.795**	**2.738**

Mol %

Na + Ca	31.52	92.80	24.65	29.10
U + Th	1.10	-	-	4.09
A-def.	67.38	7.20	75.35	66.81

Mol %

Nb	84.33	86.62	82.95	80.80
Ta	2.66	1.90	0.43	6.17
Ti	13.01	11.48	16.62	13.03

III.XIII Rutile

	MAS001 N = 1	MAS001 N = 2	MAS002 N = 2	MAS002 N = 2	MAS002 N = 3	MAS003 N = 3	MAS003 N = 1
Wt. %							
Nb_2O_5	8.79	7.02	0.67	6.64	0.85	14.83	9.00
SiO_2	0.57	0.63	0.38	0.45	0.73	1.31	0.79
TiO_2	87.60	90.03	96.60	89.87	95.77	77.64	85.69
ZrO_2	-	-	-	-	-	-	-
SnO_2	-	-	0.73	0.90	-	-	-
UO_2	-	-	-	-	-	-	-
Al_2O_3	-	0.04	0.11	0.06	0.13	0.01	0.08
Fe_2O_3	0.42	2.48	1.57	1.02	2.30	3.73	5.00
FeO	1.98	0.25	-	1.23	-	2.21	-
CaO	0.16	0.40	0.10	0.05	0.09	0.10	0.14
CuO	-	-	-	-	-	-	-
Total	99.52	100.85	100.16	100.22	99.87	99.83	100.70
Structural formulae calculated on the basis of 2 oxygens							
Nb	0.055	0.043	0.004	0.041	0.005	0.094	0.056
Si	0.008	0.009	0.005	0.006	0.010	0.018	0.011
Ti	0.908	0.914	0.972	0.922	0.964	0.820	0.879
Zr	-	-	-	-	-	-	-
Sn	-	-	0.004	0.005	-	-	-
U	-	-	-	-	-	-	-
Al	-	0.001	0.002	0.001	0.002	-	0.001
Fe^{3+}	0.004	0.025	0.016	0.011	0.023	0.039	0.051
Fe^{2+}	0.023	0.003	-	0.014	-	0.026	-
Ca	0.002	0.006	0.001	0.001	0.001	0.002	0.002
Cu	-	-	-	-	-	-	-
Total	1.000	1.000	1.004	1.000	1.006	1.000	1.000

	MAS004 N = 1	MAS007 N = 2	MAS007 N = 1	MAS007 N = 1	MAS009 N = 3	MAS009 N = 1	MAS012 N = 1
Wt. %							
Nb_2O_5	6.06	10.61	11.26	8.48	7.27	20.52	23.19
SiO_2	0.14	0.96	1.07	1.26	0.42	0.68	0.39
TiO_2	88.37	82.78	82.05	82.79	89.46	72.05	67.71
ZrO_2	-	-	1.32	2.07	1.65	0.95	0.37
SnO_2	-	-	-	-	-	-	-
UO_2	-	0.30	0.10	0.51	-	-	-
Al_2O_3	-	-	-	-	-	-	-
Fe_2O_3	5.86	2.63	1.28	3.53	-	1.04	0.29
FeO	-	1.22	1.92	-	0.76	4.84	5.91
CaO	-	0.14	0.17	0.26	0.60	0.19	0.18
CuO	-	0.33	0.37	0.51	-	-	-
Total	**100.43**	**98.96**	**99.54**	**99.41**	**100.16**	**100.26**	**100.04**
Structural formulae calculated on the basis of 2 oxygens							
Nb	0.037	0.067	0.071	0.053	0.045	0.133	0.152
Si	0.002	0.013	0.015	0.018	0.006	0.010	0.006
Ti	0.906	0.871	0.862	0.868	0.918	0.778	0.762
Zr	-	-	0.009	0.014	0.011	0.007	0.003
Sn	-	-	-	-	-	-	-
U	-	0.001	-	0.002	-	-	-
Al	-	-	-	-	-	-	-
Fe^{3+}	0.060	0.028	0.013	0.037	-	0.011	0.003
Fe^{2+}	-	0.014	0.022	-	0.009	0.058	0.072
Ca	-	0.002	0.003	0.004	0.009	0.003	0.003
Cu	-	0.003	0.004	0.005	-	-	-
Total	**1.006**	**1.000**	**1.000**	**1.001**	**0.998**	**1.000**	**1.000**

	MAS012 N = 2	MAS012 N = 2	MAS012 N = 1	MAS019 N = 2	MAS019 N = 3	MAS021 N = 3	MAS022 N = 1
Wt. %							
Nb_2O_5	19.80	16.10	21.32	1.94	4.63	1.91	10.84
SiO_2	0.52	2.33	1.26	0.39	0.48	0.36	0.29
TiO_2	73.61	77.17	69.76	93.19	88.00	95.83	84.61
ZrO_2	0.51	0.27	0.42	-	-	0.37	-
SnO_2	-	-	-	-	-	-	-
UO_2	-	-	-	-	-	-	-
Al_2O_3	-	0.09	0.06	0.27	0.24	0.35	-
Fe_2O_3	1.59	1.23	1.96	3.60	6.21	-	0.99
FeO	4.41	3.53	4.68	-	-	1.22	1.95
CaO	0.18	0.16	0.13	-	-	-	0.42
CuO	-	-	-	-	-	-	-
Total	**100.62**	**100.88**	**99.59**	**99.39**	**99.56**	**100.01**	**99.10**
Structural formulae calculated on the basis of 2 oxygens							
Nb	0.128	0.101	0.139	0.012	0.029	0.012	0.068
Si	0.007	0.032	0.018	0.005	0.007	0.005	0.004
Ti	0.789	0.807	0.759	0.949	0.907	0.967	0.888
Zr	0.004	0.002	0.003	-	-	0.002	-
Sn	-	-	-	-	-	-	-
U	-	-	-	-	-	-	-
Al	-	0.001	0.001	0.004	0.004	0.006	-
Fe^{3+}	0.017	0.013	0.021	0.037	0.064	-	0.010
Fe^{2+}	0.053	0.041	0.057	-	-	0.014	0.023
Ca	0.003	0.002	0.002	-	-	-	0.006
Cu	-	-	-	-	-	-	-
Total	**1.000**	**1.000**	**1.000**	**1.007**	**1.010**	**1.005**	**1.000**

III.XIV Thorite

	MAS001 N = 3	MAS002 N = 4	MAS006 N = 3	MAS006 N = 3	MAS006 N = 1	MAS008 N = 2	MAS008 N = 3
Wt. %							
P_2O_5	-	-	-	-	-	-	-
Nb_2O_5	-	-	-	0.78	0.10	1.01	-
SiO_2	20.37	23.35	21.18	21.34	19.03	19.75	18.81
ZrO_2	1.26	-	1.65	1.60	1.86	-	-
ThO_2	39.15	52.35	46.88	43.61	42.66	44.87	42.86
UO_2	10.76	0.92	2.76	1.07	3.92	0.59	6.92
Al_2O_3	0.89	1.32	0.61	0.58	0.60	0.66	0.62
Y_2O_3	0.74	-	7.64	7.35	8.65	6.88	6.98
La_2O_3	2.06	0.99	-	-	-	0.40	0.11
Ce_2O_3	6.54	2.01	0.53	-	-	0.71	0.71
Pr_2O_3	1.08	0.35	-	-	-	0.32	-
Nd_2O_3	2.43	0.90	-	-	-	1.05	0.57
Sm_2O_3	-	-	-	-	-	-	-
Eu_2O_3	-	-	-	-	-	-	-
Gd_2O_3	-	-	-	0.45	0.03	0.58	0.31
Tb_2O_3	-	-	-	0.06	0.08	-	-
Dy_2O_3	0.13	-	1.33	1.04	1.06	0.95	1.01
Ho_2O_3	-	-	0.64	0.28	0.47	-	-
Er_2O_3	-	-	1.18	1.17	1.22	0.75	0.37
Tm_2O_3	-	-	-	0.32	0.56	-	-
Yb_2O_3	0.14	-	1.19	1.20	0.98	0.53	0.80
Lu_2O_3	-	-	-	0.14	-	-	-
CaO	1.00	4.46	1.10	1.10	0.86	1.24	1.29
MnO	-	-	-	-	-	-	-
FeO	1.05	2.06	2.24	2.22	1.04	4.98	1.51
PbO	0.98	-	-	-	-	-	-
Total	**88.58**	**88.71**	**88.93**	**83.53**	**83.02**	**84.25**	**82.88**

	MAS001 N = 3	MAS002 N = 4	MAS006 N = 3	MAS006 N = 3	MAS006 N = 1	MAS008 N = 2	MAS008 N = 3
Structural formulae calculated on the basis of 4 cations							
P	-	-	-	-	-	-	-
Nb	-	-	-	0.017	0.002	0.022	-
Si	1.052	1.092	1.023	1.050	1.019	0.935	1.017
Zr	0.032	-	0.039	0.038	0.049	-	-
Th	0.450	0.557	0.515	0.488	0.520	0.483	0.527
U	0.124	0.010	0.030	0.012	0.047	0.006	0.083
Al	0.054	0.073	0.035	0.034	0.038	0.037	0.040
Y	0.020	-	0.196	0.192	0.246	0.173	0.201
La	0.039	0.017	-	-	-	0.007	0.002
Ce	0.124	0.034	0.009	-	-	0.012	0.014
Pr	0.020	0.006	-	-	-	0.006	-
Nd	0.045	0.015	-	-	-	0.018	0.011
Sm	-	-	-	-	-	-	-
Eu	-	-	-	-	-	-	-
Gd	-	-	-	0.007	0.001	0.009	0.006
Tb	-	-	-	0.001	0.001	-	-
Dy	0.002	-	0.021	0.016	0.018	0.014	0.018
Ho	-	-	0.010	0.004	0.008	-	-
Er	-	-	0.018	0.018	0.021	0.011	0.006
Tm	-	-	-	0.005	0.009	-	-
Yb	0.002	-	0.018	0.018	0.016	0.008	0.013
Lu	-	-	-	0.002	-	-	-
Ca	0.055	0.223	0.057	0.058	0.049	0.063	0.075
Mn	-	-	-	-	-	-	-
Fe	0.136	0.242	0.271	0.274	0.140	0.592	0.205
Pb	0.014	-	-	-	-	-	-
Total	**2.179**	**2.269**	**2.241**	**2.219**	**2.181**	**2.374**	**2.217**

	MAS008 N = 2	MAS014 N = 3	MAS014 N = 3	MAS015 N = 4	MAS016 N = 4	MAS019 N = 6	MAS019 N = 4
Wt. %							
P_2O_5	-	2.66	2.04	0.83	2.83	0.79	0.76
Nb_2O_5	-	-	-	-	-	-	-
SiO_2	18.17	17.89	17.93	20.11	18.56	20.27	20.85
ZrO_2	-	-	-	-	-	-	-
ThO_2	44.15	59.91	48.49	53.02	52.09	50.03	44.38
UO_2	0.59	1.78	4.44	0.38	0.56	5.75	4.20
Al_2O_3	0.51	0.07	0.29	0.85	0.20	0.35	0.44
Y_2O_3	7.20	-	7.25	-	-	2.37	8.28
La_2O_3	0.37	1.31	0.99	3.05	5.58	1.20	0.21
Ce_2O_3	0.66	5.97	2.98	7.32	6.06	6.21	1.43
Pr_2O_3	-	1.17	0.26	1.03	0.77	0.87	0.23
Nd_2O_3	0.33	3.52	1.90	2.09	1.15	3.27	2.12
Sm_2O_3	-	0.74	0.64	0.34	0.21	0.20	0.73
Eu_2O_3	-	-	-	-	-	-	-
Gd_2O_3	0.42	-	0.68	-	-	0.21	0.89
Tb_2O_3	0.10	-	-	-	-	-	-
Dy_2O_3	1.49	-	1.02	-	-	0.54	1.28
Ho_2O_3	0.21	-	-	-	-	-	0.10
Er_2O_3	0.70	-	0.24	-	-	0.10	0.42
Tm_2O_3	-	-	-	-	-	-	-
Yb_2O_3	0.50	-	0.10	-	-	-	0.26
Lu_2O_3	-	-	-	-	-	-	-
CaO	1.10	1.42	1.58	0.51	1.07	1.01	0.88
MnO	-	-	-	0.46	-	-	-
FeO	3.92	3.23	3.03	2.59	4.02	-	1.68
PbO	-	-	-	-	0.35	-	-
Total	**80.42**	**99.67**	**93.86**	**92.58**	**93.45**	**93.17**	**89.14**

	MAS008 N = 2	MAS014 N = 3	MAS014 N = 3	MAS015 N = 4	MAS016 N = 4	MAS019 N = 6	MAS019 N = 4
Structural formulae calculated on the basis of 4 cations							
P	-	0.105	0.082	0.034	0.111	0.034	0.031
Nb	-	-	-	-	-	-	-
Si	0.947	0.831	0.849	0.972	0.860	1.040	1.018
Zr	-	-	-	-	-	-	-
Th	0.524	0.633	0.522	0.583	0.549	0.584	0.493
U	0.009	0.18	0.047	0.004	0.006	0.066	0.046
Al	0.031	0.004	0.016	0.048	0.011	0.021	0.025
Y	0.200	-	0.183	-	-	0.065	0.215
La	0.007	0.022	0.017	0.054	0.095	0.023	0.004
Ce	0.013	0.102	0.052	0.130	0.103	0.117	0.026
Pr	-	0.020	0.004	0.018	0.013	0.016	0.004
Nd	0.006	0.058	0.032	0.036	0.019	0.060	0.037
Sm	-	0.012	0.010	0.006	0.003	0.004	0.012
Eu	-	-	-	-	-	-	-
Gd	0.007	-	0.011	-	-	0.004	0.014
Tb	0.002	-	-	-	-	-	-
Dy	0.025	-	0.016	-	-	0.009	0.020
Ho	0.003	-	-	-	-	-	0.002
Er	0.011	-	0.004	-	-	0.002	0.006
Tm	-	-	-	-	-	-	-
Yb	0.008	-	0.001	-	-	-	0.004
Lu	-	-	-	-	-	-	-
Ca	0.060	0.071	0.080	0.026	0.053	0.056	0.046
Mn	-	-	-	0.019	-	-	-
Fe	0.513	0.376	0.360	0.314	0.467	-	0.206
Pb	-	-	-	-	0.004	-	-
Total	**2.365**	**2.252**	**2.286**	**2.244**	**2.296**	**2.099**	**2.211**

	MAS021 N = 6	MAS022 N = 2	MAS022 N = 2	MAS025 N = 4	MAS029 N = 3	MAS037 N = 2
Wt. %						
P_2O_5	0.24	1.26	0.25	-	0.96	-
Nb_2O_5	-	-	1.18	-	-	-
SiO_2	21.69	18.24	19.52	21.77	19.14	19.21
ZrO_2	-	-	-	0.97	-	-
ThO_2	46.05	42.61	44.98	64.25	46.21	48.33
UO_2	0.46	1.54	0.33	-	0.77	0.72
Al_2O_3	0.87	0.72	1.00	-	0.23	0.38
Y_2O_3	6.77	7.52	4.23	0.78	8.09	6.18
La_2O_3	0.11	0.58	1.25	2.33	0.06	0.64
Ce_2O_3	0.65	2.18	2.82	4.22	0.58	3.41
Pr_2O_3	0.36	0.42	0.74	0.45	0.39	0.92
Nd_2O_3	1.09	1.53	1.67	0.80	1.55	3.10
Sm_2O_3	0.77	0.74	0.45	0.21	1.12	0.74
Eu_2O_3	0.28	-	-	-	0.70	-
Gd_2O_3	1.06	0.95	0.66	-	1.69	0.26
Tb_2O_3	0.16	-	-	-	0.29	-
Dy_2O_3	0.83	1.36	0.36	-	1.48	0.66
Ho_2O_3	0.08	0.38	0.20	-	0.75	-
Er_2O_3	0.60	0.87	0.52	-	0.64	0.86
Tm_2O_3	0.12	0.32	-	-	0.39	-
Yb_2O_3	0.14	0.66	0.78	-	0.48	0.21
Lu_2O_3	0.15	-	-	-	0.10	-
CaO	1.10	1.45	1.74	1.02	0.76	1.18
MnO	-	-	-	-	-	-
FeO	4.10	1.29	2.19	3.22	2.24	0.71
PbO	-	-	-	-	-	-
Total	**87.68**	**84.62**	**84.87**	**100.02**	**88.62**	**87.51**

	MAS021 N = 6	MAS022 N = 2	MAS022 N = 2	MAS025 N = 4	MAS029 N = 3	MAS037 N = 2
Structural formulae calculated on the basis of 4 cations						
P	0.009	0.056	0.011	-	0.041	-
Nb	-	-	0.027	-	-	-
Si	1.001	0.955	0.988	0.991	0.956	1.023
Zr	-	-	-	0.022	-	-
Th	0.483	0.508	0.518	0.665	0.525	0.586
U	0.005	0.018	0.004	-	0.009	0.009
Al	0.047	0.044	0.060	-	0.014	0.024
Y	0.166	0.209	0.114	0.019	0.215	0.175
La	0.002	0.011	0.023	0.039	0.001	0.013
Ce	0.011	0.042	0.052	0.070	0.011	0.066
Pr	0.006	0.008	0.014	0.007	0.007	0.018
Nd	0.018	0.029	0.030	0.013	0.028	0.059
Sm	0.012	0.013	0.008	0.003	0.019	0.014
Eu	0.004	-	-	-	0.012	-
Gd	0.016	0.016	0.011	-	0.028	0.005
Tb	0.002	-	-	-	0.005	-
Dy	0.012	0.023	0.006	-	0.024	0.011
Ho	0.001	0.006	0.003	-	0.012	-
Er	0.009	0.014	0.008	-	0.010	0.014
Tm	0.002	0.005	-	-	0.006	-
Yb	0.002	0.011	0.012	-	0.007	0.003
Lu	0.002	-	-	-	0.002	-
Ca	0.054	0.081	0.094	0.050	0.041	0.067
Mn	-	-	-	-	-	-
Fe	0.474	0.169	0.278	0.368	0.281	0.095
Pb	-	-	-	-	-	-
Total	**2.340**	**2.220**	**2.262**	**2.247**	**2.250**	**2.182**

III.XV Titanite (all niobium accompanied by equal amounts (apfu) of water)

	MAS003 N = 5	MAS024 N = 5	MAS024 N = 4	MAS036 N = 3	MAS036 N = 3	MAS037 N = 5
Wt. %						
Nb_2O_5	0.60	1.82	0.54	1.54	3.46	0.34
SiO_2	31.75	31.83	31.40	30.19	31.04	32.07
TiO_2	34.97	32.71	34.59	35.87	32.75	33.22
ZrO_2	-	-	-	-	1.00	-
Al_2O_3	3.69	4.87	6.02	3.15	2.70	3.22
Fe_2O_3	3.33	3.11	2.11	2.59	3.12	5.22
CaO	25.73	24.45	25.12	25.99	24.58	24.96
Total	**100.26**	**98.79**	**99.58**	**98.94**	**98.71**	**99.01**
H_2O_C	0.08	0.25	0.05	0.16	0.47	0.07
Total	**100.34**	**99.04**	**99.63**	**99.12**	**99.18**	**99.08**
Structural formulae calculated on the basis of 5 oxygens						
Nb	0.009	0.027	0.005	0.017	0.051	0.005
Si	1.025	1.033	1.011	0.990	1.018	1.048
Ti	0.849	0.798	0.838	0.884	0.808	0.817
Zr	-	-	-	-	0.017	-
Al	0.140	0.186	0.228	0.122	0.104	0.124
Fe^{3+}	0.081	0.076	0.051	0.064	0.077	0.128
Ca	0.890	0.850	0.866	0.913	0.864	0.874
H_2O	0.009	0.027	0.005	0.017	0.051	0.005
Total	**3.002**	**2.997**	**3.005**	**3.007**	**2.990**	**3.002**

III.XV Xenotime

	MAS018 N = 4	MAS018 N = 1	MAS019 N = 2	MAS019 N = 2	MAS021 N = 1	MAS021 N = 2	MAS021 N = 1
Wt. %							
SiO_2	0.50	-	0.36	-	1.33	1.36	0.23
ThO_2	0.30	-	0.62	1.68	1.85	1.84	1.48
UO_2	0.12	-	-	-	0.11	0.12	0.08
P_2O_5	34.24	34.45	34.98	35.91	33.96	34.41	35.24
Al_2O_3	-	-	-	-	0.95	0.90	0.92
Y_2O_3	44.36	42.81	41.14	42.32	39.54	40.71	40.89
La_2O_3	0.14	-	0.88	0.34	-	-	-
Ce_2O_3	0.30	0.41	1.53	0.67	-	-	-
Pr_2O_3	0.17	-	0.13	-	-	-	-
Nd_2O_3	0.20	-	0.93	0.21	-	-	-
Sm_2O_3	0.47	0.55	0.41	0.44	-	-	-
Eu_2O_3	-	0.31	-	-	-	0.03	-
Gd_2O_3	2.86	3.92	2.83	2.23	1.66	1.20	1.48
Tb_2O_3	0.62	0.54	0.70	0.98	1.15	0.33	0.77
Dy_2O_3	6.69	7.78	8.11	7.10	7.56	5.80	6.12
Ho_2O_3	1.45	1.75	1.24	1.62	2.36	1.36	1.53
Er_2O_3	4.10	4.21	4.07	3.85	4.95	5.55	4.44
Tm_2O_3	0.78	1.07	0.78	0.91	0.42	0.96	0.91
Yb_2O_3	2.17	2.32	1.81	2.52	3.61	3.97	4.21
Lu_2O_3	0.29	0.14	-	-	0.62	1.18	0.44
CaO	-	0.43	0.11	0.14	0.25	0.15	0.05
FeO	-	-	-	-	0.41	0.22	0.30
Total	**99.76**	**100.69**	**100.63**	**100.92**	**100.73**	**100.09**	**99.09**

	MAS018 N = 4	MAS018 N = 1	MAS019 N = 2	MAS019 N = 2	MAS021 N = 1	MAS021 N = 2	MAS021 N = 1
Structural formulae calculated on the basis of 4 oxygens							
Si	0.017	-	0.012	-	0.044	0.045	0.008
Th	0.002	-	0.005	0.013	0.014	0.014	0.011
U	0.001	-	-	-	0.001	0.001	0.001
P	0.976	0.983	0.991	1.007	0.954	0.964	0.992
Al	-	-	-	-	0.037	0.035	0.036
Y	0.795	0.768	0.733	0.746	0.698	0.717	0.724
La	0.002	-	0.011	0.004	-	-	-
Ce	0.004	0.005	0.019	0.008	-	-	-
Pr	0.002	-	0.002	-	-	-	-
Nd	0.002	-	0.011	0.002	-	-	-
Sm	0.005	0.006	0.005	0.005	-	-	-
Eu	-	0.004	-	-	-	0.000	-
Gd	0.032	0.044	0.031	0.024	0.018	0.013	0.016
Tb	0.007	0.006	0.008	0.011	0.013	0.004	0.008
Dy	0.073	0.085	0.087	0.076	0.081	0.062	0.066
Ho	0.016	0.019	0.013	0.019	0.025	0.014	0.016
Er	0.043	0.045	0.043	0.040	0.052	0.058	0.046
Tm	0.008	0.011	0.008	0.009	0.004	0.010	0.009
Yb	0.022	0.024	0.018	0.025	0.037	0.040	0.043
Lu	0.003	0.001	-	-	0.006	0.012	0.004
Ca	-	0.016	0.004	0.005	0.009	0.005	0.002
Fe	-	-	-	-	0.034	0.018	0.025
Total	**2.009**	**2.016**	**2.001**	**1.993**	**2.026**	**2.012**	**2.008**

	MAS022 N = 2	MAS022 N = 2	MAS026 N = 4	MAS040 N = 2	MAS040 N = 1	MAS040 N = 2
Wt. %						
SiO_2	-	0.23	0.98	0.02	0.35	0.25
ThO_2	0.64	1.12	1.14	0.45	0.37	0.24
UO_2	0.03	-	0.21	0.14	0.18	0.12
P_2O_5	35.69	36.01	35.20	35.25	34.91	35.11
Al_2O_3	1.46	1.12	-	0.53	0.52	0.45
Y_2O_3	39.34	39.57	45.53	40.21	39.59	40.06
La_2O_3	-	-	-	-	-	-
Ce_2O_3	-	-	-	-	-	-
Pr_2O_3	-	-	-	-	-	-
Nd_2O_3	-	-	0.14	-	-	-
Sm_2O_3	-	-	-	-	-	-
Eu_2O_3	0.01	0.02	-	0.03	-	0.10
Gd_2O_3	1.66	2.25	1.66	3.27	3.19	2.63
Tb_2O_3	0.61	0.70	0.53	1.05	0.90	0.60
Dy_2O_3	5.93	5.92	5.84	7.46	9.31	8.18
Ho_2O_3	1.76	0.82	1.43	1.55	2.04	1.77
Er_2O_3	5.24	4.69	4.23	4.04	4.66	5.10
Tm_2O_3	0.86	0.92	0.64	1.14	0.54	1.04
Yb_2O_3	5.07	5.29	2.29	3.99	3.71	3.98
Lu_2O_3	0.70	0.59	0.16	0.23	0.36	1.00
CaO	-	0.06	0.35	0.10	0.09	-
FeO	0.24	0.04	-	-	-	-
Total	**99.24**	**99.35**	**100.32**	**99.46**	**100.72**	**100.63**

	MAS022 N = 2	MAS022 N = 2	MAS026 N = 4	MAS040 N = 2	MAS040 N = 1	MAS040 N = 2
Structural formulae calculated on the basis of 4 oxygens						
Si	-	0.008	0.032	0.001	0.012	0.008
Th	0.005	0.008	0.009	0.003	0.003	0.002
U	0.000	-	0.002	0.001	0.001	0.001
P	1.001	1.008	0.978	1.004	0.991	0.996
Al	0.057	0.044	-	0.021	0.021	0.018
Y	0.693	0.696	0.795	0.720	0.707	0.714
La	-	-	-	-	-	-
Ce	-	-	-	-	-	-
Pr	-	-	-	-	-	-
Nd	-	-	0.002	-	-	-
Sm	-	-	-	-	-	-
Eu	0.000	0.000	-	0.000	-	0.001
Gd	0.018	0.025	0.018	0.036	0.035	0.029
Tb	0.007	0.008	0.006	0.012	0.010	0.007
Dy	0.063	0.063	0.062	0.081	0.101	0.088
Ho	0.019	0.009	0.015	0.017	0.022	0.019
Er	0.055	0.049	0.044	0.043	0.049	0.054
Tm	0.009	0.009	0.007	0.012	0.006	0.011
Yb	0.051	0.053	0.023	0.041	0.038	0.041
Lu	0.007	0.006	0.002	0.002	0.004	0.010
Ca	-	0.002	0.012	0.004	0.003	-
Fe	0.020	0.003	-	-	-	-
Total	**2.004**	**1.991**	**2.005**	**1.997**	**2.002**	**1.999**

III.XVII Zircon (includes hydrous variety)

	MAS001 N = 3	MAS005 N = 5	MAS005 N = 3	MAS006 N = 3	MAS006 N = 3	MAS007 N = 3	MAS007 N = 5	MAS009 N = 3	MAS009 N = 3	MAS011 N = 2	MAS011 N = 3
Wt. %											
SiO_2	33.08	30.96	32.78	33.02	30.34	25.80	26.71	32.59	29.25	31.78	27.70
ZrO_2	66.24	52.26	66.77	66.37	59.14	35.14	46.99	65.66	55.08	62.79	52.78
HfO_2	0.95	-	0.88	0.96	0.53	0.37	0.80	1.17	0.77	0.25	0.27
ThO_2	-	-	-	-	0.31	2.75	0.25	-	0.62	2.36	1.80
UO_2	-	-	-	-	0.63	2.15	1.02	-	0.34	1.58	0.67
Al_2O_3	-	0.42	-	-	-	1.83	1.22	0.15	0.17	-	-
Y_2O_3	-	8.26	-	-	-	8.34	3.86	-	-	-	-
La_2O_3	-	-	-	-	-	0.25	-	-	-	-	-
Ce_2O_3	-	0.25	-	-	-	0.72	0.36	-	-	-	-
Pr_2O_3	-	-	-	-	-	0.11	-	-	-	-	-
Nd_2O_3	-	-	-	-	-	0.65	-	-	-	-	-
Sm_2O_3	-	-	-	-	-	0.09	-	-	-	-	-
Gd_2O_3	-	0.51	-	-	-	0.49	0.43	-	-	-	-
Tb_2O_3	-	0.04	-	-	-	0.14	0.04	-	-	-	-
Dy_2O_3	-	1.12	-	-	-	1.27	0.53	-	-	-	-
Ho_2O_3	-	-	-	-	-	-	-	-	-	-	-
Er_2O_3	-	1.05	-	-	-	1.03	0.82	-	-	-	-
Tm_2O_3	-	0.24	-	-	-	0.38	-	-	-	-	-
Yb_2O_3	-	1.61	-	-	-	1.90	0.66	-	-	-	-
CaO	-	0.39	-	-	1.89	1.57	1.74	-	1.44	-	2.17
MnO	-	-	-	-	0.55	-	-	-	0.60	-	0.68
FeO	0.20	0.49	-	-	1.41	1.14	1.19	0.08	1.26	-	1.77
Na_2O	-	-	-	-	0.51	0.22	0.63	-	0.67	-	-
Total	**100.47**	**97.60**	**100.43**	**100.35**	**95.31**	**86.34**	**87.25**	**99.65**	**90.20**	**98.76**	**87.84**

	MAS001 N = 3	MAS005 N = 5	MAS005 N = 3	MAS006 N = 3	MAS006 N = 3	MAS007 N = 3	MAS007 N = 5	MAS009 N = 3	MAS009 N = 3	MAS011 N = 2	MAS011 N = 3
Structural formulae calculated on the basis of 4 cations											
Si	1.004	0.997	1.000	1.006	0.970	0.972	0.956	1.000	0.987	1.003	0.959
Zr	0.980	0.821	0.993	0.986	0.922	0.646	0.820	0.982	0.906	0.966	0.891
Hf	0.008	-	0.008	0.008	0.005	0.004	0.008	0.010	0.007	0.002	0.003
Th	-	-	-	-	0.002	0.024	0.002	-	0.005	0.017	0.014
U	-	-	-	-	0.004	0.018	0.008	-	0.003	0.011	0.005
Al	-	0.016	-	-	-	0.081	0.051	0.005	0.007	-	-
Y	-	0.142	-	-	-	0.167	0.074	-	-	-	-
La	-	-	-	-	-	0.003	-	-	-	-	-
Ce	-	0.003	-	-	-	0.010	0.005	-	-	-	-
Pr	-	-	-	-	-	0.002	-	-	-	-	-
Nd	-	-	-	-	-	0.009	-	-	-	-	-
Sm	-	-	-	-	-	0.001	-	-	-	-	-
Gd	-	0.005	-	-	-	0.006	0.005	-	-	-	-
Tb	-	-	-	-	-	0.002	-	-	-	-	-
Dy	-	0.012	-	-	-	0.015	0.006	-	-	-	-
Ho	-	-	-	-	-	-	-	-	-	-	-
Er	-	0.011	-	-	-	0.012	0.009	-	-	-	-
Tm	-	0.002	-	-	-	0.004	-	-	-	-	-
Yb	-	0.016	-	-	-	0.022	0.007	-	-	-	-
Ca	-	0.013	-	-	0.065	0.063	0.067	-	0.052	-	0.081
Mn	-	-	-	-	0.015	-	-	-	0.017	-	0.020
Fe	0.015	0.040	-	-	0.113	0.108	0.107	0.006	0.107	-	0.154
Na					0.032	0.016	0.044	-	0.044	-	-
Total	**2.007**	**2.078**	**2.001**	**2.000**	**2.128**	**2.185**	**2.169**	**2.003**	**2.135**	**1.999**	**2.127**

	MAS012 N = 4	MAS012 N = 4	MAS013 N = 2	MAS013 N = 2	MAS015 N = 2	MAS015 N = 1	MAS015 N = 3	MAS016 N = 3	MAS016 N = 3	MAS017 N = 3	MAS018 N = 2
Wt. %											
SiO_2	32.59	30.08	25.38	26.91	32.56	29.87	28.40	32.40	28.52	27.20	31.61
ZrO_2	65.62	58.70	39.76	48.87	65.24	58.06	53.44	65.02	57.26	47.31	62.26
HfO_2	1.04	1.01	0.59	0.46	0.64	1.28	0.74	1.47	0.93	0.39	1.33
ThO_2	-	-	2.19	0.39	0.30	0.40	0.69	0.37	0.59	3.81	0.42
UO_2	-	0.29	1.49	0.82	0.41	0.26	0.20	0.13	0.31	1.37	0.21
Al_2O_3	-	0.34	1.98	0.68	-	0.20		-	0.24	0.18	0.36
Y_2O_3	-	-	4.16	5.45	-	-	0.21	-	-	-	-
La_2O_3	-	-	0.15	-	-	-	-	-	-	-	-
Ce_2O_3	-	-	0.76	-	-	-	-	-	-	-	0.35
Pr_2O_3	-	-	0.57	-	-	-	-	-	-	-	-
Nd_2O_3	-	-	-	-	-	-	-	-	-	-	0.12
Sm_2O_3	-	-	-	-	-	-	-	-	-	-	-
Gd_2O_3	-	-	0.59	0.78	-	-	-	-	-	-	-
Tb_2O_3	-	-	-	0.12	-	-	-	-	-	-	-
Dy_2O_3	-	-	0.78	1.06	-	-	-	-	-	-	-
Ho_2O_3	-	-	-	0.21	-	-	-	-	-	-	-
Er_2O_3	-	-	1.02	1.22	-	-	-	-	-	-	-
Tm_2O_3	-	-	-	0.24	-	-	-	-	-	-	-
Yb_2O_3	-	-	0.87	1.06	-	-	-	-	-	-	-
CaO	-	1.46	1.96	1.49	0.09	0.40	1.08	-	0.92	2.02	0.45
MnO	-	1.00	0.24	0.56	-	0.21	0.54	-	0.66	0.66	-
FeO	0.11	1.89	1.43	1.93	0.16	1.01	2.83	-	2.97	1.64	0.35
Na_2O	-	0.61	0.23	0.58	-	0.44	0.40	-	0.32	0.82	-
Total	**99.36**	**95.38**	**84.15**	**92.83**	**99.40**	**92.13**	**88.53**	**99.39**	**92.72**	**85.40**	**97.46**

	MAS012 N = 4	MAS012 N = 4	MAS013 N = 2	MAS013 N = 2	MAS015 N = 2	MAS015 N = 1	MAS015 N = 3	MAS016 N = 3	MAS016 N = 3	MAS017 N = 3	MAS018 N = 2
Structural formulae calculated on the basis of 4 cations											
Si	1.002	0.956	0.952	0.920	1.002	0.988	0.956	1.003	0.926	0.980	0.994
Zr	0.984	0.910	0.727	0.815	0.979	0.937	0.877	0.981	0.906	0.831	0.954
Hf	0.009	0.009	0.006	0.004	0.006	0.012	0.007	0.013	0.009	0.004	0.012
Th	-	-	0.019	0.003	0.002	0.003	0.005	0.003	0.004	0.031	0.003
U	-	0.002	0.012	0.006	0.003	0.002	0.001	0.001	0.002	0.011	0.001
Al	-	0.013	0.088	0.027	-	0.008	0.008	-	0.009	0.008	0.013
Y	-	-	0.083	0.099	-	-	-	-	-	-	-
La	-	-	0.002	-	-	-	-	-	-	-	-
Ce	-	-	0.010	-	-	-	-	-	-	-	0.004
Pr	-	-	0.008	-	-	-	-	-	-	-	-
Nd	-	-	-	-	-	-	-	-	-	-	0.001
Sm	-	-	-	-	-	-	-	-	-	-	-
Gd	-	-	0.007	0.009	-	-	-	-	-	-	-
Tb	-	-	-	0.001	-	-	-	-	-	-	-
Dy	-	-	0.009	0.012	-	-	-	-	-	-	-
Ho	-	-	-	0.002	-	-	-	-	-	-	-
Er	-	-	0.012	0.013	-	-	-	-	-	-	-
Tm	-	-	-	0.003	-	-	-	-	-	-	-
Yb	-	-	0.010	0.011	-	-	-	-	-	-	-
Ca	-	0.050	0.079	0.055	0.003	0.014	0.039	-	0.032	0.078	0.015
Mn	-	0.027	0.008	0.016	-	0.006	0.015	-	0.018	0.020	-
Fe	0.008	0.151	0.135	0.166	0.012	0.084	0.239	-	0.242	0.148	0.028
Na	-	0.038	0.017	0.038	-	0.028	0.026	-	0.020	0.057	-
Total	**2.003**	**2.156**	**2.184**	**2.2**	**2.007**	**2.082**	**2.173**	**2.001**	**2.168**	**2.168**	**2.026**

	MAS019 N = 4	MAS020 N = 4	MAS022 N = 4	MAS024 N = 3	MAS024 N = 2	MAS025 N = 3	MAS025 N = 4	MAS026 N = 2	MAS026 N = 2	MAS026 N = 4	MAS030 N = 3
Wt. %											
SiO_2	32.58	32.55	32.13	28.72	32.26	32.53	28.43	32.89	32.58	28.99	32.93
ZrO_2	65.71	65.72	64.17	54.58	64.66	63.74	55.35	64.40	64.36	55.17	66.6
HfO_2	0.49	1.12	1.20	1.65	1.26	2.17	1.80	0.74	0.94	2.51	0.89
ThO_2	1.44	-	-	0.81	0.38	-	0.86	-	0.69	0.45	-
UO_2	-	-	-	-	-	-	0.15	-	-	-	-
Al_2O_3	-	-	0.26	0.30	-	0.71	0.36	-	-	0.27	-
Y_2O_3	-	-	-	-	-	-	-	-	-	-	-
La_2O_3	-	-	-	-	-	-	-	-	-	-	-
Ce_2O_3	-	-	-	-	-	-	-	-	-	-	-
Pr_2O_3	-	-	-	-	-	-	-	-	-	-	-
Nd_2O_3	-	-	-	-	-	-	-	-	-	-	-
Sm_2O_3	-	-	-	-	-	-	-	-	-	-	-
Gd_2O_3	-	-	-	-	-	-	-	-	-	-	-
Tb_2O_3	-	-	-	-	-	-	-	-	-	-	-
Dy_2O_3	-	-	-	-	-	-	-	-	-	-	-
Ho_2O_3	-	-	-	-	-	-	-	-	-	-	-
Er_2O_3	-	-	-	-	-	-	-	-	-	-	-
Tm_2O_3	-	-	-	-	-	-	-	-	-	-	-
Yb_2O_3	-	-	-	-	-	-	-	-	-	-	-
CaO	-	0.09	0.19	1.61	0.06	0.05	2.28	-	-	1.79	-
MnO	-	-	-	0.14	-	-	0.40	-	-	0.77	-
FeO	0.06	-	0.59	0.99	0.13	0.16	1.61	0.51	0.24	2.68	0.22
Na_2O	-	-	-	0.49	-	-	0.33	-	-	0.46	-
Total	**100.28**	**99.48**	**98.54**	**89.29**	**98.75**	**99.36**	**91.57**	**99.54**	**98.81**	**93.09**	**100.64**

| | MAS019 | MAS020 | MAS022 | MAS024 | MAS024 | MAS025 | MAS025 | MAS026 | MAS026 | MAS026 | MAS030 |
	N = 4	N = 4	N = 4	N = 3	N = 2	N = 3	N = 4	N = 2	N = 2	N = 4	N = 3
Structural formulae calculated on the basis of 4 cations											
Si	1.000	1.002	0.991	0.979	1.001	1.000	0.947	1.002	1.007	0.938	0.999
Zr	0.983	0.987	0.965	0.907	0.979	0.955	0.899	0.972	0.970	0.870	0.985
Hf	0.004	0.010	0.011	0.016	0.011	0.019	0.017	0.006	0.008	0.023	0.008
Th	0.010	-	-	0.006	0.003	-	0.007	-	0.005	0.003	-
U	-	-	-	-	-	-	0.001	-	-	-	-
Al	-	-	0.009	0.012	-	0.026	0.014	-	-	0.010	-
Y	-	-	-	-	-	-	-	-	-	-	-
La	-	-	-	-	-	-	-	-	-	-	-
Ce	-	-	-	-	-	-	-	-	-	-	-
Pr	-	-	-	-	-	-	-	-	-	-	-
Nd	-	-	-	-	-	-	-	-	-	-	-
Sm	-	-	-	-	-	-	-	-	-	-	-
Gd	-	-	-	-	-	-	-	-	-	-	-
Tb	-	-	-	-	-	-	-	-	-	-	-
Dy	-	-	-	-	-	-	-	-	-	-	-
Ho	-	-	-	-	-	-	-	-	-	-	-
Er	-	-	-	-	-	-	-	-	-	-	-
Tm	-	-	-	-	-	-	-	-	-	-	-
Yb	-	-	-	-	-	-	-	-	-	-	-
Ca	-	0.003	0.006	0.059	0.002	0.002	0.081	-	-	0.062	-
Mn	-	-	-	0.004	-	-	0.011	-	-	0.021	-
Fe	0.005	-	0.046	0.085	0.010	0.012	0.135	0.039	0.019	0.218	0.017
Na	-	-	-	0.032	-	-	0.021	-	-	0.029	-
Total	**2.002**	**2.001**	**2.028**	**2.101**	**2.006**	**2.013**	**2.133**	**2.019**	**2.009**	**2.175**	**2.008**

	MAS031 N = 3	MAS032 N = 3	MAS032 N = 1	MAS032 N = 2	MAS033 N = 1	MAS033 N = 2	MAS033 N = 3	MAS034 N = 4	MAS034 N = 7	MAS038 N = 3	MAS038 N = 2
Wt. %											
SiO_2	32.87	32.98	28.40	28.30	32.79	27.52	29.65	32.89	28.29	33.32	28.93
ZrO_2	65.43	65.95	55.92	55.47	64.81	48.43	54.69	66.97	57.54	64.91	58.31
HfO_2	1.38	1.41	1.17	0.83	0.43	-	1.03	0.48	0.78	1.10	0.86
ThO_2	-	-	0.94	1.05	-	-	-	-	0.38	-	2.28
UO_2	-	-	-	-	-	-	-	-	0.21	-	0.27
Al_2O_3	0.21	0.22	0.29	0.27	-	0.80	1.00	-	0.52	0.44	0.33
Y_2O_3	-	-	-	-	-	-	-	-	-	-	-
La_2O_3	-	-	-	-	-	-	-	-	-	-	1.11
Ce_2O_3	-	-	-	-	-	-	0.35	-	-	-	1.73
Pr_2O_3	-	-	-	-	-	-	-	-	-	-	-
Nd_2O_3	-	-	-	-	-	-	0.17	-	-	-	0.44
Sm_2O_3	-	-	-	-	-	-	-	-	-	-	-
Gd_2O_3	-	-	-	-	-	-	-	-	-	-	-
Tb_2O_3	-	-	-	-	-	-	-	-	-	-	-
Dy_2O_3	-	-	-	-	-	0.91	0.48	-	-	-	-
Ho_2O_3	-	-	-	-	-	0.32	0.19	-	-	-	-
Er_2O_3	-	-	-	-	-	0.63	0.65	-	-	-	-
Tm_2O_3	-	-	-	-	-	-	-	-	-	-	-
Yb_2O_3	-	-	-	-	-	0.83	0.66	-	-	-	-
CaO	-	-	0.18	1.27	-	1.64	1.43	-	2.40	-	1.65
MnO	-	-	-	-	0.32	-	0.32	-	0.71	-	-
FeO	0.21	-	0.27	1.44	0.68	1.05	1.32	-	0.55	0.72	1.14
Na_2O	-	-	0.83	0.43	-	0.33	0.26	-	0.68	-	-
Total	**100.10**	**100.56**	**88.00**	**89.06**	**99.03**	**82.46**	**92.20**	**100.34**	**92.06**	**100.49**	**97.05**

	MAS031 N=3	MAS032 N=3	MAS032 N=1	MAS032 N=2	MAS033 N=1	MAS033 N=2	MAS033 N=3	MAS034 N=4	MAS034 N=7	MAS038 N=3	MAS038 N=2
Structural formulae calculated on the basis of 4 cations											
Si	1.002	1.003	0.991	0.963	1.001	1.004	0.976	1.001	0.947	1.001	0.938
Zr	0.972	0.978	0.952	0.921	0.965	0.861	0.877	0.994	0.939	0.951	0.922
Hf	0.012	0.012	0.012	0.008	0.004	-	0.010	0.004	0.007	0.009	0.008
Th	-	-	0.007	0.008	-	-	-	-	0.003	-	0.017
U	-	-	-	-	-	-	-	-	0.002	-	0.002
Al	0.008	-	0.012	0.011	-	0.034	0.039	-	0.021	0.016	0.013
Y	-	-	-	-	-	-	-	-	-	-	-
La	-	-	-	-	-	-	-	-	-	-	0.013
Ce	-	-	-	-	-	-	0.004	-	-	-	0.021
Pr	-	-	-	-	-	-	-	-	-	-	-
Nd	-	-	-	-	-	-	0.002	-	-	-	0.005
Sm	-	-	-	-	-	-	-	-	-	-	-
Gd	-	-	-	-	-	-	-	-	-	-	-
Tb	-	-	-	-	-	-	-	-	-	-	-
Dy	-	-	-	-	-	0.011	0.005	-	-	-	-
Ho	-	-	-	-	-	0.004	0.002	-	-	-	-
Er	-	-	-	-	-	0.007	0.007	-	-	-	-
Tm	-	-	-	-	-	-	-	-	-	-	-
Yb	-	-	-	-	-	0.009	0.007	-	-	-	-
Ca	-	-	0.007	0.046	-	0.064	0.050	-	0.086	-	0.057
Mn	-	-	-	-	0.008	-	0.009	-	0.020	-	-
Fe	0.016	-	0.024	0.123	0.052	0.096	0.109	-	0.046	0.054	0.093
Na	-	-	0.056	0.028	-	0.021	0.017	-	0.044	-	-
Total	**2.010**	**2.002**	**2.060**	**2.109**	**2.030**	**2.114**	**2.113**	**2.000**	**2.114**	**2.031**	**2.088**

	MAS038 N = 1	MAS040 N = 4
Wt. %		
SiO_2	23.59	32.47
ZrO_2	48.11	66.37
HfO_2	0.75	0.24
ThO_2	4.00	-
UO_2	0.46	-
Al_2O_3	0.36	-
Y_2O_3	-	-
La_2O_3	3.09	-
Ce_2O_3	4.03	-
Pr_2O_3	-	-
Nd_2O_3	0.78	-
Sm_2O_3	-	-
Gd_2O_3	-	-
Tb_2O_3	-	-
Dy_2O_3	-	-
Ho_2O_3	-	-
Er_2O_3	-	-
Tm_2O_3	-	-
Yb_2O_3	-	-
CaO	3.89	-
MnO	-	-
FeO	1.03	-
Na_2O	-	-
Total	**90.09**	**99.08**

	MAS038 N = 1	MAS040 N = 4

Structural formulae calculated on the basis of 4 cations

Si	0.871	1.001
Zr	0.867	0.997
Hf	0.008	0.002
Th	0.034	-
U	0.004	-
Al	0.016	-
Y	-	-
La	0.042	-
Ce	0.055	-
Pr	-	-
Nd	0.010	-
Sm	-	-
Gd	-	-
Tb	-	-
Dy	-	-
Ho	-	-
Er	-	-
Tm	-	-
Yb	-	-
Ca	0.154	-
Mn	-	-
Fe	0.095	-
Na	-	-
Total	**2.155**	**2.000**

III.XVIII Zirconolite [Fe^{3+} recalculated using the method of Droop (1987)]

	MAS001 N = 5	MAS002 N = 3	MAS002 N = 5	MAS002 N = 3	MAS005 N = 3	MAS005 N = 5	MAS023 N = 3
Wt. %							
WO_3	0.26	-	-	-	0.59	0.38	-
Nb_2O_5	10.54	10.04	8.01	8.21	12.62	11.88	17.58
Ta_2O_5	1.90	-	-	-	1.83	1.61	0.91
SiO_2	0.79	0.60	0.59	0.40	2.82	2.01	-
TiO_2	20.58	23.06	25.60	22.67	21.43	22.50	18.18
ZrO_2	27.20	32.14	33.21	28.97	28.89	29.50	30.40
HfO_2	0.44	0.49	0.39	0.59	0.57	0.75	0.54
ThO_2	3.09	1.95	2.15	2.19	3.92	3.15	0.16
UO_2	1.14	0.78	0.75	0.89	0.42	0.47	-
Al_2O_3	0.26	0.65	0.15	0.59	0.23	0.38	0.20
Y_2O_3	1.77	2.21	2.34	4.69	7.44	8.16	1.78
La_2O_3	2.24	2.07	1.64	2.24	0.52	0.73	2.54
Ce_2O_3	6.37	6.61	5.17	7.63	2.44	2.82	7.11
Pr_2O_3	1.54	1.01	1.04	1.38	0.49	0.41	1.10
Nd_2O_3	4.10	3.54	2.54	3.34	1.59	1.49	3.67
Sm_2O_3	0.79	0.46	0.89	0.36	0.41	0.22	0.55
Gd_2O_3	0.14	-	-	0.24	1.54	2.04	-
Tb_2O_3	0.32	-	-	0.53	0.29	0.19	-
Dy_2O_3	0.84	-	-	1.40	2.05	2.59	-
Ho_2O_3	0.39	-	-	0.46	0.56	0.66	-
Er_2O_3	0.31	-	-	0.03	0.87	1.24	-
Tm_2O_3	0.40	-	-	0.32	0.21	0.19	-
Yb_2O_3	0.37	-	-	0.15	0.69	1.19	-
Lu_2O_3	0.25	-	-	0.07	0.16	-	-
Fe_2O_3	1.84	0.08	0.62	1.91	-	-	-
FeO	6.84	8.47	7.11	6.05	3.54	2.64	9.13
CaO	6.11	6.15	7.42	5.39	4.54	3.65	6.98
Total	**100.76**	**100.31**	**99.62**	**100.70**	**100.66**	**100.85**	**100.83**

	MAS001 N = 5	MAS002 N = 3	MAS002 N = 5	MAS002 N = 3	MAS005 N = 3	MAS005 N = 5	MAS023 N = 3
Structural formulae calculated on the basis of 7 oxygens							
W	0.005	-	-	-	0.010	0.007	-
Nb	0.333	0.305	0.240	0.256	0.382	0.362	0.541
Ta	0.036	-	-	-	0.033	0.030	0.017
Si	0.055	0.040	0.039	0.028	0.189	0.136	-
Ti	1.081	1.165	1.277	1.174	1.080	1.141	0.930
Zr	0.926	1.052	1.074	0.973	0.944	0.970	1.008
Hf	0.009	0.009	0.007	0.012	0.011	0.014	0.010
Th	0.049	0.030	0.032	0.034	0.060	0.048	0.002
U	0.018	0.012	0.011	0.014	0.006	0.007	-
Al	0.021	0.051	0.012	0.048	0.018	0.030	0.016
Y	0.066	0.079	0.083	0.172	0.265	0.293	0.064
La	0.058	0.051	0.040	0.057	0.013	0.018	0.064
Ce	0.163	0.163	0.126	0.192	0.060	0.070	0.177
Pr	0.039	0.025	0.025	0.035	0.012	0.010	0.027
Nd	0.102	0.085	0.060	0.082	0.038	0.036	0.089
Sm	0.019	0.011	0.020	0.009	0.009	0.005	0.013
Gd	0.003	-	-	0.005	0.034	0.046	-
Tb	0.007	-	-	0.012	0.006	0.004	-
Dy	0.019	-	-	0.031	0.044	0.056	-
Ho	0.009	-	-	0.010	0.012	0.014	-
Er	0.007	-	-	0.001	0.018	0.026	-
Tm	0.009	-	-	0.007	0.004	0.004	-
Yb	0.008	-	-	0.003	0.014	0.024	-
Lu	0.005	-	-	0.001	0.003	-	-
Fe^{3+}	0.435	0.476	0.395	0.351	-	-	-
Fe^{2+}	0.064	0.004	0.031	0.100	0.198	0.149	0.519
Ca	0.457	0.443	0.527	0.398	0.326	0.264	0.509
Total	**4.002**	**4.000**	**4.001**	**4.003**	**3.791**	**3.764**	**3.987**

	MAS023 N = 1	MAS023 N = 2
Wt. %		
WO_3	-	-
Nb_2O_5	19.66	16.49
Ta_2O_5	0.89	0.82
SiO_2	-	-
TiO_2	16.22	18.39
ZrO_2	29.49	28.98
HfO_2	0.24	0.57
ThO_2	1.08	0.85
UO_2	0.45	-
Al_2O_3	-	-
Y_2O_3	1.76	1.82
La_2O_3	1.63	1.98
Ce_2O_3	6.70	7.18
Pr_2O_3	0.78	1.19
Nd_2O_3	4.32	4.03
Sm_2O_3	0.53	0.46
Gd_2O_3	-	-
Tb_2O_3	-	-
Dy_2O_3	-	-
Ho_2O_3	-	-
Er_2O_3	-	-
Tm_2O_3	-	-
Yb_2O_3	-	-
Lu_2O_3	-	-
Fe_2O_3	-	0.15
FeO	9.69	8.90
CaO	6.88	7.02
Total	**100.32**	**98.82**

	MAS023 N = 1	MAS023 N = 2

Structural formulae calculated on the basis of 7 oxygens

	MAS023 N = 1	MAS023 N = 2
W	-	-
Nb	0.614	0.519
Ta	0.017	0.016
Si	-	-
Ti	0.843	0.963
Zr	0.994	0.984
Hf	0.005	0.011
Th	0.017	0.013
U	0.007	-
Al	-	-
Y	0.065	0.067
La	0.042	0.051
Ce	0.170	0.183
Pr	0.020	0.030
Nd	0.107	0.100
Sm	0.013	0.011
Gd	-	-
Tb	-	-
Dy		-
Ho	-	-
Er	-	-
Tm	-	-
Yb	-	-
Lu	-	-
Fe^{3+}	-	0.008
Fe^{2+}	0.560	0.518
Ca	0.509	0.524
Total	**3.981**	**4.000**